UNIVERSITY OF SOUTH BOHEMIA

FACULTY OF SCIENCE

BIOSYNTHESIS OF CHLOROPHYLL-BINDING PROTEINS

Habilitation Thesis

Roman Sobotka

České Budějovice, March 2017

Contents

About this thesis

The presented habilitation thesis is a sum of nine articles published in international journals, representing a part of my scientific work that was done during more than 10 years (2005–2016). A common theme of the selected articles is the biosynthesis of chlorophyll-binding proteins that form the functional core of photosystem I and II. The combination of chlorophyll molecules, light, and oxygen is a toxic cocktail, particularly if the light energy absorbed by chlorophylls is not immediately utilized for photosynthesis. If excited for 'too long' ($>10^{-9}$ s) chlorophylls tend to switch to a triplet excited state that can react with oxygen, forming damaging oxygen radicals. However, light absorption, oxygen production, and the synthesis of quantities of chlorophyll are processes that photosynthetic cells typically do at the same moment. The central question of this thesis is how cells regulate the synthesis of chlorophyll and chlorophyll-protein complexes in order to prevent and/or decrease oxidative stress.

The majority of the work was done at the Centre Algatech, Institute of Microbiology in Třeboň, using the cyanobacterium *Synechocystis* PCC 6803 as a model organism. The results presented in the thesis would not exist without the assistance of my colleagues and students from Třeboň. Namely, I would like to thank Josef Komenda and Martin Tichý for introducing me to biochemistry and genetics of cyanobacteria, for their guidance during initial experimental work, and for sharing and discussing ideas. I would like to thank Jana Kopečná, Lenka Bučinská, Markéta Linhartová and Peter Konik for excellent work and for their nice personality. I am thankful to all members of the Laboratory of photosynthesis for being helpful, hard-working and smart people.

A part of the work was done at Sheffield University during my postdoctoral stay and several subsequent visits in the group of Prof. Neil Hunter. Neil is an excellent scientist and I have learnt a great deal from him during our intensive and continuing collaboration. Furthermore, Neil's students Jack Chidgey and Sarah Hollingshead made an important contribution to the research described in this thesis.

I am very grateful to my wife Káťa for her tolerance, patience and love, and Filip and Kuba for their being.

Selected publications

1. **Sobotka R**, Komenda J, Bumba L, Tichý M. (2005) Photosystem II assembly in CP47 mutant of *Synechocystis* sp. PCC 6803 is dependent on the level of chlorophyll precursors regulated by ferrochelatase. ***J. Biol. Chem*.** 280: 31595-31602
2. **Sobotka R**, Dühring U, Komenda J, Peter E, Gardian Z, Tichy M, Grimm B, Wilde A. (2008) Importance of the cyanobacterial Gun4 protein for chlorophyll metabolism and assembly of photosynthetic complexes. ***J. Biol. Chem***. 283: 25794-802
3. **Sobotka R**, Tichý M, Wilde A, Hunter CN. (2011) Functional assignments for the C-terminal domains of the ferrochelatase from Synechocystis PCC 6803: the CAB domain plays a regulatory role and region II is essential for catalysis. ***Plant Physiol***. 155: 1735-47
4. Kopečná J, Komenda J, Bučinská L, **Sobotka R**. (2012) Long-term acclimation of the cyanobacterium Synechocystis PCC 6803 to high light is accompanied by an enhanced production of chlorophyll that is preferentially channeled to trimeric PSI. ***Plant Physiol***. 160: 2239-50
5. Linhartová, M, Bučinská, L, Halada, P, Ječmen, T, Šetlík, J, Komenda, J, **Sobotka, R**. (2014) Accumulation of the Type IV prepilin triggers degradation of SecY and YidC and inhibits synthesis of Photosystem II proteins in the cyanobacterium *Synechocystis* PCC 6803. ***Mol Microbiol***, 93: 1207–1223
6. Chidgey, JW, Linhartová, M, Komenda, J, Jackson, PJ, Dickman, MJ, Canniffe, DP, Koník, P, Pilný, J, Hunter, CN, **Sobotka, R**. (2014) A cyanobacterial chlorophyll synthase-HliD complex associates with the Ycf39 protein and the YidC/Alb3 insertase. ***Plant Cell*** 26: 1267-79
7. Knoppová, J, **Sobotka, R**, Tichý, M, Yu, J, Halada, P, Nixon, PJ, Komenda, J. (2014) Discovery of a chlorophyll binding protein complex involved in the early steps of Photosystem II assembly in *Synechocystis*. ***Plant Cell*** 26: 1200-1212
8. Staleva, H, Komenda, J, Shukla, MK, Šlouf, V, Kaňa, R, Polívka, T, **Sobotka, R** (2015) Mechanism of photoprotection in the cyanobacterial ancestor of plant antenna protein. ***Nature Chem Biol*** 11: 287-291
9. Hollingshead, S, Kopečná, J, Armstrong, DR, Bučinská, L, Jackson, PJ, Chen, GE, Dickman, MJ, Williamson, MP, **Sobotka, R**, Hunter, CN. (2016) Synthesis of chlorophyll-binding proteins in a fully segregated *ycf54* strain of the cyanobacterium *Synechocystis* PCC 6803**. *Front Plant Sci*** 7: 292

My role in these publications was either: key researcher (1, 2, 3, 7) or supervisor (9) or corresponding author (4, 5, 6, 8).

Photosynthetic apparatus in cyanobacteria

Oxygenic phototrophs (cyanobacteria, algae, and plants) utilize light as the source of energy for their proliferation. They are responsible for almost all primary production and for the oxygenation of the Earth's atmosphere. However, light intensity at the Earth's surface is not constant; it fluctuates from being too low to sufficiently drive photosynthetic reactions to being much higher than can be utilized, or at least safely dissipated, by the photosynthetic apparatus. Other important environmental factors like nutrient availability or temperature can also be quite varying, such that photosynthetic cells are under constant pressure to rapidly acclimate to a dynamic environment. The response could be described as an effort to restore an optimal metabolic homeostasis (energy input, redox balance, and nutrient and carbon assimilation) and thus achieve the maximal possible growth rate. Or, under really severe conditions, to at least survive.

During acclimation, the central target for the regulation is the photosynthetic electron transport chain, which is driven by the integral thylakoid membrane complexes Photosystem I and II (PSI and PSII) and cytochrome b_6f (Fig. 1). Particularly, light energy has to be carefully distributed between photosystems to maintain redox homeostasis. Photosynthetic organisms have developed a remarkable number of strategies for the reorganization and modulation of PSII, PSI, and light-harvesting antennas in order to avoid redox misbalance (Bailey and Grossman, 2008; Horton *et al.*, 1996). Since my results selected for this thesis were obtained using the model cyanobacterium *Synechocystis* PCC 6803 (hereafter *Synechocystis*), this text will further focus mostly on cyanobacteria. Nevertheless, given the close evolutionary relationship between cyanobacteria and chloroplasts, and the similarity of the structure and function of their thylakoid complexes, the mechanisms regulating the biogenesis and stoichiometry of photosystems are expected to be generally common to all oxygenic phototrophs.

While both photosystems are large and complicated assemblages of proteins that bind a number of Chl molecules, PSI binds the majority of Chls. In cyanobacteria, where PSI is uniquely organised in trimers (PSI[3]), there are about 300 Chls per PSI[3] and only about 70 Chls in a PSII dimer (Fig. 1; Kopečná *et al.*, 2012). The large array of Chls in PSI is adequate to harvest the energy powering this complex, while PSII activity relies mainly on the energy delivered from extrinsic antennae (Page *et al.*, 2012). Cyanobacteria (and red

algae) do not use chlorophyll (Chl)-based light-harvesting systems, which are typical for plants. Instead, most of the light that powers PSII complexes is harvested by large extrinsic phycobilisome complexes containing linear tetrapyrroles (phycobilins) as chromophores (Fig. 1).

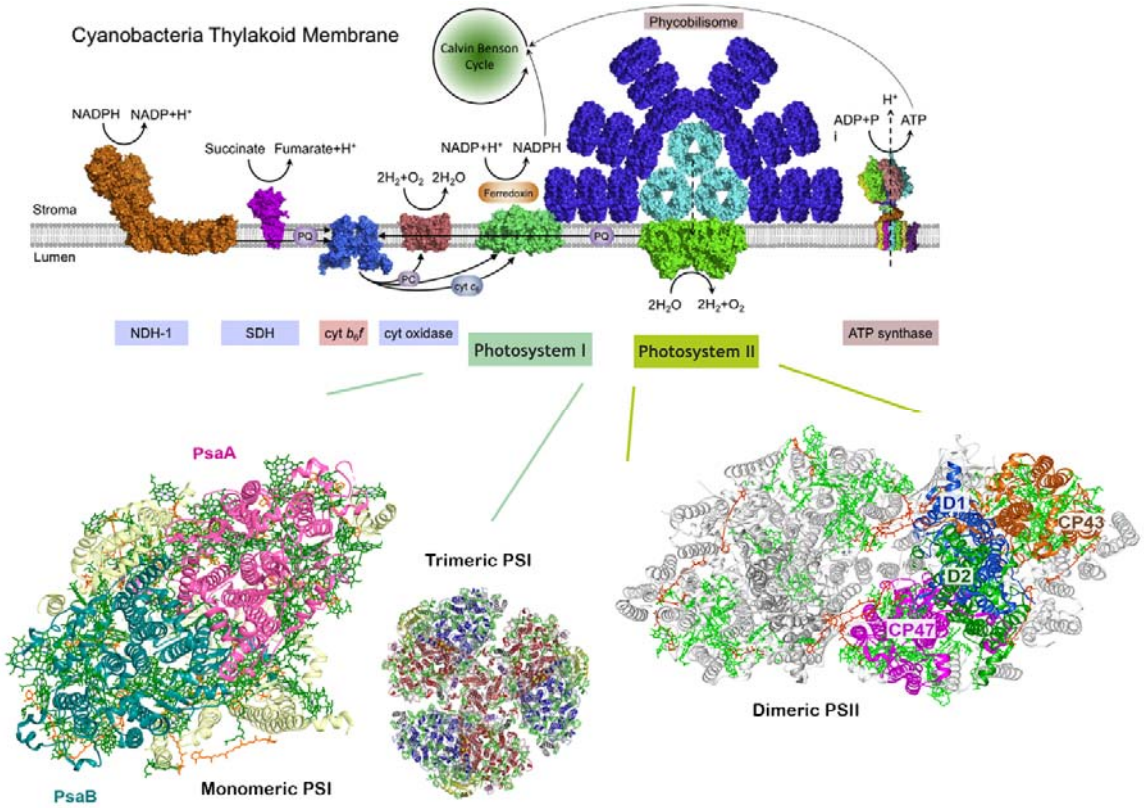

Figure 1. Cyanobacterial thylakoid membranes harbour the elements of both photosynthetic and respiratory electron transfer chain. This schematic model shows photosynthetic complexes with extrinsic phycobilisomes as well as respiratory membrane complexes from a side view (top; modified from (Liu, 2016). Crystal structures of trimeric PSI (Jordan *et al.*, 2001) and dimeric PSII (Umena *et al.*, 2011) are shown from stromal side (below). A detailed view of a (monomeric) PSI unit is also shown (left). Individual Chl-binding subunits (PsaA/B, D1, D2, CP47 CP43) of both photosystems are highlighted by different colours. In cyanobacteria almost all Chl molecules (~95%) are bound to these five proteins (Xu *et al.*, 2004).

This inherent light-harvesting capacity of PSI and PSII determines how cyanobacteria control their excitation. Whereas phycobilisomes can be quickly de-attached from PSII and/or the energy absorbed by phycobilisomes can be dissipated (Stoitchkova *et al.*, 2007; Kirilovsky and Kerfeld, 2013), the total PSI excitation can be reduced only via decreasing the number of PSI complexes per cell. Indeed, a typical response of *Synechocystis* to high-light, cold, or to nutrient limitation is a fast downregulation of the level of PSI[3] and

phycobilisomes, while maintaining a rather constant level of PSII. Over the course of just a few hours the PSI/PSII ratio can change remarkably (Kopečná *et al.*, 2012). Altering the PSI level is, however, a complicated and 'risky' task. Under non-stress conditions PSI[3] is the site where the majority (>80%) of cellular Chl is located in *Synechocystis* and this complex is also the main sink for the *de novo* synthesized Chl molecules (Kopečná *et al.*, 2015b). As already noted in the foreword, Chl is readily excited by visible light and if the absorbed light energy is not utilized quickly enough, Chls tend to switch to a triplet excited state and generate damaging reactive oxygen species (ROS). Therefore, any pool of unquenched Chls, either as free molecules in the lipid bilayer, or bound to unassembled 'free' proteins, is potentially highly toxic, particularly under high light intensities. In addition, most intermediates of Chl biosynthesis are also phototoxic. The cell must therefore minimize the levels of assembly intermediates of PSI/PSII biogenesis and avoid accumulation of free Chl as well as its biosynthetic intermediates. The biogenesis of Chl-proteins is further complicated by the fact that the lifetime of Chl molecules is much longer than that of the proteins that they bind, suggesting that Chl molecules are reutilized many times (Vavilin *et al.*, 2005). Additionally, because of the high sensitivity of PSII to ROS, oxygenic phototrophs have evolved a unique mechanism to repair damaged PSII by replacing the most sensitive D1 subunit (Fig. 1; Komenda *et al.*, 2007). However, this means that to maintain a constant pool of active PSII under stress conditions, the cell has to co-ordinate *de novo* PSII synthesis with the synthesis of extra D1 subunit for the repair, according to the rate of PSII damage. The levels of PSI and PSII have to be controlled by a sophisticated regulatory mechanism that synchronizes Chl biosynthesis and recycling, and the synthesis and assembly of photosystem subunits. This regulation has to further reflect PSII damage and its repair, as well as the actual growth rate. In the following two chapters I describe the current knowledge about Chl biosynthesis and biogenesis of Chl-proteins. The last chapter is more speculative, dealing with an emerging picture of the Chl-protein biosynthetic machinery.

Chlorophyll biosynthetic pathway

Oxygenic phototrophs generally synthesize all tetrapyrroles (Chl, heme, bilins) via a common branched pathway (Fig. 2). The initial precursor, 5-aminolaevulinic acid (ALA) is made in three steps from glutamate through glutamyl-tRNA, and is subsequently converted

in several steps to protoporphyrin IX, the last common precursor of Chl and heme biosynthesis. Insertion of Fe^{2+} into this porphyrin macrocycle by ferrochelatase (FeCH) leads to heme, whereas the insertion of Mg^{2+} by magnesium chelatase leads to Mg-protoporphyrin IX, the first intermediate of the Chl branch. Chl synthesis continues with formation of the isocyclic 'fifth' ring by Mg-protoporphyrin methyl transferase and Mg-protoporphyrin cyclase (cyclase), reduction of a peripheral vinyl group to an ethyl group by divinyl reductase, followed or preceded by the reduction of the macrocyclic ring system to form a chlorin by protochlorophyllide oxidoreductase. Chl is completed by the addition of a polyisoprene alcohol to the tetrapyrrole by a teamwork of the Chl-synthase and geranyl-geranyl reductase enzymes (reviewed in Sobotka, 2014).

Cyanobacteria growing under non-stress conditions produce large quantities of Chl and bilins to maintain a constant Chl and phycobilisome content per cell during fast proliferation. However, this changes very quickly when a stress factor arises, and the total metabolite flow through the tetrapyrrole pathway can show dramatic changes (Kopečná *et al.*, 2015a). Still, tetrapyrrole synthesis must be accomplished to always avoid the accumulation of "free" tetrapyrrole intermediates, which is complicated by the fact that Chl, heme, and bilins are needed in differing amounts according to environmental conditions. In contrast to the relatively 'safe' bilin molecules, a leakage in the control over Chl-protein biogenesis is followed by the formation of destructive ROS (Papenbrock *et al.*, 2001). According to the current model the tetrapyrrole pathway possesses two critical regulatory points: the formation of ALA, and the branch point towards Chl and heme.

There is good evidence that the formation of ALA in plants and algae is allosterically inhibited by heme (Brzezowski *et al.*, 2015) and a heme feedback loop probably operates in cyanobacteria as well (Sobotka *et al.*, 2008b). The mechanism regulating substrate flow into Chl and heme branches remains unknown; however, the regulatory role of Mg- and Fe-chelatases (FeCH) is obvious (Sobotka *et al.*, 2008a; Czarnecki and Grimm, 2012). FeCH is an enzyme of special interest regarding the regulation of tetrapyrrole biosynthesis. Firstly, via heme production, FeCH likely regulates the flux into both the heme and Chl branches of the pathway. Secondly, differential consumption of the common substrate protoporphyrin IX by FeCH and Mg-chelatase might also control partitioning at the Chl/heme branch point. Our work on the regulation of Chl biosynthesis demonstrated that FeCH is indeed a global regulator of the tetrapyrrole pathway (Fig. 2; Sobotka *et al.*, 2005;

Sobotka *et al.*, 2011). FeCH activity/level is strongly upregulated in various PSII mutants that exhibit inhibited Chl biosynthesis as well as in the PSI-less strains. The limited Chl biosynthesis in these mutants is indeed due to the high FeCH activity, as the Chl formation can be restored by using a specific FeCH inhibitor (Sobotka *et al.*, 2005).

An intriguing feature of FeCH from cyanobacterial and chloroplast sources is the conserved hydrophobic C-terminal extension (Cab or Hlip domain) with a high degree of similarity to the first and third helixes of the plant LHCII light-harvesting complex, including a Chl-binding motif. In fact, this FeCH Cab/Hlip domain highly resembles the single transmembrane helix proteins called high-light-inducible proteins (Hlips) that are encoded in all sequenced cyanobacterial genomes. These proteins possess a Chl-binding motif and, as shown recently, they can indeed bind Chl molecules (Chidgey *et al.*, 2014); see Fig. 4 for a model of the hypothetical Hlip dimer). It is very likely that the modern cyanobacterial and plastid FeCH resulted from an ancient fusion with a Hlip.

Interestingly, a *Synechocystis* mutant possessing a truncated FeCH lacking the Cab/Hlip domain has an unaltered pigment composition under low light intensities but it is sensitive to high light and accumulates chlorophyllide (Sobotka *et al.*, 2011). Similarly to other Hlips (see below), the one fused with FeCH is also likely to be important for the re-usage of Chl molecules released from degraded Chl-proteins. Whether this Cab/Hlip domain plays a role in controlling FeCH activity (*e.g.* via binding of Chl molecules) remains an open question. It appears, however, that the FeCH level is increased under certain stress conditions such as high-light or cold stress; (Kopečná *et al.*, 2012; Kopf *et al.*, 2014) and these are the same conditions that lead to a strongly reduced level of PSI[3] (Sobotka, R. unpublished results).

Insertion of chlorophyll molecules into apoproteins

The main Chl-binding subunits of PSI (PsaA, PsaB) and PSII (D1, D2, CP43, CP47; Fig. 1) are relatively large and strongly hydrophobic transmembrane proteins. In cyanobacteria, as well as in chloroplasts, these proteins are synthesized on membrane-bound ribosomes and the elongating nascent chains are co-translationally inserted into the thylakoid membrane (Kim *et al.*, 1994; Chua *et al.*, 1976; Tyystjarvi *et al.*, 2001).

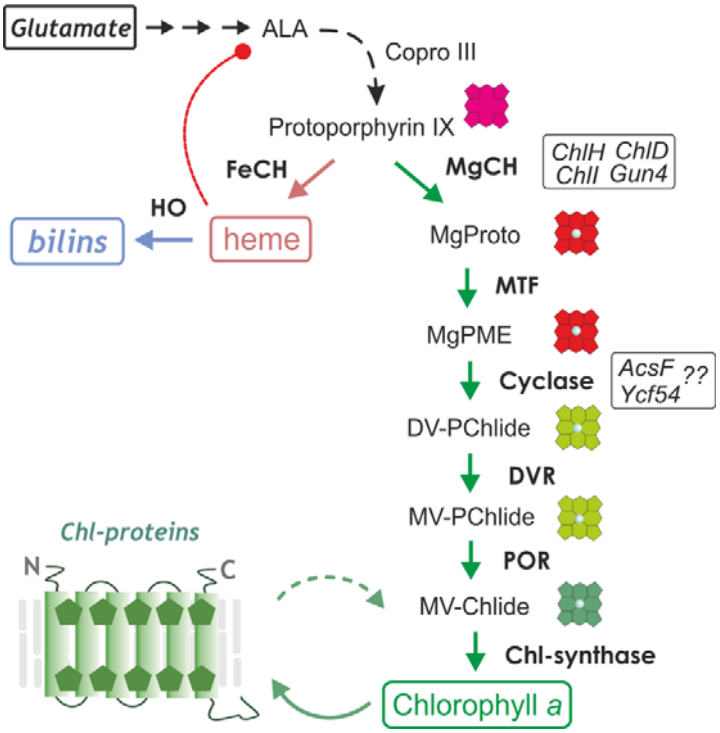

Figure 2. A scheme of the tetrapyrrole biosynthetic pathway and its connection to Chl-protein synthesis and Chl recycling. Chl precursor monovinyl chlorophyllide (MV-Chlide) is not only an intermediate of de novo Chl biosynthesis but also of the constant process of Chl recycling (Vavilin *et al.*, 2005; Kopečná *et al.*, 2015b). It is generally expected that heme acts as an allosteric inhibitor of ALA formation, though the mechanism waits for explanation. Abbreviations: MgCH, Mg-chelatase; MTF, Mg-protoporphyrin IX methyltransferase; DVR, divinyl-(proto)chlorophyllide reductase; POR, protochlorophyllide oxidoreductase. Copro III, Coproporphyrinogen III; Mg-proto, Mg-protoporphyrin IX, MgPME Mg-protoporphyrin IX monomethyl ester, DV/MV-PChlide, monovinyl/divinyl protochlorophyllide. Mg-chelatase and cyclase enzymes require several other proteins for their activity (Sobotka *et al.*, 2008a; Hollingshead *et al.*, 2012), which are also indicated.

To be integrated and folded into the correct conformation, membrane proteins generally require the assistance of a translocon system. Briefly, the newly synthesized membrane protein is quickly recognized in the cytosol by a conserved signal recognition particle and the ribosome–SRP complex is then targeted to the membrane-associated FtsY receptor and transferred to a membrane-bound translocation apparatus. It usually includes the SecYEG translocon and an associated insertase/foldase YidC. The heterotrimeric SecYEG complex forms a protein-conducting channel, which is essential for the insertion of the membrane protein. Transmembrane segments probably escape the channel laterally and are handed over to YidC before entering the lipid phase. The role of YidC is not clear yet, but it has

been suggested to support the partitioning of transmembrane segments into the lipid bilayer and facilitate the folding of nascent membrane proteins (Nagamori *et al.*, 2004).

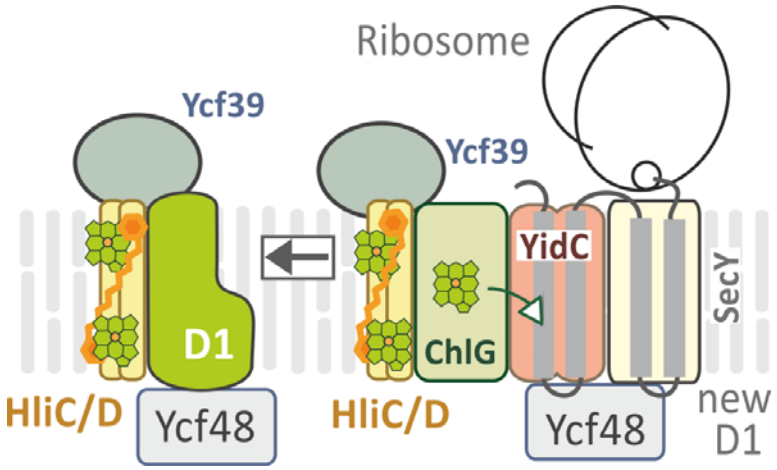

Figure 3. A scheme of the Chl-protein (D1) synthesis in *Synechocystis*. The D1 protein is synthesized and inserted into the membrane by teamwork of SecY translocase and YidC insertase. Ycf48 is a PSII assembly factor, which is involved in D1 synthesis (Komenda *et al.*, 2008); possibly by stabilizing the luminal loops of the nascent chain. Chl molecules are inserted into helixes fixed in the YidC directly from Chl-synthase (ChlG; (Chidgey *et al.*, 2014). Hlip proteins (HliC and HliD) play a role in Chl recycling and in photoprotection of the unassembled D1 protein. Ycf39 is another assembly factor, whose function remains enigmatic (Knoppová *et al.*, 2014).

A fundamental difference between the synthesis of non-Chl and Chl-containing membrane proteins is the critical role of Chl for the completion of translation and for the stable incorporation into membranes. Both *in vivo* and *in vitro* studies on higher plants suggest that Chl has to be inserted into the core subunits of PSI/PSII co-translationally (at least to PsaA/B, CP43 and CP47), probably as a prerequisite for correct protein folding. It remained unclear till recently how Chl molecules are delivered into the vicinity of a translocon to provide Chls for nascent apoprotein chains. We demonstrated that the last enzyme of Chl biosynthesis, Chl-synthase is associated with Hlip proteins (HliC and HliD) as well as with Ycf39 (a putative assembly factor for PSII); and this whole enzymatic complex is attached to YidC insertase (Fig. 3; (Chidgey *et al.*, 2014). Hlips associated with Chl-synthase were shown to bind Chl and carotenoids (Niedzwiedzki *et al.*, 2016). In a parallel study, the same pair of Hlips and the Ycf39 protein have been found to form a tight complex with a newly synthesized D1 protein (Knoppová *et al.*, 2014). These observations led to a model of D1 synthesis where Chl is inserted into the synthesized D1 directly from

Chl-synthase. As discussed in the next chapter, Hlips are required for an efficient re-usage of Chl molecules (Fig. 3) and have an important photoprotective function.

Regulation of the chlorophyll-protein biosynthetic machinery

During the last decade evidence has accumulated suggesting that photosystems are produced by large macromolecular 'factories' termed biosynthetic centres (Komenda *et al.*, 2012). These factories are probably organized as functional membrane nanodomains (probably phosphatidylglycerol-rich; (Kopečná *et al.*, 2015b), and our recent work outlined what this machinery looks like in cyanobacteria. As described above, the heart of the biosynthetic complex is the Sec translocase associated with the YidC insertase, Chl synthase and Hlips (Chidgey *et al.*, 2014; Knoppová *et al.*, 2014). At the moment we can only speculate that this basic arrangement is the same for the synthesis of both PSI and PSII Chl-subunits. However, the synthesis of PSI appears to be independent of the synthesis of PSII, since blocking the translocons by a toxic protein prepilin abolishes the synthesis of PSII subunits, but has no significant effect on the synthesis of PSI (Linhartová *et al.*, 2014).

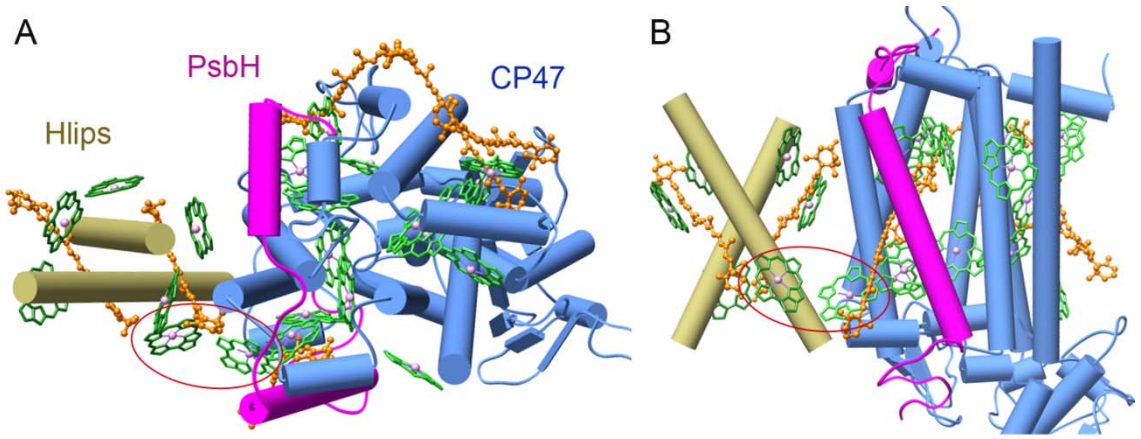

Figure 4. A hypothetical model of HliA/B pair (grey) bound to the CP47 protein (blue) viewed from stromal side perpendicularly to the membrane plane (A) or in parallel with this plane (B). The putative Hlip pair binds 6 Chls and 2 β-carotenes (Staleva *et al.*, 2015) and is attached to CP47 in the vicinity of the small subunit PsbH (magenta; Promnares *et al.*, 2006). The Hlip pair can quench the energy absorbed by CP47 via interaction of its Chls and/or β-carotenes with accessible Chls of CP47 (circled).

An apparent difference in the synthesis of individual Chl-proteins is how sensitive they are to the availability of *de novo* (freshly made) Chl. This feature seems to be important for the regulation of the PSI/PSII ratio in the cell (Kopečná *et al.*, 2012; Kopečná *et al.*, 2015b). As noted above, cyanobacteria utilize the majority of *de novo* Chl molecules for the building of long-lived PSI[3] complexes; not surprisingly, as this complex binds the majority of Chl in the cell. However, it appears that the machinery for the synthesis of PSI[3] complexes cannot utilize 'old' Chl released from the degraded Chl-proteins. Importantly, a relatively strict requirement for *de novo* Chl has also been observed for the synthesis of the Chl-binding PSII subunit CP47 (Fig. 1; Sobotka *et al.*, 2008a; Hollingshead *et al.*, 2016). The synthesis of the structurally similar CP43 subunit also requires *de novo* Chl, though it is less sensitive to Chl deficiency (Hollingshead *et al.*, 2016; Kopečná *et al.*, 2015b). In contrast, the short-lived Chl-binding PSII subunits D1 and D2 are synthesized even in strains with drastically reduced *de novo* Chl biosynthesis (Hollingshead *et al.*, 2016), most likely via recycling of a small pool of Chl. Hlips are Chl-binding proteins (Staleva *et al.*, 2015) that are essential for long Chl life-time (days) in the cell (Yao *et al.*, 2012) and their expression is strongly induced under stress conditions (He *et al.*, 2001). *Synechocystis* contains four small Hlips (HliA-D). HliD and HliC tightly associate with newly synthesized D1 (Fig. 3); whereas HliA, HliB and HliC were found to be bound to the newly synthesized CP47 (Fig. 4; (Komenda and Sobotka, 2016). In addition, HliD and HliC form a complex also with Chl-synthase (Niedzwiedzki *et al.*, 2016). The fifth Hlip is fused with FeCH as described above. Mutants lacking Hlips are generally stress-sensitive (reviewed in Komenda and Sobotka, 2016). Hlips are specifically implicated in PSII biogenesis; no Hlips have been found to associate with PSI (Komenda and Sobotka, 2016). These observations implicate that the downregulation of Chl biosynthesis restricts the production of PSI[3], which depends on *de novo* Chl, while PSII complexes are synthesized even under conditions of low availability of *de novo* Chl. Furthermore, due to a fast Chl recycling, the synthesis of D1 and D2 can be enhanced to replace damaged D1/D2 during stress conditions.

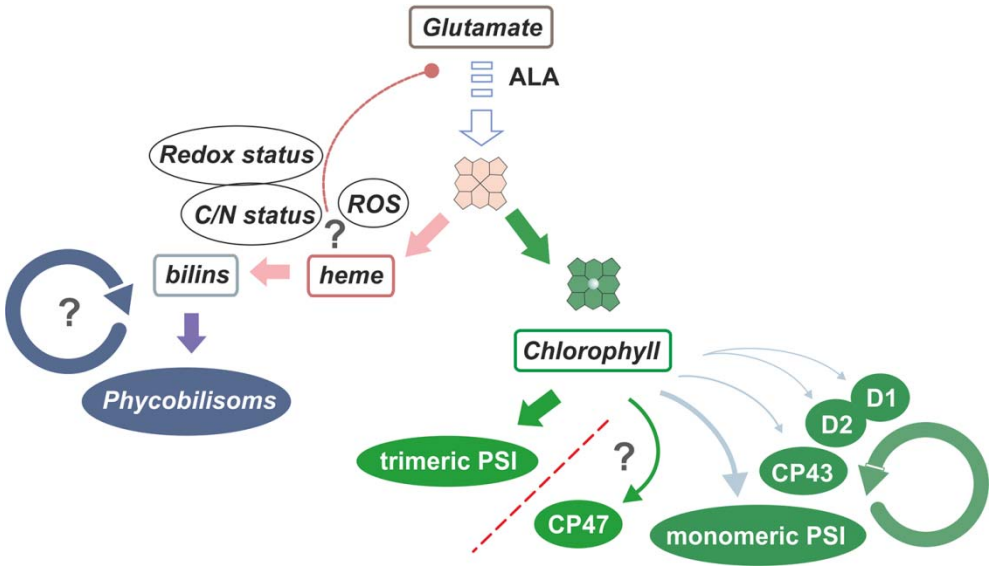

Figure 5. A working model of how cyanobacterial cells control the synthesis of PSI and PSII complexes. It is widely accepted that there is a negative feedback loop that operates from the heme branch and inhibits the metabolic flow through the whole tetrapyrrole pathway (Brzezowski *et al.*, 2015). Based on the available data I propose that the activity of FeCH and perhaps also of the following enzyme heme oxygenase is tightly controlled by cellular redox, C/N status and by the level of ROS. The availability of *de novo* Chl molecules dictates the maximal capacity of the cell to produce PSI trimers (Kopečná *et al.*, 2012). A pool of recycled Chl molecules serves for the synthesis of PSII subunits but also maintains a stable level of monomeric PSI, which has yet an unknown role in the cell. Enigmatic remains the synthesis of CP47 since this subunit is more sensitive to Chl deficiency than D1, D2 or CP43. CP47 might therefore act as a sensor that helps the cell to maintain an indispensable level of *de novo* Chl synthesis and thereby prevents severe depletion of PSI[3].

Based on our data I propose that the biosynthetic centres producing PSI[3] can be quickly switched off along with the reduction of *de novo* Chl biosynthesis if there is a need for lower PSI levels (*e.g.* high-light stress). The FeCH enzyme is potentially a key player in this regulation; however, the mechanism controlling FeCH activity/level has not been discovered yet. A prompt integration of Hlips into PSII biosynthetic centres under stress conditions ensures effective Chl reutilization and channelling of the remaining *de novo* Chl molecules into newly synthesized CP47 and CP43 proteins.

References

Bailey, S., and Grossman, A. (2008) Photoprotection in cyanobacteria: regulation of light harvesting. *Photochem Photobiol* **84**: 1410-1420.

Brzezowski, P., Richter, A. S., and Grimm, B. (2015) Regulation and function of tetrapyrrole biosynthesis in plants and algae. *Biochim Biophys Acta* **1847**: 968-985.

Chidgey, J. W., Linhartová, M., Komenda, J., Jackson, P. J., Dickman, M. J., Canniffe, D. P., *et al.* (2014) A cyanobacterial chlorophyll synthase-HliD complex associates with the Ycf39 protein and the YidC/Alb3 insertase. *Plant Cell* **26**: 1267-1279.

Chua, N. H., Blobel, G., Siekevitz, P., and Palade, G. E. (1976) Periodic variations in the ratio of free to thylakoid-bound chloroplast ribosomes during the cell cycle of *Chlamydomonas reinhardtii*. *J Cell Biol* **71**: 497-514.

Czarnecki, O., and Grimm, B. (2012) Post-translational control of tetrapyrrole biosynthesis in plants, algae, and cyanobacteria. *J Exp Bot* **63**: 1675-1687.

He, Q., Dolganov, N., Bjorkman, O., and Grossman, A. R. (2001) The high light-inducible polypeptides in Synechocystis PCC6803. Expression and function in high light. *J Biol Chem* **276**: 306-314.

Hollingshead, S., Kopečná, J., Armstrong, D. R., Bučinská, L., Jackson, P. J., Chen, G. E., *et al.* (2016) Synthesis of chlorophyll-binding proteins in a fully segregated Δ*ycf54* strain of the cyanobacterium *Synechocystis* PCC 6803. *Front Plant Sci* **7**: 292.

Hollingshead, S., Kopečná, J., Jackson, P. J., Canniffe, D. P., Davison, P. A., Dickman, M. J., *et al.* (2012) Conserved chloroplast open-reading frame *ycf54* is required for activity of the magnesium protoporphyrin monomethylester oxidative cyclase in *Synechocystis* PCC 6803. *J Biol Chem* **287**: 27823-27833.

Horton, P., Ruban, A. V., and Walters, R. G. (1996) Regulation of Light Harvesting in Green Plants. *Annu Rev Plant Physiol Plant Mol Biol* **47**: 655-684.

Jordan, P., Fromme, P., Witt, H. T., Klukas, O., Saenger, W., and Ktrauss, N. (2001) Three-dimensional structure of cyanobacterial photosystem I at 2.5 A resolution. *Nature* **411**: 909-917.

Kim, J., Klein, P. G., and Mullet, J. E. (1994) Synthesis and turnover of photosystem II reaction center protein D1. Ribosome pausing increases during chloroplast development. *J Biol Chem* **269**: 17918-17923.

Kirilovsky, D., and Kerfeld, C. A. (2013) The Orange Carotenoid Protein: a blue-green light photoactive protein. *Photochem Photobiol Sci* **12**: 1135-1143.

Knoppová, J., Sobotka, R., Tichý, M., Yu, J., Koník, P., Halada, P., *et al.* (2014) Discovery of a chlorophyll binding protein complex involved in the early steps of photosystem II assembly in *Synechocystis*. *Plant Cell* **26**: 1200-1212.

Komenda, J., Dobakova, M., and Tichy, M. (2007) Advances in understanding mechanisms underlying photosystem II assembly and repair in cyanobacteria. *Photosynth Res* **91**: 202-202.

Komenda, J., Nickelsen, J., Tichý, M., Prášil, O., Eichacker, L. A., and Nixon, P. J. (2008) The cyanobacterial homologue of HCF136/YCF48 is a component of an early

photosystem II assembly complex and is important for both the efficient assembly and repair of photosystem II in *Synechocystis* sp PCC 6803. *J Biol Chem* **283**: 22390-22399.

Komenda, J., and Sobotka, R. (2016) Cyanobacterial high-light-inducible proteins - Protectors of chlorophyll-protein synthesis and assembly. *Biochim Biophys Acta* **1857**: 288-295.

Komenda, J., Sobotka, R., and Nixon, P. J. (2012) Assembling and maintaining the Photosystem II complex in chloroplasts and cyanobacteria. *Curr Opin Plant Biol* **15**: 245-251.

Kopečná, J., Cabeza de Vaca, I., Adams, N. B., Davison, P. A., Brindley, A. A., Hunter, C. N., *et al.* (2015a) Porphyrin Binding to Gun4 Protein, Facilitated by a Flexible Loop, Controls Metabolite Flow through the Chlorophyll Biosynthetic Pathway. *J Biol Chem* **290**: 28477-28488.

Kopečná, J., Komenda, J., Bučinská, L., and Sobotka, R. (2012) Long-term acclimation of the cyanobacterium *Synechocystis* sp PCC 6803 to high light is accompanied by an enhanced production of chlorophyll that is preferentially channeled to trimeric Photosystem I. *Plant Physiol* **160**: 2239-2250.

Kopečná, J., Pilný, J., Krynická, V., Tomčala, A., Kis, M., Gombos, Z., *et al.* (2015b) Lack of phosphatidylglycerol inhibits chlorophyll biosynthesis at multiple sites and limits chlorophyllide reutilization in the cyanobacterium *Synechocystis* 6803. *Plant Physiol*.

Kopf, M., Klahn, S., Scholz, I., Matthiessen, J. K., Hess, W. R., and Voss, B. (2014) Comparative analysis of the primary transcriptome of *Synechocystis* sp. PCC 6803. *DNA Res* **21**: 527-539.

Linhartová, M., Bučinská, L., Halada, P., Ječmen, T., Šetlík, J., Komenda, J., *et al.* (2014) Accumulation of the Type IV prepilin triggers degradation of SecY and YidC and inhibits synthesis of Photosystem II proteins in the cyanobacterium *Synechocystis* PCC 6803. *Mol Microbiol* **93**: 1207-1223.

Liu, L. N. (2016) Distribution and dynamics of electron transport complexes in cyanobacterial thylakoid membranes. *Biochim Biophys Acta* **1857**: 256-265.

Nagamori, S., Smirnova, I. N., and Kaback, H. R. (2004) Role of YidC in folding of polytopic membrane proteins. *J Cell Biol* **165**: 53-62.

Niedzwiedzki, D. M., Tronina, T., Liu, H., Staleva, H., Komenda, J., Sobotka, R., *et al.* (2016) Carotenoid-induced non-photochemical quenching in the cyanobacterial chlorophyll synthase-HliC/D complex. *Biochim Biophys Acta* **1857**: 1430-1439.

Page, L. E., Liberton, M., and Pakrasi, H. B. (2012) Reduction of photoautotrophic productivity in the cyanobacterium Synechocystis sp. strain PCC 6803 by phycobilisome antenna truncation. *Appl Environ Microbiol* **78**: 6349-6351.

Papenbrock, J., Mishra, S., Mock, H. P., Kruse, E., Schmidt, E. K., Petersmann, A., *et al.* (2001) Impaired expression of the plastidic ferrochelatase by antisense RNA synthesis leads to a necrotic phenotype of transformed tobacco plants. *Plant J* **28**: 41-50.

Promnares, K., Komenda, J., Bumba, L., Nebesářová, J., Vácha, F., and Tichý, M. (2006) Cyanobacterial small chlorophyll-binding protein ScpD (HliB) is located on the periphery of photosystem II in the vicinity of PsbH and CP47 subunits. *J Biol Chem* **281**: 32705-32713.

Sobotka, R. (2014) Making proteins green; biosynthesis of chlorophyll-binding proteins in cyanobacteria. *Photosynth Res* **119**: 223-232.

Sobotka, R., Duerhring, U., Komenda, J., Peter, E., Gardian, Z., Tichý, M., *et al.* (2008a) Importance of the cyanobacterial GUN4 protein for chlorophyll metabolism and assembly of photosynthetic complexes. *J Biol Chem* **283**: 25794-25802.

Sobotka, R., Komenda, J., Bumba, L., and Tichý, M. (2005) Photosystem II assembly in CP47 mutant of *Synechocystis* sp PCC 6803 is dependent on the level of chlorophyll precursors regulated by ferrochelatase. *J Biol Chem* **280**: 31595-31602.

Sobotka, R., McLean, S., Žuberová, M., Hunter, C. N., and Tichý, M. (2008b) The C-terminal extension of ferrochelatase is critical for enzyme activity and for functioning of the tetrapyrrole pathway in *Synechocystis* strain PCC 6803. *J Bacteriol* **190**: 2086-2095.

Sobotka, R., Tichý, M., Wilde, A., and Hunter, C. N. (2011) Functional Assignments for the Carboxyl-Terminal Domains of the Ferrochelatase from *Synechocystis* PCC 6803: The CAB Domain Plays a Regulatory Role, and Region II Is Essential for Catalysis. *Plant Physiol* **155**: 1735-1747.

Staleva, H., Komenda, J., Shukla, M. K., Šlouf, V., Kaňa, R., Polívka, T., *et al.* (2015) Mechanism of photoprotection in the cyanobacterial ancestor of plant antenna proteins. *Nat Chem Biol* **11**: 287-291.

Stoitchkova, K., Zsiros, O., Javorfi, T., Pali, T., Andreeva, A., Gombos, Z., *et al.* (2007) Heat- and light-induced reorganizations in the phycobilisome antenna of Synechocystis sp. PCC 6803. Thermo-optic effect. *Biochim Biophys Acta* **1767**: 750-756.

Tyystjarvi, T., Herranen, M., and Aro, E. M. (2001) Regulation of translation elongation in cyanobacteria: membrane targeting of the ribosome nascent-chain complexes controls the synthesis of D1 protein. *Mol Microbiol* **40**: 476-484.

Umena, Y., Kawakami, K., Shen, J. R., and Kamiya, N. (2011) Crystal structure of oxygen-evolving photosystem II at a resolution of 1.9 A. *Nature* **473**: 55-60.

Vavilin, D., Brune, D. C., and Vermaas, W. (2005) N-15-labeling to detennine chlorophyll synthesis and degradation in *Synechocystis* sp PCC 6803 strains lacking one or both photosystems. *Biochim Biophys Acta* **1708**: 91-101.

Xu, H., Vavilin, D., Funk, C., and Vermaas, W. F. J. (2004) Multiple deletions of small cab-like proteins in the cyanobacterium *Synechocystis* sp PCC 6803 - Consequences for pigment biosynthesis and accumulation. *J Biol Chem* **279**: 27971-27979.

Yao, D. C. I., Brune, D. C., Vavilin, D., and Vermaas, W. F. J. (2012) Photosystem II component lifetimes in the cyanobacterium *Synechocystis* sp. strain PCC 6803: small Cab-like proteins stabilize biosynthesis intermediates and affect early steps in chlorophyll synthesis. *J Biol Chem* **287**: 682-692.

Publication I

THE JOURNAL OF BIOLOGICAL CHEMISTRY
Vol. 280, No. 36, Issue of September 9, pp. 31595–31602, 2005

Printed in U.S.A.

Photosystem II Assembly in CP47 Mutant of *Synechocystis* sp. PCC 6803 Is Dependent on the Level of Chlorophyll Precursors Regulated by Ferrochelatase*[S]

Received for publication, June 1, 2005, and in revised form, July 14, 2005
Published, JBC Papers in Press, July 18, 2005, DOI 10.1074/jbc.M505976200

Roman Sobotka‡§¶, Josef Komenda‡§, Ladislav Bumba‖, and Martin Tichy‡§

From the ‡Institute of Physical Biology, University of South Bohemia, 373 33 Nove Hrady, the §Department of Autotrophic Microorganisms, Institute of Microbiology, Opatovicky mlyn, 379 71 Trebon, and the ‖Institute of Plant Molecular Biology, Branisovska 31, 370 05 Ceske Budejovice, Czech Republic

Accumulation of chlorophyll and expression of the chlorophyll (Chl)-binding CP47 protein that serves as the core antenna of photosystem II are indispensable for the assembly of a functional photosystem II. We have characterized the CP47 mutant with an impaired photosystem II assembly and its two spontaneous pseudorevertants with their much improved photoautotrophic growth. The complementing mutations in these pseudorevertants were previously mapped to the ferrochelatase gene (1). We demonstrated that complementing mutations dramatically decrease ferrochelatase activity in pseudorevertants and that this decrease is responsible for their improved photoautotrophic growth. Photoautotrophic growth of the CP47 mutant was also restored by *in vivo* inhibition of ferrochelatase by a specific inhibitor. The decrease in ferrochelatase activity in pseudorevertants was followed by increased steady-state levels of Chl precursors and Chl, leading to CP47 accumulation and photosystem II assembly. Similarly, supplementation of the CP47 mutant with the Chl precursor Mg-protoporphyrin IX increased the number of active photosystem-II centers, suggesting that synthesis of the mutated CP47 protein is enhanced by an increased Chl availability in the cell. The probable role of ferrochelatase in the regulation of Chl biosynthesis is discussed.

The photosystem-II (PSII)[1] core complex of higher plants, algae, and cyanobacteria consists of the chlorophyll-binding proteins D1, D2, CP43, and CP47 and two subunits of cytochrome b_{559}. These proteins are assembled into the PSII complex in an ordered manner, and the mutation or inactivation of a single protein frequently leads to PSII destabilization and its disappearance from the thylakoids (2, 3).

From several cofactors that are associated with the PSII core, chlorophyll (Chl) has been shown to be essential for PSII biogenesis. Both *in vitro* and *in vivo* analyses of expression and accumulation of PSII chlorophyll-binding proteins have suggested that cotranslational binding of Chl is required for correct apoprotein folding and stable integration into the thylakoid membrane (4–6). Mutation studies of Chl ligands and *in vitro* reconstitution of Chl-binding proteins indicate that, without Chl, apoproteins do not fold correctly and are recognized and degraded by specific proteases (7–9). However, the process of delivery and incorporation of Chl into apoproteins, as well as the role of Chl in protein folding, remain to be elucidated.

It is generally accepted that expression of Chl-binding proteins is synchronized with Chl biosynthesis to ensure formation of a proper amount of Chl for assembly of the photosynthetic apparatus and to avoid harmful accumulation of non-assembled (free) Chl and its precursors (10, 11). This regulation is rather complicated: because Chl shares a common biosynthetic pathway with heme, and demand for these cofactors varies considerably depending on environmental and growth conditions (reviewed in Ref. 12). Therefore, photosynthetic organisms have to balance fluxes through these two biosynthetic branches and coordinate them with apoprotein formation.

An important role in this process may be played by Mg- and Fe-chelatases lying at the branch point of the common tetrapyrrole pathway. Here, magnesium chelatase and ferrochelatase (FeCH) compete for the same substrate, protoporphyrin IX (Proto IX), to insert either magnesium for Chl biosynthesis or ferrous ion for heme, and in cyanobacteria also for phycobilin biosynthesis. To guarantee a balanced flow of precursors in the pathway, expression or activities of these chelatases are apparently controlled by light (13), diurnal and circadian rhythmicity (14, 15), and by the redox state of photosynthetic electron transport (16).

Recently, Tichy and Vermaas (1) described a C1.8 mutant of the cyanobacterium *Synechocystis* PCC 6803 carrying a mutation in the Chl-binding CP47 protein comprising the core antenna of PSII (see Fig. 1). The mutant exhibited very poor photoautotrophic growth, however fully autotrophic pseudorevertants were formed at high frequency. Interestingly, in two C1.8 pseudorevertants (P1.8.1 and P1.8.2), complementing mutations were mapped to the FeCH gene, and their sequencing revealed point mutations in this gene (see Fig. 1).

In this study we have characterized the *Synechocystis* C1.8 mutant and its photoautotrophic pseudorevertants in detail to explain how mutations in FeCH may functionally complement mutation in the CP47 protein. The results clearly indicate that, at least in this mutant, FeCH activity is controlling PSII assembly, most probably by modulation of chlorophyll availability in the cell.

* This work was supported by the Grant Agency of the Czech Academy of Sciences (Project B5817301 to R. S.), by Institutional Research Concept AV0Z50200510 (to J. K. and M. T.), and by the Ministry of Education, Youth and Sports (Project MSM6007665808 to J. K. and M. T). The costs of publication of this article were defrayed in part by the payment of page charges. This article must therefore be hereby marked "*advertisement*" in accordance with 18 U.S.C. Section 1734 solely to indicate this fact.

[S] The on-line version of this article (available at http://www.jbc.org) contains supplemental Figs. S1 and S2 and Table S1.

¶ To whom correspondence should be addressed: Tel.: 420-384-722-268; Fax: 420-384-721-246; E-mail: sobotka@alga.cz.

[1] The abbreviations used are: PSII, photosystem II; WT, wild type; Chl, chlorophyll; DCMU, 3-(3,4-dichlorophenyl)-1,1-dimethylurea; TES, *N*-[tris(hydroxymethyl)methyl]-2-aminoethanesulfonic acid; FeCH, ferrochelatase; Proto IX, protoporphyrin IX; PChlide, protochlorophyllide; Mg-proto IX, Mg-protoporphyrin IX.

TABLE I

Growth rate, Chl content, and oxygen evolution of Synechocystis 6803 strains

WT, CP47 mutants, and pseudorevertants were grown photoautotrophically and photomixotrophically in normal and low light to OD_{730} 0.4–0.5. Values given are the averages from three different determinations.

Strain	Normal light				Low light	
	Doubling time		Chlorophyll,[b] +glu.	O_2 evolution,[c] +glu.	Doubling time, +glu.	Chlorophyll, +glu.
	−glu.[a]	+glu.				
	h		*50 μmol·m⁻²·s⁻¹*		*h*	*5 μmol·m⁻²·s⁻¹*
WT	14	10	4.5 ± 0.2	550	19	3.7 ± 0.2
ΔCP47	NG[d]	13	3.2 ± 0.2	0	19	3.6 ± 0.2
Δ1	NG	17	1.9 ± 0.1	0	19	3.7 ± 0.2
C1.8	65	14	3.4 ± 0.2	250	19	3.6 ± 0.2
P1.8.1	14	10	6.6 ± 0.2	530	19	4.4 ± 0.2
P1.8.2	15	10	5.4 ± 0.2	500	19	4.4 ± 0.2

[a] 5 mM glucose (glu.).
[b] $\mu g \cdot ml^{-1} \cdot OD_{730}^{-1}$.
[c] $\mu mol \cdot O_2 \cdot mg\ Chl^{-1} \cdot h^{-1}$.
[d] NG, no growth (strain did not grow under these conditions).

EXPERIMENTAL PROCEDURES

Strains and Growth Conditions—The ΔCP47 deletion mutant, in which most of the *psbB* gene coding for CP47 is replaced by a spectinomycin-resistance cassette, was prepared by Eaton-Rye and Vermaas (29). The deletion mutant Δ1CP47 (Δ1), lacking four amino acid residues (Ile^{265}–Phe^{268}, Fig. 1) of the CP47 protein, has been prepared by Haag *et al.* (17). The poorly photoautotrophic C1.8 mutant has been constructed by combinatorial mutagenesis performed on Δ1 (1). Two photoautotrophic pseudorevertants originating from C1.8–P1.8.1 and P1.8.2 carry point mutations in the FeCH gene that cause amino acid substitution S50Y and S321F, respectively (1). Other PSII mutants used in this report are (name and inactivated genes): ΔCP43, *psbC*; ΔD1, *psbA1*, *-2*, and *-3* (18); and Δc559, *psbEFLJ* (19).

Synechocystis strains were grown in liquid BG-11 medium (20) supplemented by 10 mM TES at 30 °C and 50 μmol m^{-2} s^{-1} (normal light) or 5 μmol m^{-2} s^{-1} (low light) on the rotary shaker. Strains were grown on 5 mM glucose unless photoautotrophic conditions are indicated.

Oxygen Evolution—Light-saturated (3500 μmol m^{-2} s^{-1}) steady-state rate of oxygen evolution was measured directly with samples taken from liquid cultures (OD_{730} = 0.5–0.7) using a Clark-type electrode in the presence of 1 mM potassium ferricyanate and 0.1 mM dimethyl-*p*-benzoquinone at 29 °C.

Determination of Chl and Carotenoids—Chl and carotenoids were extracted from cell pellets (50 ml, OD_{730} ~ 0.5) by 100% methanol. Chl content was measured spectrophotometrically on a Spectronic Unicam UV500 spectrophotometer (21). Carotenoids were separated by HPLC on a Vydac 201TP54 column (250 mm × 4.6 mm, C-18 reversed-phase silica gel). The column was eluted with a linear gradient of solvent B (methanol and acetone, 6:4, v/v) in solvent A (methanol and 0.5 M ammonium acetate, 8:2, v/v, pH 7.0) at a flow rate of 1.2 ml/min as follows: 0–80% in 3 min, 80–100% in the next 10 min, and then followed by 100% solvent B for 5 min. Carotenoid species were identified by their absorption spectra and by their typical retention times.

Electron Microscopy—Cells were washed twice in 50 mM phosphate buffer (pH 7.4) and fixed in a solution containing 2% glutaraldehyde in 50 mM phosphate buffer (pH 7.4) for 2 h. This was followed by three washes in phosphate buffer and post-fixated in 1% OsO_4 in 50 mM phosphate buffer (pH 7.4) for 1 h. The cells were again washed three times, and the samples were dehydrated in acetone and embedded in Spurr's resin. Thin sections were cut with a diamond knife and post-stained for 30 min with 5% aqueous uranyl acetate followed by lead citrate for 80 s and examined with a Jeol 1010 electron microscope equipped with charge-coupled device video camera Lhesa 72WA and image acquisition software VideoTIP (Tescan).

Radiolabeling of the Cells, Membrane Preparation, and Protein Analysis Using Two-dimensional Native/SDS Electrophoresis and Immunoblotting—Radiolabeling of cells using a mixture of L-[^{35}S]methionine and L-[^{35}S]cysteine (>1000 Ci $mmol^{-1}$, Tran^{35}S-label, ICN, final activity, 400 μCi ml^{-1}) and isolation of membranes was performed as described in a previous study (2). For two-dimensional analysis, isolated membranes were solubilized with *n*-dodecyl-β-maltoside (*n*-dodecyl-β-maltoside/Chl = 20, w/w), and the obtained complexes were separated by blue-native electrophoresis at 4 °C in 5–14% polyacrylamide gel according to a previous study (22) in the first dimension, and by electrophoresis in a denaturing 12–20% linear-gradient polyacrylamide gel containing 7 M urea in the second dimension (2). Proteins separated in the gel were transferred onto a polyvinylidene difluoride membrane. The membrane was incubated with specific primary antibodies and then with secondary antibody-horseradish peroxidase conjugate (Sigma). The primary antibodies used in the study were raised in rabbits against: (i) residues 58–86 of the spinach D1 polypeptide; (ii) 12 last residues of the *Synechocystis* D2 polypeptide; (iii) residues 380–394 of barley CP47; and (iv) the whole isolated CP43 (2). For autoradiography, the gel or the membrane with labeled proteins was exposed to x-ray film at laboratory temperature for 2–3 days.

Ferrochelatase Activity Assay—For the determination of FeCH activity in thylakoids, 50 ml of cells (OD_{730} ~ 0.5) were washed in the thylakoid buffer containing 100 mM Tris/HCl pH 8.0, 1 mM EDTA, 1 mM dithiothreitol, and 20% glycerol (v/v). The cell suspension was transferred into 0.5-ml microcentrifuge tubes, mixed with glass beads, and broken in a MiniBeadBeater. The homogenate was centrifuged at 32,000 × *g* for 20 min at 4 °C. Pelleted thylakoids were washed in EDTA-free thylakoid buffer and centrifuged at 32,000 × *g*. Finally, thylakoids were re-suspended in EDTA-free thylakoid buffer containing 1% Triton X-100 and frozen at −70 °C.

The standard assay was performed in a cuvette containing 1.5 ml of assay buffer (100 mM Tris/HCl, pH 8.0, 0.03% Tween 80, 0.1 μM $ZnSO_4$, and 0.3 μM protoporphyrin IX) at 35 °C. The reaction was started with thylakoids and the formation of zinc-protoporphyrin IX recorded spectrofluorometrically using a Spectronic Unicam series 2 spectrofluorometer (23) and zinc-protoporphyrin IX (Sigma) as a standard.

Quantification of Chlorophyll Intermediates—For quantitative determination of protoporphyrin IX (Proto IX), Mg-protoporphyrin IX (Mg-proto IX) monomethyl ester, and protochlorophyllide (PChlide), pigments were extracted from cell pellets (150 ml, OD_{730} ~ 0.5) by three successive extractions with methanol containing 0.1% of NH_4OH. Supernatants were combined, and the solvent was evaporated under vacuum to dryness. Extracts were dissolved in a small volume of basic methanol and immediately subjected to HPLC analysis with a Vydac 201TP54 column (250 mm × 4.6 mm, C-18 reversed-phase silica gel). The column was eluted with a linear gradient of solvent B (methanol and acetone, 9:1, v/v) in solvent A (methanol and 0.5 M ammonium acetate, 7:3, v/v, pH 7.0) at a flow rate of 1.5 ml/min. The 100% of solvent B was reached after 20 min. HPLC peaks corresponding to PChlide were identified from their absorption spectra. Positions corresponding to Proto IX and Mg-proto IX monomethyl ester were identified from comparison with authentic standards (Sigma and Frontier Scientific, Logan, UT).

HPLC fractions containing PChlide (retention time, 12.5–13.5 min), Mg-proto IX monomethyl ester (14–14.5 min), and Proto IX (17–17.8 min) were collected and concentrations of the corresponding compounds determined fluorometrically using a Spectronic Unicam series 2 spectrofluorometer.

Protoheme Determination—Protoheme was extracted from 0.5 liter of cells (OD_{730} ~ 0.5) by acidic acetone according to Ref. 24, and its concentration was determined from the reduced-minus-oxidized difference spectrum as described by Stillman and Gassman (25) with ammonium persulfate used for sample oxidation.

Chlorophyll Fluorescence Induction—A P.S.I. fluorometer (Photon System Instrument, Brno, Czech Republic) was used to record Chl fluorescence induction in the presence of 10 μM DCMU. PSII fluorescence was induced by a 60-ms pulse of light supplied by blue light-

emitting diodes. Induction curves were measured directly in liquid cultures (OD_{730} = 0.5) after 2-min dark adaptation. The cells treated by Mg-proto IX were washed three times in BG-11 medium to eliminate traces of this compound.

RESULTS

Mutant Characterization—The growth characteristics, Chl content and oxygen evolution of strains used in this study are listed in Table I. In normal light, all three CP47 mutants (ΔCP47, Δ1, and C1.8) exhibited slower growth rate and lower Chl accumulation than WT. Interestingly, growth impairment and decrease in Chl level were more pronounced in the Δ1 mutant with a short deletion in the E loop of the CP47 protein (Fig. 1*A*) than in the ΔCP47 strain lacking most of the CP47 gene. The growth rates and Chl levels were not affected in low light, indicating the light sensitivity of the CP47 mutants. This is supported by the significantly increased levels of carotenoids shown in normal light. Particularly myxoxanthophyll, important in defense against light stress (26), was highly increased in all CP47 mutants (see Supplemental Table S1). In contrast, carotenoid levels in both strains were comparable to WT in low light (data not shown). The phenotype of the poorly photoautotrophic C1.8 mutant was consistent with its original characterization (1).

Transmission electron microscopy revealed that cells of Δ1 growing in normal light were much smaller than WT cells and displayed highly fragmented thylakoid membranes (Fig. 2). This was in contrast to the almost normal membrane organization in the corresponding ΔCP47 mutant (Fig. 2), confirming the strong adverse effect of the Δ1 mutation. Membrane organization in C1.8 was similar to that in the ΔCP47 mutant (not shown).

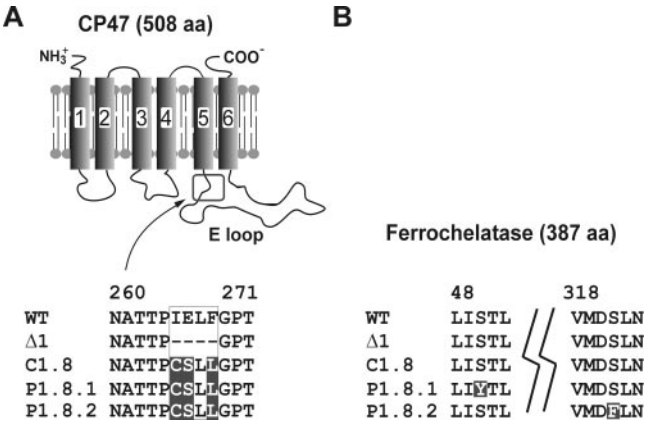

FIG. 1. **Mutations in CP47 and FeCH genes in relevant strains.** *A*, alignment of the amino acid sequences 260–271 of CP47 from WT, Δ1, C1.8, and two C1.8 pseudorevertants. The region probed by combinatorial mutagenesis is *boxed*. The approximate position of Δ1 mutation in CP47 protein is also shown. *B*, alignment of the amino acid sequence of FeCH showing the secondary mutations in P1.8.1 and P1.8.2 strains at positions 50 and 321, respectively.

The rate of photoautotrophic growth and oxygen-evolving capacity of the pseudorevertants were comparable to that of WT (Table I), however, significantly higher levels of Chl, carotenoids and phycobilinoproteins accumulated in both strains (Table I and Supplemental Fig. S1). This concomitant increase of photosynthetic pigments in pseudorevertants suggests a higher abundance of photosystems and phycobilisomes in their cells. Indeed, electron microscopy revealed an atypical organization of thylakoid membranes in the cells of the P1.8.1 pseudorevertant. In addition to several concentric thylakoid membranes typical for *Synechocystis* 6803, new centric membranes were found in P1.8.1 (Fig. 2, *C–E*).

CP47 Accumulation and Photosystem II Assembly—We analyzed the effect of the mutation in the Δ1 and C1.8 strains on stability and accumulation of PSII core proteins and PSII assembly in CP47 mutants and pseudorevertants. To follow the accumulation of PSII core proteins, solubilized thylakoid membranes were analyzed by SDS-PAGE, the separated proteins blotted and exposed to a mix of antisera against CP47, CP43, D1, and D2. As shown in Fig. 3, the Δ1 mutant has no detectable amounts of CP47, similar to that of the deletion mutant ΔCP47. In the C1.8 mutant, about 20% of the WT steady-state level of CP47 was estimated, showing an improved CP47 translation/stability in comparison to Δ1. The accumulation of CP47 in pseudorevertants was comparable to WT (Fig. 3).

De novo synthesis and assembly of mutated CP47 into PSII was followed by a combination of protein pulse-chase radiolabeling and two-dimensional native/SDS electrophoresis. In thylakoid membranes of Δ1, no signal of CP47 was detected and the synthesis of labeled proteins was essentially identical to that of ΔCP47 (data not shown, for ΔCP47 see Ref. 2), indicating that the synthesis and/or incorporation of CP47 into the thylakoid membrane was completely disrupted.

In C1.8, only a very weak signal of labeled proteins assembled into the PSII complex and RC47 subcomplex (consisting of D1, D2, cytochrome b_{559}, and CP47) was detected (Fig. 4). Instead, the D1-D2-cytochrome b_{559} subcomplex and free CP43 accumulated substantially, suggesting that PSII assembly was blocked at the CP47 insertion step. The very low level of unas-

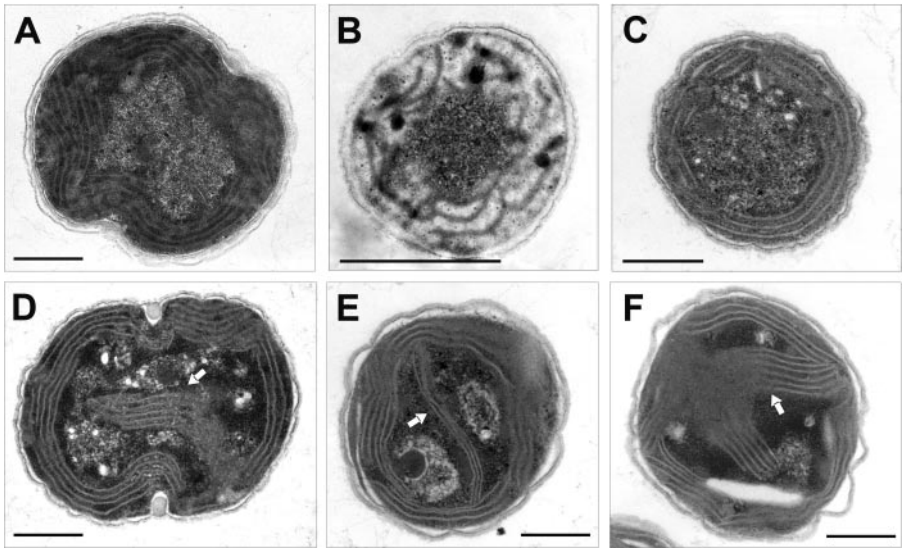

FIG. 2. **Transmission electron microscopy of *Synechocystis* 6803 cells.** WT (*A*), Δ1 (*B*), ΔCP47 (*C*), and P1.8.1 cells (*D–F*). Atypical membrane structures in P1.8.1 cells are shown by *arrows*. *Scale bar* = 500 nm.

sembled CP47 indicates that the C1.8 mutation does not affect the assembly of CP47 into PSII.

In the pseudorevertants, the amount of synthesized CP47, as well as the rate of its assembly into PSII, were found to be very similar to WT. After a 30-min chase, the signal intensity of CP47 did not significantly decline, implying normal stability of the newly synthesized CP47 carrying the C1.8 mutation (Fig. 4). This indicates that the C1.8 strain is impaired at the level of CP47 synthesis. The mutated CP47 protein, once synthesized, is stable and is assembled normally into a functional PSII.

In Vitro FeCH Activity in C1.8 Strains—Because the effect of both complementing mutations on FeCH was not evident from the sequence alignments, and it was hypothesized that they may influence FeCH activity (1), we decided to compare *in vitro* FeCH activity in the CP47 mutants and both pseudorevertants. Because no FeCH activity was found in the soluble fraction, isolated thylakoid membranes were used for the FeCH assay using Proto IX and zinc as a substrate.

Surprisingly, in both the C1.8 and Δ1 mutants, FeCH activity was significantly higher than in WT (Fig. 5*A*). In the pseudorevertants, FeCH activity decreased dramatically below the WT level resulting in a 30- to 40-fold decrease in comparison to the C1.8 mutant (Fig. 5*A*). This indicates that both complementing mutations strongly inhibit FeCH activity. To determine whether the increase in FeCH activity observed in the Δ1 and C1.8 mutants is characteristic only of a mutation in this region of CP47, we also measured FeCH activity in other strains with impaired PSII assembly. In all PSII mutants tested, a significant increase in FeCH activity was observed, showing that up-regulation of FeCH activity is related to partly or completely destabilized PSII (Fig. 5*B*). To exclude the possibility that increased FeCH activity results from changes induced by photoheterotrophic metabolism in PSII mutants, FeCH activity was also measured in WT grown in the presence of a PSII inhibitor, DCMU. No significant increase in FeCH activity was observed under such conditions (Fig. 5*B*).

In Vivo Inhibition of FeCH—To test whether decreased FeCH activity in the pseudorevertants is responsible for their photosynthetic phenotype, we used *N*-methylprotoporphyrin IX, which is a specific and potent inhibitor of FeCH (27). In the presence of 10 μM *N*-methylprotoporphyrin IX in the growth medium, photoautotrophic growth of C1.8 dramatically improved (doubling time changed from 65 to 16 h), whereas growth of WT was slightly inhibited (see Supplemental Fig. S2). No growth was observed in the Δ1 strain, even when the concentration of the inhibitor was increased to 50 μM (not shown).

To show that the improved photoautotrophic growth is due to increased PSII accumulation in the pseudorevertants, 77K fluorescence emission spectroscopy was used to monitor the accumulation of PSII *in vivo*. Upon Chl excitation at 435 nm, the presence of the 695-nm emission peak, which is characteristic of CP47 assembled into PSII, can be used to monitor the assembly of PSII core complexes (8). Absence of the 695-nm peak in the C1.8 strain corresponds to low levels of assembled PSII in this strain. After treatment of C1.8 with *N*-methylprotoporphyrin IX, significant 695-nm emission was observed (Fig. 6*A*). Moreover, appearance of the 695-nm emission peak was accompanied by increased oxygen-evolving capacity of the cells (Fig. 6*B*). The improved PSII activity was also accompanied by increased overall Chl accumulation in C1.8 cells (Fig. 6*B*). No changes in Chl accumulation were observed when 10 μM *N*-methylprotoporphyrin IX was added to the WT and Δ1 strains (not shown). These data show that the decreased FeCH activity in the C1.8 strain is necessary for PSII assembly and for the improved photoautotrophic growth.

Chlorophyll and Heme Precursor Levels—To determine the effect of CP47 and FeCH mutations on the Chl/heme biosynthetic pathway, levels of Proto IX, Mg-proto IX monomethyl ester, PChlide, and protoheme were quantified in the WT, Δ1, and C1.8 mutants, and the two pseudorevertants were grown in normal light.

The Δ1 and C1.8 mutations in CP47, which lead to the increased FeCH activity, caused about 5-fold decrease in the level of Proto IX, the last common intermediate of both Chl and heme biosynthesis, and ~2-fold decrease of the Chl precursors Mg-proto IX monomethyl ester and PChlide (Fig. 7). In contrast, in the pseudorevertants with decreased FeCH activity, precursor levels increased above WT levels (~3-fold increase in

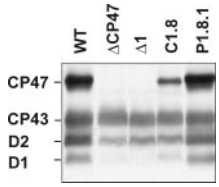

FIG. 3. **Accumulation of PSII core proteins in *Synechocystis* 6803 mutants.** Thylakoid membranes from analyzed strains were prepared, 3 μg of Chl was loaded for each sample, and amounts of CP47, CP43, D1, and D2 PSII proteins were determined by immunolabeling.

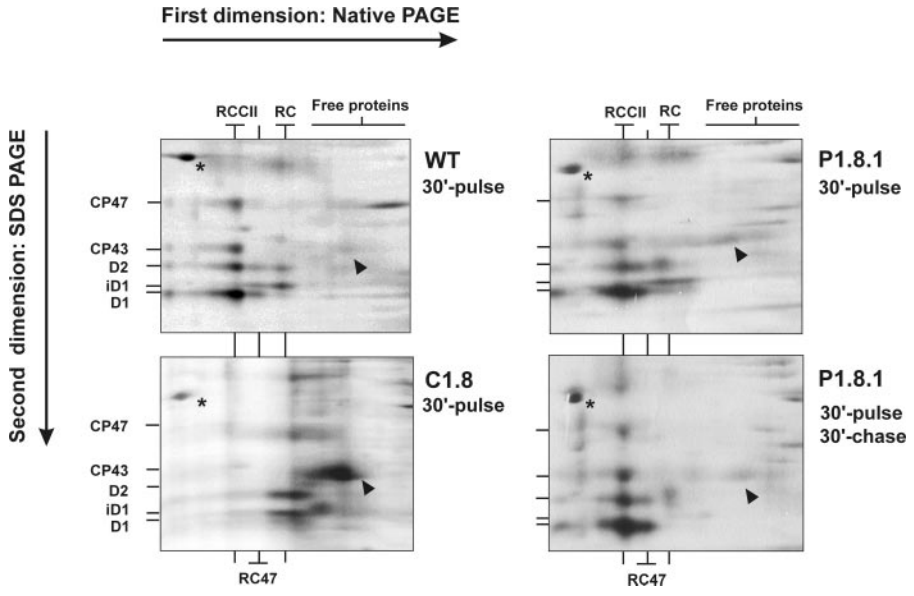

FIG. 4. **PSII core protein expression and PSII assembly determined by two-dimensional PAGE.** Cells were radiolabeled with [^{35}S]methionine and their thylakoid membranes prepared. Analysis of thylakoid protein complexes and their protein composition was performed by a combination of blue-native and SDS-PAGE. *iD1*, intermediate D1; *RCCII*, PSII core complex; *RC47*, cyt559-D1-D2-CP47 complex; *RC*, cyt559-D1-D2 complex (2). Free CP43 protein is shown by *black arrows* and ATPase by *asterisk*.

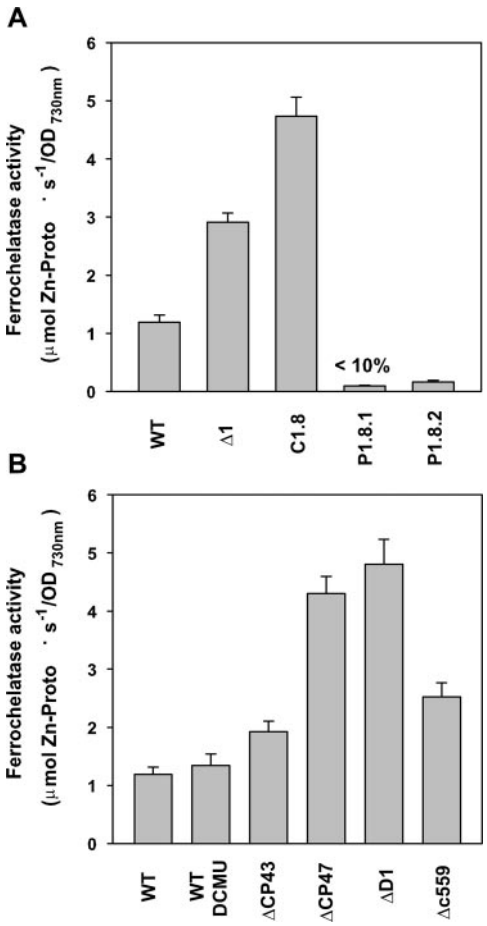

FIG. 5. ***In vitro* activity of FeCH determined by continuous spectrofluorometric assay.** FeCH activity was determined in Δ1, C1.8 and C1.8 pseudorevertants (*A*) and WT treated by 10 μM DCMU (*B*) for 48 h and in several PSII mutants with inactivated PSII components: *psbC* (Δ*CP43*), *psbB* (Δ*CP47*), three *psbA* (Δ*D1*), or both subunits of cytochrome b_{559} (Δ*c559*). The values are the mean of three independent experiments.

the level of Proto IX and ~2-fold increase in the level of Chl precursors). These data demonstrate that the decrease in FeCH activity in pseudorevertants resulted in a significant increase in the Chl precursor levels. Unexpectedly, drastic changes in FeCH activity had no effect on protoheme accumulation (Fig. 7).

To determine whether the increased accumulation of Chl precursors in the pseudorevertants is sufficient to restore PSII assembly in C1.8, the formation of the 695-nm Chl emission peak was followed after supplementation with Mg-protoporphyrin IX (Mg-proto IX), an early precursor of Chl. In C1.8 cultures supplemented with 200 μM Mg-proto IX for 2 days, the 695-nm peak became visible and was even more pronounced in cells supplemented with 400 μM Mg-proto IX (Fig. 6*C*). No such increase was detected in Δ1. No effect of Mg-proto IX on the FeCH activity was detected, suggesting that the improved PSII assembly is the direct effect of Mg-proto IX supplementation.

The improved PSII assembly in the C1.8 mutant after Mg-proto IX supplementation was further confirmed by measurement of variable fluorescence of Chl (F_v), which is specific for photochemically active PSII. In untreated C1.8 cells, F_v reached only ~20% of that in WT (Fig. 6*D*), which is in agreement with the expected PSII accumulation in this strain. After 48-h incubation in 400 μM Mg-proto IX, F_v in C1.8 significantly increased, indicating a higher accumulation of PSII. No fluorescence induction was found in the Δ1 mutant (not shown).

DISCUSSION

Deletion of the Δ1 Region of CP47 Protein Disrupts Its Expression and Is Responsible for the Photosensitivity of the Mutant—The Chl-binding protein CP47 possesses six transmembrane domains with a large lumenal loop joining helices 5 and 6 (Fig. 1). The function of this loop has been extensively probed by partial deletions in which domains consisting of several amino acid residues have been removed (reviewed in Ref. 28). Deletion of four amino acid residues in the Δ1 domain resulted in a non-photoautotrophic phenotype (17) and the complete loss of CP47 protein from thylakoid membranes (Fig. 3). Interestingly, the phenotype of the Δ1 deletion mutant was different from that of the ΔCP47 mutant lacking most of the *psbB* gene (29). In contrast to ΔCP47, cells of Δ1 were severely damaged in normal light, although they accumulated high levels of carotenoids (Fig. 2 and Supplemental Table S1). It appears that the expression of the modified Δ1 CP47 protein is more deleterious for cell viability than its complete deletion. No full-length CP47 protein is detectable in thylakoid membranes of this strain, even by the highly sensitive radiolabeling technique, indicating that the Δ1 region is essential for the completion of CP47 translation or for the stable incorporation of CP47 into thylakoid membranes.

The mechanism of Δ1 photosensitivity is not clear. We have not seen increased levels of photoreactive Proto IX and Mg-porphyrins in this strain (Fig. 7). Possibly, Proto IX precursors can be slowly oxidized and also form photodynamically active compounds (30). Alternatively, non-assembled (free) Chl can be responsible for the Δ1 photosensitivity. As Chl molecules bind to the CP47 apoprotein cotranslationally (5), free Chl in Δ1 can originate from prematurely degraded uncompleted CP47. As will be shown later, we favor this explanation.

The Effect of C1.8 Mutation Is Suppressed by Decreased FeCH Activity—The C1.8 mutant with three substitutions in the Δ1 region (Fig. 1) exhibits very limited photoautotrophic growth due to the seriously impaired CP47 synthesis (Fig. 4). We have provided clear evidence that expression of the mutated CP47 and consequently the autotrophic capacity of C1.8 can be fully restored by lowering FeCH activity. The severe decrease in FeCH activity was observed in two spontaneous photoautotrophic C1.8 pseudorevertants with secondary mutations in the FeCH gene (Fig. 5). A proportional decrease in FeCH activity was observed in the mutant carrying the P1.8.2 point mutation in the FeCH gene in the WT background, showing that this mutation is solely responsible for the decrease in FeCH activity.[2] Treatment with the specific inhibitor of FeCH resulted again in restored PSII assembly and photoautotrophic growth (Fig. 6, *A* and *B*, and Supplemental Fig. S2), demonstrating that the photosynthetic phenotype of the C1.8 pseudorevertants can be exclusively attributed to the lack of FeCH activity.

Decreased FeCH Activity in the C1.8 Pseudorevertants Increases Chl Accumulation and PSII Assembly—It is not immediately obvious how the decreased activity of the heme-producing enzyme can stabilize the expression of the Chl-binding CP47 protein. We have shown that the decrease in FeCH activity resulted in the increased accumulation of Proto IX, Mg-proto IX monomethyl ester, and PChlide (Fig. 7).

This is similar to FeCH-antisense plants, where decrease in FeCH activity resulted in accumulation of Proto IX (31). Moreover, a significant increase in PChlide and Chl levels was reported in plants genetically engineered for increased production of Proto IX (32, 33). A similar effect has been observed in other

[2] L. A. Eichacker, B. Müller, J. Kim, and J. E. Mullet, unpublished data.

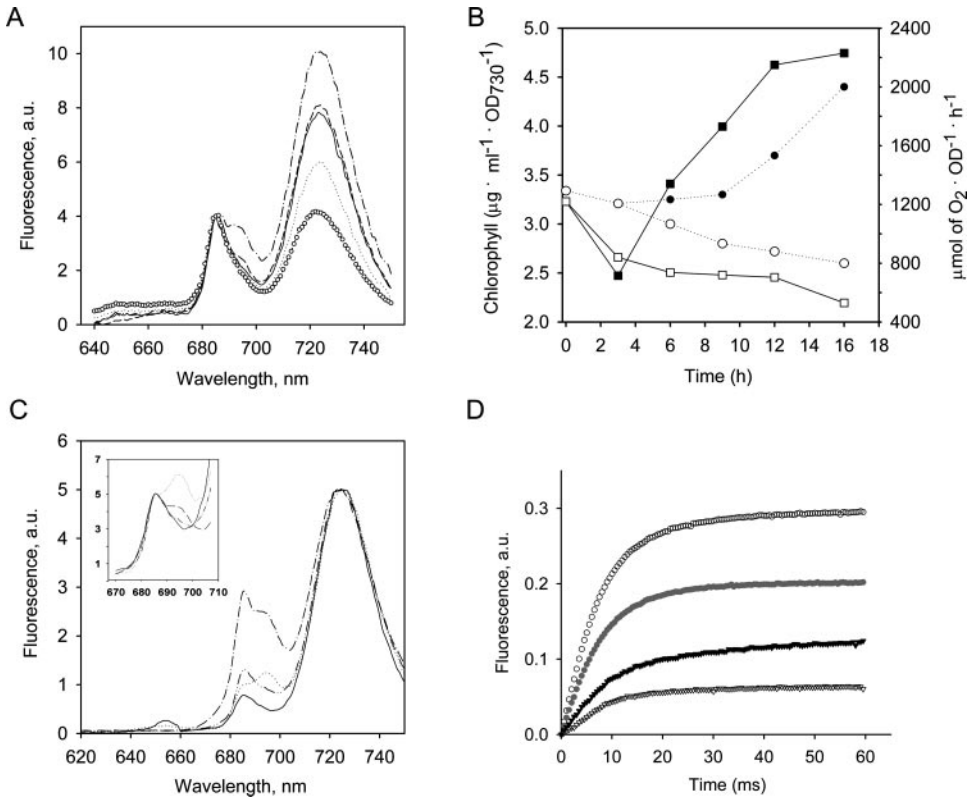

FIG. 6. **Analysis of PSII assembly and Chl accumulation in C1.8 mutant treated by FeCH inhibitor or supplemented by Mg-proto IX.** *A*, 77K fluorescence emission spectra of the C1.8 cells treated by 10 μM FeCH inhibitor *N*-methylprotoporphyrin IX for 0 h (*solid line*), 3 h (*dotted line*), 6 h (*dashed line*), and 12 h (*dashed and dotted line*). Control C1.8 cells after 12 h (*circles*). Excitation was at 435 nm, and fluorescence intensities were normalized to the fluorescence yield at 685 nm; *a.u.*, arbitrary units. *B*, Chl content (*circles*) and oxygen-evolving activity (*squares*) in C1.8 mutant growing autotrophically (*open symbols*) and in the same strain treated by 10 μM FeCH inhibitor (*closed symbols*). C1.8 cells grown photomixotrophically were harvested, washed, and resuspended into autotrophic growth medium. After 12 h of autotrophic growth, 10 μM *N*-methylprotoporphyrin IX was added (0 h). *C*, 77 K fluorescence emission spectra of the WT (*dotted line*), C1.8 (*solid line*), and C1.8 cells treated by 200 μM Mg-proto IX (*dash-dot-dot-dash line*) and 400 μM Mg-proto IX (*dash-dot-dash line*) for 48 h. Mg-proto IX (Frontier Scientific, Logan, UT) was added to C1.8 growing at low light to reduce the effects of Mg-proto IX photoreactivity. Excitation was at 435 nm and fluorescence intensities were normalized to the fluorescence yield at 725 nm; *a.u.*, arbitrary units. The *inset* shows emission of PSII-associated chlorophyll normalized to 685 nm. *D*, Chl fluorescence induction of *Synechocystis* cells in the presence of 10 μM DCMU. *WT*, control (*open circles*); WT treated by 400 μM Mg-proto IX (*gray circles*); C1.8, control (*open triangles*); C1.8 treated by 400 μM Mg-proto IX (*black triangles*). Curves were normalized to the F_0.

photosynthetic bacteria. *In vivo* inhibition of FeCH enhanced bacteriochlorophyll synthesis in the aerobic bacterium *Erythrobacter longus* (34) and led to the accumulation and excretion of Mg-proto IX in *Rhodopseudomonas sphaeroides* (35).

We have shown that supplementation of the C1.8 mutant with Mg-proto IX also improved PSII accumulation (Fig. 6, *C* and *D*), indicating that the increased level of Chl precursors is the reason for PSII assembly in the C1.8 pseudorevertants. Surprisingly, increased Chl biosynthesis in the pseudorevertants was followed by the formation of extra thylakoid membranes with aberrant localization (Fig. 2). It looks like the increased pool of Chl leads to the accumulation of Chl-binding proteins and initiates the formation of extra thylakoid membranes. This suggests an important role of tetrapyrroles in the control of the accumulation of pigment-protein complexes and the proliferation of thylakoid membranes in the cyanobacterial cell.

Interestingly, a 10-fold decrease in FeCH activity had no effect on the protoheme level, and no symptoms of heme deficiency were observed. Although cyanobacteria utilize large amounts of heme for the biosynthesis of phycobilins (chromophores of the major light-harvesting structures), we have not observed any decrease in content of phycobilisomes in the cells (Supplemental Fig. S1). This is similar to our unsuccessful attempt to genetically inactivate FeCH, where no changes in phycobiliprotein levels were detectable until very late in the segregation process. A similar excess of FeCH capacity has been observed in other organisms: 10-fold decrease in FeCH activity in the purple bacterium *R. sphaeroides*, or 16-fold lower activity of FeCH in *Bacillus subtilis*, had no effect on cell viability (35, 36).

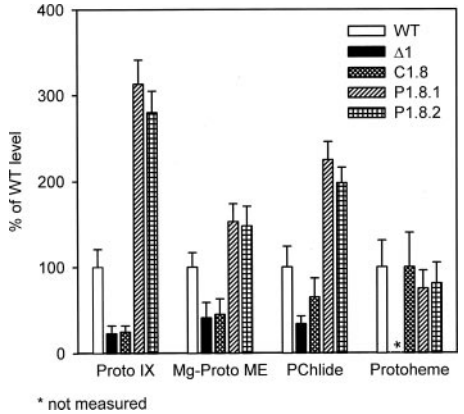

FIG. 7. **Protoheme and Chl precursor levels in the CP47 mutants and pseudorevertants.** Chl precursor pigments were extracted from cells by extraction with methanol and quantified by a combination of HPLC and spectrofluorometry. Protoheme was extracted by acidic acetone, and its concentration was determined from the reduced-minus-oxidized difference spectrum (see "Experimental Procedures"). The values are the mean of three independent experiments and are given as a percentage of WT.

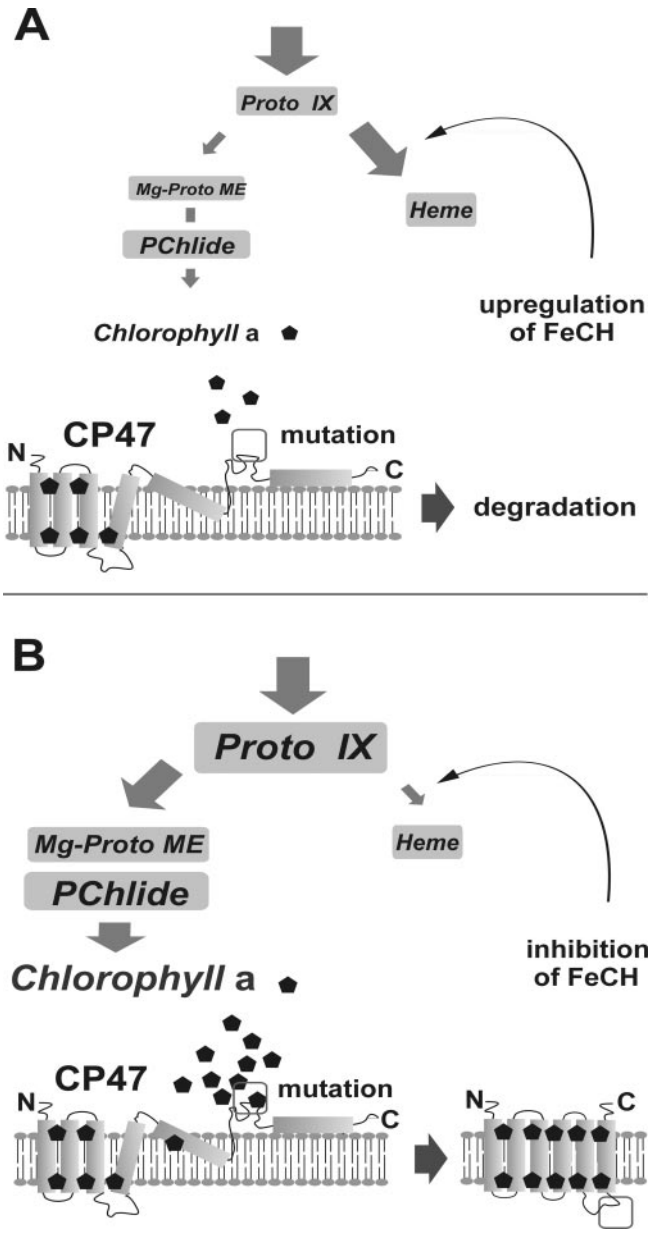

FIG. 8. **Model describing effect of the C1.8 mutation and its complementation by inactivation of FeCH.** *A*, the C1.8 mutation prevents proper Chl binding to the CP47 apoprotein; an uncomplete holoprotein is degraded. Up-regulation of FeCH activity results in decreased levels of Chl precursors, further impairing synthesis of CP47. *B*, decreased FeCH activity in the pseudorevertants (or after treatment with FeCH inhibitor) increases Chl supply and results in the improved synthesis of mutated CP47 holoprotein that is stable and assembles normally into PSII.

Inversely, up-regulation of FeCH activity found in several PSII mutants (Fig. 5) may be responsible for the decreased accumulation of Chl precursors in these strains (Fig. 7). In *Rhodobacter capsulatus*, overexpression of FeCH led to a decrease of aminolevulinate synthase activity and to dramatically lowered levels of bacteriochlorophyll (37).

C1.8 Mutation Influences Synthesis of CP47 but Not Its Function or Assembly into PSII—During PSII assembly, CP47 is attached to the D1-D2-cytochrome b_{559} subcomplex followed by the insertion of CP43 (2). We have shown that in the C1.8 strain, PSII assembly is blocked at the CP47 insertion step most probably due to low levels of available CP47. Pseudorevertants carrying the same C1.8 mutation in CP47, but with an improved supply of Chl, synthesized the mutated CP47 protein with normal stability and assembled almost normal amounts of functional PSII complexes. This argues that C1.8 mutation influences mostly the synthesis of CP47 and not its final stability or functionality. The CP47 protein binds 16 Chl molecules, several of them having been shown to be critical for protein stability (3). By translation assays, it was revealed that Chl binding is required for the stability and membrane association of CP47 translation intermediates. Interestingly, ribosome pausing was observed after synthesis of helix 5 of the CP47 protein.[3] This pausing could be related to Chl attachment and folding of the CP47 protein.

Increased FeCH Activity in PSII Mutants: Possible Role of the C-terminal Extension of FeCH—The reasons for increased FeCH activity in PSII mutants are not known. We have shown by DCMU treatment that this increase is not caused by blocked photosynthetic electron transport or by the switch from photoautotrophic to photoheterotrophic growth. Interestingly, highly increased FeCH activity was found also in a PSI-less mutant,[2] suggesting that FeCH activity is increased in mutants that may have a problem with chlorophyll placement. In higher plants, increase in FeCH activity has been reported as a response to environmental stresses such as wounding, oxidative stress, and viral infection (38). However, there are two different FeCH isozymes in plants (39) and only the FeCH-1 isozyme, ubiquitously expressed throughout the plant, was responsible for the described increase. In contrast, FeCH-2 localized in plastids, was repressed (38). Plant FeCH-2 is a homologue of cyanobacterial FeCH with a putative membrane-spanning region carrying the characteristic Chl-binding motif (40).

This C-terminal extension of FeCH, found only in organisms with oxygenic photosynthesis, is proposed as being involved in the modulation of FeCH activity and in the regulation of Chl/heme biosynthesis through Chl binding (30). Our data indirectly support this hypothesis. Firstly, point mutation in Ser-321 leading to a 40-fold decrease in FeCH activity in the P1.8.2 pseudorevertant is localized in the region connecting FeCH with this putative transmembrane region. Secondly, we demonstrated that changes in FeCH activity in C1.8 influence Chl biosynthesis, suggesting that changes in FeCH activity could regulate Chl biosynthesis even in WT. Lastly, our data indicate that the most photosensitive PSII$^-$ strains (in the order $\Delta 1 >$ cyt559 $>$ ΔCP47 $>$ ΔCP43) have also the highest FeCH activity when grown in low light.[2] We speculate that free Chl accumulating in PSII$^-$ strains as a consequence of degraded Chl-binding proteins may both induce photosensitivity of PSII$^-$ strains and up-regulate FeCH activity by binding to its transmembrane domain.

In the working model depicted in Fig. 8, the $\Delta 1$ region located near to the C-terminal of the CP47 protein is important for Chl-attachment during translation and for proper protein folding. In the C1.8 mutant, only a small fraction of translated CP47 proteins is completed due to the affected Chl binding to the CP47 protein. In pseudorevertants, the completion of properly folded CP47 is improved due to the increased Chl supply. Because the C1.8 mutation apparently only affects the synthesis of the CP47 protein and not its function or assembly into PSII, up-regulation of the Chl pathway allows the C1.8 mutant to grow fully photoautotrophically.

In conclusion, we have demonstrated that FeCH activity is controlling PSII assembly in the C1.8 mutant by the modulation of chlorophyll availability in the cell. The fact that FeCH activity can be easily regulated by a specific inhibitor makes the C1.8 strain a useful tool for studying tetrapyrrole metabolism and connection between Chl synthesis and the assembly of

[3] R. Eichacker *et al.*, unpublished data.

Chl-binding complexes. We are currently analyzing several C1.8 pseudorevertants in which secondary mutations did not map into the FeCH gene, to identify other proteins involved in the regulation of tetrapyrrole biosynthesis.

Acknowledgments—We thank Eva Prachova for her technical assistance, Michal Koblizek for reading the manuscript, Drs. P. Nixon, L. Eichacker, and R. Barbato for specific antisera, and Profs. W. Vermaas and H. Pakrasi for the PSII mutants.

REFERENCES

1. Tichy, M., and Vermaas, W. (2000) *Eur. J. Biochem.* **267,** 6296–6301
2. Komenda, J., Reisinger, V., Müller, B. C., Dobáková, M., Granvogl, B., and Eichacker, L.A. (2004) *J. Biol. Chem.* **279,** 48620–48629
3. Shen, G. Z., Eaton-Rye, J. J., and Vermaas, W. F. J. (1993) *Biochemistry* **32,** 5109–5115
4. Müller, B., and Eichacker, L. A. (1999) *Plant Cell* **11,** 2365–2377
5. Eichacker, L. A., Helfrich, M., Rüdiger, W., and Müller, B. (1996) *J. Biol. Chem.* **271,** 32174–32179
6. He, Q., and Vermaas, W. (1998) *Proc. Natl. Acad. Sci. U. S. A.* **95,** 5830–5835
7. Manna, P., and Vermaas, W. (1997) *Eur. J. Biochem.* **247,** 666–672
8. Shen, G., and Vermaas, W. F. J. (1994) *Biochemistry* **33,** 7379–7388
9. Paulsen, H., H., Finkenzeller, B., and Kühlein, N. (1993) *Eur. J. Biochem.* **215,** 809–816
10. Yaronskaya, E., Ziemann, V., Walter, G., Averina, N., Börner, T., and Grimm, B. (2003) *Plant J.* **35,** 512–522
11. Thomas, H. (1997) *New Phytol.* **136,** 163–181
12. Cornah, J. E., Terry, M. J., and Smith, A. G. (2003) *Trends Plant Sci.* **8,** 224–229
13. Hihara, Y., Kamei, A., Kanehisa, M., Kaplan, A., and Ikeuchi, M. (2001) *Plant Cell* **13,** 793–806
14. Papenbrock, J., Mock, H.P., Kruse, E., and Grimm, B. (1999) *Planta* **208,** 264–273
15. Matsumoto, F., Obayashi, T., Sasaki-Sekimoto, Y., Ohta, H., Takamiya, K., and Masuda, T. (2004) *Plant Physiol.* **135,** 2379–2391
16. Hihara, Y., Sonoike, K., Kanehisa, M., and Ikeuchi, M. (2003) *J. Bacteriol.* **185,** 1719–1725
17. Haag, E., Eaton-Rye, J. J., Renger, G., and Vermaas, W. F. J. (1993) *Biochemistry* **32,** 4444–4454
18. Yu, J. J., and Vermaas, W. F. J. (1990) *Plant Cell* **2,** 315–322
19. Pakrasi, H. B., Diner, B. A., Williams, J. G. K., and Arntzen, C. J. (1989) *Plant Cell* **1,** 591–597
20. Rippka, R., Deruelles, J., Waterbury, J. B., Herman, M., and Stanier, R. Y. (1979) *J. Gen. Microbiol.* **111,** 1–61
21. Porra, R. J., Thompson, W. A., and Kriedemann, P. E. (1989) *Biochim. Biophys. Acta* **975,** 384–394
22. Schägger, H., and von Jagow, G. (1991) *Anal. Biochem.* **199,** 223–231
23. Camadro, J. M., and Labbe, P. (1988) *J. Biol. Chem.* **263,** 11675–11682
24. Xu, H., Vavilin, D., and Vermaas, W. (2002) *J. Biol. Chem.* **277,** 42726–42732
25. Stillman, L. C., and Gassman, M. L. (1978) *Anal. Biochem.* **91,** 166–172
26. Steiger, S., Schäfer, L., and Sandmann, G. (1999) *J. Photochem. Photobiol. B: Biol.* **52,** 14–18
27. De Matteis, F., Gibbs, A. H., and Smith, A. G. (1980) *Biochem. J.* **189,** 645–648
28. Bricker, T. M., and Frankel, L. K. (2002) *Photosyn. Res.* **72,** 131–146
29. Eaton-Rye, J. J., and Vermaas, W. F. J. (1991) *Plant Mol. Biol.* **17,** 1165–1177
30. Vavilin, D. V., and Vermaas, W. F. J. (2002) *Physiol. Plant.* **115,** 9–24
31. Papenbrock, J., Mishra, S., Mock, H. P., Kruse, E., Schmidt, E. K., Petersmann, A., Braun, H. P., and Grimm, B. (2001) *Plant J.* **28,** 41–50
32. Jung, S., Yang, K., Lee, D., and Back, K. (2004) *Plant Sci.* **167,** 789–795
33. Zavgorodnyaya, A., Papenbrock, J., and Grimm, B. (1997) *Plant J.* **12,** 169–178
34. Shiba, T. (1992) *J. Gen. Appl. Microbiol.* **38,** 439–446
35. Houghton, J. D., Honeybourne, C. L., Smith, K. M., Tabba, H. D., and Jones, O. T. G. (1982) *Biochem. J.* **208,** 479–486
36. Olsson, U., Billberg, A., Sjövall, S., Al-Karadaghi, S., and Hansson, M. (2002) *J. Bacteriol.* **184,** 4018–4024
37. Kanazireva, E., and Biel, A. J. (1995) *J. Bacteriol.* **177,** 6693–6694
38. Singh, D. P., Cornah, J. E., Hadingham, S., and Smith, A. G. (2002) *Plant Mol. Biol.* **50,** 773–788
39. Suzuki, T., Masuda, T., Singh, D. P., Tan, F.-C., Tsuchiya, T., Shimada, H., Ohta, H., Smith, A. G., and Takamiya, K. (2002) *J. Biol. Chem.* **277,** 4731–4737
40. Funk, C., and Vermaas, W. (1999) *Biochemistry* **38,** 9397–9404

Publication II

THE JOURNAL OF BIOLOGICAL CHEMISTRY VOL. 283, NO. 38, pp. 25794–25802, September 19, 2008

Importance of the Cyanobacterial Gun4 Protein for Chlorophyll Metabolism and Assembly of Photosynthetic Complexes*

Received for publication, May 16, 2008, and in revised form, July 11, 2008 Published, JBC Papers in Press, July 14, 2008, DOI 10.1074/jbc.M803787200

Roman Sobotka[‡§1], Ulf Dühring[¶1], Josef Komenda[‡§], Enrico Peter[¶], Zdenko Gardian[‖], Martin Tichy[‡§], Bernhard Grimm[¶], and Annegret Wilde[¶2]

From the [‡]Institute of Physical Biology, University of South Bohemia, 37333 Nove Hrady, Czech Republic, [§]Department of Autotrophic Microorganisms, Institute of Microbiology, Opatovicky mlyn, 37971 Trebon, Czech Republic, [¶]Institute of Biology, Humboldt-University Berlin, Chausseestrasse 117, 10115 Berlin, Germany, and [‖]Institute of Plant Molecular Biology, Branisovska 31, 37005 Ceske Budejovice, Czech Republic

Gun4 is a porphyrin-binding protein that activates magnesium chelatase, a multimeric enzyme catalyzing the first committed step in chlorophyll biosynthesis. In plants, GUN4 has been implicated in plastid-to-nucleus retrograde signaling processes that coordinate both photosystem II and photosystem I nuclear gene expression with chloroplast function. In this work we present the functional analysis of Gun4 from the cyanobacterium *Synechocystis* sp. PCC 6803. Affinity co-purification of the FLAG-tagged Gun4 with the ChlH subunit of the magnesium chelatase confirmed the association of Gun4 with the enzyme in cyanobacteria. Inactivation of the *gun4* gene abolished photoautotrophic growth of the resulting *gun4* mutant strain that exhibited a decreased activity of magnesium chelatase. Consequently, the cellular content of chlorophyll-binding proteins was highly inadequate, especially that of proteins of photosystem II. Immunoblot analyses, blue native polyacrylamide gel electrophoresis, and radiolabeling of the membrane protein complexes suggested that the availability of the photosystem II antenna protein CP47 is a limiting factor for the photosystem II assembly in the *gun4* mutant.

The three major tetrapyrrole end products chlorophyll (Chl),[3] heme, and phycobilins are synthesized in a branched metabolic pathway with protoporphyrin IX (P_{IX}) as the last common precursor (1–4). The iron branch insertion of Fe^{2+} into P_{IX} by ferrochelatase leads to the formation of protoheme, whereas in the magnesium branch magnesium chelatase catalyzes the chelation of Mg^{2+} into P_{IX}, thereby directing tetrapyrroles into Chl synthesis.

Cyanobacteria and plants accumulate various tetrapyrrole species in different quantities in the cell. Unlike plants, which use Chl-containing antenna complexes for light harvesting, the major light-harvesting antennae of cyanobacteria consist of phycobiliproteins, which contain covalently bound phycobilines originating from heme. Thus, in cyanobacteria P_{IX} might be directed into the iron branch to a much larger extent than in plants. Regulation of the P_{IX} distribution at the branch point between the magnesium and iron pathways as well as coordination of tetrapyrrole and cognate apoprotein synthesis are substantial in order to avoid accumulation of photoreactive intermediates during tetrapyrrole synthesis. For instance, in plants the genes coding for the light-harvesting Chl-*a*/*b*-binding proteins (*LHCB*) and for Chl biosynthesis proteins are simultaneously up-regulated in the light (5–7).

In a search for *Arabidopsis thaliana* mutants that are deregulated in the communication between plastids and the nucleus several *gun* (genome uncoupled) mutants have been identified (8). The *GUN2*, *GUN3*, *GUN4*,and *GUN5* genes encode proteins that are involved in tetrapyrrole biosynthesis (9, 10). Two of the gene products, GUN2 (heme oxygenase) and GUN3 (biliverdin reductase), function in heme degradation. *GUN5* encodes the ChlH subunit of the magnesium chelatase complex (9), whereas *GUN4* encodes a protein that interacts with magnesium chelatase (10). *GUN4*-related genes were found only in photosynthetic organisms. In plants *GUN4* either is encoded in the nucleus or retained in the chloroplast genome as is the case with several algae, where it was previously designated as *ycf53*.

All cyanobacterial genomes sequenced so far contain one or more *gun4*-related genes, with the exception of the ancient cyanobacterium *Gloeobacter violaceus* PCC7421. An *A. thaliana GUN4* mutant forms white-yellow tissue under standard conditions or pale green tissue in dim light (10). The *A. thaliana* Gun4 protein was co-purified with the ChlH subunit of magnesium chelatase and binds P_{IX} as well as magnesium protoporphyrin IX (MgP_{IX}) (10). *In vitro* enzyme assays revealed a dramatically increased efficiency of the enzymatic Mg^{2+} insertion into P_{IX} in the presence of Gun4, especially at low Mg^{2+} concentrations (10, 11). Accordingly, the crystal structures of Gun4 proteins from two cyanobacterial species bare a specific por-

* This work was supported by Deutsche Forschungsgemeinschaft Grants SFB429 and TPA8 (to A. W. and B. G.), by Institutional Research Concept AV0Z50200510, by Ministry of Education of the Czech Republic project MSM6007665808 (to J. K.), and by Grant Agency of the Czech Academy of Sciences project IAA500200713 (to R. S. and M. T.). The costs of publication of this article were defrayed in part by the payment of page charges. This article must therefore be hereby marked "*advertisement*" in accordance with 18 U.S.C. Section 1734 solely to indicate this fact.

[1] These authors equally contributed to this work.

[2] Present address and to whom correspondence should be addressed: Institute of Microbiology and Molecular Biology, Justus-Liebig-University Giessen, Heinrich-Buff-Ring 26-32, 35392 Giessen, Germany. Tel.: 496419935545; Fax: 496419935549; E-mail: Annegret.Wilde@mikro.bio.uni-giessen.de.

[3] The abbreviations used are: Chl, chlorophyll; P_{IX}, protoporphyrin IX; PS, photosystem; DM, β-dodecyl maltoside; BN-PAGE, blue native PAGE; GT, glucose-tolerant; HPLC, high performance liquid chromatography; MES, 4-morpholineethanesulfonic acid.

phyrin binding site supporting a function of Gun4 in tetrapyrrole trafficking (11, 12).

In a previous report we described an incompletely segregated *gun4* mutant of *Synechocystis* sp. PCC 6803 (hereafter *Synechocystis* 6803), arguing for substantial roles of Gun4 in cell metabolism (13). Here, we succeeded in generating a fully segregated *gun4* mutant strain in the glucose-tolerant (GT) *Synechocystis* 6803 wild-type background. The analysis of this strain revealed that the absence of Gun4 strongly decreased Chl biosynthesis and completely abolished photoautotrophic growth. These mutant properties correlated with a drastically impaired assembly of the two photosystems (PS). Among all Chl-binding proteins the accumulation of the PSII subunit CP47 was most strongly affected in the *gun4* mutant. The regulatory interaction between Chl synthesis and PS accumulation is discussed.

EXPERIMENTAL PROCEDURES

Culture Conditions—*Synechocystis* 6803 wild-type (GT) and mutant strains were grown at 30 °C in BG-11 medium (14) containing 5 mM glucose under continuous irradiance of 5 μmol of photons m^{-2} s^{-1} (low light intensity) or 50 μmol of photons $m^{-2}s^{-1}$ (medium light intensity) in rotating Erlenmeyer flasks. For microaerobic growth, the strains were grown under medium light in a 1% CO_2, 99% N_2 atmosphere. The GT strain originates from the laboratory of W. Vermaas (Arizona State University). Transformants of *Synechocystis* 6803 were selected on media with increasing concentrations of kanamycin (5 μg up to 40 μg ml^{-1}). The *gun4* mutant strain was prepared as described in Wilde *et al.* (13). Complete segregation of the mutants was confirmed by PCR using primers 5′-CTTCCGCTGGATCACCTTTA-3′ and 5′-GGTAATGACTTCCCCGAAGA-3′.

Construction of a Synechocystis 6803 Strain Expressing the 3×FLAG-tagged Gun4 Protein—The coding sequence of the *Synechocystis* 6803 *gun4* gene was amplified using the primers 5′-CATATGTCTGATAATTTGACCGAACTCTCC-3′ and 5′-AGATCTTTACCAACCGTATTGGGACC-3′. An NdeI site that overlaps with the ATG start codon of the *gun4* gene was introduced by the forward primer. The PCR product was subcloned into the pDrive vector (Qiagen, Hilden, Germany). Two complementary oligonucleotides encoding the 3×FLAG peptide (Sigma-Aldrich) were hybridized, thus creating NdeI-compatible overhangs, and then ligated into the NdeI site of the pDrive-*gun4* construct. The resultant construct was verified by sequencing. Using NdeI and BglII restriction enzymes, a DNA fragment encoding the FLAG-tagged Gun4 was excised and then ligated into pSK9 vector for chromosomal integration under the control of the copper dependent *petJ* promoter (15), which supports low level expression in BG-11 medium. *gun4* mutant cells were transformed with the resultant vector pSKgun4FLAG. Transformants were selected on BG-11 agar plates containing 7 μg ml^{-1} chloramphenicol. For strong expression of the fusion protein under the control of the *petJ* promoter, cells were grown for at least 7 days in BG-11 medium lacking copper in the trace metal mix.

Determination of Enzyme Activity—Cell cultures (800 ml) were pelleted and disrupted with glass beads in PBS, pH 7.5, and cell debris was removed by centrifugation. Samples were subdivided for assays of magnesium chelatase and ferrochelatase activities, which were performed according to Papenbrock *et al.* (16). A typical assay mix contained 1 mM dithiothreitol (DTT), 0.1% bovine serum albumin, 25 mM ATP, 20 mM $MgCl_2$, and 100 μM P_{IX} for magnesium chelatase or 1 mM DTT, 1% Tween 80, 2.5 mM palmitic acid, 10 mM $ZnSO_4$, and 50 μM P_{IX} for ferrochelatase. The reactions were started by the addition of P_{IX} dissolved in DMSO, and the assay mixtures were further incubated at 28 °C. Reactions were stopped after 0, 20, 40, and 60 min by the addition of an equal volume of methanol to the reaction mixture followed by freezing in liquid nitrogen. After the initial methanol extraction all samples were extracted twice with acetone, methanol, 0.1 N NH_4OH (10:9:1; v/v/v). Reaction products were quantified by HPLC using authentic porphyrin standards.

Determination of Porphyrins—Steady state levels of magnesium porphyrins were analyzed in the exponential growth phase of the cell culture ($OD_{750\ nm}$ ~ 0.5–0.9). Pelleted cells were resuspended in methanol and incubated on ice for 15 min. After a short centrifugation, supernatants were collected, and the pellets were resuspended in methanol, acetone, 0.1 N NH_4OH (10:9:1; v/v/v). Supernatants were combined after centrifugation at 13,000 × *g* for 5 min and prepared for HPLC analysis. Extracted porphyrinogens were oxidized by the addition of 5 μl of 1 M acetic acid and 5 μl of 2-butanone peroxide per 200 μl of extract and separated by HPLC (Agilent-1100, Agilent, Waldborn, Germany) on a RP 18 column (Novapak C18, 4-μm particle size, 3.9 × 150 mm; Millipore, Eschborn, Germany) at a flow rate of 1 ml min^{-1}. Porphyrins were eluted with a linear gradient of solvent B (90% methanol, 0.1 M ammonium acetate, pH 5.2) in solvent A (10% methanol, 0.1 M ammonium acetate, pH 5.2) as follows: 0 to 100% in 7 min followed by 100% solvent B for 17 min. The eluate was monitored by fluorescence detection. The excitation and emission wavelengths were, respectively: for Proto, 405 and 625 nm; for ZnProto, 416 and 589 nm; for MgProto and MgProtoME, 420 and 595 nm, respectively. Porphyrins were identified and quantified using authentic standards (Fluka, Germany; Porphyrin Products, UT). For quantification of P_{IX} precipitated in growth medium, 100 ml of culture at OD_{750} ~ 0.4 were filtered through 4-μm cellulose filters to collect precipitated pigments in growth media. The filter was frozen in liquid nitrogen, powdered in a 2-ml Eppendorf tube, and dissolved in 0.5 ml of alkaline acetone. Acetone was then extracted with 250 μl of hexane to remove Chl. P_{IX} was diluted 50× in DMSO and quantified spectrofluorometrically using an authentic standard (Sigma).

Radioactive Labeling of Cells and Preparation of Membranes—Radiolabeling of cells using a mixture of [^{35}S]Met and [^{35}S]Cys (Trans-label, MP Biochemicals, Irvine, CA; final activity, 400 μCi ml^{-1}) was performed at 30 °C for 20 min under illumination with 125 μmol of photons m^{-2} s^{-1} as described in a previous study (17). For preparation of membrane and cytosolic protein fractions, cells (OD_{750} ~ 0.5) were washed and resuspended in thylakoid buffer containing 25 mM Hepes, pH 7.4, 10 mM $MgCl_2$, 5 mM $CaCl_2$, and 20% glycerol. The cell suspension was mixed with glass beads and broken in a Mini Bead Beater, and the resulted homogenate was divided into two halves. To prepare a whole cell extract, the first part was solubilized by 1%

β-dodecyl maltoside (DM) and centrifuged at 32,000 × *g* for 10 min at 4 °C to discard unbroken cells. The second part was centrifuged at 100,000 × *g* for 30 min at 4 °C, and the supernatant containing soluble proteins was transferred to a new tube. Pelleted membranes were washed 3 times in thylakoid buffer and resuspended in the same buffer containing 1% DM, and unbroken cells were discarded by centrifugation. To prove whether proteins are tightly bound to the membrane, an additional washing step with 2 M NaCl was applied.

Protein Analyses—Analysis of membrane proteins under native conditions was performed by Blue Native (BN)-PAGE using the buffer system of Schägger and von Jagow (18). The isolated membranes were resuspended in 25 mM MES/NaOH, pH 6.5, containing 10 mM $CaCl_2$, 10 mM $MgCl_2$, and 25% glycerol. The membranes were then solubilized with DM (DM: Chl = 40 for WT and 160 for *gun4*$^-$, respectively, w/w) and analyzed at 4 °C in a 4–16% polyacrylamide gel. Protein composition of complexes was then assessed by electrophoresis in a denaturing 12–20% linear gradient polyacrylamide gel containing 7 M urea (19). The whole lanes from the BN gel were excised, incubated for 30 min in 25 mM Tris/HCl, pH 7.5, containing 1% SDS (w/v), and placed on the top of the denaturing gel; two lanes were analyzed in a single denaturing gel. Proteins separated in the gel were either stained by Coomassie Blue or transferred onto a membrane for immunodetection. One-dimensional SDS-PAGE was carried out as described by Jänsch *et al.* (20). For immunodetection proteins were transferred from gels onto nitrocellulose or polyvinylidene difluoride membranes and immunolabeled with specific antibodies. The primary antibodies used in the study were raised in rabbits against (i) residues 58–86 of the spinach D1 polypeptide, (ii) residues 380–394 of barley CP47, (iii) whole recombinant Gun4 and ferrochelatase proteins from *Synechocystis* 6803 overexpressed in *Escherichia coli* using the pQE80 expression vector (Qiagen) and purified with nickel-nitrilotriacetic acid-agarose. The antibodies against *Synechocystis* 6803 ChlH and ChlD subunits of the magnesium chelatase were kindly provided by Prof. Neil C. Hunter (University of Sheffield). Protein signals were visualized using the Immobilon Western (Millipore, Bedford, MA) or Supersignal West Pico (Pierce) chemiluminescence detection systems. Purification of 3×FLAG-tagged Gun4 from *Synechocystis* 6803 was performed from solubilized whole cell extracts as previously described (21).

Electron Microscopy—Cells were washed twice in 50 mM phosphate buffer, pH 7.2, and fixed in a solution containing 2% glutaraldehyde in 50 mM phosphate buffer for 2 h. This was followed by 3 washes in phosphate buffer and post-fixated in 1% OsO_4 in 50 mM phosphate buffer for 1 h. Finally, the cells were washed 3 times and embedded in 2% agarose. The segments of agarose with cells were dehydrated in isopropyl alcohol and embedded in Spurr's resin. Thin sections were cut with a diamond knife and post-stained for 30 min with 5% aqueous uranyl acetate followed by lead citrate for 80 s. The samples were examined with a Jeol 1010 electron microscope equipped with CCD camera MegaView III and image processing software Analysis (3.1.110).

Absorption Spectra and Pigment Measurements—Absorption spectra of whole cells were measured with a UV-2401 PC spectrophotometer equipped with an integrating sphere (Shimadzu). Chl was extracted from cell pellets (10 ml, $OD_{750} \sim 0.5$) with 100% methanol, and its content was measured spectrophotometrically (22).

77 K Fluorescence Emission Spectra—77 K fluorescence emission spectra were measured in liquid nitrogen with an Aminco spectrofluorimeter (Spectronic Unicam) using membranes washed twice with excess of thylakoid buffer. 100 μl of the sample at Chl concentration of 14 μg ml^{-1} were used for the measurement with 2 μM rhodamine as an internal standard. The spectra were normalized to rhodamine peak (573 nm) and multiplied by relative Chl:absorbance ratio for individual strains to indicate their Chl fluorescence per cell. 77 K fluorescence emission spectra were collected using excitation wavelength 435 nm to excite Chl*a*.

RESULTS

Mutant Characterization—We had previously analyzed the role of *Synechocystis* 6803 Gun4 in tetrapyrrole biosynthesis using a *gun4* mutant strain that was not fully segregated under different growth conditions. These *gun4* mutant cells had exhibited lower magnesium and ferrochelatase activities accompanied by the accumulation of P_{IX}, the substrate of both enzymes. In the present study we used a GT *Synechocystis* 6803 strain for mutational analysis. This different lineage of the original *Synechocystis* 6803 strain is widely used for the dissection and analysis of photosynthetic mutants. Fully segregated PSI, PSII, and Chl biosynthesis mutants could be generated in this genetic background (23, 24).

PCR analysis (Fig. 1) revealed that *gun4* mutant in the GT substrain of *Synechocystis* 6803 (hereafter designated *gun4*$^-$) was completely segregated. In contrast to previous results obtained with the PCC strain of *Synechocystis* 6803 (13), no chromosomal wild-type copies of the *gun4* gene were detected. *Gun4* inactivation was confirmed by immunoblot analysis, demonstrating the complete lack of Gun4 in protein extracts from the mutant (compare Fig. 3*A*). Because Gun4-deficient cells lost the ability to grow photoautotrophically, all media were supplemented with 5 mM glucose to support the growth of the *gun4* mutant cells. At a medium light intensity (50 μmol of photons m^{-2} s^{-1}) *gun4* mutant cells grew slowly, lost more than 90% of Chl, and accumulated large amounts of P_{IX} (Table 1). In addition, P_{IX} also strongly accumulated in the growth medium leading to the formation of brown porphyrin aggregates. When these aggregates were separated from cells by filtration, more than eight times more P_{IX} was found in *gun4*$^-$ cells compared with the wild type (data not shown). In addition, mutant cells lost substantial amounts of thylakoid membranes (Fig. 2*B*) at medium light intensity. In contrast, at low light intensity (5 μmol of photons m^{-2} s^{-1}) growth of the *gun4* mutant on glucose (Table 1) was improved, its thylakoid structure (Fig. 2*C*) rather resembled that of wild type, and endogenous accumulation of P_{IX} was decreased (Table 1). However, even under low light conditions, the Chl content in the mutant was only about 25% that of the wild-type level (Table 1), and the content of the Chl precursor MgP_{IX} monomethyl ester was strongly reduced (Table 1). Similar effects were observed when the *gun4* mutant was grown under microaerobic conditions at

medium light intensity. Chl content in the mutant increased from 8 to 15%, and the cells contained more thylakoid membranes than under aerobic conditions (Fig. 2*D*). The negative influence of both light and aerobic conditions on the formation of thylakoid membranes and Chl contents in the *gun4* mutant suggests increased light sensitivity and photooxidative damage in the absence of Gun4 at medium light intensity. To prove whether oxidative stress contributes to the *gun4*$^-$ phenotype even at low light intensities, the mutant was grown microaerobically under these light conditions. No further increase in Chl accumulation was observed compared with aerobic growth at low light, and the Chl content in the mutant remained at 25% that of the wild-type level. In addition, the amount of Chl also was not enhanced in *gun4* mutant cells, grown aerobically in the dark (data not shown). It was concluded that low light intensity did not photosensitize the mutant cells and did not cause light-dependent oxidative stress. Thus, strains were grown at low light intensities for further experiments.

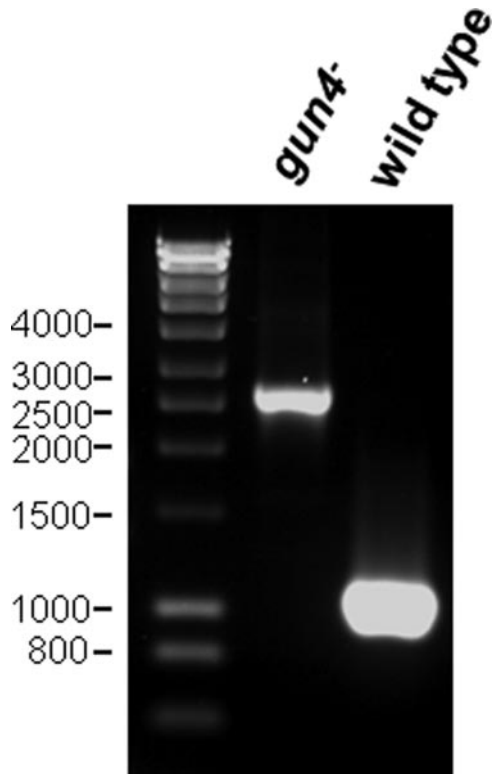

FIGURE 1. **Inactivation of the *gun4* gene in *Synechocystis* 6803 (GT strain).** Wild-type and mutant gene copies were amplified using total chromosomal DNA from wild-type and *gun4*$^-$ strains as templates. PCR amplification of the *gun4* gene yielded a correct 1.1-kilobase pair product in the wild type. The mutant *gun4* copy gave rise to a larger PCR fragment of 2.6 kilobase pairs due to the insertion of the kanamycin resistance cassette (1.5 kilobase pairs). The sizes of the DNA marker fragments are indicated on the *left*.

Localization of Gun4, Ferrochelatase, and Magnesium Chelatase in the Cyanobacterial Cell—Gun4 is proposed to function at the branch point of Chl and heme biosynthesis. To localize Gun4 and the two metal chelatases in cyanobacterial cells, whole cell extracts of wild-type and *gun4* mutant cells were fractionated. Proteins of the cytosolic and membrane fractions were separated by SDS-PAGE, blotted, and probed with antibodies. Fig. 3*A* shows that the ferrochelatase is tightly bound to the membrane, as there is no significant decrease in signal intensity after additional washing of the membranes or treatment with 2 M NaCl. In contrast, the ChlH subunit of magnesium chelatase was detected both in the soluble and in the membrane fractions, whereas the ChlD subunit of the magnesium chelatase appears to be exclusively located in the soluble fraction. Gun4 was mainly detected as a soluble protein and appeared in the membrane fraction only to a minor degree. The substantially lower signal of Gun4 in the membrane fraction after treatment with 2 M NaCl suggests peripheral association of this protein with membranes (Fig. 3*A*).

In the fully segregated *gun4* mutant no immune-reacting protein band was detectable using the anti-Gun4 antiserum (Fig. 3*A*). Interestingly, in contrast to an equal distribution of wild type ChlH subunit of the magnesium chelatase between soluble and membrane fractions, in the *gun4* mutant this protein seems be localized mainly in the soluble fraction (Fig. 3*A*). Intriguingly, *gun4*$^-$ cells contained unequivocally lower amounts of ChlH and ferrochelatase (Fig. 3*B*) than the wild type. This finding corroborates the decreased activities of both enzymes *in vivo* (Fig. 3*C*). Whereas the loss of ferrochelatase activity was proportional to the loss of protein, loss of magnesium chelatase activity could not entirely be attributed to the ChlH deficiency, supporting a direct role of Gun4 for retaining the enzyme activity (10).

Affinity Purification of 3×FLAG-tagged Gun4—A possible explanation for the decreased activity of both chelatases in the *gun4* mutant might be their physical interaction with Gun4. To identify and specify interacting protein partners of Gun4, *gun4* mutant cells were engineered to express a 3×FLAG-tagged Gun4 protein. For this purpose we used a vector harboring the *petJ* promoter, which is induced by copper deficiency and a platform for stable insertion of the construct into the *Synechocystis* 6803 chromosome. Absorption spectra of whole cells confirmed that expression of 3×FLAG-Gun4 complemented

TABLE 1
Phenotypical analysis of *gun4* mutant in comparison to the wild type
Values represent the mean ± S.D. of at least three independent experiments using different cultures harvested in logarithmic growth phase.

Strain	Low light intensity[a]		Medium light intensity[b]	
	Wild type	*gun4*$^-$	Wild type	*gun4*$^-$
Doubling time (h)	19 ± 0.5	21 ± 0.5	10 ± 0.2	25 ± 0.5
Chlorophyll (μg·mg protein^{-1})	11.3 ± 1.1	2.7 ± 0.2	11.8 ± 1.0	0.9 ± 0.4
Phycocyanin (μg·mg protein^{-1})	153 ± 36	154 ± 32	163 ± 45	131 ± 43
Protoporphyrin IX (pmol·mg protein^{-1})	17.2 ± 10.9	61.6 ± 51.2	4.7 ± 2.0	205.0 ± 100
Mg-protoporphyrin IX (pmol·mg protein^{-1})	1.17 ± 0.46	0.15 ± 0.06	1.00 ± 0.22	0.16 ± 0.06
Mg-protoporphyrin IX monomethyl ester (pmol·mg protein^{-1})	4.51 ± 0.87	0.98 ± 0.51	3.88 ± 1.12	0.72 ± 0.33

[a] 5 μmol of photons m^{-2} s^{-1} in medium containing 5 mM glucose.
[b] 50 μmol of photons m^{-2} s^{-1} in medium containing 5 mM glucose.

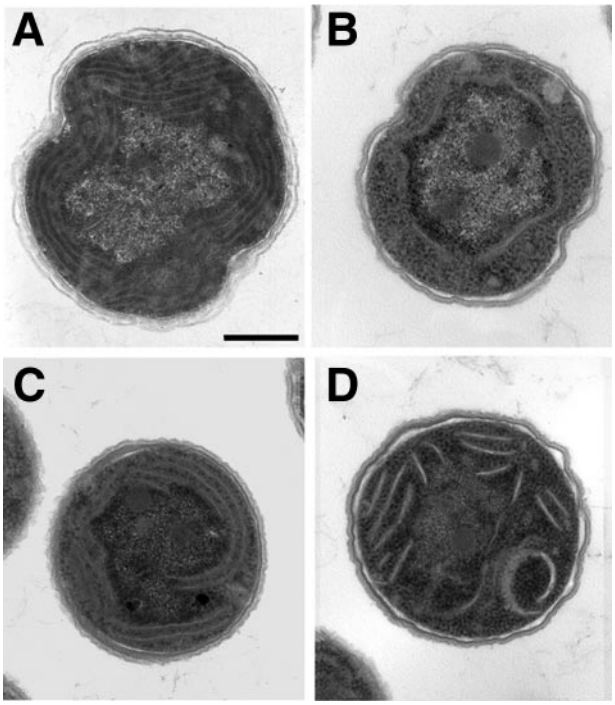

FIGURE 2. **Transmission electron microscopy of *Synechocystis* 6803 cells.** *A*, wild-type cells grown aerobically under medium light conditions. *B*, *gun4* mutant cells grown aerobically under medium light intensity. *C*, *gun4* mutant cells grown aerobically under low light intensity. *D*, *gun4* mutant cells grown microaerobically under medium light conditions. *Scale bar* = 500 nm.

the *gun4* mutation (Fig. 4*A*), indicating the generation and activity of a functional fusion protein. The 3×FLAG-Gun4 fusion protein was expressed during growth in copper-deficient medium and immunoprecipitated with anti-FLAG M2 affinity gel (Sigma-Aldrich) as described (21). The 3×FLAG-Gun4 protein was eluted by the addition of a 3×FLAG peptide and separated by SDS-PAGE (Fig. 4, *C* and *D*). Cells expressing the non-tagged Gun4 were used as the negative control. Among the proteins co-purified with Gun4, only ChlH was identified by immunoblot analysis (Fig. 4*C*). The other magnesium chelatase subunits ChlI and ChlD as well as ferrochelatase did apparently not associate with Gun4. Immunoblot analysis demonstrates that the magnesium chelatase subunits ChlH and ChlD as well as the ferrochelatase were present in similar amounts in cells expressing 3×FLAG Gun4 and control cells (data not shown). In addition, *in vitro* pulldown assays did not indicate an interaction between recombinant Gun4 and ferrochelatase (data not shown). No other putative interacting proteins were detected in the eluate fraction from the *gun4*$^-$:*gun4*FLAG strain after affinity purification of the 3×FLAG-Gun4 protein (Fig. 4*D*).

Absence of Gun4 Affects Accumulation of Both PSII and PSI—The drastically reduced Chl content in the *gun4* mutant (Table 1) was necessarily associated with lower amounts of the Chl-binding protein complexes PSII and PSI. Indeed, semi-quantitative measurements of 77 K fluorescence spectra of membranes using rhodamine as the internal standard revealed an almost complete loss of PSII complexes and a large decrease in the amount of PSI complexes in *gun4*$^-$ cells compared with the wild type (Fig. 4*B*). The pronounced loss of PSII complexes containing the CP47 protein (PsbB) was indicated by the absence of the 695-nm emission peak in *gun4*$^-$, similar to the Δ*psbB* deletion mutant (25), which served as reference in this study (Fig. 4*B*).

The Chl deficiency in *gun4*$^-$ gave us a unique opportunity to investigate consequences of very limited Chl supply for assembly and stability of Chl-binding proteins under standard light conditions. Therefore, we performed a detailed comparison of protein complexes of membranes isolated from wild-type and *gun4* mutant cells applying BN-PAGE (Fig. 5*A*). Apparently, on the per cell basis the contents of both PSI (RCCI) and PSII (RCCII) complexes were dramatically decreased in *gun4* mutant cells compared with wild-type cells (about 25% PSI and maximally 10% PSII of the wild-type level). The PSI trimer was the prevailing form in both strains, but the PSI trimer/PSI monomer ratio was apparently decreased in the mutant. In addition, the relative content of the dimeric form of PSII core com-

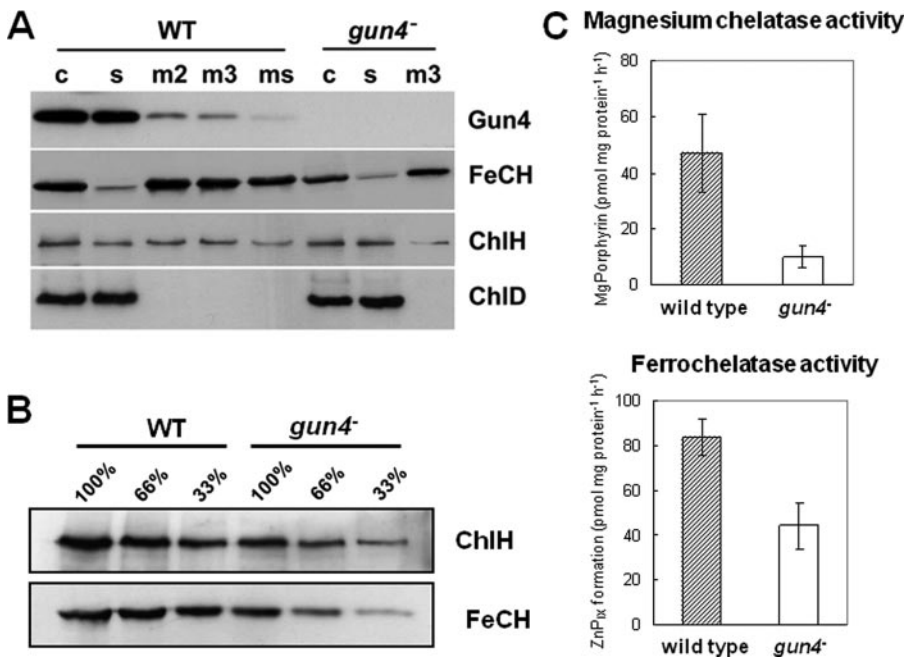

FIGURE 3. **Localization, quantification, and activities of both chelatases.** *A*, subcellular localization of Gun4, ferrochelatase (*FeCH*), and the magnesium chelatase ChlH and ChlD subunits. Membranes have been washed 2 (m2) or 3 (m3) times in thylakoid buffer followed by an additional wash with 2 M NaCl in thylakoid buffer (ms). Membrane fractions (*m*), crude (*c*), and soluble extracts (*s*) of wild-type and *gun4* mutant cells were separated by SDS-PAGE and transferred to nitrocellulose membranes. The amount of Chl corresponding to 150 μl of cells at A_{730} = 1 was loaded per each lane. Polyclonal antibodies used for the immunoblots are shown on the *right*. *B*, accumulation of the ChlH subunit of magnesium chelatase and ferrochelatase in the crude cell extract were determined by immunodetection. *Numbers* indicate relative protein loading based on the amount of cells. *C*, activities of magnesium and ferrochelatase measured in wild-type and *gun4* mutant cells.

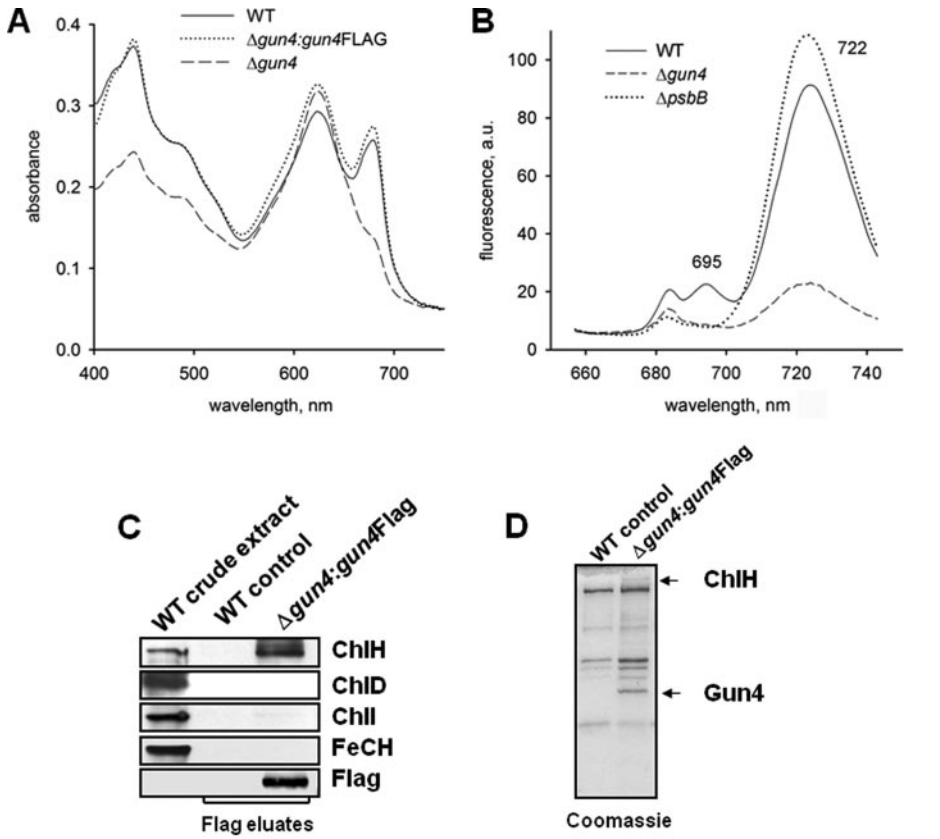

FIGURE 4. **Phenotype of *gun4* mutant cells and affinity purification of Gun4.** *A*, absorption spectra of *Synechocystis* 6803 wild-type (*WT*) and mutant cells lacking Gun4 (*gun4*$^-$) or expressing a FLAG-tagged version of Gun4 (Δ*gun4*:gun4FLAG). Cells were grown with 5 mM glucose in the medium. Peaks at 620 and 682 nm represent phycocyanin and Chl absorption, respectively. Spectra of whole cells were measured with a UV-2401 PC spectrophotometer (Shimadzu, Kyoto, Japan). *B*, semiquantitative 77 K fluorescence emission spectra of thylakoid membranes from *Synechocystis* 6803 wild-type and mutant cells lacking Gun4 (Δ*gun4*) or CP47 (Δ*psbB*). Rhodamine was used as an internal standard, and the spectra were normalized to indicate Chl fluorescence per cell. Peaks at 685/695 and 722 nm represent PSII and PSI complexes, respectively. *a.u.*, absorbance units. *C*, affinity purification of 3×FLAG-Gun4 and identification of magnesium and ferrochelatase (*FeCH*) subunits by immunodetection. Solubilized extracts of *gun4* mutant cells engineered to express 3×FLAG-Gun4 were immunoprecipitated with anti-FLAG M2-agarose (Sigma-Aldrich). FLAG-Gun4 complexes were eluted with 3×FLAG peptide, resolved by SDS-PAGE, stained with Coomassie (*D*) or blotted onto a nitrocellulose membrane and immunodetected (*C*). Wild-type eluate was used as a control.

plex (RCCII(2)) was lower in the mutant than in the wild type. The two-dimensional gel separation of proteins from wild-type membranes and the corresponding immunoblots revealed the presence of the CP47 protein in the core complex lacking CP43 (RC47) and in the region of unassembled proteins. Both free CP47 and CP47 integrated in RC47 were missing in thylakoids of *gun4*$^-$. Moreover, the mutant accumulated two distinct complexes lacking CP47 previously designated as RC* and RCa (26). These complexes contain mature D1 or its partially processed form iD1, D2, cytochrome *b* 559, and PsbI and are typical for strains impaired in synthesis and/or stability of CP47 (17, 26). Thus, the results suggest that the insufficient accumulation of CP47 limits the assembly and accumulation of complete PSII core complexes. In contrast to the Chl-containing PSs, the ATP synthase was present in both strains in equal amounts showing that accumulation of membrane protein complexes lacking Chl was not changed after inactivation of the *gun4* gene.

The differential effect of the *gun4* deletion on accumulation of Chl-binding proteins was further supported by semiquantitative immunoblot analysis (Fig. 6). Consistent with the BN-PAGE data, the ATP synthase was present in similar amounts in wild type and *gun4*$^-$, whereas the amount of the PSI protein PsaD corresponded to about 25% that of the wild-type level. Among the PSII proteins, CP43 accumulated to 25% that of the wild-type level, whereas the D1 protein and especially CP47 were hardly detectable. Negligible cellular contents of CP47 corresponded with a non-detectable oxygen-evolving capacity of PSII, and no variable fluorescence was observed in the *gun4* mutant (not shown).

Because two-dimensional BN/SDS-PAGE was performed with thylakoids isolated from radioactively labeled cells, the analysis also provided information on the synthesis of PSII subunits and their assembly into complexes in both strains (Fig. 5*B*, autoradiograms). In wild-type cells the labeled D1 and D2 subunits were mainly found in RCCII(1) and RCCII(2), and their distribution between both complexes was approximately equal. Small amounts of labeled D1 and D2 (about 10% of the overall levels) were detected in the above-mentioned complexes RC* and RCa. However, these RC complexes accumulated only transiently, quickly disappeared during the chase (data not shown), and were not detected by immunoblot analysis. The inner PSII antennae CP43 and CP47 were labeled less strongly and were present in the core complexes as well as in the fraction of unassembled proteins. In this fraction the labeling of CP43 was particularly strong. The labeling pattern in *gun4*$^-$ thylakoids was different. The autoradiogram revealed that all four large PSII proteins in the assembled core complex RCCII(1) were labeled weakly and nearly to the same extent. The labeling of these proteins in RCCII(2) was hardly detectable. About 70% of the labeled D2, D1, and its partially processed form, iD1, were found in the RC* and RCa complexes. The remaining 30% were found in the core complexes (Fig. 5*B*, see Ref. 26). Moreover, the labeled proteins in RC* and RCa were detectable even after the 30 min of the radioactive chase (data not shown), showing that the complexes are not easily transformed into the core complexes. In the fraction of unassembled proteins, a strong labeling of CP43, but no labeling of CP47, was observed. The results confirmed that the insufficient synthesis of CP47 most probably limits the assembly and accumulation of the complete PSII core complexes. Similar transcript levels of the CP47-encoding gene *psbB* in wild type and *gun4*$^-$ (not shown) showed

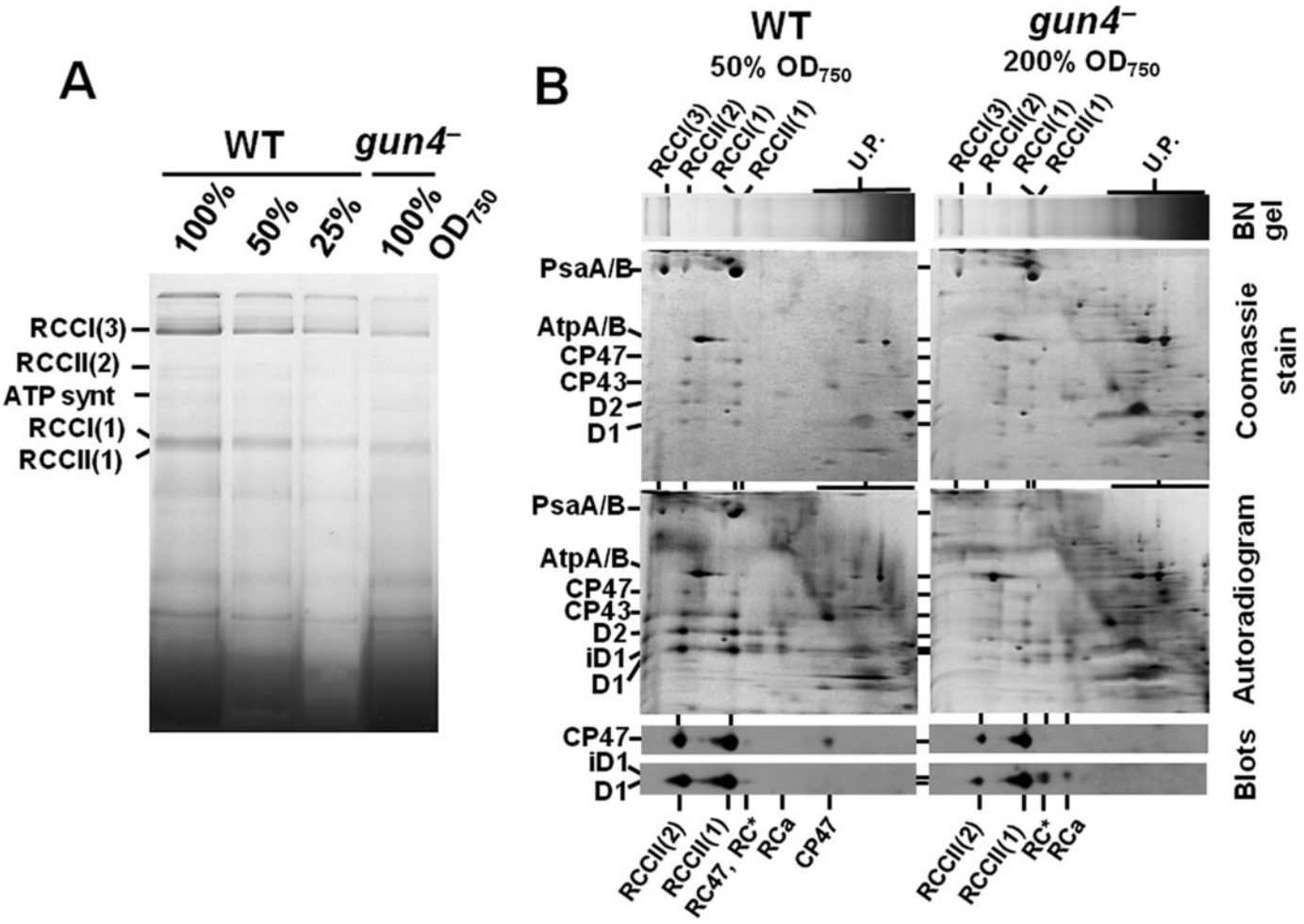

FIGURE 5. **Analysis of membrane protein complexes and their assembly in wild-type and *gun4* mutant cells.** *A*, membrane protein complexes from wild-type and *gun4* mutant labeled *in vivo* with ^{35}[S]Met/Cys were separated in 4–16% BN gel as described under "Experimental Procedures." Amounts of Chl corresponding to designated amounts of cells were loaded per each lane. *B*, two-dimensional analysis of membrane protein complexes separated in *A*. Equal amounts of Chl corresponding to the half (50% A_{750}) and double (200% A_{750}) amounts of wild-type and *gun4*$^-$ cells were loaded, respectively. Lanes from the BN-gel were excised and placed on top of the 12–20% denaturating gel. The two-dimensional gels were either stained by Coomassie Blue (Coomassie gels), dried, and exposed to phosphorimaging plates (Autoradiograms) or electroblotted onto a polyvinylidene difluoride membrane that was immunodecorated using antibodies raised against D1 and CP47 proteins (*blots*). Designation of complexes: *RCCI(3)* and *RCCI(1)*, trimeric and monomeric PSI complexes, respectively; *RCCII(2)* and *RCCII(1)*, dimeric and monomeric PSII core complexes, respectively; *RC47*, the monomeric PSII core complex lacking CP43; *RC** and *RCa*, reaction center complexes accumulating in PSII mutants lacking CP47 (24); *U.P.*, unassembled proteins; *iD1* designates D1 processing intermediate.

that the limitation in the accumulation of CP47 occurred at the posttranscriptional level.

DISCUSSION

In a previous work we did not succeed in preparing a fully segregated cyanobacterial *gun4* mutant in *Synechocystis* 6803. However, generation of such a mutant was feasible in a GT substrain of *Synechocystis* 6803. The *gun4* mutant was further examined for the function of Gun4 in tetrapyrrole biosynthesis and consecutive processes of protein assembly of the photosynthetic apparatus. Although *A. thaliana* GUN4 was reported to be nonessential for plant growth (10), here we show that the complete loss of *gun4* expression in a cyanobacterium prevents photoautotrophic growth. The Chl content in the *gun4* mutant grown at medium light intensities was dramatically reduced to about 8% that of the wild-type amount. At low light intensities the *gun4* mutant accumulated about 25% that of the wild-type Chl content. The better viability of the *gun4*$^-$ cells under low light or microaerobic conditions may be explained by the increased accumulation of P_{IX} in this mutant (Table 1) as P_{IX} is known to cause photooxidative damage (27). Recently, a very similar phenotype has been observed in a *Synechocystis* 6803 mutant that also accumulated large quantities of P_{IX}, resulting from a mutation in the ferrochelatase gene (28). However, at low light intensities under microaerobic conditions no further improvement in Chl accumulation was observed, with the *gun4* mutant accumulating about 25% of the wild-type Chl content. This suggests that the low light *gun4*$^-$ phenotype can be mostly attributed to the lack of Chl precursors and not to enhanced photooxidative stress.

In agreement with the predicted function of Gun4 (10), the absence of this protein adversely affected the magnesium chelatase activity resulting in a limited supply of magnesium porphyrins for Chl synthesis (Table 1). In *Synechocystis* 6803, the Gun4 protein is present mainly as a soluble protein with a small fraction bound to the membrane (Fig. 3*A*). This is consistent with the situation described in *A. thaliana*, where the

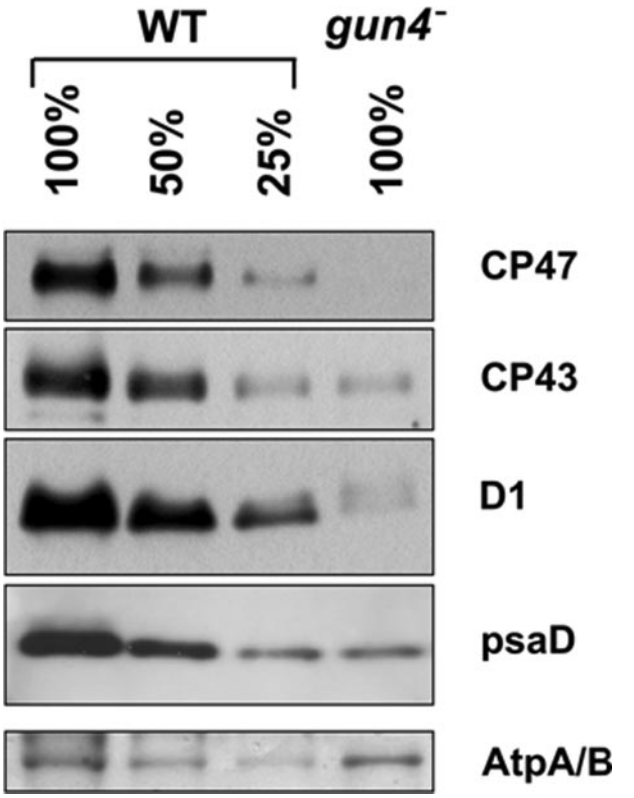

FIGURE 6. **Semiquantitative immunoblot analysis of PSII and PSI subunits in wild type and *gun4* mutant.** Wild-type and *gun4* mutant membrane fractions were separated by SDS-PAGE and transferred to a polyvinylidene difluoride membrane. Different amounts of Chl corresponding to designated amounts of cells were loaded per each lane. Immunodetection was performed using polyclonal antibodies raised against the PSII subunits CP47, CP43, and D1, and the PSI subunit PsaD. ATPase band stained on the membrane with Ponceau red indicates protein loading.

majority of GUN4 was localized in the stroma and clearly smaller amounts in the envelope and thylakoid membranes (10). Moreover, the same authors reported that unlike the soluble GUN4, which probably is present as a monomer, the thylakoid-bound GUN4 was identified as part of a >500 kDa complex also containing the ChlH subunit (10). We have confirmed that cyanobacterial Gun4 is associated with ChlH as well (Fig. 4*C*) and showed that the accumulation of ChlH is influenced by absence of Gun4 (Fig. 3*B*). Interestingly, the proportion of the membrane-bound ChlH seemed to be decreased in the *gun4* mutant as well (Fig. 3*A*). Therefore, Gun4 is possibly important for association of ChlH with the membrane, maybe as a part of a membrane-bound magnesium chelatase complex.

The absence of the Gun4 protein also resulted in a decreased accumulation of ferrochelatase. Because no direct physical interaction between Gun4 and ferrochelatase was detected, the lack of Chl in *gun4*$^-$ may influence the cellular content of ferrochelatase. The plant ferrochelatase as well as its cyanobacterial counterpart contains a highly conserved Chl binding motif within the C-terminal domain (2). Thus, we cannot exclude that a putative Chl binding to this domain is important for the synthesis or stability of ferrochelatase.

The *gun4* mutant provided a new opportunity to analyze the effect of Chl deficiency on photosynthetic membrane proteins in cyanobacterial cells grown under standard light conditions. Previously, a comparably detailed study in the cyanobacterium *Plectonema boryanum* revealed that a mutation in *chlL*, which encodes a subunit of the light-independent protochlorophyllide oxidoreductase (29), leads to Chl deficiency during growth in nearly complete darkness. However, the consequences of Chl deficiency in the dark might significantly differ from those in the light, which is supported by the data of Kada *et al.* (29). The depletion of PSI Chl proteins was much faster than the depletion of PSII in the *chlL*$^-$ strain. We assume that this difference is associated with the different stabilities of PSI and PSII Chl proteins in the dark and under illumination, respectively. Recently, it has been shown that the half-life of PSII-bound Chl in illuminated cells is remarkably shorter than that of the PSI-bound Chl (30). Within PSII, the turnover rate of unassembled CP43 is slower than that of other PSII Chl-binding proteins. In the absence of several PSII proteins, CP43 still accumulates to a larger extent (17). In the *gun4*$^-$ mutant the cellular level of CP43 corresponded to the level of PSI proteins, both of which were reduced to about 25% that of the wild-type level. Moreover, the unassembled protein was clearly visible in the Coomassie-stained two-dimensional gel (Fig. 5*B*). Immunoblot analyses detected the incompletely processed form of D1, which is referred to as iD1, as a component of the RC complexes in the *gun4* mutant but not in wild-type cells (Fig. 5*B*, *blot*). The presence of the incompletely processed form of the D1 protein was reported to be closely related to Chl deficiency, underlying the hypothesis that maturation of D1 occurs after binding of Chl to the protein (31). Here we show that the incompletely processed form of D1 is present in the RC complexes and that the effect of Chl deficiency on the D1 maturation is indirect and related to the absence of CP47. Not until CP47 binds to the RC complexes can the complete and fast D1 maturation proceed.

Despite the presence of RC complexes, the subsequent PSII assembly intermediate RC47, which usually is formed from RC complexes after binding of CP47 (17), is absent in the *gun4* mutant. Because unassembled CP47 is not detectable in the mutant either (Fig. 5*B*, *blot*), it is clear that the accumulation of CP47 is strongly compromised in the mutant. A similar effect was detected in a CP47 mutant that harbors a few amino acid changes in the E-loop of the protein (32). This mutation resulted in a lowered cellular amount of functional PSII accompanied by an increased accumulation of RC complexes. Possibly, Chl deficiency limits the translation of CP47 to a greater extent than the translation of D1 due to the requirement of co-translational Chl binding to the CP47 apoprotein.

In conclusion, our results demonstrate that Gun4 plays an essential role in the magnesium branch of tetrapyrrole biosynthesis and dramatically affects the Chl content in the cell. 77 K fluorescence emission spectra as well as protein analyses demonstrated that Chl deficiency arising from the inactivation of *gun4* affects accumulation of both photosystems. The more extensive deficiency of PSII most probably was related to the insufficient accumulation of CP47. This Chl-binding protein appears to be the protein most sensitive to changes in the Chl availability and may, therefore, represent an important target for the mutual regulation of tetrapyrrole biosynthesis and formation of new PSII complexes.

Acknowledgments—We thank Prof. C. Neil Hunter (University of Sheffield) for the antibodies against the subunits of magnesium chelatase, Gisa Baumert and Kerstin Kaminski for technical assistance, and Dennis Dienst for critical reading of the manuscript. The vector psk9 was a kind gift of Prof. S. Zinchenko (Moscow State University).

REFERENCES

1. Papenbrock, J., and Grimm, B. (2001) *Planta* **213,** 667–681
2. Vavilin, D. V., and Vermaas, W. F. (2002) *Physiol. Plant* **115,** 9–24
3. Grossman, A. R., Lohr, M., and Im, C. S. (2004) *Annu. Rev. Genet.* **38,** 119–173
4. Beale, S. I. (2005) *Trends Plant Sci.* **10,** 309–312
5. Herrin, D. L., Battey, J. F., Greer, K., and Schmidt, G. W. (1992) *J. Biol. Chem.* **267,** 8260–8269
6. Plumley, G. F., and Schmidt, G. W. (1995) *Plant Cell* **7,** 689–704
7. Brusslan, J. A., and Peterson, M. P. (2002) *Photosynth. Res.* **71,** 185–194
8. Susek, R. E., Ausubel, F. M., and Chory, J. (1993) *Cell* **74,** 787–799
9. Mochizuki, N., Brusslan, J. A., Larkin, R., Nagatani, A., and Chory, J. (2001) *Proc. Natl. Acad. Sci. U. S. A.* **98,** 2053–2058
10. Larkin, R. M., Alonso, J. M., Ecker, J. R., and Chory, J. (2003) *Science* **299,** 902–906
11. Davison, P. A., Schubert, H. L., Reid, J. D., Iorg, C. D., Heroux, A., Hill, C. P., and Hunter, C. N. (2005) *Biochemistry* **44,** 7603–7612
12. Verdecia, M. A., Larkin, R. M., Ferrer, J. L., Riek, R., Chory, J., and Noel, J. P. (2005) *PLoS Biol* **3,** e151
13. Wilde, A., Mikolajczyk, S., Alawady, A., Lokstein, H., and Grimm, B. (2004) *FEBS Lett.* **571,** 119–123
14. Rippka, R., Desrulles, J., Waterbury, J. B., Herdman, M., and Stanier, R. Y. (1979) *J. Gen. Microbiol.* **11,** 419–436
15. Tous, C., Vega-Palas, M. A., and Vioque, A. (2001) *J. Biol. Chem.* **276,** 29059–29066
16. Papenbrock, J., Mock, H. P., Kruse, E., and Grimm, B. (1999) *Planta* **208,** 264–273
17. Komenda, J., Reisinger, V., Muller, B. C., Dobakova, M., Granvogl, B., and Eichacker, L. A. (2004) *J. Biol. Chem.* **279,** 48620–48629
18. Schägger, H., and von Jagow, G. (1991) *Anal. Biochem.* **199,** 223–231
19. Komenda, J., Lupinkova, L., and Kopecky, J. (2002) *Eur. J. Biochem.* **269,** 610–619
20. Jänsch, L., Kruft, V., Schmitz, U. K., and Braun, H. P. (1996) *Plant J.* **9,** 357–368
21. Dühring, U., Irrgang, K. D., Lünser, K., Kehr, J., and Wilde, A. (2006) *Biochim. Biophys. Acta* **1757,** 3–11
22. Porra, R. J., Thompson, W. A., and Kriedmann, P. E. (1989) *Biochim. Biophys. Acta* **975,** 384–394
23. Shen, G., and Vermaas, W. F. J. (1994) *J. Biol. Chem.* **269,** 13904–13910
24. He, Q., Brune, D., Nieman, R., and Vermaas, W. (1998) *Eur. J. Biochem.* **253,** 161–172
25. Eaton-Rye, J. J., and Vermaas, W. F. J. (1991) *Plant Mol. Biol.* **17,** 1165–1177
26. Dobakova, M., Tichy, M., and Komenda, J. (2007) *Plant Physiol.* **145,** 1681–1691
27. Yang, H., Inokuchi, H., and Adler, J. (1995) *Proc. Natl. Acad. Sci. U. S. A.* **92,** 7332–7336
28. Sobotka, R., McLean, S., Zuberova, M., Hunter, C. N., and Tichy, M. (2008) *J. Bacteriol.* **190,** 2086–2095
29. Kada, S., Koike, H., Satoh, K., Hase, T., and Fujita, Y. (2003) *Plant Mol. Biol.* **51,** 225–235
30. Vavilin, D., and Vermaas, W. (2007) *Biochim. Biophys. Acta* **1767,** 920–929
31. He, Q., and Vermaas, W. (1998) *Proc. Natl. Acad. Sci. U. S. A.* **95,** 5830–5835
32. Sobotka, R., Komenda, J., Bumba, L., and Tichy, M. (2005) *J. Biol. Chem.* **280,** 31595–31602

Publication III

Functional Assignments for the Carboxyl-Terminal Domains of the Ferrochelatase from *Synechocystis* PCC 6803: The CAB Domain Plays a Regulatory Role, and Region II Is Essential for Catalysis[1][W]

Roman Sobotka*, Martin Tichy, Annegret Wilde, and C. Neil Hunter

Institute of Microbiology, Department of Autotrophic Microorganisms, 379 81 Trebon, Czech Republic (R.S., M.T.); Institute of Physical Biology, University of South Bohemia, 373 33 Nove Hrady, Czech Republic (R.S., M.T.); Institute of Microbiology and Molecular Biology, Justus-Liebig-University Giessen, 35392 Giessen, Germany (A.W.); and Department of Molecular Biology and Biotechnology, University of Sheffield, Sheffield S10 2TN, United Kingdom (C.N.H.)

Ferrochelatase (FeCH) catalyzes the insertion of Fe^{2+} into protoporphyrin, forming protoheme. In photosynthetic organisms, FeCH and magnesium chelatase lie at a biosynthetic branch point where partitioning down the heme and chlorophyll (Chl) pathways occurs. Unlike their mammalian, yeast, and other bacterial counterparts, cyanobacterial and algal FeCHs as well as FeCH2 isoform from plants possess a carboxyl-terminal Chl *a/b*-binding (CAB) domain with a conserved Chl-binding motif. The CAB domain is connected to the FeCH catalytic core by a proline-rich linker sequence (region II). In order to dissect the regulatory, catalytic, and structural roles of the region II and CAB domains, we analyzed a FeCH ΔH347 mutant that retains region II but lacks the CAB domain and compared it with the ΔH324-FeCH mutant that lacks both these domains. We found that the CAB domain is not required for catalytic activity but is essential for dimerization of FeCH; its absence causes aberrant accumulation of Chl-protein complexes under high light accompanied by high levels of the Chl precursor chlorophyllide. Thus, the CAB domain appears to serve mainly a regulatory function, possibly in balancing Chl biosynthesis with the synthesis of cognate apoproteins. Region II is essential for the catalytic function of the plastid-type FeCH enzyme, although the low residual activity of the ΔH324-FeCH is more than sufficient to furnish the cellular demand for heme. We propose that the apparent surplus of FeCH activity in the wild type is critical for cell viability under high light due to a regulatory role of FeCH in the distribution of Chl into apoproteins.

Cyanobacteria, algae, and plants synthesize chlorophyll (Chl), heme, and linear tetrapyrroles such as phycobilins via a common branched pathway. At the beginning of tetrapyrrole biosynthesis, the initial precursor, 5-aminolevulinic acid (ALA), is made from Glu via glutamyl-tRNA and is subsequently converted in several steps to protoporphyrin IX (PP_{IX}), the last common precursor for both Chl and heme biosynthesis. Insertion of Fe^{2+} into this porphyrin macrocycle by ferrochelatase (FeCH) leads to heme, whereas insertion of Mg^{2+} by magnesium chelatase leads to magnesium-protoporphyrin IX (MgP), the first biosynthetic intermediate on the "green" Chl branch (for review, see Tanaka and Tanaka, 2007).

Because the levels of heme and Chl vary according to cell development, growth, or light conditions, special regulatory mechanisms have evolved that control heme and Chl formation and coordinate their levels with the synthesis of the corresponding apoproteins (Müller and Eichacker, 1999). Stringent control of this pathway is particularly essential for oxygenic organisms such as plants and cyanobacteria that have to cope with the problem of photooxidation. Chl and its intermediates are readily excited by light and, unquenched, form reactive oxygen species under aerobic conditions. Therefore, for organisms carrying out oxygenic photosynthesis, it is essential to minimize cellular levels of unbound "free" tetrapyrroles.

The mechanisms that control and regulate Chl/heme biosynthesis mostly remain to be elucidated, although it is well established that the total metabolic flow through the pathway is controlled at the point of ALA formation, a rate-limiting step for the whole pathway (for review, see Tanaka and Tanaka, 2007; Masuda and Fujita, 2008). The biosynthetic step controlling ALA formation is most probably that cata-

[1] This work was supported by Institutional Research Concept number AV0Z50200510 (to M.T.), by the Ministry of Education of the Czech Republic (project no. MSM6007665808 to R.S.), by the Czech Science Foundation (project no. P501/10/1000 to R.S.), by the Deutsche Forschungsgemeinschaft (grant no. SFB429 to A.W), and by the Biotechnology and Biological Sciences Research Council of the United Kingdom (to C.N.H.).

* Corresponding author; e-mail sobotka@alga.cz.

The author responsible for distribution of materials integral to the findings presented in this article in accordance with the policy described in the Instructions for Authors (www.plantphysiol.org) is: Roman Sobotka (sobotka@alga.cz).

[W] The online version of this article contains Web-only data.
www.plantphysiol.org/cgi/doi/10.1104/pp.110.167528

lyzed by glutamyl-tRNA reductase. This is the first enzyme in the pathway and is modulated by a wide range of regulatory signals, in line with the idea that this is the central controller of total tetrapyrrole flux (Kumar et al., 1996; Tanaka et al., 1996; McCormac et al., 2001). Another key regulatory site is at the branch point between Chl and heme biosynthesis, where distribution of PP_{IX} has to be carefully balanced according to the actual demand for both essential pigments. These regulatory mechanisms that govern the distribution of PP_{IX} remain to be elucidated, although the roles of both chelatases have become apparent (Papenbrock et al., 2000, 2001; Sobotka et al., 2005).

FeCH is an enzyme of special interest regarding the regulation of tetrapyrrole biosynthesis. FeCH activity may regulate the flux down both the heme and Chl branches of the pathway via increased production of heme, which is expected to inhibit the synthesis of ALA at the start of the pathway through feedback control (Weinstein et al., 1993; Vothknecht et al., 1998; Goslings et al., 2004). Differential consumption of the common substrate PP_{IX} by FeCH and magnesium chelatase might also control partitioning at the Chl/heme branch point (for review, see Cornah et al., 2003). Finally, a mechanism whereby the Chl branch exerts control over the heme pathway would provide an even more sophisticated mode of control at this biosynthetic branch point. We have recently demonstrated that FeCH activity influences Chl biosynthesis, as decreased activity of this enzyme was followed by a significant increase in the rate of ALA formation, in the level of Chl precursors, and in the accumulation of Chl-protein complexes (Sobotka et al., 2005, 2008b).

An intriguing feature of FeCH from cyanobacterial and algal sources is the hydrophobic C-terminal Chl *a/b*-binding (CAB) domain, with a high degree of similarity to the first and third helices of the plant light-harvesting complex II (LHCII) including a Chl-binding motif (Supplemental Fig. S1; Dolganov et al., 1995). Interestingly, the CAB domain is also a part of the FeCH isoform II responsible for the production of most of the heme in chloroplasts of higher plants (Papenbrock et al., 2001). This highly conserved CAB domain is connected to the FeCH catalytic core by a more variable region II, a short, hydrophobic, and Pro-rich sequence (Fig. 1A; Supplemental Fig. S1). This segment is preserved even in a few organisms harboring a plastid-type FeCH enzyme that lacks the CAB domain. This was shown for two cyanobacteria, *Synechococcus* JA-2-3Ab and JA-2-3B′a (Supplemental Fig. S1; Kilian et al., 2008) and for the green alga *Chromera velia* (L. Koreny, R. Sobotka, and M. Obornik, unpublished data; Supplemental Fig. S1). The only known plastid-type FeCH lacking both region II and the CAB domain is from the cyanobacterium *Gloeobacter*, which also lacks thylakoid membranes (Supplemental Fig. S1).

Although the functions of both the CAB domain and region II are unknown, we have recently demonstrated that deletion of both of these FeCH features in the

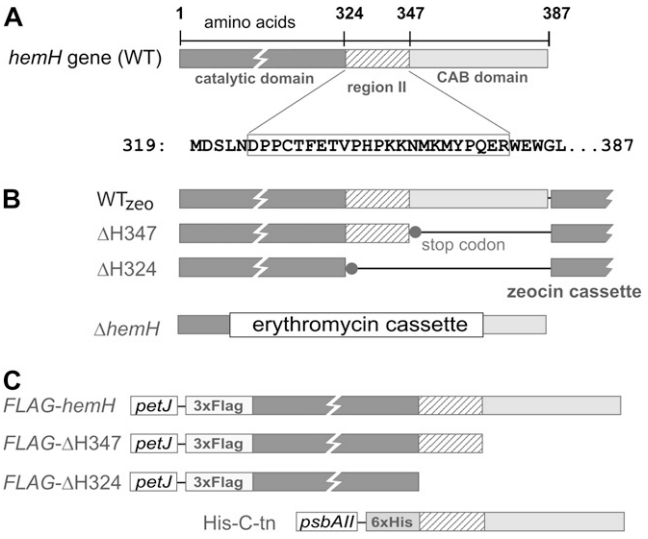

Figure 1. A, Schematic presentation of the *Synechocystis* FeCH (coded by the *hemH* gene) with catalytic and C-terminal CAB domains connected by region II. WT, Wild type. B, Strains with truncated FeCH used in this study; WT_{zeo} and ΔH324 were already described (Sobotka et al., 2008b). The Δ*hemH* deletion was combined with the *FLAG-hemH* background (see below) to construct the *FLAG-hemH*/Δ*hemH* strain, which expressed the tagged version as the only FeCH enzyme in the cell. C, Constructs used to express full-length and truncated versions of FeCH fused to a protein tag in *Synechocystis*. 3xFLAG-tagged FeCHs were expressed under the control of the *Synechocystis petJ* promoter; the His-C-tn strain expressed the 63-residue-long C-terminal fragment of *Synechocystis* FeCH as a small His_6-tagged protein under the control of the *Synechocystis psbAII* promoter.

ΔH324 strain of the cyanobacterium *Synechocystis* sp. PCC 6803 (hereafter *Synechocystis*) dramatically reduces the stability and activity of FeCH and leads to a large accumulation of its substrate, PP_{IX} (Sobotka et al., 2008b; Fig. 1B). In addition, analysis of both full-length and truncated ΔH324 recombinant FeCHs demonstrated that the C-terminal extension comprising region II and the CAB domain is essential for dimerization of the enzyme (Sobotka et al., 2008b).

In order to dissect the functional and structural roles of region II and the CAB domain, we have analyzed in this work another FeCH mutant, ΔH347, that retains region II but lacks the CAB domain (Fig. 1B). We have found comparable levels of the FeCH protein and of in vitro activity for the wild type and truncated ΔH347-FeCH, in marked contrast with the very low residual activity of the "fully truncated" ΔH324-FeCH. However, deletion of the CAB domain prevented the ΔH347 strain from growing at higher light intensities and affected the cellular accumulation of tetrapyrroles. In particular, we have found that although the ΔH347 mutant contains a decreased level of PP_{IX}, it specifically accumulates chlorophyllide (Chlide) and fails to reduce cellular levels of Chl-protein complexes under high light. Analysis of the full-length and truncated FeCHs purified from *Synechocystis* under native con-

ditions demonstrated that whereas the full-length enzyme forms a dimer, the ΔH347-FeCH is active as a monomer. The essential role of the CAB domain for the dimerization of FeCH in vivo was further confirmed by copurification of the full-length FeCHs from the cell using the tagged C-terminal segment of FeCH as bait.

RESULTS

The C-Terminal Domains of FeCH Are Required for the Acclimation of *Synechocystis* to High Light

To address the proposed role of the FeCH CAB domain in the regulation of tetrapyrrole metabolism and also to elucidate the function of region II, we constructed the *Synechocystis* mutant ΔH347, which retains the 23-residue region II but lacks the last 40 residues that constitute the putative transmembrane CAB domain (Fig. 1). Another FeCH mutant, ΔH324, prepared for previous work (Sobotka et al., 2008b), was also included in this study. This mutant differs from ΔH347 only by the additional absence of region II at the end of the FeCH catalytic domain (Fig. 1B); thus, a direct comparison of both strains should help to discriminate between the effects of both region II and the CAB domain.

First, we compared the photoautotrophic growth of both mutants and of the control wild-type strain, WT_{zeo} (Fig. 1B), under different light intensities. Under low light (5 μmol photons m^{-2} s^{-1}), all strains had comparable growth rates and also very similar levels of photosynthetic pigments (Table I; Supplemental Fig. S2). However, at normal light (40 μmol photons m^{-2} s^{-1}), the ΔH324 mutant grew significantly more slowly, and with a further increase in light intensity to 150 μmol photons m^{-2} s^{-1}, we observed a rapid loss of photosynthetic pigments. A further increase in light intensity abolished the growth of this strain (Table I; Supplemental Fig. S2). The effect of increased light intensity on the ΔH347 mutant was much less pronounced; its growth was only slightly impaired at normal light, and this strain was able to grow up to 200 μmol photons m^{-2} s^{-1} (hereafter high light; Table I). Further increase in light intensity to 250 μmol photons m^{-2} s^{-1} also completely inhibited the growth of the ΔH347 mutant, whereas the growth of the control WT_{zeo} strain was not significantly affected (Table I). Interestingly, the ΔH347 mutant did not exhibit any "bleaching" at high light, as we observed for ΔH324; on the contrary, the ΔH347 mutant retained about 40% more Chl per cell than the WT_{zeo} strain after approximately 40 h at high light (Table I; Supplemental Fig. S2). This is noteworthy, as a substantial decrease in Chl level is a typical response of *Synechocystis* to high light (Hihara et al., 1998; see control WT_{zeo} strain in Table I and Supplemental Fig. S2).

These results demonstrate that both the CAB and the region II domains are essential for photosynthetic growth of *Synechocystis* at high light intensities. However, the presence of region II of FeCH substantially improves acclimation to high light, and furthermore, the phenotypes of both FeCH mutants clearly differ under increased light intensities: whereas the ΔH324 strain loses most of its pigments probably due to the destruction of thylakoid membranes, the ΔH347 mutant retains a higher level of Chl, indicating that the viability of ΔH324 and ΔH347 mutants upon a shift to high light is abolished by different processes.

The CAB Domain Is Important for Regulation of the Tetrapyrrole Pathway

A remarkable feature of the ΔH324 strain was the excretion of PP_{IX} into the growth medium at levels high enough to produce a brown color (Sobotka et al., 2008b). As we did not observe this effect in ΔH347, we compared the accumulation of PP_{IX} and Chl intermediates in both mutants grown at normal light levels to elucidate the effect of these two protein truncations on tetrapyrrole metabolism. Surprisingly, we found that levels of tetrapyrroles in these strains are very different: whereas the ΔH324 accumulates high levels of PP_{IX} and also other intermediates in the Chl branch (Fig. 2A; Sobotka et al., 2008b), ΔH347 contains less than 20% of the PP_{IX} found in the control WT_{zeo} strain. On the other hand, levels of magnesium protoporphyrins and protochlorophyllide (PChlide) in the ΔH347 strain are not significantly affected, with the exception of the approximately 2.5-fold increase in the content of the last Chl precursor, Chlide (Fig. 2A).

The observed low PP_{IX} content of the ΔH347 mutant could indicate reduced ALA formation at the beginning of the pathway; however, measurements of ALA-synthesizing capacity revealed only a slightly increased

Table I. *Growth rate and Chl content of studied Synechocystis strains under different light regimes*

n.g., No growth (strain did not grow under these conditions).

Strain	Light Intensity (μmol photons m^{-2} s^{-1})							
	5		40		200		250	
	Doubling Time	Chl	Doubling Time	Chl	Doubling Time	Chl	Doubling Time	Chl
	h	$\mu g\ mL^{-1}\ OD_{750}^{-1}$	*h*	$\mu g\ mL^{-1}\ OD_{750}^{-1}$	*h*	$\mu g\ mL^{-1}\ OD_{750}^{-1}$	*h*	$\mu g\ mL^{-1}\ OD_{750}^{-1}$
WT_{zeo}	58	5.5 ± 0.1	13.7	5.1 ± 0.2	9.8	2.6 ± 0.15	12.1	2.1 ± 0.1
ΔH347	61	5.5 ± 0.15	14.6	5.7 ± 0.2	21	3.6 ± 0.25	n.g.	n.g.
ΔH324	56	5.8 ± 0.2	20.1	4.9 ± 0.3	n.g.	n.g.	n.g.	n.g.

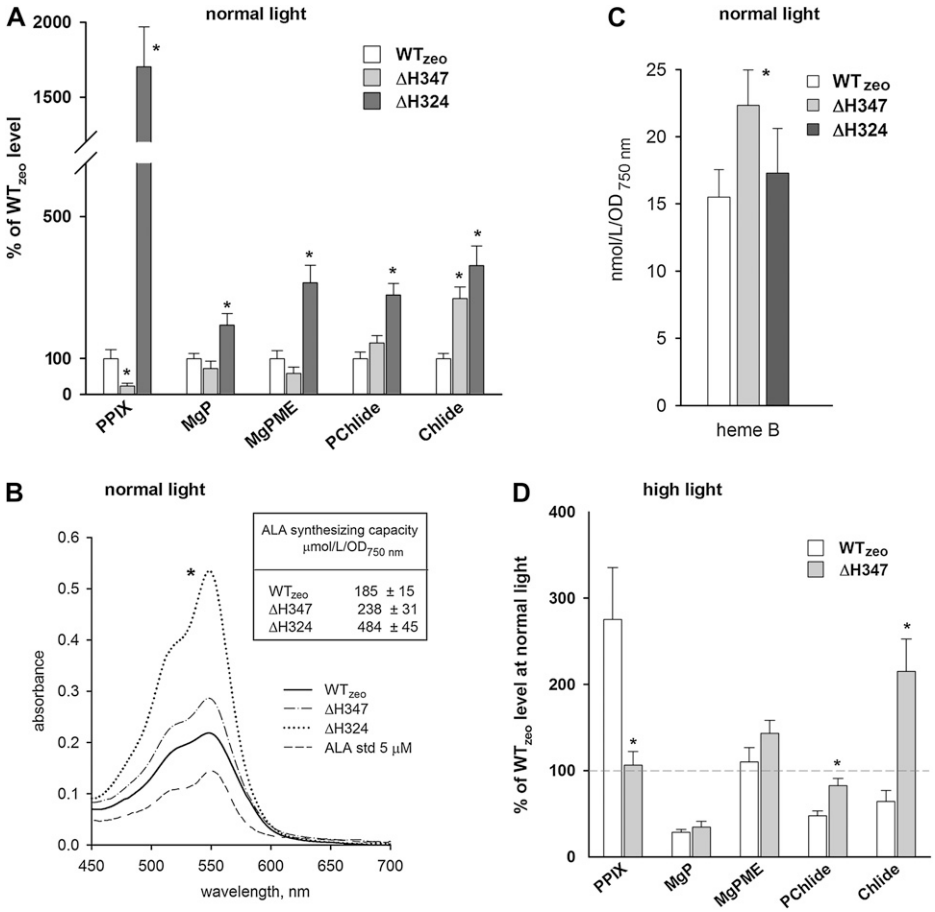

Figure 2. Analysis of pigments in *Synechocystis* mutant strains. A, Quantification of the relative contents of PP_{IX}, MgP, magnesium protoporphyrin IX methylester (MgPME), PChlide, and Chlide in *Synechocystis* cells growing at normal light (40 μmol photons m^{-2} s^{-1}) and harvested at OD_{750} = 0.35 to 0.4. Chl precursors were extracted with methanol/0.2% NH_4OH and quantified by a combination of HPLC and spectrofluorometry. Values shown represent means ± SD from three independent measurements; asterisks indicate significant differences tested using a paired *t* test ($P = 0.05$). B, ALA-synthesizing capacity as determined in a 100-mL cell suspension with OD_{750} = 0.4 treated for 4 h with levulinic acid to inhibit ALA condensation into porphobilinogen. Representative absorption spectra of developed assays as obtained for each strain together with 5 μM standard of ALA are also presented. C, Quantification of noncovalently bound heme B (protoheme) in cells growing at normal light. Heme was extracted by 90% acetone/2% HCl, separated, and quantified using HPLC. Error bars and the *t* test of statistical significance are as in A. D, Quantification of the relative contents of Chl precursors in *Synechocystis* cells growing for approximately 40 h at high light (200 μmol photons m^{-2} s^{-1}) and harvested at OD_{750} = 0.35 to 0.4. Obtained values from three measurements were compared with values for the control WT_{zeo} strain growing at normal light. The dashed line indicates 100% in comparison with values at normal light (A). Asterisks indicate statistically significant differences in precursor levels between WT_{zeo} and ΔH347 at high light as tested using a paired *t* test ($P = 0.05$).

rate of ALA formation in the ΔH347 mutant in comparison with WT_{zeo} (Fig. 2B). This contrasts with a significantly elevated ALA formation in the ΔH324 mutant, which is probably responsible for the accumulation of PP_{IX} in this strain (Fig. 2B; Sobotka et al., 2008b). So, detected changes in tetrapyrrole biosynthesis in ΔH347 do not appear to be caused predominantly by elevated metabolic flow through the whole pathway, as in the case of the ΔH324 mutant, but rather by different events at the heme/Chl branch point between heme and Chl branches influencing the PP_{IX} pool and at the final steps of the pathway resulting in the accumulation of Chlide.

The low pool of PP_{IX} in ΔH347 could be explained by a rapid "uncontrolled" consumption of PP_{IX} either by magnesium chelatase or by truncated ΔH347-FeCH. The first possibility is not consistent with the almost normal level of MgP in ΔH347. Moreover, we did not observe higher cellular levels of the magnesium chelatase subunits (Fig. 3A). The second possibility, a rapid consumption of PP_{IX} by mutated ΔH347-FeCH, could be reflected in higher levels of cellular heme or phycobilins. To determine levels of heme B (protoheme), total noncovalently bound heme was extracted by acetic acetone as described in "Materials and Methods," separated by HPLC, and quantified spec-

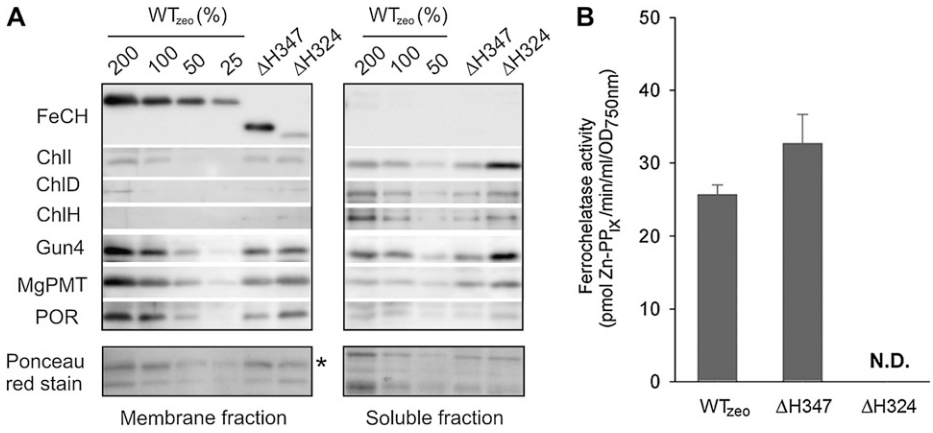

Figure 3. Accumulation of enzymes of tetrapyrrole biosynthesis, and in vitro activity of FeCH in *Synechocystis* strains. A, Membrane and soluble protein fractions were prepared as described in "Materials and Methods," separated by SDS electrophoresis, and blotted to a membrane. Enzymes were detected by specific antibodies. The amount of proteins loaded for 100% of each sample corresponded to 150 μL of cells at OD_{750} = 1. ChlI, ChlD, and ChlH are subunits of magnesium chelatase (Jensen et al., 1996), and Gun4 is another protein required for the activity of magnesium chelatase (Larkin et al., 2003; Sobotka et al., 2008a). MgPMT, Magnesium-protoporphyrin methyl transferase; POR, light-dependent PChlide oxidoreductase. Below are blotted proteins stained with Ponceau red shown as a loading control; the peripheral subunit of ATPase is marked by an asterisk. B, In vitro FeCH activity in membranes as determined by a continuous spectrofluorometric assay. Activities were monitored as an increase in fluorescence of zinc-PP_{IX} using excitation and emission wavelengths of 420 and 590 nm, respectively. N.D., Not detected.

troscopically. Indeed, the heme content of ΔH347 was significantly increased (Fig. 2C). Interestingly, the heme content of the ΔH324 mutant was not affected (Fig. 2C), suggesting that the ΔH324-FeCH is able to produce enough of the heme required for normal cellular function, despite a barely detectable in vitro activity of this truncated enzyme (Sobotka et al., 2008b; see below). We did not observe significant changes in phycobilisome levels in any of the strains studied, implying that the accumulation of the light-harvesting apparatus is under tight control and is not influenced by disturbances in tetrapyrrole biosynthesis (Supplemental Fig. S2).

The enlarged pool of Chlide in the ΔH347 mutant is not easy to explain with regard to the position of FeCH in the pathway and normal or lower levels of other Chl precursors. It should also be noted that the ΔH347 mutation did not significantly alter the accumulation or cell localization of enzymes in the Chl pathway, including the enzyme producing Chlide, PChlide oxidoreductase (Fig. 3A). However, Chlide is the last precursor of the Chl biosynthesis pathway; thus, its accumulation could be related to the failure of ΔH347 to adjust the levels of Chl-protein complexes according to light conditions. Therefore, we compared the levels of Chl precursors in WT_{zeo} and ΔH347 at high light when the growth rate of ΔH347 was retarded (Table I). Whereas the content of Chlide in the control strain decreased when compared with the situation in normal light, the content of Chlide in the ΔH347 remained almost unchanged (Fig. 2D), suggesting that the FeCH CAB domain is required for regulation of the final step (s) of Chl biosynthesis, which could include the attachment of Chl to proteins and Chl turnover (see "Discussion").

To summarize, it is evident that the two different truncations at the FeCH C terminus have very different consequences for tetrapyrrole metabolism. Elimination of both region II and the CAB domain from FeCH results in a greatly elevated synthesis of PP_{IX} and a consequent increase in the flux down the green branch of tetrapyrrole biosynthesis. In contrast, the ΔH347 strain that retains region II contains only a small PP_{IX} pool but exhibits increased accumulation of Chlide under different light regimes. These results highlight the importance of region II and the CAB domain of FeCH for both its enzymatic and regulatory functions.

Region II Is Critical for Both the Stability and Enzyme Activity of *Synechocystis* FeCH

We have shown previously that truncation of the whole C-terminal domain of *Synechocystis* FeCH strongly impairs the stability and activity of the resulting ΔH324 enzyme (Sobotka et al., 2008b). To elucidate the completely different effect of the ΔH347 mutation on tetrapyrrole metabolism, we compared the activity and stability of mutated and full-length FeCHs.

To assess the localization and cellular levels of the ΔH347-FeCH, a whole-cell extract of the ΔH347 mutant was fractionated into cytosolic and membrane fractions, separated by SDS-PAGE, and subjected to immunodetection using anti-FeCH antibody raised against recombinant *Synechocystis* FeCH. The ΔH347-FeCH was detected only in the membrane fraction

despite the lack of the putative transmembrane CAB domain. However, in contrast to the ΔH324 enzyme, both the FeCH levels and in vitro FeCH activities were comparable in membrane fractions from the ΔH347 and WT_{zeo} strains (Fig. 3). As we did not observe any in vitro activity for the ΔH324 enzyme, it is evident that the presence of region II dramatically improves both the stability and the activity of *Synechocystis* FeCH.

To further determine possible structural functions for both the region II and CAB C-terminal FeCH domains, we analyzed enzymes purified under nondenaturing conditions from *Synechocystis* using the 3xFLAG tag (FLAG hereafter). To show that the presence of the tag did not interfere with the enzyme function, we deleted the native *hemH* gene in the *FLAG-hemH* strain, resulting in a strain expressing just the tagged FeCH version (Fig. 1B). The *FLAG-hemH*/Δ*hemH* strain did not display any apparent effects of FeCH deficiency, such as retarded growth or accumulation of PP_{IX}, and the in vitro activity of the FLAG-FeCH in the cell extract corresponded with the enzyme content (data not shown).

Both full-length and truncated FeCHs were expressed in *Synechocystis* and purified from cell extracts under native conditions using anti-FLAG resin; the migration of purified proteins on SDS electrophoresis corresponded to theoretical masses of 46.2, 41.7, and 38.9 kD for the FLAG-FeCH, FLAG-ΔH347, and FLAG-ΔH324, respectively (Fig. 4A). Activities of purified FeCHs were compared using an in vitro assay (Fig. 4B). Consistent with previous results on recombinant FeCHs (Sobotka et al., 2008b), deletion of both the region II and the CAB domains dramatically impaired activity of the ΔH324-FeCH (less than 5% of the full-length enzyme activity; Fig. 4B). The specific activity of the FLAG-ΔH347 enzyme was also about 20% of that of the wild-type enzyme. Intriguingly, the rate of incorporation of zinc into PP_{IX} by ΔH347-FeCH rapidly decreases in the first 50 s of the assay, whereas the rate of incorporation of zinc by the full-length tagged enzyme is almost linear for at least 10 min (Fig. 4B). It should be noted that the activity of nontagged ΔH347-FeCH in purified membranes exhibits the same decrease in the rate of zinc-PP_{IX} formation (data not shown). This implies that although the CAB domain is important for functioning of the FeCH, further truncation involving region II affects the FeCH accumulation and activity much more strongly.

The CAB Domain Is Necessary for the Dimerization of *Synechocystis* FeCH in Vivo

Using recombinant *Synechocystis* FeCHs, we have previously shown that deletion of the C terminus in ΔH324-FeCH abolishes dimerization of the recombinant enzyme and leads to the loss of its activity (Sobotka et al., 2008b). This led us to the assumption that, in agreement with the situation in mitochondrial FeCH (Grzybowska et al., 2002; Ohgari et al., 2005), the dimer is the active form of the *Synechocystis* FeCH. Given that the purified ΔH347-FeCH is fairly active and the same enzyme is fully active in membranes (Fig. 3B), we speculated that region II might promote dimerization, resulting in an active enzyme. However, on a native gel, the purified FLAG-ΔH347-FeCH migrated strictly as a monomer, in contrast to the dimeric full-length FLAG-FeCH (Fig. 5A). To facilitate further analysis of enzyme dimerization, all three purified tagged enzymes were separated using size-exclusion chromatography, and the FeCH activity of the column fractions was measured. According to the A_{280} (Fig. 5B), the full-length FeCH migrates as a broad peak mainly as a dimer but with a significant fraction of monomers and also a small proportion of higher mass aggregates (compare with Fig. 5A), whereas both truncated enzymes migrate in a sharp peak corresponding to monomers with bound detergent molecules (Fig. 5B). Note that it is generally problematic to determine the mass of membrane proteins on gel fil-

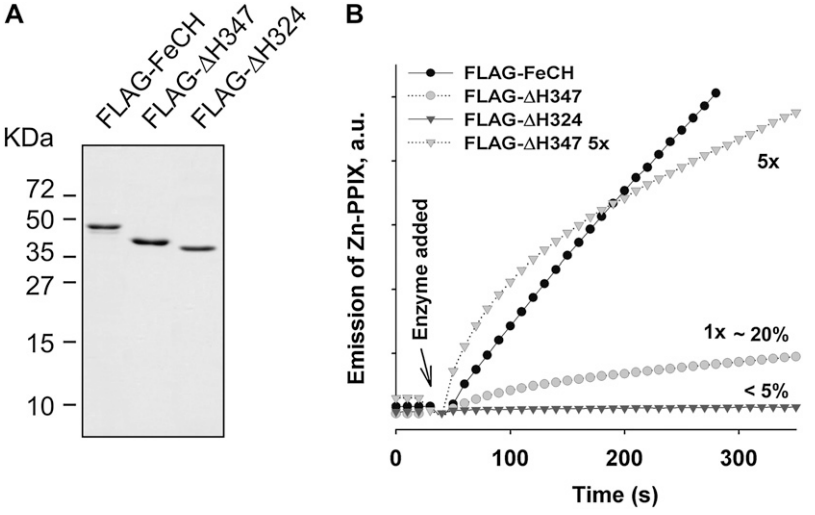

Figure 4. Full-length and truncated FeCH enzymes purified from *Synechocystis*. A, FLAG-tagged full-length and truncated FeCHs were purified under native conditions on the anti-FLAG affinity gel, separated by SDS electrophoresis, and stained by Coomassie Brilliant Blue; approximately 0.5 μg of protein was loaded in each line. B, In vitro activities of purified FeCH enzymes as determined by continuous spectrofluorometric assay. Activities were monitored as an increase in fluorescence of zinc-PP_{IX} using excitation and emission wavelengths of 420 and 590 nm, respectively; 1x indicates that approximately 0.1 μg of enzyme was assayed. Relative activities of truncated enzymes in comparison with the full-length FeCH (100%) are also indicated.

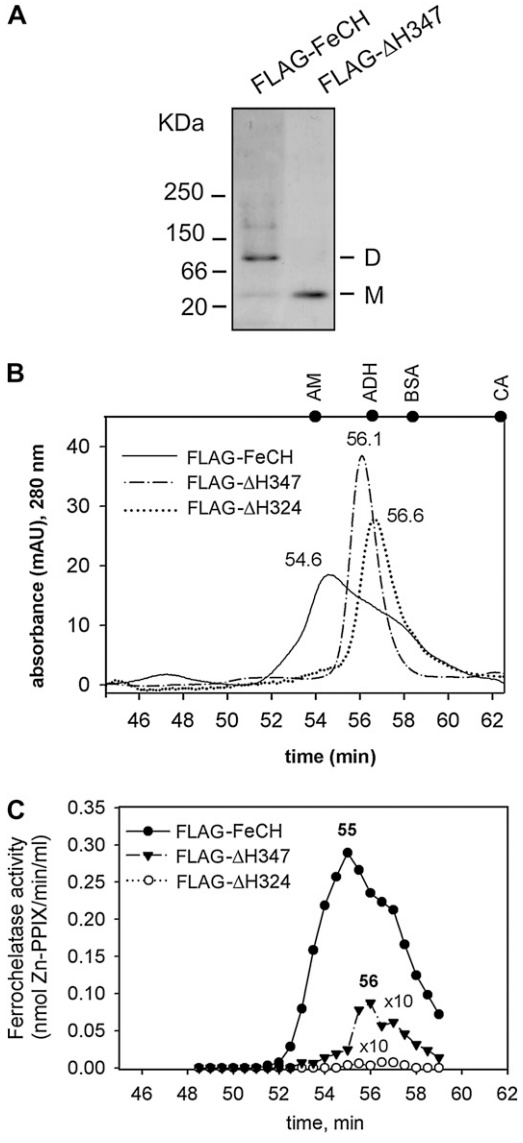

Figure 5. Aggregation state of purified FeCHs. A, Approximately 0.5 μg of the purified wild-type and truncated FeCH was separated by nondenaturing electrophoresis and stained by Coomassie Brilliant Blue. M and D indicate the positions of FeCH monomer and dimer, respectively. B, Gel filtration of the FLAG-FeCH and truncated FeCH enzymes on the BioSep SEC-S3000 column. Approximately 1 μg of each protein was separated. Positions of standards are shown at the top of the graph: AM = β-amylase (200 kD); ADH = alcohol dehydrogenase (150 kD); BSA = bovine serum albumin (66 kD); CA = carbonic anhydrase (29 kD). C, FeCH activity in 0.5-min fractions as eluted from the gel filtration column during separation of purified FeCH enzymes (described in B). The whole volume of each fraction (75 μL) was assayed immediately after elution in an in vitro FeCH assay. Obtained values for truncated enzymes were multiplied 10-fold to compare activity profiles.

tration, as calibration of a column with soluble proteins leads to inaccurate results (Zouni et al., 2005). However, the results in Figure 5 are internally consistent and show that although the mass of the FLAG-ΔH347 protein is only 2.8 kD larger than that of FLAG-ΔH324, its mobility is 0.5 min slower, which corresponds to approximately 25 kD according to our column calibration (Fig. 5B). This could indicate that the loss of region II is accompanied by a significant difference in the conformation of the FeCH protein.

The FeCH activity profile for the collected fractions for the full-length enzyme corresponded well with the protein absorbance, including an obvious shoulder at the position of a predicted monomer (Fig. 5C). This result indicates similar in vitro specific activities for both the dimeric and monomeric forms of the enzyme. The maximum activity of the FLAG-ΔH347-FeCH was measured in the elution peak fraction resembling the monomeric form. Therefore, we expect that the FLAG-ΔH347 was active in the assay in a monomeric form. It should be noted that a substantial portion of the total FLAG-ΔH347 activity was lost during gel filtration, suggesting a lower stability for this truncated enzyme when compared with the full-length FeCH, which was still highly active when eluted from the column (Fig. 5C). As expected, no activity was detected when a similar amount of the FLAG-ΔH324 was analyzed by the same method (Fig. 5C).

Although previous results strongly support a model where the CAB domain is responsible for FeCH dimerization and the ΔH347-FeCH is therefore a partially active monomer in vivo, it cannot be excluded that dimerization of *Synechocystis* FeCH is driven by having a high concentration of pure protein. To obtain further evidence that the full-length FeCH physically interacts with another FeCH molecule in vivo, we employed the *FLAG-hemH* strain expressing both the FLAG-FeCH and nontagged wild-type FeCH. As these two enzyme forms have different mobilities on SDS-PAGE, they can be distinguished by immunodetection using a combination of anti-FeCH and anti-FLAG antibodies (Fig. 6A). After isolation of the FLAG-FeCH on an anti-FLAG affinity gel, the smaller native FeCH was specifically copurified with FLAG-FeCH, and it was the only copurified protein visible on the Coomassie Brilliant Blue-stained gel (Fig. 6A).

To resolve the question of whether the CAB domain alone is sufficient to promote the formation of dimeric FeCH and to investigate whether another part of this enzyme is essential for FeCH-FeCH interaction in vivo, we prepared a *Synechocystis* strain expressing the FeCH C terminus, consisting of region II and the CAB domain, as a small His_6-tagged protein (His-C-tn; Fig. 1C). This artificial protein, lacking the extrinsic catalytic domain, was expressed both in the wild type and the ΔH347 strains and used as in vivo bait for FeCH. If the CAB domain is the only segment required for the FeCH dimerization, the His-C-tn protein would form a stable complex only with the full-length FeCH but not with the truncated ΔH347 enzyme. The His-C-tn protein was purified on a nickel column under native conditions and subjected to gel electrophoresis, and coisolated FeCH was detected by anti-FeCH antibody (Fig. 6B). The full-length FeCH clearly copurified with His-C-tn in contrast to ΔH347-FeCH,

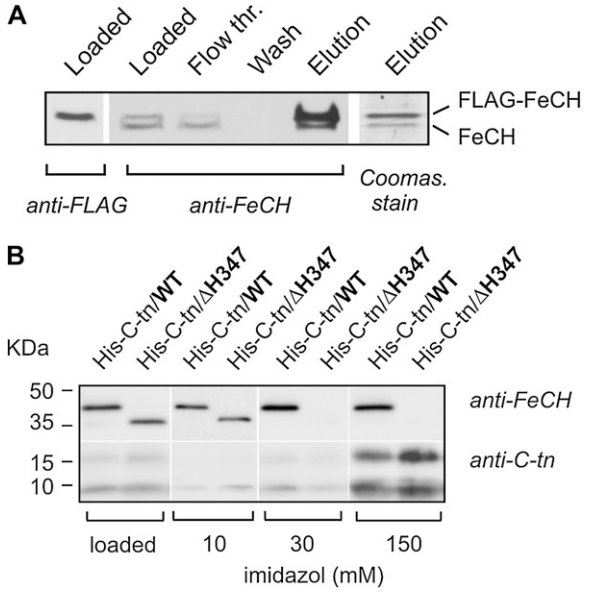

Figure 6. A, Purification of the FLAG-FeCH in a complex with nontagged FeCH. FLAG-FeCH was purified from the *FLAG-hemH* strain possessing both tagged and nontagged forms of this enzyme; purification was carried out under native conditions on the anti-FLAG affinity gel as described in "Materials and Methods." Each purification step was separated by SDS electrophoresis and blotted, and both FeCH forms were detected by anti-FeCH antibody; eluted proteins separated by SDS electrophoresis were also stained by Coomassie Brilliant Blue. The position of the FLAG-FeCH was resolved by anti-FLAG antibody. B, Purification of the FeCH C-terminal fragment and its copurification with the full-length FeCH and the ΔH347-FeCH lacking the CAB domain. The 63-residue-long C-terminal fragment of *Synechocystis* FeCH was expressed as a His-tagged protein (His-C-tn) in the wild type (WT) and in the ΔH347 backgrounds and purified from both strains using Ni^{2+} affinity chromatography. As the polyclonal anti-FeCH antibody recognized the C-terminal parts of the protein only weakly, the His-C-tn was detected using an antibody raised against a synthetic peptide corresponding to region II of the *Synechocystis* FeCH (amino acids 333–348). The amount of membrane protein loaded for each sample corresponded to 150 μL of cells at OD_{750} = 1, 1/50th the volume of each washing step (20 μL from 1 mL), and 1/25th the total elution volume. The imidazole elution is described in "Materials and Methods."

confirming in vivo dimerization via the CAB domain (Fig. 6B). Moreover, the His-C-tn protein formed a stable dimer with another His-C-tn molecule, which partly persisted even during separation by denaturing SDS electrophoresis (Fig. 6B). Based on these data, it can be concluded that the CAB domains have affinity for one another and that this domain is strictly required for dimerization of the *Synechocystis* FeCH in vivo.

DISCUSSION

Cyanobacterial and algal FeCHs as well as the plant FeCH2 isoform possess a unique conserved C-terminal CAB domain with a putative Chl-binding motif (Supplemental Fig. S1). The CAB domain and the FeCH catalytic core are connected by a "linker" (region II), which is quite variable in its length and sequence among organisms (Supplemental Fig. S1). Recently, we have demonstrated that the elimination of both region II and the CAB domain from FeCH in the *Synechocystis* ΔH324 mutant dramatically impaired the activity and stability of the truncated FeCH (Sobotka et al., 2008b). Given the essential role of dimerization for the function of human and yeast FeCHs (Grzybowska et al., 2002; Ohgari et al., 2005), the low activity of the ΔH324-FeCH was originally attributed to the absence of the CAB domain, yielding a monomeric enzyme (Sobotka et al., 2008b). However, newly discovered thermophilic *Synechococcus* strains possessing putative monomeric FeCHs lacking the CAB domain but still preserving the short region II (Kilian et al., 2008; Supplemental Fig. S1) stimulated us to mimic these naturally occurring FeCH variants by preparing the ΔH347 strain lacking only the CAB domain. Importantly, elimination of the CAB domain yielded an enzyme with comparable specific activity to the wild-type FeCH (Fig. 3). Direct comparison of ΔH347 with the ΔH324-FeCH lacking both the region II and CAB domains reveals the crucial importance of region II and enabled us, to our knowledge for the first time, to explore the role of the FeCH CAB domain in the regulation of tetrapyrrole biosynthesis.

Our earlier work on the ΔH324 strain (Sobotka et al., 2008b) posed an intriguing question as to why this mutant, possessing a strongly impaired FeCH, does not display any depletion in phycobilins, which are produced by oxidation of heme (Supplemental Fig. S2). Our work here helps to address this issue by demonstrating that the low activity of ΔH324-FeCH is more than sufficient to furnish the cellular demand for heme (Fig. 2C). However, it is still unclear why the wild-type cell maintains FeCH at levels much higher than those actually required by the demands placed on heme biosynthesis. It is noteworthy that under low light or microaerobic conditions, the ΔH324 mutant resembles the wild-type phenotype: it exhibits normal pigmentation and growth rate and does not release PP_{IX} into the growth medium (Table I; Supplemental Fig. S2; R. Sobotka, unpublished data). These data suggest that under low-stress conditions, traces of FeCH activity are sufficient. Nonetheless, at increased light intensity, the growth of the ΔH324 mutant is significantly retarded, and a further increase in light intensity to 150 μmol photons m^{-2} s^{-1} caused cell bleaching, probably due to the destruction of thylakoid membranes (Table I; Supplemental Fig. S2). It appears that under such conditions, the high content of FeCH found in the wild type is essential for cell viability to avoid accumulation of the high levels of phototoxic PP_{IX} and other porphyrins found in the ΔH324 mutant.

Based on these data and on our previous results (Sobotka et al., 2005), we expect that the FeCH enzyme is involved in the regulation of tetrapyrrole biosynthesis and that the high content of the enzyme per cell, in relation to the biosynthetic demand for heme, has

regulatory implications. Our previous work suggested a regulatory role for FeCH: the cellular FeCH activity increased 3- to 4-fold in *Synechocystis* mutants impaired in PSII assembly and led to a decrease in metabolic flow through the tetrapyrrole pathway (Sobotka et al., 2005). The cell could balance the distribution of PP_{IX} between both chelatases and could also combat the detrimental effects of a stressful and fluctuating environment using a surplus of "silent" FeCH to dissipate escalating levels of phototoxic PP_{IX}. In the cyanobacterium *Thermosynechococcus elongatus*, FeCH was found to physically interact with protoporphyrinogen oxidase, the enzyme that produces its substrate PP_{IX} (Masoumi et al., 2008). It is possible that the delivery of PP_{IX} to FeCH is controlled via the formation of such a complex and, if needed, the FeCH quickly interacts with protoporphyrinogen oxidase and channels photosensitizing PP_{IX} into the safer heme metabolite, with the bonus of inhibiting ALA synthesis via a heme feedback loop (see below). In our model, FeCH activity, which includes its access to PP_{IX}, modulates the flow of this metabolite into the heme or Chl branches. The ΔH347 strain shows higher content of noncovalently bound heme but has a low pool of PP_{IX}, although its ALA capacity is comparable to the wild type (Fig. 2). This indicates that the ΔH347 mutant is deficient in the control of PP_{IX} distribution, and we speculate that deletion of the CAB domain facilitates the access of truncated FeCH to PP_{IX}.

According to current models of the regulation of tetrapyrrole biosynthesis, increased consumption of PP_{IX} by FeCH should inhibit the GluTR enzyme via a heme feedback loop (for recent reviews, see Tanaka and Tanaka, 2007; Masuda and Fujita, 2008). However, although an allosteric inhibition of GluTR by heme in plants is supported by convincing evidence, the model of free heme directly interacting with the GluTR and modulating the activity of this enzyme is probably oversimplified. In *Chlamydomonas*, inhibition of the GluTR activity by heme depends on the presence of an unidentified soluble protein (Srivastava et al., 2005), and heme paradoxically stimulates expression of the gene coding for GluTR (Vasileuskaya et al., 2005). In nonphotosynthetic bacteria, heme controls proteolytic degradation of GluTR, and in the acidophilic bacterium *Acidithiobacillus ferrooxidans*, heme also regulates the activity of glutamyl-tRNA synthase (Wang et al., 1999; Levicán et al., 2007). The role of heme in the tetrapyrrole signaling network is thus quite complex, and it is not so surprising that the increased protoheme level in the ΔH347 strain did not result in a decreased rate of ALA formation (Fig. 2B). It should be noted that the ΔH324 strain, where ALA synthesis is clearly stimulated, has a practically unchanged protoheme content per cell, so there might be a specific pool of heme used for signaling. However, as almost nothing is known about mechanisms balancing the production of different heme forms (B, A, C) together with linear tetrapyrroles, a regulatory role of a putative heme pool remains speculative.

As we already discussed, the ΔH324 dies at high light probably due to massive accumulation of PP_{IX} and also other porphyrins. The growth of the ΔH347 mutant is also impaired by high light intensities, although it does not accumulate any tetrapyrroles other than Chlide (Table I); interestingly, at the same time, this strain contains approximately 40% more Chl per cell than WT_{zeo}. We expect that the failure of ΔH347 to grow at high light is not caused primarily by a high concentration of phototoxic tetrapyrroles but due to an inability of this strain to control the synthesis and turnover of Chl-protein complexes. A similar "stay-green" phenotype was already described in the *Synechocystis pmgA* mutant, which had lost the ability to regulate photosystem stoichiometry, particularly to decrease the level of PSI relative to PSII upon a switch to high light (Hihara et al., 1998). Such an adjustment of the PSI/PSII ratio was shown to be essential for the survival of *Synechocystis* when grown at 300 μmol photons m^{-2} s^{-1} (Sonoike et al., 2001), and since PSI contains most of the Chl in the cell, the process of high-light acclimation results in a remarkable decrease in total Chl content per cell (see WT_{zeo} in Table I). Interestingly, the down-regulation of PSI was reported to be determined primarily by limited availability of Chl for the synthesis of PSI subunits (Muramatsu et al., 2009); thus, this process can be affected by an elevated level of Chlide, the last Chl precursor. On the other hand, the regulation of the PSI/PSII ratio cannot be accomplished simply by a total restriction of Chl formation but rather by Chl redirection, as, in contrast to PSI, the synthesis of PSII subunits is accelerated under high-light stress due to a faster turnover of PSII (Nowaczyk et al., 2006). We expect that a sophisticated mechanism exists ensuring the distribution of Chl to Chl-binding proteins under changing environmental conditions and that such an apparatus has to recycle Chlide originating from degraded Chl-protein complexes via Chl turnover (Vavilin and Vermaas, 2007).

The presence of a Chl-binding motif in the FeCH CAB domain led us to the speculation that this domain is involved in the mechanism proposed above to balance Chl biosynthesis, Chl turnover, and the synthesis of particular Chl-protein complexes. Using the FLAG-tagged FeCH and its C terminus as bait, we have provided clear evidence that the CAB domain mediates a specific interaction between FeCH molecules in vivo. In the FeCH dimer, the interacting CAB domains should resemble the "cross helix" structure found in the LHCII complex of higher plants; the Chl-binding motif ExxNGR is preserved in the CAB domain (Supplemental Fig. S1; Liu et al., 2004). Our data thus support the possibility of Chl(ide) interacting with the CAB domain and may form an (alternative) route for the transfer of Chl(ide) to photosystem apoproteins. In this context, it is interesting that both cyanobacteria and plants contain high/early light-inducible proteins (ELIP/HLIP), which are structurally very similar to the FeCH CAB domain, including a conserved Chl-binding motif (Dolganov et al., 1995).

These proteins, which quickly accumulate at high levels upon a switch to high light, might form part of a dynamic network of interacting CAB domains in the membrane that perhaps transiently form a complex with the FeCH CAB domain, yielding a monomeric enzyme that is virtually fully active but localized adjacent to different protein complexes, with different affinity to Chl or with different access to PP_{IX}. Indeed, both ELIP and HLIP were found to regulate Chl biosynthesis (Xu et al., 2002; Tzvetkova-Chevolleau et al., 2007) and to physically interact with Chl-binding proteins (Promnares et al., 2006).

The CAB domain apparently has an important role also in the stability of *Synechocystis* FeCH; in contrast to the comparable membrane-associated catalytic activities of the wild type and the ΔH347-FeCH, the specific activity of the purified FLAG-ΔH347-FeCH was much lower (Fig. 4). This low specific activity is probably caused by lower stability of the enzyme, as the purified FLAG-ΔH347 enzyme lost its activity much faster than the full-length enzyme, which made it difficult for example to measure the activity of FLAG-ΔH347-FeCH separated by gel filtration. It is probable that one of the reasons for higher stability of the full-length FeCH is its dimerization.

The critical role of region II for the activity of *Synechocystis* FeCH is noteworthy, regarding its rather low sequence similarity among different groups of organisms and its position at the end of the extrinsic catalytic domain of the enzyme. The only common features perceptible from amino acid alignments are the rather hydrophobic nature of this sequence and a higher frequency of Pro residues (Supplemental Fig. S1). When compared with the structure of the spinach (*Spinacia oleracea*) LHCII (Liu et al., 2004), the FeCH CAB domain best corresponds to the third helix and the Pro-rich region II can be aligned with the stromal loop connecting the second and third helices (Supplemental Fig. S1). Indeed, this short sequence in LHCII contains five Pro residues that bend this region to form a curled but relatively flat structure on the membrane surface (Supplemental Fig. S3). So, the FeCH Pro-rich domain could form a similar structure, although we cannot account for the importance of this domain for enzyme activity/stability. A clue could be the unusual kinetics of the ΔH347-FeCH in our assay (Fig. 4B). The rapid decline in the initial rate of chelation is specific only for the ΔH347 enzyme, as the activity of recombinant ΔH324, although very weak, exhibits a linear rate of zinc-PP_{IX} formation (R. Sobotka, unpublished data). Also, this effect is not caused by low stability of the ΔH347 enzyme in the assay, as the purified FLAG-ΔH347-FeCH can be incubated in assay buffer without zinc for at least 15 min with no decrease in activity (data not shown). The observed kinetics could be related to zinc uptake by FeCH, which is known to be quite complex, as zinc, even at low concentrations, inhibits the release of product from the enzyme (Davidson et al., 2009). To clarify this question, a detail enzymological study is required.

We conclude that this study, based on a combined analysis of several *Synechocystis* strains and purified FeCHs, has demonstrated both regulatory and structural roles for the FeCH CAB domain and, unexpectedly, revealed a critical role of region II for the catalytic function of the plastid-type FeCH enzyme. In addition, as the mitochondrial FeCH is known to be active only as a homodimer (Grzybowska et al., 2002; Ohgari et al., 2005), the *Synechocystis* FeCH can be described as a new type of dimeric FeCH, since the deletion of the C-terminal CAB domain, responsible for dimerization, did not abolish the catalytic activity of the resulting monomeric enzyme.

MATERIALS AND METHODS

Growth Conditions

If not stated otherwise, *Synechocystis* strains were grown photoautotrophically in liquid BG-11 medium (Rippka et al., 1979) supplemented by 10 mM TES at 30°C and 40 μmol photons m^{-2} s^{-1} (normal light) on the rotary shaker. To induce the expression of tagged FeCHs from the *petJ* promoter (see below), *FLAG-hemH*/Δ*hemH*, *FLAG*-ΔH347, and *FLAG*-ΔH324 strains were grown in BG-11 medium lacking copper in the trace metal mix.

Construction of *Synechocystis* Mutants

Construction of the WT_{zeo} strain and the ΔH324 mutant has been described by Sobotka et al. (2008b). Essentially the same approach was adopted for the preparation of the ΔH347 mutant, with a stop codon in the *hemH* gene at amino acid position 347 (for all oligonucleotides used for strain preparation, see Supplemental Table S1).

To obtain the *FLAG-hemH* strain expressing 3xFLAG-tagged FeCH (FLAG-FeCH), the coding sequence of the *hemH* gene (locus *slr0839*) encoding the FeCH was subcloned into the pDrive vector (Qiagen). Subsequently, two complementary oligonucleotides encoding the 3xFLAG peptide (Sigma-Aldrich) were hybridized, thus creating *Nde*I-compatible overhangs, and then ligated into the *Nde*I site of the pDrive-*hemH* construct, thereby eliminating the second *Nde*I site. Using *Nde*I and *Bgl*II restriction enzymes (sites were introduced by the primers; Supplemental Table S1), a DNA fragment encoding the FLAG-FeCH was excised and then ligated into pSK9 vector for chromosomal integration under the control of the copper-dependent *petJ* promoter (Tous et al., 2001). The plasmid was transformed into *Synechocystis* wild type, and transformants were selected on BG-11 agar plates containing 7 μg mL^{-1} chloramphenicol.

In order to inactivate the entire FeCH gene and thus obtain a strain expressing the FLAG-FeCH as the only FeCH enzyme in the cell (*FLAG-hemH*/Δ*hemH* strain), the original *hemH* gene in the *FLAG-hemH* strain was replaced by an erythromycin resistance cassette using PCR-mediated insertion (Lee et al., 2004; Sobotka et al., 2008b). To prepare the *FLAG*-ΔH347 and *FLAG*-ΔH324 strains expressing truncated FeCHs, modified *hemH* genes containing stop codons were amplified from the ΔH347 and ΔH324 mutants and cloned into the pSK9 plasmid as described above.

The *Synechocystis* His-C-tn strain expresses the 63-residue-long C-terminal fragment of *Synechocystis* FeCH as a His_6-tagged protein under the control of the *psbAII* promoter. To prepare this strain, the *hemH* gene fragment was amplified by PCR using gene-specific primers with artificial restriction sites for *Nde*I and *Bgl*II and containing six His codons (CAC) in the forward primer (Supplemental Table S1). After restriction, the PCR fragment was cloned into *Nde*I and *Bam*HI sites of the pSBA plasmid containing the upstream and downstream regions of the *Synechocystis psbAII* gene (Lagarde et al., 2000). The plasmid was transformed into the *Synechocystis* psbAII-KS strain as described previously (Lagarde et al., 2000).

Fractionation of *Synechocystis* Cells

A total of 50 mL of cells (optical density at 750 nm [OD_{750}] ~ 0.5) was washed and resuspended in buffer A containing 20 mM HEPES, pH 7.4, 10 mM

$MgCl_2$, 5 mM $CaCl_2$, and 20% glycerol. The cell suspension was mixed with glass beads and broken in a Mini-BeadBeater-16 (BioSpec), and the resulting homogenate was centrifuged at 50,000*g* for 30 min at 4°C. The supernatant containing soluble proteins was transferred to a new tube. Pelleted membranes were washed two times in buffer A, resuspended, and solubilized in the same buffer containing 1% dodecyl-β-maltoside, and unbroken cells and unsolubilized material were discarded by centrifugation.

Western Blot and Immunoblotting

Unless otherwise stated, proteins were denatured by 2% SDS and 1% dithiothreitol for 30 min at room temperature and separated on a denaturing 12% SDS-polyacrylamide gel. Proteins separated on the gel were transferred onto a polyvinylidene difluoride membrane. The membrane was incubated with specific primary antibodies and then with secondary antibody conjugated to horseradish peroxidase (Sigma). The anti-FeCH was raised in rabbits against recombinant *Synechocystis* glutathione *S*-transferase-FeCH expressed in *Escherichia coli*. The anti-FeCH C-terminal antibody (anti-C-tn) was raised in rabbits against residues 332 to 347 of the *Synechocystis* FeCH. The antibodies against *Synechocystis* magnesium chelatase subunits, Gun4 and Magnesium-protoporphyrin methyl transferase, were raised in rabbits using recombinant proteins prepared in *E. coli*.

Affinity Purification of 3xFLAG-Tagged FeCHs from *Synechocystis*

Two liters of *FLAG-hemH*/Δ*hemH* and *FLAG*-ΔH347 cells and 4 L of *FLAG*-ΔH324 cells harvested at OD_{750} = 0.7 to 0.8 were washed and resuspended in buffer A (see above) containing protease inhibitors (complete protease inhibitor cocktail; Roche). The cell suspension was mixed with glass beads and broken in a Mini-BeadBeater-16 using six 1-min cycles. Membranes were pelleted by centrifugation at 50,000*g* for 20 min at 4°C, washed in buffer A, and resuspended in 10 mL of the same buffer containing 1% dodecyl-β-maltoside. Membranes were solubilized by gentle mixing for 30 min at 10°C, and unbroken cells were discarded by centrifugation. Proteins were loaded onto a column containing approximately 100 μL of anti-FLAG M2 affinity gel (Sigma) and then washed with 15 mL of buffer A containing 0.04% dodecyl-β-maltoside (buffer A-DDM). The FLAG-tagged FeCH was eluted into buffer A-DDM by incubation of the M2 affinity gel with 3xFLAG peptide (100 μg mL^{-1}) for 30 min.

Affinity Purification of the His-C-tn Protein from *Synechocystis*

For purification of the C-terminal fragment of *Synechocystis* FeCH (His-C-tn protein), membranes from 250 mL of cells (OD_{750} ~ 0.7–0.8) were washed and resuspended in buffer B (20 mM HEPES, pH 7.7, 10 mM $MgCl_2$, 5 mM $CaCl_2$, 0.1 M NaCl, and 10% glycerol) containing protease inhibitor (complete protease inhibitor cocktail; Roche). Cells were broken and membrane proteins were prepared in the same way as already described for the purification of FLAG-FeCHs. Proteins were loaded onto a column containing approximately 75 μL of His-select resin (Sigma) charged with Ni^{2+} and preequilibrated with buffer B containing 0.04% dodecyl-β-maltoside (buffer B-DDM). To remove any loosely bound contaminants, the column was first washed with 8 mL of buffer B-DDM and then successively with 1 mL of buffer B-DDM containing 10 mM, 20 mM, and 30 mM imidazole. The His-C-tn protein was eluted with buffer B-DDM containing 150 mM imidazole.

FeCH Activity Assay

FeCH activity was monitored spectrofluorometrically at 35°C by directly recording the rate of zinc-PP_{IX} formation using a Spectronic Unicam series 2 spectrofluorometer. The reaction mixture (1.5 mL final volume) contained 100 mM Tris-HCl (pH 8.0), 0.03% Tween 80, 5 μM PP_{IX}, and 1 μM $ZnSO_4$. The measurement of FeCH activity in the cell membrane fraction was initiated by adding proteins in amounts corresponding to 0.3 mL of cells at OD_{750} = 1. This value was calculated from the Chl content in the analyzed sample and Chl level per OD_{750} of the particular strain.

Quantification of Chl and Chl Precursors

For Chl quantification, pigments were extracted from cell pellets (5 mL, OD_{750} ~ 0.4) with 100% methanol, and Chl content was measured spectrophotometrically (Porra et al., 1989).

For quantitative determination of Chl precursors in the cells, 75 mL of culture at OD_{750} = 0.35 to 0.4 was filtered through a 4-μm cellulose filter to remove all precipitated pigments in growth medium and harvested. Pigments were extracted by 1 mL of methanol/0.2% NH_4OH using a Mini-BeadBeater-16 with two breaking cycles. Subsequently, the sample was centrifuged and the supernatant containing extracted pigments was collected. The pellet was then extracted again by 0.3 mL of methanol/0.2% NH_4OH with one breaking cycle, and the combined supernatants were mixed with 150 μL of 1 M NaCl. This solution was extracted two times by 400 μL of hexane to remove Chl and β-carotene, concentrated to 750 μL on a vacuum evaporator, and extracted two times by 400 μL of petroleum ether (boiling range, 45°C–60°C) to remove zeaxanthin. Remaining solution was evaporated to dry on a vacuum evaporator. Pigments were than resuspended in 140 μL of methanol/0.2% NH_4OH and mixed with 60 μL of water, and precipitated myxoxanthophylls were discarded by centrifugation. Samples were immediately separated by HPLC (Agilent-1200) on a reverse phase column (Nova-Pak C18, 4 μm particle size, 3.9 × 150 mm; Waters) using 30% methanol in 0.5 M ammonium acetate and 100% methanol as solvents A and B, respectively. Porphyrins were eluted with a linear gradient of solvent B (65%–75% in 30 min) at a flow rate of 0.9 mL min^{-1} at 40°C. HPLC fractions containing MgP (retention time of approximately 6.5 min), Chlide (approximately 8.5 min), PChlide (approximately 11.5 min), magnesium protoporphyrin IX methylester (approximately 13 min), and PP_{IX} (approximately 15 min) were collected, and concentrations of the corresponding compounds were determined fluorometrically using a Spectronic Unicam series 2 spectrofluorometer.

Quantification of Hemes and Determination of ALA-Synthesizing Capacity

For quantification of heme B (protoheme), a sample of cell debris, already extracted by methanol/0.2% NH_4OH for quantification of Chl precursors, was extracted further by 1 mL of acetone:water:HCl (90:8:2). After centrifugation, the solution was evaporated to dry on a vacuum evaporator, resuspended in 100 μL of acetone, and immediately separated by HPLC on a Nova-Pak C18 column (4-μm particle size, 3.9 × 150 mm; Waters) using a linear gradient from 50% to 80% solvent B (40% acetone in methanol) in solvent A (30% methanol in 0.5 M ammonium acetate) in 30 min at a flow rate of 1 mL min^{-1} at 40°C. Heme B was detected by a diode array detector (Agilent-1200) and quantified using an authentic hemin standard (Sigma).

To determine ALA-synthesizing capacity, a total of 100 mL of *Synechocystis* cells at OD_{750} = 0.4 was supplemented with 5 mM Glc and 15 mM levulinic acid/KOH, pH 7.5, to enhance ALA formation but inhibit its condensation into porphobilinogen. After 4 h, cells were harvested, resuspended in 0.3 mL of double-distilled water, and mixed with 20 μL of 50% TCA. Precipitated proteins were discarded by centrifugation, and the supernatant was adjusted to pH 6.7 by 90 μL of 0.5 M Na_3PO_4. The supernatant was then mixed with 12 μL of ethylacetoacetate, boiled for 15 min at 100°C, cooled on ice, and cleared by centrifugation. A total of 450 μL of modified Ehrlich's reagent was added to the supernatant, and the content of ALA was determined by A_{553} (Mauzerall and Granick, 1956) on a Shimadzu 2000 spectrophotometer.

Native Electrophoresis and Size-Exclusion Chromatography

Nondenaturing PAGE was performed with the precast 4% to 16% NativePAGE Bis-Tris Gel (Invitrogen) at 10 V cm^{-1} at 4°C using the XCell SureLock cell (Invitrogen). Cathode buffer contains 0.25 mM Tricine, 7.5 mM Bis-Tris-HCl, pH 7.0, 0.05% sodium deoxycholate, and 0.02% dodecyl-β-maltoside; anode buffer contains 0.25 mM Bis-Tris-HCl, pH 7.0. Approximately 0.25 μg of protein in buffer A-DDM was loaded for each sample, and after electrophoresis, the gel was stained with Coomassie Brilliant Blue.

Gel filtration chromatography was carried out on the BioSep SEC-S3000 300- × 7.80-mm column (Phenomenex) connected to a photodiode array detector (Agilent-1200). The column was equilibrated with buffer A containing 0.1% dodecyl-β-maltoside. The flow rate was 0.15 mL min^{-1}.

Supplemental Data

The following materials are available in the online version of this article.

Supplemental Figure S1. Amino acid alignment among the C-terminal ends of FeCH proteins from evolutionarily distant Chl-producing organisms.

Supplemental Figure S2. Whole-cell absorbance spectra of *Synechocystis* strains grown under different light regimes.

Supplemental Figure S3. Crystal structure of the spinach LHCII with the highlighted stromal loop connecting the second and third helices.

Supplemental Table S1. Oligonucleotides used for the construction of *Synechocystis* mutant strains.

ACKNOWLEDGMENTS

We thank Eva Prachova for her technical assistance and Ulf Dühring for preparation of the pSK9-*FLAG-hemH* construct. The vector pSK9 was a kind gift of Prof. S. Zinchenko.

Received October 15, 2010; accepted November 9, 2010; published November 16, 2010.

LITERATURE CITED

Cornah JE, Terry MJ, Smith AG (2003) Green or red: what stops the traffic in the tetrapyrrole pathway? Trends Plant Sci **8:** 224–230

Davidson RE, Chesters CJ, Reid JD (2009) Metal ion selectivity and substrate inhibition in the metal ion chelation catalyzed by human ferrochelatase. J Biol Chem **284:** 33795–33799

Dolganov NA, Bhaya D, Grossman AR (1995) Cyanobacterial protein with similarity to the chlorophyll a/b binding proteins of higher plants: evolution and regulation. Proc Natl Acad Sci USA **92:** 636–640

Goslings D, Meskauskiene R, Kim C, Lee KP, Nater M, Apel K (2004) Concurrent interactions of heme and FLU with Glu tRNA reductase (HEMA1), the target of metabolic feedback inhibition of tetrapyrrole biosynthesis, in dark- and light-grown *Arabidopsis* plants. Plant J **40:** 957–967

Grzybowska E, Góra M, Plochocka D, Rytka J (2002) *Saccharomyces cerevisiae* ferrochelatase forms a homodimer. Arch Biochem Biophys **398:** 170–178

Hihara Y, Sonoike K, Ikeuchi M (1998) A novel gene, *pmgA*, specifically regulates photosystem stoichiometry in the cyanobacterium *Synechocystis* species PCC 6803 in response to high light. Plant Physiol **117:** 1205–1216

Jensen PE, Gibson LCD, Henningsen KW, Hunter CN (1996) Expression of the *chlI*, *chlD*, and *chlH* genes from the cyanobacterium *Synechocystis* PCC6803 in *Escherichia coli* and demonstration that the three cognate proteins are required for magnesium-protoporphyrin chelatase activity. J Biol Chem **271:** 16662–16667

Kilian O, Steunou AS, Grossman AR, Bhaya D (2008) A novel two domain-fusion protein in cyanobacteria with similarity to the CAB/ELIP/HLIP superfamily: evolutionary implications and regulation. Mol Plant **1:** 155–166

Kumar AM, Csankovszki G, Söll D (1996) A second and differentially expressed glutamyl-tRNA reductase gene from *Arabidopsis thaliana*. Plant Mol Biol **30:** 419–426

Lagarde D, Beuf L, Vermaas W (2000) Increased production of zeaxanthin and other pigments by application of genetic engineering techniques to *Synechocystis* sp. strain PCC 6803. Appl Environ Microbiol **66:** 64–72

Larkin RM, Alonso JM, Ecker JR, Chory J (2003) GUN4, a regulator of chlorophyll synthesis and intracellular signaling. Science **299:** 902–906

Lee J, Lee HJ, Shin MK, Ryu WS (2004) Versatile PCR-mediated insertion or deletion mutagenesis. Biotechniques **36:** 398–400

Levicán G, Katz A, de Armas M, Núñez H, Orellana O (2007) Regulation of a glutamyl-tRNA synthetase by the heme status. Proc Natl Acad Sci USA **104:** 3135–3140

Liu Z, Yan H, Wang K, Kuang T, Zhang J, Gui L, An X, Chang W (2004) Crystal structure of spinach major light-harvesting complex at 2.72 A resolution. Nature **428:** 287–292

Masoumi A, Heinemann IU, Rohde M, Koch M, Jahn M, Jahn D (2008) Complex formation between protoporphyrinogen IX oxidase and ferrochelatase during haem biosynthesis in *Thermosynechococcus elongatus*. Microbiology **154:** 3707–3714

Masuda T, Fujita Y (2008) Regulation and evolution of chlorophyll metabolism. Photochem Photobiol Sci **7:** 1131–1149

Mauzerall D, Granick S (1956) The occurrence and determination of δ-amino-levulinic acid and porphobilinogen in urine. J Biol Chem **219:** 435–446

McCormac AC, Fischer A, Kumar AM, Söll D, Terry MJ (2001) Regulation of HEMA1 expression by phytochrome and a plastid signal during de-etiolation in Arabidopsis thaliana. Plant J **25:** 549–561

Müller B, Eichacker LA (1999) Assembly of the D1 precursor in monomeric photosystem II reaction center precomplexes precedes chlorophyll *a*-triggered accumulation of reaction center II in barley etioplasts. Plant Cell **11:** 2365–2377

Muramatsu M, Sonoike K, Hihara Y (2009) Mechanism of downregulation of photosystem I content under high-light conditions in the cyanobacterium *Synechocystis* sp. PCC 6803. Microbiology **155:** 989–996

Nowaczyk MM, Hebeler R, Schlodder E, Meyer HE, Warscheid B, Rögner M (2006) Psb27, a cyanobacterial lipoprotein, is involved in the repair cycle of photosystem II. Plant Cell **18:** 3121–3131

Ohgari Y, Sawamoto M, Yamamoto M, Kohno H, Taketani S (2005) Ferrochelatase consisting of wild-type and mutated subunits from patients with a dominant-inherited disease, erythropoietic protoporphyria, is an active but unstable dimer. Hum Mol Genet **14:** 327–334

Papenbrock J, Mishra S, Mock HP, Kruse E, Schmidt EK, Petersmann A, Braun HP, Grimm B (2001) Impaired expression of the plastidic ferrochelatase by antisense RNA synthesis leads to a necrotic phenotype of transformed tobacco plants. Plant J **28:** 41–50

Papenbrock J, Mock HP, Tanaka R, Kruse E, Grimm B (2000) Role of magnesium chelatase activity in the early steps of the tetrapyrrole biosynthetic pathway. Plant Physiol **122:** 1161–1169

Porra RJ, Thompson WA, Kriedemann PE (1989) Determination of accurate extinction coefficients and simultaneous equations for assaying chlorophyll a and b extracted with four different solvents: verification of the concentration of chlorophyll standards by atomic absorption spectroscopy. Biochim Biophys Acta **975:** 384–394

Promnares K, Komenda J, Bumba L, Nebesarova J, Vacha F, Tichy M (2006) Cyanobacterial small chlorophyll-binding protein ScpD (HliB) is located on the periphery of photosystem II in the vicinity of PsbH and CP47 subunits. J Biol Chem **281:** 32705–32713

Rippka R, Deruelles J, Waterbury JB, Herman M, Stanier RY (1979) Generic assignments, strain histories and properties of pure cultures of cyanobacteria. J Gen Microbiol **111:** 1–61

Sobotka R, Dühring U, Komenda J, Peter E, Gardian Z, Tichy M, Grimm B, Wilde A (2008a) Importance of the cyanobacterial Gun4 protein for chlorophyll metabolism and assembly of photosynthetic complexes. J Biol Chem **283:** 25794–25802

Sobotka R, Komenda J, Bumba L, Tichy M (2005) Photosystem II assembly in CP47 mutant of *Synechocystis* sp. PCC 6803 is dependent on the level of chlorophyll precursors regulated by ferrochelatase. J Biol Chem **280:** 31595–31602

Sobotka R, McLean S, Zuberova M, Hunter CN, Tichy M (2008b) The C-terminal extension of ferrochelatase is critical for enzyme activity and for functioning of the tetrapyrrole pathway in *Synechocystis* strain PCC 6803. J Bacteriol **190:** 2086–2095

Sonoike K, Hihara Y, Ikeuchi M (2001) Physiological significance of the regulation of photosystem stoichiometry upon high light acclimation of *Synechocystis* sp. PCC 6803. Plant Cell Physiol **42:** 379–384

Srivastava A, Lake V, Nogaj LA, Mayer SM, Willows RD, Beale SI (2005) The *Chlamydomonas reinhardtii gtr* gene encoding the tetrapyrrole biosynthetic enzyme glutamyl-trna reductase: structure of the gene and properties of the expressed enzyme. Plant Mol Biol **58:** 643–658

Tanaka R, Tanaka A (2007) Tetrapyrrole biosynthesis in higher plants. Annu Rev Plant Biol **58:** 321–346

Tanaka R, Yoshida K, Nakayashiki T, Masuda T, Tsuji H, Inokuchi H, Tanaka A (1996) Differential expression of two hemA mRNAs encoding glutamyl-tRNA reductase proteins in greening cucumber seedlings. Plant Physiol **110:** 1223–1230

Tous C, Vega-Palas MA, Vioque A (2001) Conditional expression of RNase P in the cyanobacterium *Synechocystis* sp. PCC6803 allows detection of precursor RNAs: insight in the in vivo maturation pathway of transfer and other stable RNAs. J Biol Chem **276:** 29059–29066

Tzvetkova-Chevolleau T, Franck F, Alawady AE, Dall'Osto L, Carrière F, Bassi R, Grimm B, Nussaume L, Havaux M (2007) The light stress-induced protein ELIP2 is a regulator of chlorophyll synthesis in *Arabidopsis thaliana*. Plant J **50:** 795–809

Vasileuskaya Z, Oster U, Beck CF (2005) Mg-protoporphyrin IX and heme

control HEMA, the gene encoding the first specific step of tetrapyrrole biosynthesis, in *Chlamydomonas reinhardtii*. Eukaryot Cell **4:** 1620–1628

Vavilin D, Vermaas W (2007) Continuous chlorophyll degradation accompanied by chlorophyllide and phytol reutilization for chlorophyll synthesis in *Synechocystis* sp. PCC 6803. Biochim Biophys Acta **1767:** 920–929

Vothknecht UC, Kannangara CG, von Wettstein D (1998) Barley glutamyl tRNAGlu reductase: mutations affecting haem inhibition and enzyme activity. Phytochemistry **47:** 513–519

Wang L, Elliott M, Elliott T (1999) Conditional stability of the HemA protein (glutamyl-tRNA reductase) regulates heme biosynthesis in *Salmonella typhimurium*. J Bacteriol **181:** 1211–1219

Weinstein JD, Howell RW, Leverette RD, Grooms SY, Brignola PS, Mayer SM, Beale SI (1993) Heme inhibition of δ-aminolevulinic acid synthesis is enhanced by glutathione in cell-free extracts of *Chlorella*. Plant Physiol **101:** 657–665

Xu H, Vavilin D, Funk C, Vermaas W (2002) Small Cab-like proteins regulating tetrapyrrole biosynthesis in the cyanobacterium *Synechocystis* sp. PCC 6803. Plant Mol Biol **49:** 149–160

Zouni A, Kern J, Frank J, Hellweg T, Behlke J, Saenger W, Irrgang KD (2005) Size determination of cyanobacterial and higher plant photosystem II by gel permeation chromatography, light scattering, and ultracentrifugation. Biochemistry **44:** 4572–4581

Publication IV

Long-Term Acclimation of the Cyanobacterium *Synechocystis* sp. PCC 6803 to High Light Is Accompanied by an Enhanced Production of Chlorophyll That Is Preferentially Channeled to Trimeric Photosystem I[1][W]

Jana Kopečná, Josef Komenda, Lenka Bučinská, and Roman Sobotka*

Institute of Microbiology, Department of Phototrophic Microorganisms, Academy of Sciences, 37981 Trebon, Czech Republic; and Faculty of Science, University of South Bohemia, 370 05 Ceske Budejovice, Czech Republic

Cyanobacteria acclimate to high-light conditions by adjusting photosystem stoichiometry through a decrease of photosystem I (PSI) abundance in thylakoid membranes. As PSI complexes bind the majority of chlorophyll (Chl) in cyanobacterial cells, it is accepted that the mechanism controlling PSI level/synthesis is tightly associated with the Chl biosynthetic pathway. However, how Chl is distributed to photosystems under different light conditions remains unknown. Using radioactive labeling by ^{35}S and by ^{14}C combined with native/two-dimensional electrophoresis, we assessed the synthesis and accumulation of photosynthetic complexes in parallel with the synthesis of Chl in *Synechocystis* sp. PCC 6803 cells acclimated to different light intensities. Although cells acclimated to higher irradiances (150 and 300 $\mu E\ m^{-2}s^{-1}$) exhibited markedly reduced PSI content when compared with cells grown at lower irradiances (10 and 40 $\mu E\ m^{-2}\ s^{-1}$), they grew much faster and synthesized significantly more Chl, as well as both photosystems. Interestingly, even under high irradiance, almost all labeled de novo Chl was localized in the trimeric PSI, whereas only a weak Chl labeling in photosystem II (PSII) was accompanied by the intensive ^{35}S protein labeling, which was much stronger than in PSI. These results suggest that PSII subunits are mostly synthesized using recycled Chl molecules previously released during PSII repair-driven protein degradation. In contrast, most of the fresh Chl is utilized for synthesis of PSI complexes likely to maintain a constant level of PSI during cell proliferation.

Photosynthetic autotrophs are completely dependent on light as the only source of energy for their proliferation. However, light intensity can swiftly change due to variable environmental conditions, sometimes being too low to sufficiently drive photosynthetic reactions, and other times being even higher than can be utilized, or at least safely dissipated, by a photosynthetic apparatus. In the latter case, the excessive part of the absorbed energy can be ultimately transformed into energy of reactive oxygen species, which has a destructive impact on key cellular components: nucleic acids, lipids, pigments, and proteins. To cope with light fluctuations, cyanobacteria as well as algae and plants possess complex regulatory machinery to optimize the utilization of light energy and to protect photosynthetic apparatus against the damage induced by excessive light. This machinery involves the regulation of size and number of light-harvesting antennas (Anderson et al., 1995; Walters, 2005), dissipation of light energy by nonphotochemical quenching (El Bissati et al., 2000; Müller et al., 2001), redistribution of light energy between photosystems by state transition (Mullineaux and Emlyn-Jones, 2005; Fujimori et al., 2005), or adapting the capacity of carbon dioxide (CO_2) fixation (Demmig-Adams and Adams, 1992).

One of the most prominent responses to light intensity, and also to its spectral quality, is a selective regulation of the abundance of PSI in the thylakoid membrane, which controls the frequency of excitation of photosystems to optimize the entire photosynthetic electron flow (Chow et al., 1990; Muramatsu and Hihara, 2012). Given that the PSII level is much more stable, this process establishes a specific stoichiometry between both photosystems (PSI/PSII ratio) depending on particular light conditions (Neale and Melis, 1986; Murakami and Fujita, 1991; Walters and Horton, 1994). A dynamic adjustment of the PSI/PSII ratio has been shown to be required for maintaining a high quantum efficiency of photosynthesis in plants (Chow et al., 1990) and algae (Melis et al., 1996). In cyanobacteria, a physiological significance of photosystem stoichiometry was demonstrated on mutants of the cyanobacterium *Synechocystis* sp. PCC 6803 (hereafter, Synechocystis). The *pmgA* mutant has lost the ability to

[1] This work was supported by projects Algatech (CZ.1.05/2.1.00/03.0110) and RVO61388971 and by projects P501/10/1000 and P501/12/G055 of the Grant Agency of the Czech Republic. L.B. was supported by the Grant Agency of the University of South Bohemia.

* Corresponding author; e-mail sobotka@alga.cz.

The author responsible for distribution of materials integral to the findings presented in this article in accordance with the policy described in the Instructions for Authors (www.plantphysiol.org) is: Roman Sobotka (sobotka@alga.cz).

[W] The online version of this article contains Web-only data.
www.plantphysiol.org/cgi/doi/10.1104/pp.112.207274

selectively decrease the PSI content during acclimation to high light (HL) and its growth is severely inhibited under prolonged HL conditions (Hihara et al., 1998; Sonoike et al., 2001). A similar defect in maintaining reduced PSI content in HL has been demonstrated in a Synechocystis strain lacking the putative chlorophyll (Chl)-binding domain of ferrochelatase. The growth of this mutant has been completely abolished by HL (Sobotka et al., 2011). The mechanism responsible for the HL-induced selective decrease in PSI content is not clear; however, the process appears to be under control of the redox state of the cytochrome b_6f complex (Murakami and Fujita, 1993). In a proposed model, a signal from cytochrome b_6f downregulates Chl biosynthesis, particularly formation of an early Chl intermediate aminolevulinic acid (ALA), and it seems to be a limited Chl availability that determines the PSI content (Fujita et al., 1990; Muramatsu et al., 2009). Consistently with this model, transcription of *psaA/B* genes coding for large Chl-binding PSI core subunits is not a rate-limiting step in the PSI accumulation, while de novo Chl synthesis is blocked immediately after being transferred to HL conditions (Muramatsu et al., 2009). On the other hand, Chl is required during the repair/replacement of PSII complexes that are photodamaged much faster than PSI complexes (Nowaczyk et al., 2006; Nixon et al., 2010). Therefore, the synthesis of Chl-binding PSII subunits, especially the fast turning over D1 subunit, should be much faster in comparison with PSI subunits (Yao et al., 2012a, 2012b). It raises the question of how an enhanced synthesis of PSII subunits is achieved if less de novo-synthesized Chl is produced under HL conditions to keep PSI at a reduced level. Chl is produced via a quite long and branched pathway together with heme and other tetrapyrroles, and the formation of ALA is a particularly critical step controlling the accumulation of the whole spectrum of phototoxic intermediates of Chl/heme biosynthesis (for review, see Czarnecki and Grimm, 2012; see Supplemental Fig. S1 for a scheme of tetrapyrrole pathway). However, controlling PSI content by the metabolic flow through the whole tetrapyrrole pathway does not seem to be flexible enough to balance the formation of all tetrapyrrole cofactors. The de novo Chl biosynthesis is expected to be tightly synchronized with synthesis of Chl-binding proteins (Komenda et al., 2012) but a cross talk between Chl and Chl-protein biosyntheses has to also reflect the fact that the lifetime of Chl molecules is much longer than that of proteins (Vavilin et al., 2005; Vavilin and Vermaas 2007; Yao et al., 2012a, 2012b); therefore, a potential role of the recycled Chl in controlling Chl-protein biogenesis must be addressed as well. In this study, we focused on the correlation between synthesis of both photosystems and Chl biosynthesis in Synechocystis cells fully acclimated to different light intensities. Using radioactive labeling of proteins and Chl by ^{35}S and ^{14}C, respectively, we found that the rate of de novo Chl formation, as well as synthesis of both photosystems, is significantly enhanced in HL, despite the markedly reduced cellular level of PSI. Our data suggest that there is no simple correlation between the actual synthesis of PSI and PSII core subunits and the synthesis and distribution of de novo Chl; de novo Chl was found to be predominantly directed to the PSI trimer, whereas the Chl-binding PSII subunits seem to be mostly synthesized using the recycled Chl molecules previously released during Chl-protein degradation. It appears that the particular level of PSI needed for the optimal photosynthetic performance at a given light intensity is reached by a precise equilibrium between the rate of cell proliferation, the rate of Chl biosynthesis, and the distribution of Chl into individual Chl-proteins.

RESULTS

Acclimation of the Synechocystis Cells to Various Irradiances

To understand how Chl biosynthesis is synchronized with the varying demand for Chl-binding subunits of PSI/PSII, we analyzed the Synechocystis wild type acclimated to different light intensities. Cells were first grown for 5 d under continuous illumination at 40 μE m^{-2} s^{-1} (moderate light [ML]) and subsequently moved for 24 h to either lower light (LL; 10 μE m^{-2} s^{-1}) or higher light intensities (HL1, 150 μE m^{-2} s^{-1}; HL2, 300 μE m^{-2} s^{-1}). Absorption spectra of cells normalized per optical density at 750 nm (OD_{750}) are shown in Figure 1A. Whereas the shift to LL did not result in significant changes in the cell pigmentation (data not shown; see Table I for Chl level), amounts of Chl and phycobilisomes per cell were markedly lowered as a response to higher irradiance (Fig. 1A). Chl concentration at HL2 reached about 50% of that observed at ML (Table I; Supplemental Fig. S2). Levels of carotenoids also decreased, except for myxoxanthophyll, the level of which more than doubled after 24 h at HL2 (Supplemental Fig. S2). Growth rates of the cultures were accelerating with light intensity reaching the maximum at HL2 (Table I), a further increase in light intensity to 600 μE m^{-2} s^{-1} started to inhibit growth (data not shown), although cell pigmentation did not significantly alter when compared with HL2 (see Supplemental Fig. S3 for the whole-cell spectra). Supplementing growth media with 5 mM $NaHCO_3$ did not affect the growth rate or Chl level at HL2 (Table I), implying that under our growth conditions with a higher concentration of CO_2 in the growth chamber, the proliferation of Synechocystis cells was not significantly limited by CO_2 availability. To gather information about the functional status of PSII during acclimation to HL, we also determined the ratio of variable to maximal fluorescence (F_v/F_m). When cells grown at ML were moved to HL2, the F_v/F_m ratio declined rapidly (Supplemental Fig. S4); nevertheless, in the following 6 h it recovered to the initial value. This suggests that even under HL2, cells coped relatively quickly with the initial damage of PSII, and fully acclimated cells did not contain a significant portion of nonfunctional PSII complexes and grew much faster than at ML.

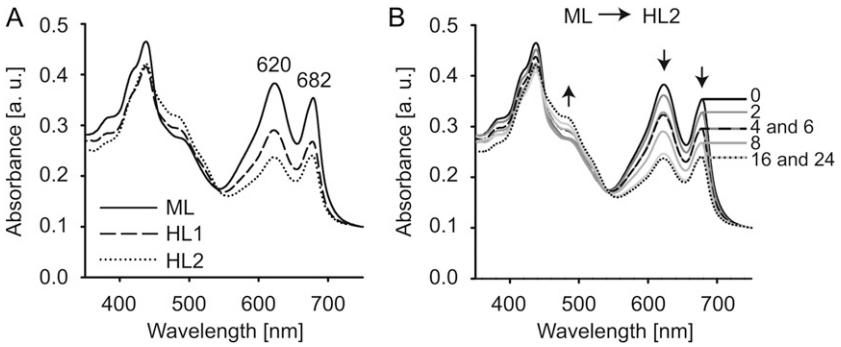

Figure 1. Whole-cell absorption spectra of the Synechocystis cells acclimated to different light intensities. A, Absorption spectra of Synechocystis cells grown photoautotrophically for 24 h under 40 μE m^{-2} s^{-1} (ML), 150 μE m^{-2} s^{-1} (HL1), and 300 μE m^{-2} s^{-1} (HL2). Peaks at 620 and 682 nm represent phycocyanin and Chl absorption, respectively. B, Time course of changes in absorption spectra of cells shifted from ML to HL2 (time 0). Cell spectra measured after 4 (dashed line) and 6 h (solid line) are practically identical, which suggests a lag phase in acclimation to HL2. Spectrum at 24 h is designated by the dotted line. a.u., Absorbance units.

A time-course analysis of changes in whole-cell spectra during acclimation to HL2 showed a rapid decrease in Chl and phycobilisome level in the first 4 h followed by a lag phase between the fourth and sixth hours when no apparent changes were observed (Fig. 1B). The second decrease in Chl and phycobilisome content was observed between the sixth and 16th hour. A prolonged cultivation had no additional effect on the pigment content (Fig. 1B). Observed changes at HL were also reflected in the cell ultrastructure; as shown in Figure 2, cells from HL2 possessed less abundant and less compact thylakoid membrane structures when compared with ML. A distinct feature of HL2 acclimated cells was a very high abundance of glycogen granules that were almost missing in ML grown cells (Fig. 2). Using electron microscopy, we did not observe any significant variability in size among cells from different light conditions even though the growth rate was quite different (Fig. 2). Assessment of cell size and distribution within particular cultures using a cell counter showed that only the cells at HL2 were in average slightly bigger; therefore, their number corresponding to OD_{750} = 1 was somewhat lower. Nevertheless, cell mass corresponding to OD_{750} = 1 was quite stable in all cultures grown under various irradiances (data not shown).

Accumulation and Synthesis of PSI and PSII in HL-Acclimated Cells

In the Synechocystis cells, practically all Chl is associated with photosystems and more than 80% is associated with PSI under ML (Shen et al., 1993). In order to determine how total levels of PSI and PSII are correlated with the drop in the cellular Chl level under HL, we first separated membranes from cultures acclimated to LL, ML, HL1, and HL2 by SDS-PAGE and then probed with antibodies against PSII and PSI subunits (Fig. 3A). As expected, an increase in light intensities reduced the amount of both PSI and PSII per cell (Fig. 3A). However, a decrease in the PSI level was much more pronounced. The following separation of photosynthetic complexes using clear-native electrophoresis (CN-PAGE) combined with detection of Chl fluorescence in gel allowed us to assess the content of particular oligomeric forms of PSI and PSII (Fig. 3B). Interestingly, the amount of both PSI and PSII monomers per cell was not significantly altered by HL, which contrasts with the dramatically downregulated amount of trimeric PSI and the clearly lowered level of PSII dimer (Fig. 3B).

To assess how de novo synthesis of PSI/PSII complexes corresponds to changes in their accumulation at a cellular level, cells acclimated to ML and HL2 were radioactively labeled using [^{35}S]Met/Cys mixture for 30 min and separated by CN-PAGE. After exposing the CN gel to a phosphor imager plate, we found rather similar labeling of the PSI trimer in both cultures while the labeling of the PSII dimer and both PSI and PSII monomers was at least doubled (Fig. 4A). Taking into account a much lower level of PSI trimer per cell in the HL2 cells, the results indicate significantly faster synthesis of all four complexes at this light intensity. To see how the individual Chl-binding PSII core subunits D1, D2, CP43, and CP47 contributed to the PSII monomer

Table I. *Growth rate and Chl content of Synechocystis cells under different growth regimes*

Values shown represent means ± SD from three independent measurements.

Light Intensity	Doubling Time	Chl
	(hours ± SD)	(μg mL^{-1} OD_{750}^{-1})
LL (10 μE m^{-2} s^{-1})	32.8 ± 1.3	5.9 ± 0.08
ML (40 μE m^{-2} s^{-1})	15.8 ± 0.8	5.5 ± 0.12
HL1 (150 μE m^{-2} s^{-1})	10.4 ± 1.3	3.6 ± 0.12
HL2 (300 μE m^{-2} s^{-1})	7.2 ± 0.3	2.5 ± 0.09
HL2 + 5 mM $NaHCO_3$	7.1 ± 0.3	2.4 ± 0.10

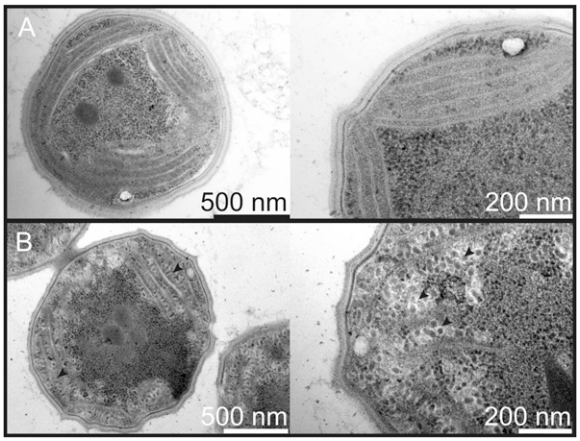

Figure 2. Transmission electron microscopy of the Synechocystis cells. Representative stained ultrathin sections of cells grown photoautotrophically for 24 h under ML (A) and HL2 (B); black arrows indicate glycogen granules.

and dimer labeling, we separated them in a second dimension using SDS-PAGE (Fig. 4B). Although their total level was lower at HL2, particularly in the dimeric PSII, the synthesis of all four proteins was clearly enhanced in both PSII complexes. We also observed a higher accumulation and synthesis of components of ATPase and FtsH2 and FtsH3 proteases at HL2 (Fig. 4B).

Light-Driven Up-Regulation of the Tetrapyrrole Biosynthetic Pathway

Acclimation of the cells to HL2 led to a fast down-regulation of PSI and phycobilisome levels (Fig. 1) and resulted in a reduction of the thylakoid membrane system (Fig. 2). On the other hand, synthesis of Chl-proteins was accelerated (Fig. 4). To evaluate Chl biosynthesis in the acclimated cells, we analyzed this metabolic pathway in detail. First, using a set of specific antibodies, we estimated levels of enzymes involved in the synthesis of heme and Chl in the cells acclimated to the particular light intensities by western blot (Fig. 5; see Supplemental Fig. S1 for a scheme of the tetrapyrrole pathway). Total levels of almost all enzymes, including the heme-producing ferrochelatase, were upregulated by light and light also induced association of enzymes with membranes. The enzymes reached the highest level at HL1 but further increase in irradiance to HL2 resulted in a drop of certain enzymes/enzyme subunits (Mg-protoporphyrin monomethyl ester cyclase, light-dependent protochlorophyllide oxidoreductase, Gun4, and geranylgeranyl reductase). An interesting exception was the D subunit of Mg-chelatase, which exhibited an opposite mode of regulation with the highest concentration reached under LL. Moreover, only at this light intensity was a large portion of the D subunit of Mg-chelatase protein bound to the membranes.

Although these data suggested that the heme/Chl biosynthetic pathway was upregulated after 24 h of acclimation to increased irradiance, the Chl content per cell started to fall quickly after the light shift and the process finished in 16 h (Fig. 1B). Therefore, the changes in enzyme levels were checked after 2 and 4 h after the shift to HL2 and most of the monitored proteins started to accumulate or at least showed little variation (Fig. 5B). A characteristic feature of Chl biosynthesis up-regulation was an enhanced association of Mg-chelatase subunits H and I with membranes, which was visible after 4 h at HL2 (Fig. 5B). In contrast to the other monitored enzymes, the amount of geranylgeranyl reductase underwent a rapid and significant decline in 2 h after the shift to HL2 and then recovered only very slowly (Fig. 5).

As enzyme levels could not necessarily reflect changes in metabolic flow through the pathway, accumulation of Chl precursors was also quantified. To preserve steady-state levels of precursors, which are probably transient and quickly change during cell handling, we developed a very sensitive method based on HPLC equipped with two fluorescence detectors (see "Material and Methods"). This enabled us to detect very low abundant intermediates of the Chl biosynthesis pathway in extracts from 2-mL cell cultures prepared just in several minutes (Fig. 6A). Employing this method, we observed that the growth at increased irradiance induced an accumulation

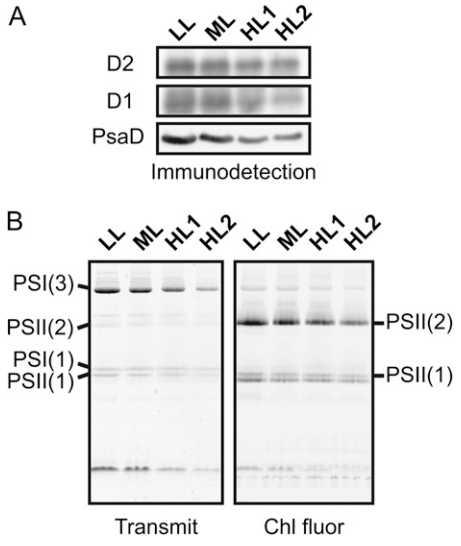

Figure 3. Accumulation of PSI and PSII in Synechocystis cells acclimated to different light intensities. A, Total amount of PSI and PSII detected using specific antibodies against PSII subunits D1 and D2 and PSI subunit PsaD. Membrane proteins corresponding to 100 μL of cells at OD_{750} = 1.0 were loaded per lane, separated by SDS-PAGE, and blotted. B, Separation of monomers and oligomers of PSI and PSII using CN-PAGE. After separation, the gel was scanned in transmittance mode (Transmit) using a LAS 4000 imager (Fuji), and to better visualize PSII complexes, Chl fluorescence in gel (Chl fluor) was detected after excitation by blue light using the same equipment. Proteins were loaded as in A. Designation of complexes: PSI(1) and PSI(3), Monomer and trimer of PSI, respectively; PSII(1) and PSII(2), monomer and dimer of PSII, respectively.

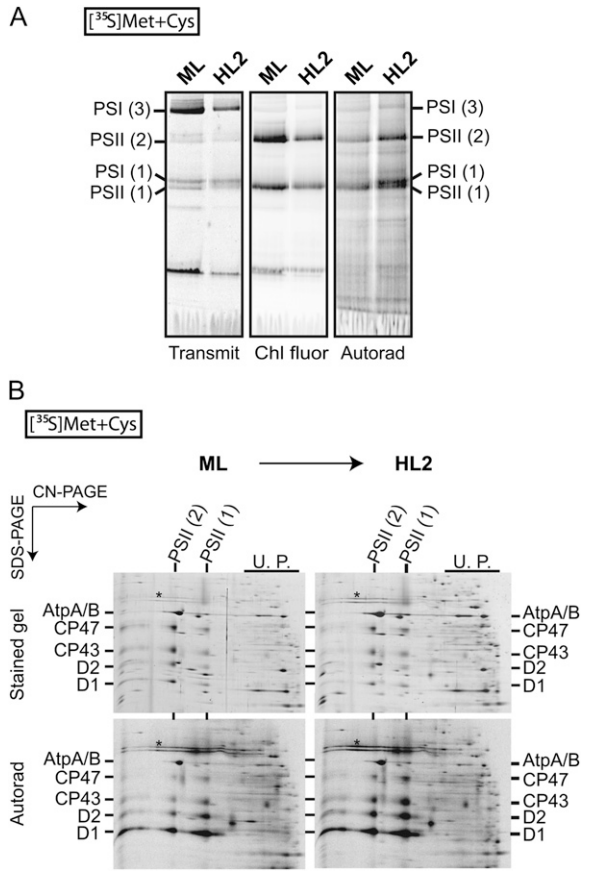

Figure 4. Synthesis of PSI and PSII complexes in Synechocystis cells acclimated to ML and HL2. A, Cells were radiolabeled with [^{35}S]Met/Cys mixture using a 30-min pulse, membrane protein complexes were separated by CN-PAGE, and labeled proteins visualized using a phosphor imager (Autorad). The gel was scanned using a LAS 4000 imager as described in Figure 3B. B, Separation of identical radiolabeled samples by two-dimensional CN/SDS-PAGE. Gel was stained with Coomassie blue and labeled proteins then detected by a phosphor imager (Autorad). Designation of the complexes is as in the legend to Figure 3. U.P., Unassembled proteins. FtsH2/3 proteases are marked with an asterisk.

of Mg-protoporphyrin monomethyl ester and protochlorophyllide, whereas pools of other Chl precursors appeared to be quite stable (Fig. 6B). Finally, to assess the capacity of the whole tetrapyrrole pathway to produce Chl, we followed incorporation of [^{14}C]Glu into Chl molecules. Briefly, cells were acclimated to tested light conditions for 24 h and then supplemented with 180 μM [^{14}C]Glu for 30 min. Chl (as well as geranylgeranyl-Chl) was immediately extracted by an excess of methanol and converted to Mg-chlorin as described in "Material and Methods." The solution containing Mg-chlorin was separated on a silica thin-layer chromatography (TLC) plate and exposed to an x-ray film. We found that the incorporation of [^{14}C]Glu into Chl is much faster at both HL1 and HL2 than at ML; in contrast, the labeling at LL was very weak (Fig. 6C; see Supplemental Fig. S5 for a color version). Together, these data suggest that the acclimation of the Synechocystis cells to HL results in a great upregulation of Chl biosynthesis despite the total relative decline in the cellular level of Chl.

Distribution of a Newly Synthesized Chl into Chl-Proteins and Complexes

Formation of an early precursor ALA is accepted as a critical check point controlling the metabolic flow through the whole tetrapyrrole pathway (Czarnecki and Grimm, 2012). Labeling of Chl by [^{14}C]Glu then ensures that the total capacity of the pathway can be assessed involving the ALA barrier as well as all other regulatory steps located down the pathway (Supplemental Fig. S1). Moreover, as Glu is also used for protein synthesis, radiolabeling with [^{14}C]Glu enabled us to assess the approximate portions of Glu incorporated into the proteins and Chl. Membrane proteins were isolated from HL2 cells, separated by two-dimensional CN/SDS-PAGE and exposed to an x-ray film. Chl migrates on the SDS gel faster than proteins and can be easily distinguished as spots on the bottom of the gel, below the edge of proteins, designated by the arrowheads in Figure 7. We found that the majority of the metabolized [^{14}C]Glu was used for the synthesis of Chl. Moreover, even at HL2, most of the labeled Chl was directed to the PSI trimer (Fig. 7A). On the protein side, the strongest radioactive signal was localized in the D1 protein and much less in other PSII subunits; higher molecular mass labeled proteins were probably core subunits of PSI and ATP synthase (Fig. 7A).

To trace the fate of Chl in ML- and HL2-acclimated cells more precisely, we labeled Chl using [^{14}C]ALA, and this allowed us to detect new Chl directly in the protein complexes visualized by CN-PAGE. After a 30-min pulse, the Chl labeling in PSII was apparently enhanced in HL2. However, flux of the newly made Chl into the trimeric PSI dominated under both conditions with additional enhancement at HL2 when compared with ML (Fig. 7B). This result contrasted to the very weak [^{35}S] labeling of PSI trimer when compared with PSII monomer/dimer and, intriguingly, also to PSI monomer (Fig. 4A), suggesting a specific channeling of labeled Chl into the PSI trimer. However, one has to be careful to assess Chl distribution just according to intensity of Chl labeling in individual PSI/PSII complexes. One PSI trimer contains 288 Chl molecules (Jordan et al., 2001), which is about 4 times more than the sum of Chls and pheophytins in a PSII dimer (Umena et al., 2011) and about 8 times more than number of Chls and pheophytins in a PSII monomer. We used the same methodology as for the [^{35}S] labeling to quantify the distribution of labeled Chl in PSI and PSII complexes in cells acclimated to HL2 and labeled by [^{14}C]ALA (Table II). As expected, the majority (58%) of Chl was located in trimeric PSI, while only 18% in PSI monomer and 24% in PSII complexes. To take into account different protein/Chl ratios in each complex, we calculated what portion of labeled

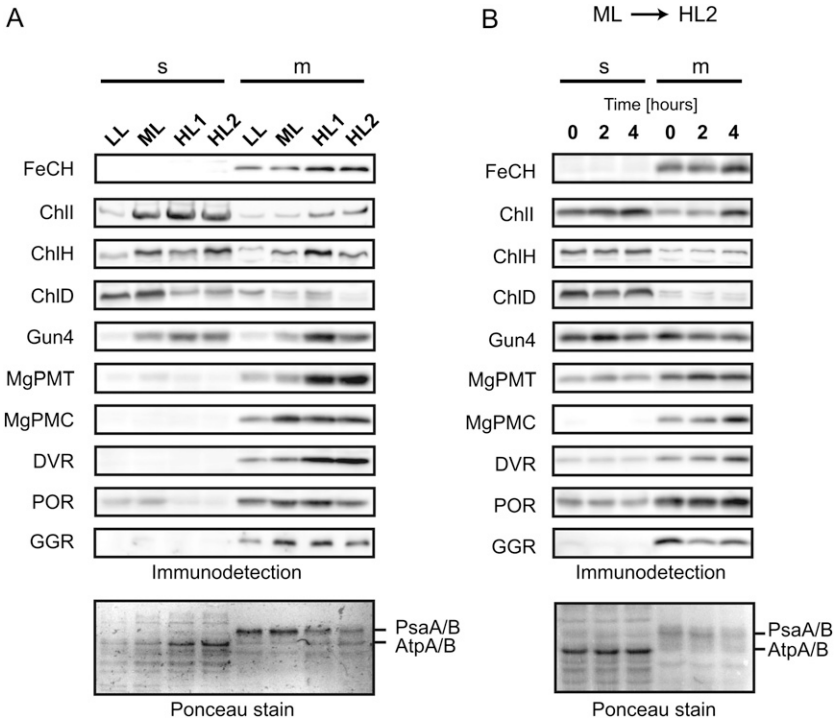

Figure 5. Accumulation and localization of enzymes of the tetrapyrrole biosynthetic pathway. A, Membrane and soluble protein fractions were prepared from acclimated cells as described in "Materials and Methods," separated by SDS-PAGE, and blotted to a polyvinylidene difluoride membrane. The amount of proteins loaded per lane correspond to 100 μL of cells at $OD_{750} = 1.0$. These proteins were probed with specific antibodies: FeCH, ferrochelatase; ChlI, ChlH, and ChlD, subunits of Mg-chelatase; Gun4, a protein required for the activity of Mg-chelatase; MgPMT, Mg-protoporphyrin methyl transferase; MgPMC, Mg-protoporphyrin monomethyl ester oxidative cyclase (Sll1214); DVR, 3,8-divinyl chlorophyllide 8-vinyl reductase; POR, light-dependent protochlorophyllide oxidoreductase; GGR, geranylgeranyl reductase. m, Membrane protein fraction; s, soluble protein fraction. B, Short-term changes in enzyme levels after the shift from ML to HL2. Synechocystis cells were harvested at the indicated time and analyzed as in A. Ponceau-stained proteins blotted onto a membrane are shown as a loading control.

Chl would theoretically be present in each PSI/PSII complex in the case that the protein labeling corresponds to Chl labeling and new Chls are evenly distributed to individual complexes. Less than 10% of labeled Chl should be bound to PSI trimers due to the very weak synthesis of this complex (Table II). The fact that 6 times more of the new Chl is bound to PSI trimer than expected from protein labeling demonstrates a crucial role of a precise distribution of de novo and recycled Chl in the biogenesis of photosystems.

DISCUSSION

Growth of cyanobacteria under high irradiance induces a fast decrease in harvesting capacity by reducing the number and size of phycobilisomes and abundance of PSI in the thylakoid membranes. However, the total excitation pressure is not the only factor controlling changes in the harvesting capacity. Although an adjustment of PSI and phycobilisome content is characteristic for light acclimation, a regulation of antenna size appears to be initiated by any redox imbalance of the electron transport chain (Wallner et al., 2012), and the actual abundance/ratio of photosynthetic complexes then results from the combined effects of light intensity and quality, temperature, or nutrient availability (Murakami and Fujita, 1991; Murakami et al., 1997; Miskiewicz et al., 2002). Light acclimation can be viewed as a set of regulatory events activated to restore a redox equilibrium in the cell. Indeed, a defect in the mechanism balancing the excitation of PSI and PSII, like the one caused by the *pmgA* mutation, generates a detrimental redox poise (Sonoike et al., 2001) and presumably locks the mutant cell in a perpetual unsuccessful effort to achieve the redox equilibrium.

The cytochrome b_6f complex was shown to serve as a redox sensor, triggering acclimatory machinery in cyanobacteria (Murakami and Fujita, 1993), though it remains unknown how this signal is transduced and processed in the cell. Undoubtedly, the tetrapyrrole pathway is an important target of this regulation. In cyanobacteria, the main flow of tetrapyrrole biosynthesis intermediates is directed to the synthesis of Chl and phycobilins that serve as the main light-harvesting pigments bound to the PSII-associated phycobilisome antenna. During light acclimation, Chl and intermediates of its biosynthesis deserve special care due to their phototoxic nature and high concentration of Chl in the cell. A tight coordination between synthesis of Chl and Chl apoproteins is expected to be crucial for the viability of the photosynthetic cell as formation of a pool of unquenched Chl or its intermediates would generate harmful reactive oxygen species.

The PSI trimer is the site where the majority of Chl is placed in the cyanobacterial cell, and as we show in this work, this complex is almost an exclusive sink for de novo Chl (Fig. 7B). For the reasons described above, a relatively fast down-regulation of the PSI level during the acclimation to HL has to be reflected by a regulation of Chl biosynthesis or/and Chl trafficking in the cell. A relation between the regulation of the PSI level and Chl biosynthesis is likely to be even more intimate since de novo Chl appears to be a rate-limiting factor for the translation of the PSI core subunits (Eichacker et al., 1996). It is expected that the PSI level is controlled via the regulation of Chl synthesis; thereby, the Chl limitation is the key factor causing the

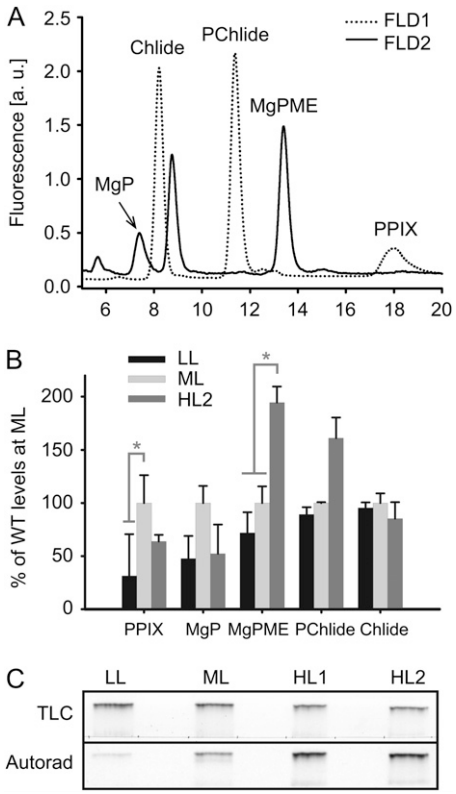

Figure 6. Levels of Chl precursors and the rate of Chl formation in cells acclimated to different light intensities. A, Separation and detection of Chl precursors using HPLC equipped with two fluorescence detectors (FLD1 and FLD2). Precursors were extracted from 2 mL of HL2-acclimated cells by a successive extraction using 70% and 80% methanol and immediately injected into the HPLC; for details, see "Materials and Methods." a.u., Arbitrary units; PP_{IX}, protoporphyrin IX; MgP, Mg-protoporphyrin IX; MgPME, Mg-protoporphyrin IX methylester; PChlide, protochlorophyllide; Chlide, chlorophyllide. B, Relative levels of Chl precursors in the Synechocystis cells acclimated to LL, ML, and HL2. Values shown represent means ± SD from three independent measurements. Asterisks indicate statistically significant differences in precursor levels as tested using a paired Student's *t* test ($P = 0.05$). WT, The wild type. C, Chl radiolabeled by [^{14}C]Glu was extracted using methanol/0.2% NH_4OH from cells cultivated under different light conditions (LL, ML, HL1, and HL2), converted into Mg-chlorin, and separated on a TLC plate. Radiolabeled Mg-chlorin was detected using an x-ray film (Autorad); amount of Mg-chlorin loaded per TLC lane corresponds to the cellular level of Chl under relevant light conditions.

decrease in PSI level at HL (Fujita et al., 1990; Muramatsu et al., 2009). The proposed mechanism is based on an assumption that a surplus of PsaA/B proteins is continuously translated but finally degraded due to a shortage in Chl. Although it seems to be a waste of energy, it might also provide a crucial function to ensure that there is always a place where Chl molecules can be safely incorporated even when synthesized in excess. Moreover, it is obvious from Figure 2, that Synechocystis cells are packed with glycogen when grown at HL2; thus, some energy can be easily sacrificed for a tight control over Chl-(protein) biosynthesis.

Although there is compelling evidence that both the transcription rate and stability of the *psaA/B* transcript are carefully regulated during light acclimation (Hihara et al., 2001; Herranen et al., 2005), the abundance of the *psaA/B* transcript does not appear to limit PSI synthesis consistently with the proposed regulatory role of Chl. In an elegant experiment Muramatsu et al. (2009) demonstrated that a Synechocystis strain engineered to have a constantly upregulated *psaA/B* transcript was still able to reduce the PSI level under HL.

Results so far published on an interplay between the Chl biosynthesis and the PSI/PSII stoichiometry concern a time period spanning up to 16 h after the shift to

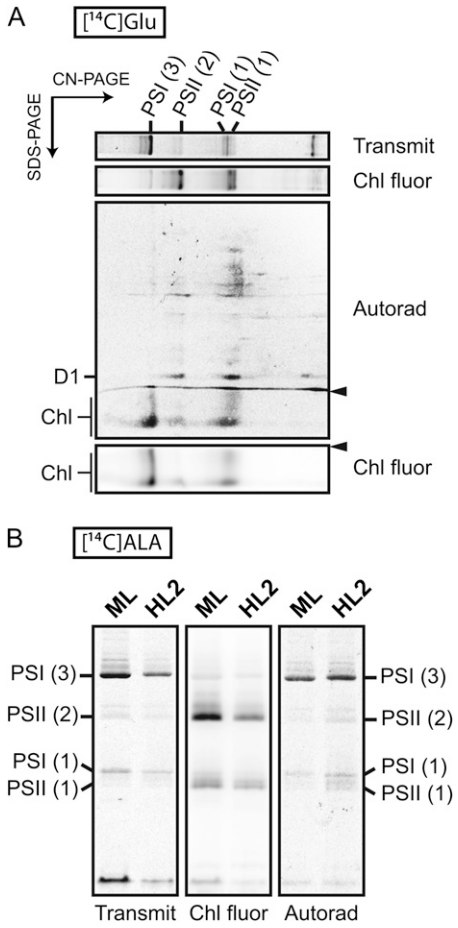

Figure 7. Radiolabeling of Chl molecules by [^{14}C]Glu and [^{14}C]ALA and detection of labeled Chl in Chl-protein complexes. A, Synechocystis cells acclimated to HL2 were radiolabeled with [^{14}C]Glu in a 30-min pulse and membrane proteins were then separated by two-dimensional CN/SDS-PAGE. Radioactivity was detected by a phosphor imager (Autorad). Position of particular complexes is indicated on the top; Chl molecules running ahead of proteins (below the protein edge line designated by arrowheads) on the SDS gel were also visualized by Chl fluorescence (Chl fluor). B, Cells acclimated to ML and HL2 were radiolabeled with [^{14}C]ALA for 30 min, and membrane proteins were separated by CN-PAGE. Proteins loaded in each lane correspond to 200 μL of cells at $OD_{750} = 1.0$; all abbreviations used are described in Figure 3.

Table II. *Quantification of proteins and Chl labeling in individual PSI and PSII complexes*

The same Synechocystis cell culture acclimated to HL2 was labeled separately by [^{35}S]Met/Cys mixture or by [^{14}C]ALA for 30 min and isolated cell membranes separated as a dilution series by CN-PAGE (see Figs. 4 and 7; Supplemental Fig. S6). After exposure of gels in a phosphor imager, bands of individual complexes were quantified using ImageQuant TL 7.0 software (GE Healthcare).

Complex	Protein Labeling: [^{35}S]Met+Cys			Chl Labeling: [^{14}C]ALA			
	Protein Labeling[a]	Normalized Labeling[b]	Normalized Labeling[c]	Measured Chl Labeling[a]	Measured Chl Labeling	Expected Chl Labeling[d]	Measured/ Expected
			(%)		(%)		
PSI trimer	0.36×10^6	0.21×10^6	2.1	29.44×10^6	58.8	9.3	6.31
PSI monomer	1.46×10^6	2.57×10^6	26.3	5.92×10^6	17.5	38.4	0.46
PSII dimer	2.15×10^6	1.86×10^6	19.0	8.76×10^6	11.8	21.9	0.54
PSII monomer	2.98×10^6	5.78×10^6	52.6	5.98×10^6	11.9	30.4	0.39

[a]Absolute values of protein and Chl labeling in PSI and PSII complexes obtained using ImageQuant software and a calibration curve for each complex (Supplemental Fig. S6). [b][^{35}S] labeling normalized to a total number of Met and Cys in D1, D2, CP43, and CP47 core proteins for PSII complexes and PsaA and PsaB core proteins for PSI. Although synthesis rates of individual PSII core proteins are different (see Fig. 5), all four proteins contain a similar number of Met and Cys and then their different syntheses can be neglected. [c]Actual synthesis of PSI/PSII complexes expressed in relative values. [d]Expected Chl labeling simulates a situation when labeled Chls are evenly distributed to individual complexes synthesized in rates determined by [^{35}S] labeling. Calculation is based on known number of Chl molecules bound to each complex (see text).

HL when visible changes in the cell pigmentation are observed (for review, see Muramatsu and Hihara, 2012; see also Fig. 1). However, almost no attention has been paid to how an optimal PSI/PSII ratio is maintained in the cyanobacterial cells already acclimated to HL, even though this is the ultimate optimum to which the whole process of acclimation is directed. In this work, we analyzed in detail the Synechocystis cells acclimated to four different irradiances; the highest one used (HL2) is close to the saturated (optimal) intensity for Synechocystis providing energy for the fastest proliferation that this cyanobacterium is probably able to achieve. Doubling time 7 h (Table I) for these cells was close to 6 h described by Hihara et al. (2001) for the same light intensity. Taking into account that the cell growth rate was twice and more than 4 times faster at HL2 than at ML and LL, respectively, it is trivial to calculate that cells have to start to produce 4 times more Chl after acclimation at HL2 just to maintain a constant Chl content per cell; it does not matter what exactly the content is. In fact, the rate of Chl formation at HL2 should be elevated more than an order of magnitude since the half-life of Chl molecules was determined by ^{15}N labeling to be at least 4 times shorter in Synechocystis cells growing at HL2 (approximately 50 h) when compared with very stable Chls found in cells acclimated to ML (half-life $>$ 200 h; Vavilin et al., 2007). This expectation corresponds well to the more intensive de novo Chl labeling (Fig. 6C), to the higher level of enzymes of the tetrapyrrole pathway (Fig. 5), and to the significantly increased levels of late Chl precursors Mg-protoporphyrin monomethyl ester and protochlorophyllide in the HL2-acclimated cells (Fig. 6B).

In light of our results and the published data, the process of acclimation to HL could be divided into two phases. In the first moment after the shift to HL, an intensive irradiation catches cells off guard and causes photooxidation demonstrated by a decrease in F_v/F_m (Supplemental Fig. S4). Cells start to mobilize a broad spectrum of protective mechanisms, including synthesis of myxoxanthophyll, an acceleration of the PSII repair cycle, and a massive expression of high light-induced proteins (HLIPs) belonging to family of Chl *a*/*b* binding proteins (for review, see Muramatsu and Hihara, 2012). According to microarray and expression data, the transcription of the *psaA/B* genes is strongly reduced (Hihara et al., 2001; Herranen et al., 2005), and because the ALA formation is also ceased (Muramatsu et al., 2009), it is likely that the PSI synthesis is minimal during an initial phase of acclimation. However, the cells continue dividing and result in the observed fast drop in PSI level in the first 4 h at HL2 caused by a simple dilution (Fig. 1B). Interestingly, levels of enzymes involved in Chl biosynthesis appear to be similar or increasing during this early time of acclimation (Fig. 5B) despite the reported decrease in their transcripts (Hihara et al., 2001). Our results are consistent with the observation of Muramatsu et al. (2009) that glutamyl-tRNA reductase, the first enzyme of Chl biosynthesis, also accumulates after 6 h of cultivating Synechocystis cells under HL. An important exception is geranylgeranyl reductase, the level of which is strongly reduced shortly after the shift to HL2 (Fig. 5B), indicating its specific degradation or an unspecific, light-induced destruction. However, the observed decrease in geranylgeranyl reductase level is unlikely a consequence of the regulatory response as this enzyme is essential for the synthesis of phytol and its inactivation in Synechocystis resulted in a Chl deficient and light sensitive strain (Shpilyov et al., 2005). A more plausible explanation is that the geranylgeranyl reductase is relatively easily damaged by light and requires a protective mechanism, which, however, is not efficient enough at the time immediately after the shift from ML to HL2. Regarding this possibility, it is interesting that LIL3 protein from the Chl *a*/*b* binding family is essential for the accumulation of geranylgeranyl reductase in higher plants (Tanaka et al., 2010). As mentioned above, cyanobacteria possess similar Chl *a*/*b*

binding proteins called HLIPs that are almost absent under LL intensities but very quickly accumulate upon exposure of cells to various stress conditions, including HL (He et al., 2001; see also below).

Based on our data, we propose that the synthesis of PSII subunits does not rely on the availability of the de novo Chl to such an extent as the trimeric PSI (Fig. 7B); thus, the synthesis of the most light-sensitive D1 subunit can be accelerated even when the availability of de novo Chl is limited during the initial phase of the HL acclimation. After this initial emergency phase, the photoprotective mechanisms start to work and in 6 h of the HL2 acclimation the F_v/F_m returns to the value observed under ML (Supplemental Fig. S4). At that particular moment, cells were already growing rapidly (J. Kopecna and R. Sobotka, unpublished data); thus, the rate of Chl formation has to be boosted to prevent an excessive loss of the thylakoid membranes. The adjustment of the PSI level and the level of phycobilisomes in proceeding approximately 10 h is probably based on a sophisticated regulatory network seeking for a balance among the redox state, Chl availability, growth rate, antenna size, and probably a number of other parameters. The two different phases of the HL acclimation are in line with the phenotype of the *pmgA* mutant; there is no change in the PSI level during the first phase, but in the second phase the PSI accumulates more than it should be (Hihara et al., 1998), indicating that due to the *pmgA* mutation, more Chl than necessary is directed to PSI.

Once the new equilibrium under HL is achieved, the levels of photosystems and phycobilisomes remain constant when the culture is kept at a similar (low) optical density that prevents shading (Fig. 1B; 16 and 24 h). As discussed above, the HL2-acclimated cells have to up-regulate Chl production to support fast growth. Labeling using [^{14}C]Glu or [^{14}C]ALA demonstrated that the main sink for the newly synthesized Chl is the trimeric PSI, a stable, Chl-rich building block of the thylakoid membranes. On the other hand, our study confirmed enhanced synthesis of PSII subunits in comparison with PSI proteins at all studied irradiances (Fig. 4). The HL sensitivity of the PSII complex to the light-induced damage necessitates a higher turnover rate of its protein subunits (especially the D1 protein) than subunits of PSI (Yao et al., 2012b). A significant disproportion between strong protein labeling versus weak Chl labeling in PSII complexes shows that the resynthesis of PSII Chl-proteins largely occurs at the expense of the recycled Chl previously released from degraded Chl-proteins. PSII complexes are completely replaced by new ones in less than a day, but the lifetime of total Chl in Synechocystis cells is much longer (see above; Vavilin et al., 2005; Yao et al., 2012a). Moreover, Xu et al. (2004) suggested that the preexisting Chl molecules in a periphery of PSI could be released and redistributed for PSII biosynthesis in the etiolating cyanobacterial cells. The exact mechanism of the Chl recycling process is not known; nevertheless, it seems to include a dissociation of the phytol chain and the chlorophyllide ring (Vavilin and Vermaas, 2007) upon PSII protein degradation and their subsequent reassociation before or during their reuse in the biogenesis of new PSII Chl-proteins (Vavilin et al., 2005; Vavilin and Vermaas, 2007). Nonetheless, despite the apparent importance of the Chl recycling, there should always be a certain input of newly synthesized Chl that replaces the lost/degraded Chl released from PSII and that also maintains sufficient Chl quantity for the enhanced de novo/repair-related PSII synthesis under the increased irradiance. The labeling of pigments showed that the input of the newly synthesized Chl into the PSII complex is enhanced after the HL2 acclimation (Fig. 7B).

The input of the de novo Chl into PSII synthesis seems to be largely independent on the main flow of the tetrapyrrole intermediates directed to PSI trimer and might represent a separate branch of the pathway. We speculate that Chl biosynthesis occurs in Chl biosynthesis centers, which contain some common general components, such as Chl biosynthesis enzymes, but may differ in regulatory proteins that are specific for individual Chl proteins (Komenda et al., 2012). In this regard, it is intriguing that the monomeric PSI is synthesized faster than the trimeric PSI but contains much less labeled Chl (Figs. 4A and 7B; Table II). This indicates that cyanobacteria possess a portion of PSI serving perhaps a specific function, which is not assembled into a trimer, has a faster turnover, and is synthesized utilizing recycled Chls. Such separated biogenesis of PSI complexes would be consistent with our idea of protein/complex-specific Chl biosynthesis centers in the cell. The small membrane proteins called HLIPs (also named small chlorophyll *a*/*b* binding proteins [SCPs]) possessing the conserved Chl *a*/*b* binding motif are promising candidates for factors controlling a precise distribution of Chl into apoproteins. HLIPs seem to play a crucial role in Chl recycling. In Synechocystis HLIP-less mutants, the half-life of Chl molecules is not affected under LL; however, under HL2, Chl is degraded much faster in the mutant than in the wild type (Vavilin et al., 2007). HLIPs also somehow modulate early steps of the Chl biosynthesis (Xu et al., 2002; Yao et al., 2012a) and physically interact with PSII assembly intermediates. Furthermore, cyanobacterial and plastidic ferrochelatase enzymes are fused at the C terminus with a HLIP protein forming the so-called CAB domain. A deletion of this domain in Synechocystis has no effect on the ferrochelatase activity or stability, but the resulting mutant accumulates significantly higher Chl level under HL (Sobotka et al., 2011).

In higher plants, particularly in matured leaves, the regulation of the harvesting capacity and the PSI/PSII ratio has to differ from cyanobacteria as plants do not contain phycobilisomes and the dilution of the thylakoid membranes by a slowly dividing chloroplast is minimal compared with fast-growing cyanobacteria. Interestingly, Chl labeling in Arabidopsis (*Arabidopsis thaliana*) was found to be accelerated after a long-term acclimation

to HL (Beisel et al., 2010), which implies that light upregulates the Chl formation in both plants and cyanobacteria. However, in another radiolabeling experiment carried out on HL-exposed rye (*Secale cereale*) chloroplasts, de novo Chl was localized predominantly in PSII, much less in PSI or in light-harvesting antennas (Feierabend and Dehne, 1996). Thus, opposed to cyanobacteria, most of the Chl produced in plant chloroplasts is probably used to support the PSII repair cycle since the need for synthesis of the new PSI complexes is very limited. Nonetheless, since the tetrapyrrole biosynthesis and the structure of the photosynthetic apparatus is so well conserved in both cyanobacteria and chloroplasts, we expect that, in principle, molecular mechanisms harmonizing the synthesis of Chl and photosystem subunits are shared generally by all oxygenic phototrophs.

MATERIALS AND METHODS

Growth Conditions

A nonmotile, Glc-tolerant strain of Synechocystis (*Synechocystis* sp. PCC 6803; Williams, 1988) obtained from the laboratory of Peter. J. Nixon (Imperial College, London) was grown photoautotrophically in BG11 medium (Rippka et al., 1979). Sixty milliliters of a liquid culture was grown at 28°C in a rotating 250-mL Erlenmeyer flask in a growing chamber under continuous illumination of 40 μE m^{-2} s^{-1} (ML). For described experiments, cells grown at ML were diluted to OD_{750} = 0.25 and shifted to 10 μE m^{-2} s^{-1} (LL), diluted to OD_{750} = 0.1 and shifted to 150 μE m^{-2} s^{-1} (HL1), or diluted to OD_{750} = 0.06 and shifted to 300 μE m^{-2} s^{-1} (HL2). After 24 h, cells were harvested in an exponential growth phase (OD_{750} = approximately 0.3). In all experiments, illumination was provided by cool-white fluorescent tubes (Osram).

Absorption Spectra and Determination of Chl Content

Absorption spectra of whole cells were measured at room temperature with a UV-3000 spectrophotometer (Shimadzu). Chl was extracted from cell pellets (2 mL, OD_{750} = approximately 0.3) with 100% (v/v) methanol, and its concentration was measured spectrophotometrically according to Porra et al. (1989).

Radioactive Labeling of Proteins and Preparations of Cell Membranes

Cells (50 μg of Chl) in an exponential growth phase (OD_{750} = approximately 0.3) were harvested by centrifugation, washed, and resuspended in fresh BG11 with 20 mM TES to a final volume 475 μL. The cell suspension was shaken in 10-mL glass tubes for 30 min at 30°C at the same light conditions as acclimated before for 24 h. [^{35}S]Met/Cys mixture (>1,000 Ci/mmol; Amersham Biosciences) was then added with the final activity of 500 μCi mL^{-1}, and illumination was continued for another 30 min. After this time period, cells were immediately frozen in liquid nitrogen. To prepare cyanobacterial membranes and cytosolic proteins, harvested cells were washed, resuspended in the thylakoid buffer containing 25 mM MES/NaOH, pH 6.5, 5 mM $CaCl_2$, 10 mM $MgCl_2$, and 20% glycerol, and broken using glass beads. The broken cells were pelleted (20,000*g*, 15 min). The supernatant represented the soluble fraction, while the sediment was resuspended in the excess volume of the thylakoid buffer, pelleted, and resuspended again in the thylakoid buffer to obtain the membrane fraction.

Electrophoresis and Immunoblotting

Analysis of membrane proteins under native conditions was performed by CN-PAGE as described by Wittig and Schägger (2008). The isolated membranes were resuspended in 25 mM MES/NaOH, pH 6.5, containing 5 mM $CaCl_2$, 10 mM $MgCl_2$, and 20% glycerol. The membranes were then solubilized in 1% *n*-dodecyl-β-maltoside and analyzed at 4°C in a 4% to 14% or 4% to 12% polyacrylamide gel. Individual proteins in membrane complexes were resolved in the second dimension by SDS-PAGE in a 12% to 20% linear gradient polyacrylamide gel containing 7 M urea (Sobotka et al., 2008). One-dimensional SDS-PAGE and immunodetection was carried out as described by Sobotka et al. (2008). The primary antibodies against subunits of Mg-chelatase and against Mg-protoporphyrin methyltransferase, light-dependent protochlorophyllide oxidoreductase, and geranylgeranyl reductase were kindly provided by Prof. C. Neil Hunter (University of Sheffield), ferrochelatase and Gun4 antibodies were kindly provided by Prof. Annegret Wilde (Justus-Liebig University, Giessen), and antibody against the plant homolog of the cyclase component Sll1214 was purchased from Agrisera.

Electron Microscopy

A small volume of the Synechocystis cells acclimated to ML and HL2 was concentrated in a sealed 200-μL tip by centrifugation at 5,000 rpm for 5 min. The obtained cell pellet was loaded into a specimen carrier (200-μm deep; Leica), pretreated with 1% lecithin in chloroform, and then ultra-rapidly frozen in a high-pressure freezer (EM Pact2; Leica). Samples were freeze-substituted in a solution of 1% tannic acid and 0.5% glutaraldehyde in acetone using an automatic freeze substitution unit (AFS, EM; Leica) as follows: 72 h at −85°C, three times rinsed with acetone for 1 h followed by a change of solution to 1% osmium/acetone, 4 h at −85°C, 5 h warming up to −25°C, 12 h at −25°C, and 6 h warming up to 4°C. Samples were removed from specimen carriers and rinsed three times in acetone at room temperate. Resin infiltration was done stepwise with 20%, 25%, 33%, 50%, 66%, and 80% steps with low viscosity Spurr's resin in acetone (SPI Supplies) for 3 h each. After infiltration with 100% resin overnight, the samples were polymerized for 48 h at 60°C. Ultrathin sections were cut on an ultramicrotome (UCT; Leica), collected on copper grids with a formvar coating, and stained with uranyl acetate for 5 min followed by lead citrate for 1 min. Sections were examined in a transmission electron microscope (JEOL 1010) equipped with a Mega View III camera (SIS).

Chl Radiolabeling, Extraction, and Detection Using TLC

The procedure of labeling Chl was identical to the protein labeling except that 180 μM of [^{14}C]Glu or [^{14}C]ALA (specific activity approximately 55 mCi/mmol; American Radiolabeled Chemicals) was used instead of [^{35}S]Met/Cys. Chl was extracted from pelleted cells using 750 μL of methanol/0.2% NH_4OH (v/v), cell debris pelleted by centrifugation, and supernatant collected. This step was repeated and supernatants combined, and NaCl was added to the final concentration of 100 mM. This solution was mixed with 400 μL of hexan and the upper phase taken. The hexan extraction was repeated three times, combined, and completely evaporated in a SpeedVac (Eppendorf). The pellet was resuspended in 0.5% KOH/methanol (v/v) and incubated at room temperature for 15 min to convert Chl to phytol-less Mg-chlorin. The suspension was then washed three times with 200 μL of hexan, concentrated by evaporation to 50 μL, and washed with 100 μL of petroleum ether (boiling range 45°C to 60°C). The solution of Mg-chlorin was dried by evaporation in a SpeedVac, resuspended in 30 μL of methanol/chloroform (1:1, v/v), and loaded on a TLC plate (SIL G-25; Macherey-Nagel). The mobile phase used was methanol/10 mM $Na_XH_YPO_4$, pH 6.8 (3:1, v/v); the dried TLC plate was exposed to an x-ray film for 5 d.

Quantification of Chl Precursors

For quantitative determination of Chl precursors in the cells, 2 mL of culture at OD_{750}= 0.35 was harvested. Pigments were extracted with 100 μL of 70% methanol, the sample was centrifuged, and the supernatant containing the extracted pigments was collected. The pellet was then extracted again using 100 μL of 80% methanol. Supernatants were combined and immediately separated by HPLC (Agilent 1200) on a reverse-phase column (Nova-Pak C18, 4-mm particle size, 3.9 3 150 mm; Waters) using 30% methanol in 1 M ammonium acetate, pH 6.7, and 100% methanol as solvents A and B, respectively. Porphyrins were eluted with a linear gradient of the solvent B (67%–74% in 20 min) at a flow rate of 0.9 mL min^{-1} at 40°C. Porphyrins were detected by two fluorescence detectors. The first fluorescence detector was set to 435/675 nm (excitation/emission wavelengths) for 0 to 11 min, 435/640 nm for 11 to 14 min, and 400/640 nm for 14 to 25 min, and the second fluorescence detector was set at 416/595 nm throughout the experiment. For retention times of individual precursors, see Figure 5A.

Supplemental Data

The following materials are available in the online version of this article.

Supplemental Figure S1. A scheme of the tetrapyrrole biosynthetic pathway in cyanobacteria.

Supplemental Figure S2. Levels of major carotenoids and chlorophyll determined in Synechocystis cells acclimated to LL, ML, and HL2.

Supplemental Figure S3. Whole-cell spectra of Synechocystis wild-type cells grown for 24 h at HL2 (300 μE m^{-2} s^{-1}) and at 600 μE m^{-2} s^{-1}.

Supplemental Figure S4. Time course of changes in F_v/F_m ratios following shift of Synechocystis cells from ML (40 μE m^{-2} s^{-1}) to HL2 (300 μE m^{-2} s^{-1}).

Supplemental Figure S5. Color figure of [^{14}C]-labeled Mg-chlorin separated on a TLC plate.

Supplemental Figure S6. A dilution series of [^{35}S]-labeled membranes separated by CN-electrophoresis and a calibration curve used for quantification of labeled PSII(2) complex.

ACKNOWLEDGMENTS

We thank Prof. C. Neil Hunter (Sheffield University, UK) and Prof. Annegret Wilde (Justus-Liebig-University, Giessen, Germany) for antibodies and Ondřej Komárek (Institute of Microbiology, Trebon, Czech Republic) for the measurement of variable Chl fluorescence of Synechocystis cells.

Received September 14, 2012; accepted October 2, 2012; published October 4, 2012.

LITERATURE CITED

Anderson JM, Chow WS, Park YI (1995) The grand design of photosynthesis: Acclimation of the photosynthetic apparatus to environmental cues. Photosynth Res **46:** 129–139

Beisel KG, Jahnke S, Hofmann D, Köppchen S, Schurr U, Matsubara S (2010) Continuous turnover of carotenes and chlorophyll a in mature leaves of Arabidopsis revealed by $^{14}CO_2$ pulse-chase labeling. Plant Physiol **152:** 2188–2199

Chow WS, Melis A, Anderson JM (1990) Adjustments of photosystem stoichiometry in chloroplasts improve the quantum efficiency of photosynthesis. Proc Natl Acad Sci USA **87:** 7502–7506

Czarnecki O, Grimm B (2012) Post-translational control of tetrapyrrole biosynthesis in plants, algae, and cyanobacteria. J Exp Bot **63:** 1675–1687

Demmig-Adams B, Adams WW (1992) Photoprotection and other responses of plants to high light stress. Annu Rev Plant Physiol Plant Mol Biol **43:** 599–626

Eichacker LA, Helfrich M, Rüdiger W, Müller B (1996) Stabilization of chlorophyll *a*-binding apoproteins P700, CP47, CP43, D2, and D1 by chlorophyll *a* or Zn-pheophytin *a*. J Biol Chem **271:** 32174–32179

El Bissati K, Delphin E, Murata N, Etienne AL, Kirilovsky D (2000) Photosystem II fluorescence quenching in the cyanobacterium *Synechocystis* PCC 6803: involvement of two different mechanisms. Biochim Biophys Acta **1457:** 229–242

Feierabend J, Dehne S (1996) Fate of the porphyrin cofactors during the light-dependent turnover of catalase and of the photosystem II reaction-center protein D1 in mature rye leaves. Planta **198:** 413–422

Fujimori T, Higuchi M, Sato H, Aiba H, Muramatsu M, Hihara Y, Sonoike K (2005) The mutant of sll1961, which encodes a putative transcriptional regulator, has a defect in regulation of photosystem stoichiometry in the cyanobacterium *Synechocystis* sp. PCC 6803. Plant Physiol **139:** 408–416

Fujita Y, Murakami A, Ohki K (1990) Regulation of the stoichiometry of thylakoid components in the photosynthetic system of cyanophytes: Model experiments showing that control of the synthesis or supply of Chl *a* can change the stoichiometric relationship between the two photosystems. Plant Cell Physiol **31:** 145–153

He Q, Dolganov N, Bjorkman O, Grossman AR (2001) The high light-inducible polypeptides in *Synechocystis* PCC6803. Expression and function in high light. J Biol Chem **276:** 306–314

Herranen M, Tyystjärvi T, Aro EM (2005) Regulation of photosystem I reaction center genes in *Synechocystis* sp. strain PCC 6803 during light acclimation. Plant Cell Physiol **46:** 1484–1493

Hihara Y, Kamei A, Kanehisa M, Kaplan A, Ikeuchi M (2001) DNA microarray analysis of cyanobacterial gene expression during acclimation to high light. Plant Cell **13:** 793–806

Hihara Y, Sonoike K, Ikeuchi M (1998) A novel gene, *pmgA*, specifically regulates photosystem stoichiometry in the cyanobacterium *Synechocystis* species PCC 6803 in response to high light. Plant Physiol **117:** 1205–1216

Jordan P, Fromme P, Witt HT, Klukas O, Saenger W, Krauss N (2001) Three-dimensional structure of cyanobacterial photosystem I at 2.5 A resolution. Nature **411:** 909–917

Komenda J, Sobotka R, Nixon PJ (2012) Assembling and maintaining the photosystem II complex in chloroplasts and cyanobacteria. Curr Opin Plant Biol **15:** 245–251

Melis A, Murakami A, Nemson JA, Aizawa K, Ohki K, Fujita Y (1996) Chromatic regulation in *Chlamydomonas reinhardtii* alters photosystem stoichiometry and improves the quantum efficiency of photosynthesis. Photosynth Res **47:** 253–265

Miskiewicz E, Ivanov AG, Huner NPA (2002) Stoichiometry of the photosynthetic apparatus and phycobilisome structure of the cyanobacterium *Plectonema boryanum* UTEX 485 are regulated by both light and temperature. Plant Physiol **130:** 1414–1425

Müller P, Li XP, Niyogi KK (2001) Non-photochemical quenching. A response to excess light energy. Plant Physiol **125:** 1558–1566

Mullineaux CW, Emlyn-Jones D (2005) State transitions: an example of acclimation to low-light stress. J Exp Bot **56:** 389–393

Murakami A, Fujita Y (1991) Regulation of photosystem stoichiometry in the photosynthetic system of the cyanophyte *Synechocystis* PCC 6714 in response to light-intensity. Plant Cell Physiol **32:** 223–230

Murakami A, Fujita Y (1993) Regulation of stoichiometry between PSI and PSII in response to light regime for photosynthesis observed with *Synechocystis* PCC 6714: relationship between redox state of Cyt $b_{6\text{-}f}$ complex and regulation of PSI formation. Plant Cell Physiol **34:** 1175–1180

Murakami A, Kim SJ, Fujita Y (1997) Changes in photosystem stoichiometry in response to environmental conditions for cell growth observed with the cyanophyte *Synechocystis* PCC 6714. Plant Cell Physiol **38:** 392–397

Muramatsu M, Hihara Y (2012) Acclimation to high-light conditions in cyanobacteria: from gene expression to physiological responses. J Plant Res **125:** 11–39

Muramatsu M, Sonoike K, Hihara Y (2009) Mechanism of downregulation of photosystem I content under high-light conditions in the cyanobacterium *Synechocystis* sp. PCC 6803. Microbiology **155:** 989–996

Neale PJ, Melis A (1986) Algal photosynthetic membrane complexes and the photosynthesis-irradiance curve: a comparison of light-adaptation responses in *Chlamydomonas reinhardtii* (Chlorophyta). J Phycol **22:** 531–538

Nixon PJ, Michoux F, Yu J, Boehm M, Komenda J (2010) Recent advances in understanding the assembly and repair of photosystem II. Ann Bot (Lond) **106:** 1–16

Nowaczyk MM, Hebeler R, Schlodder E, Meyer HE, Warscheid B, Rögner M (2006) Psb27, a cyanobacterial lipoprotein, is involved in the repair cycle of photosystem II. Plant Cell **18:** 3121–3131

Porra RJ, Thompson WA, Kriedmann PE (1989) Determination of accurate extinction coefficients and simultaneous equations for assaying chlorophylls *a* and *b* extracted with four different solvents: verification of the concentration of chlorophyll standards by atomic absorption spectroscopy. Biochim Biophys Acta **975:** 384–394

Rippka R, Deruelles J, Waterbury JB, Herdman M, Stanier RY (1979) Generic assignments, strain histories and properties of pure cultures of cyanobacteria. J Gen Microbiol **111:** 1–61

Shen G, Boussiba S, Vermaas WFJ (1993) Synechocystis sp PCC 6803 strains lacking photosystem I and phycobilisome function. Plant Cell **5:** 1853–1863

Shpilyov AV, Zinchenko VV, Shestakov SV, Grimm B, Lokstein H (2005) Inactivation of the geranylgeranyl reductase (ChlP) gene in the cyanobacterium *Synechocystis* sp. PCC 6803. Biochim Biophys Acta **1706:** 195–203

Sobotka R, Dühring U, Komenda J, Peter E, Gardian Z, Tichý M, Grimm B, Wilde A (2008) Importance of the cyanobacterial Gun4 protein for chlorophyll metabolism and assembly of photosynthetic complexes. J Biol Chem **283:** 25794–25802

Sobotka R, Tichý M, Wilde A, Hunter CN (2011) Functional assignments for the carboxyl-terminal domains of the ferrochelatase from *Synechocystis* PCC 6803: the CAB domain plays a regulatory role, and region II is essential for catalysis. Plant Physiol **155:** 1735–1747

Sonoike K, Hihara Y, Ikeuchi M (2001) Physiological significance of the regulation of photosystem stoichiometry upon high light acclimation of Synechocystis sp. PCC 6803. Plant Cell Physiol **42:** 379–384

Tanaka R, Rothbart M, Oka S, Takabayashi A, Takahashi K, Shibata M, Myouga F, Motohashi R, Shinozaki K, Grimm B, et al (2010) LIL3, a light-harvesting-like protein, plays an essential role in chlorophyll and tocopherol biosynthesis. Proc Natl Acad Sci USA **107:** 16721–16725

Umena Y, Kawakami K, Shen JR, Kamiya N (2011) Crystal structure of oxygen-evolving photosystem II at a resolution of 1.9 Å. Nature **473:** 55–60

Vavilin D, Brune DC, Vermaas WFJ (2005) ^{15}N-labeling to determine chlorophyll synthesis and degradation in *Synechocystis* sp. PCC 6803 strains lacking one or both photosystems. Biochim Biophys Acta **1708:** 91–101

Vavilin D, Vermaas WFJ (2007) Continuous chlorophyll degradation accompanied by chlorophyllide and phytol reutilization for chlorophyll synthesis in *Synechocystis* sp. PCC 6803. Biochim Biophys Acta **1767:** 920–929

Vavilin D, Yao D, Vermaas WFJ (2007) Small Cab-like proteins retard degradation of photosystem II-associated chlorophyll in *Synechocystis* sp. PCC 6803: kinetic analysis of pigment labeling with ^{15}N and ^{13}C. J Biol Chem **282:** 37660–37668

Wallner T, Hagiwara Y, Bernát G, Sobotka R, Reijerse EJ, Frankenberg-Dinkel N, Wilde A (2012) Inactivation of the conserved open reading frame *ycf34* of *Synechocystis* sp. PCC 6803 interferes with the photosynthetic electron transport chain. Biochim Biophys Acta **1817:** 2016–2026

Walters RG (2005) Towards an understanding of photosynthetic acclimation. J Exp Bot **56:** 435–447

Walters RG, Horton P (1994) Acclimation of *Arabidopsis thaliana* to the light environment: changes in composition of the photosynthetic apparatus. Planta **195:** 248–256

Williams JGK (1988) Construction of specific mutations in photosystem II photosynthetic reaction center by genetic engineering methods in *Synechocystis* 6803. Methods Enzymol **167:** 766–778

Wittig I, Schägger H (2008) Features and applications of blue-native and clear-native electrophoresis. Proteomics **8:** 3974–3990

Xu H, Vavilin D, Funk C, Vermaas W (2002) Small Cab-like proteins regulating tetrapyrrole biosynthesis in the cyanobacterium *Synechocystis* sp. PCC 6803. Plant Mol Biol **49:** 149–160

Xu H, Vavilin D, Funk C, Vermaas W (2004) Multiple deletions of small Cab-like proteins in the cyanobacterium Synechocystis sp. PCC 6803: consequences for pigment biosynthesis and accumulation. J Biol Chem **279:** 27971–27979

Yao DC, Brune DC, Vavilin D, Vermaas WF (2012a) Photosystem II component lifetimes in the cyanobacterium *Synechocystis* sp. strain PCC 6803: small Cab-like proteins stabilize biosynthesis intermediates and affect early steps in chlorophyll synthesis. J Biol Chem **287:** 682–692

Yao DC, Brune DC, Vermaas WF (2012b) Lifetimes of photosystem I and II proteins in the cyanobacterium *Synechocystis* sp. PCC 6803. FEBS Lett **586:** 169–173

Publication V

Molecular Microbiology (2014) 93(6), 1207–1223 ■
doi:10.1111/mmi.12730
First published online 12 August 2014

Accumulation of the Type IV prepilin triggers degradation of SecY and YidC and inhibits synthesis of Photosystem II proteins in the cyanobacterium *Synechocystis* PCC 6803

Markéta Linhartová,[1,2] Lenka Bučinská,[1,2] Petr Halada,[3] Tomáš Ječmen,[4] Jiří Šetlík,[1] Josef Komenda[1,2] and Roman Sobotka[1,2]*

[1]*Institute of Microbiology, Academy of Sciences, Opatovický mlýn, 37981 Třeboň, Czech Republic.*
[2]*Faculty of Sciences, University of South Bohemia, Branišovská 31, 37005 České Budějovice, Czech Republic.*
[3]*Institute of Microbiology, Academy of Sciences, Vídeňská 1083, 14220 Prague 4, Czech Republic.*
[4]*Department of Biochemistry, Faculty of Science, Charles University in Prague, Hlavova 8, 128 43 Prague, Czech Republic.*

Summary

Type IV pilins are bacterial proteins that are small in size but have a broad range of functions, including motility, transformation competence and secretion. Although pilins vary in sequence, they possess a characteristic signal peptide that has to be removed by the prepilin peptidase PilD during pilin maturation. We generated a *pilD* (*slr1120*) null mutant of the cyanobacterium *Synechocystis* 6803 that accumulates an unprocessed form of the major pilin PilA1 (pPilA1) and its non-glycosylated derivative (NpPilA1). Notably, the *pilD* strain had aberrant membrane ultrastructure and did not grow photoautotrophically because the synthesis of Photosystem II subunits was abolished. However, other membrane components such as Photosystem I and ATP synthase were synthesized at levels comparable to the control strain. Proliferation of the *pilD* strain was rescued by elimination of the *pilA1* gene, demonstrating that PilA1 prepilin inhibited the synthesis of Photosystem II. Furthermore, NpPilA1 co-immunoprecipitated with the SecY translocase and the YidC insertase, and both of these essential translocon components were degraded in the mutant. We propose that unprocessed prepilins inactivate an identical pool of translocons that function in the synthesis of both pilins and the core subunits of Photosystem II.

Accepted 23 July, 2014. *For correspondence. E-mail sobotka@alga.cz; Tel. (+42) 384 340491; Fax (+42) 384 340415.

Introduction

Bacterial Type IV pilins, pseudopilins and the related archaeal flagellins form a large family of proteins with an extraordinary broad spectrum of functions. They are implicated in motility, genetic transformation, cell aggregation, secretion or even serve as electrically conductive nanowires (reviewed in Giltner *et al.*, 2012). The signature of Type IV pilins is a cleavable N-terminal signal peptide (SP) followed by a conserved hydrophobic segment (Fig. 1). The C-terminal domain forms a globular head faced to periplasmic space and, although its sequence is usually quite divergent, the available crystal structures are highly conserved and contain four-stranded anti-parallel β-sheets (Giltner *et al.*, 2012).

In the current model of pilin biogenesis, pilins are co-translationally inserted into the membrane by the Sec pathway (Arts *et al.*, 2007; Francetic *et al.*, 2007). The SP is then removed by a dedicated membrane-bound prepilin peptidase called PilD, and the same enzyme also methylates the amino-terminal residue (Holt *et al.*, 2005; reviewed in Dalbey and Kuhn, 2012). PilD belongs to a family of aspartyl proteases (Dalbey and Kuhn, 2012) and cleaves prepilins roughly proximal to the membrane surface, consistently with the recently published structure of the related presenilin protease (Li *et al.*, 2013). The cleavage of the SP is necessary for further processing of all known Type IV pilins into functional structures (Giltner *et al.*, 2012).

It is unclear how mature pilins are extruded from the lipid bilayer and polymerized into long fibres. According to the current knowledge, pilus assembly requires the interaction of at least 15 proteins (Carbonnelle *et al.*, 2006). The core components of the assembly machinery are the PilQ secretin, a channel in the outer membrane through which the pilus fibre (polymerized pilins) exits the cell, and PilC, which forms a platform in the inner membrane. PilQ is a large multimer exposed within the periplasm, and the other components of the assembly machinery are most likely arranged around the PilQ-PilC scaffold in a compact structure spanning the entire cell envelope (Burrows, 2012; Tammam *et al.*, 2013). The hexameric ATPase PilB associates with PilC (Takhar *et al.*, 2013) and generates force to move pilins from the inner membrane under

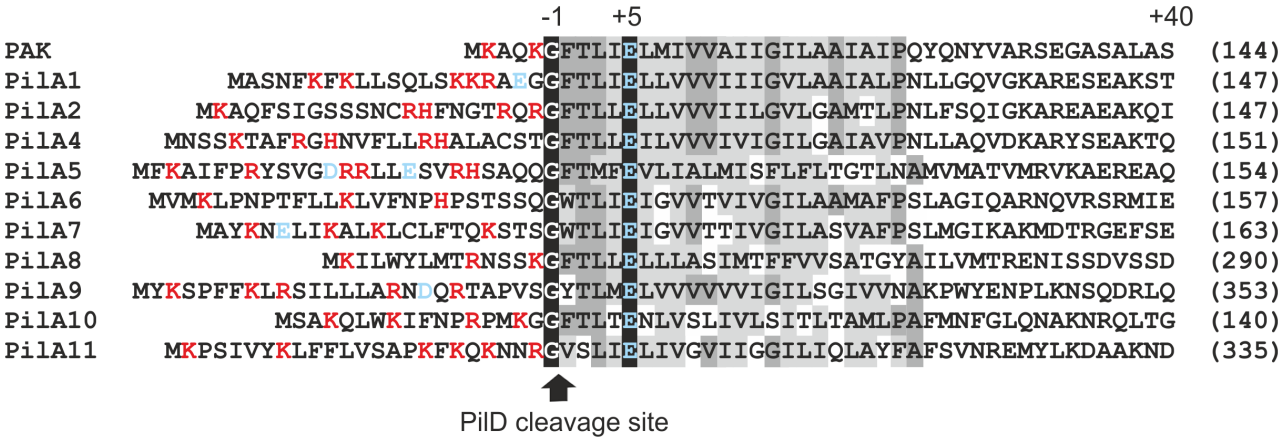

Fig. 1. Alignment of putative pilin proteins encoded in the *Synechocystis* genome and the canonical Type IV pilin (PAK) from *Pseudomonas aeruginosa*. The leader peptide and first 40 N-terminal residues were aligned based on the PilD peptidase cleavage site (marked by an arrow). The cleavage domain contains hydrophobic amino acids between the conserved glycine (– 1) and glutamic acid (+ 5) residues. The membrane segment is shown in grey, the positively and negatively charged amino acid residues in the leader peptide and in the membrane segment are highlighted in red and blue, respectively, and the total length of each mature protein is indicated on the right.

assistance of other critical components (PilM, PilN, PilO and PilP). Pilin polymerization is reversible, and cycles of pilus assembly and disassembly underlie twitching motility (Burrows, 2012).

Cyanobacteria form an important bacterial phylum that emerged at the dawn of life on Earth (Knoll, 2008). These organisms have evolved an efficient photoautotrophic metabolism based on oxidation of water molecules, which is powered by energy of photons. The evolution of cyanobacteria relying on oxygenic photosynthesis and possessing an endogenous thylakoid membrane system had to result in substantial remodelling of the original bacterial structures. Indeed, more than a hundred protein families universally shared by cyanobacteria have no counterparts in other bacteria (Mulkidjanian *et al*., 2006). Although cyanobacteria are highly specialized, many typical bacterial structures have been preserved over billions of years after the branching of cyanobacteria and bacteria; an example is Type IV pilus-based motility (Bhaya *et al*., 2000). However, genomic data show that cyanobacterial strains often contain unusually high numbers of type IV pilin-like genes (Table S1). For instance, the genome of the cyanobacterium *Acaryochloris marina* contains at least 16 genes with the typical pilin signature (Table S1). The genome of the best-studied cyanobacterium *Synechocystis* PCC 6803 (hereafter referred to as *Synechocystis*) encodes 10 putative Type IV pilin proteins (Fig. 1), and only four of these proteins (PilA1, PilA9, PilA10, PilA11) are essential for motility (Bhaya *et al*., 2000; 2001; Yoshihara *et al*., 2001). The functions of other pilin-like proteins remain unknown. Surprisingly, He and Vermaas (1999) observed that cyanobacterial pilins are implicated in the biogenesis of Photosystem II (PSII). They analysed a multiple *Synechocystis* mutant that synthesized chlorophyll only under light conditions and also lacked Photosystem I (PSI). After incubation in the dark, the mutant cells were almost entirely depleted of chlorophyll; therefore, these mutant cells enabled the study of early events in PSII biogenesis, which were unmasked by the absence of abundant chlorophyll complexes. Notably, the first observable green complex during re-greening contained typical pilin proteins (He and Vermaas, 1999). The authors also demonstrated that the appearance of this first chlorophyll complex was significantly delayed when two pilin genes (*pilA1, pilA2*) were inactivated (He and Vermaas, 1999).

In this study, we assessed the photosynthetic performance of *Synechocystis* mutants lacking pilins or proteins essential for the biogenesis of pilus fibres. Interestingly, unlike other tested strains that showed no obvious growth phenotypes, the *pilD* null strain lacking the prepilin peptidase proliferated only when the growth medium was supplemented with glucose. We demonstrated that the loss of photoautotrophy in *pilD* was caused exclusively by the toxicity of the unprocessed form (prepilin) of the major pilin PilA1. The presence of the prepilin in membranes strongly impaired the synthesis of PSII subunits but not PSI and induced the degradation of Sec translocons. These data suggest that the PilA1 prepilin interferes with the translocon machinery required for the synthesis of pilins and PSII.

Results

The Synechocystis pilD *(*slr1120*) mutant accumulates two forms of PilA1 prepilin*

The pilin mutants used in this study (listed in Table 1) were derived from the glucose-tolerant *Synechocystis* WT-V

Table 1. Characteristics of *Synechocystis* strains used in this study.

Strain	Resistance	Mutation	Ref. for construct	Photoautotrophic growth
pilA1-2	Zeo	del[a]:89–782	This study	+
pilA2	Spec	ins[b]:57	Bhaya *et al.* (2000)	+
pilA4	Kan	del:206–528(+54)[c]	He and Vermaas (1999)	+
pilA5-8	Zeo	del:74–2190	This study	+
pilA9-11	Zeo	del:100–2479	This study	+
pilB1	Zeo	del:113–614	This study	+
pilQ	Cm	del:72–955	This study	+
pilD	Kan	del:4–570	Bhaya *et al.* (2000)	–
pilD/pilA1-2	Kan, Zeo		This study	+
pilD/pilA2	Kan, Spec		This study	–

a. Replacement of the indicated gene region (in base pairs) by the antibiotic-resistance cassette.
b. Insertion of the antibiotic-resistance cassette into the gene after nucleotide 57.
c. The deletion includes the first 54 bp down-stream of the *pilA4* gene.
Photoautotrophic growth was monitored by growing the mutant cells on BG11 plates under moderate-light conditions (40 $\mu E\ s^{-1}\ m^{-2}$) or high-light conditions (300 $\mu E\ s^{-1}\ m^{-2}$) for 2 weeks. + indicates that the proliferation of the strain was comparable to the WT under both tested conditions. The antibiotic-resistance genes conferred resistance to Zeo (zeocin), Spec (spectinomycin), Kan (kanamycin) or Cm (chloramphenicol).

sub-strain (Trautmann *et al.*, 2012). Unlike the original *Synechocystis* PCC strain, the WT-V sub-strain is non-motile because of a mutation in the SpkA signalling kinase (Kamei *et al.*, 2001); however, the biogenesis and the assembly of pilus fibres are not affected (Fig. S1). The use of the WT-V sub-strain (hereafter WT) genetic background eliminates the 'false-positive' phenotypes that might be observed if the immotile mutants were compared with a motile control.

The studied pilin mutants exhibited no obvious growth defects under moderate- and high-light conditions, with the exception of the *pilD* (*slr1120*) strain that lacks the putative prepilin peptidase. This strain was strictly mixotrophic and survived for a prolonged time (days) only on agar plates supplemented with glucose (Fig. 2A). Similarly, the *pilD* cells grew slowly in liquid culture with glucose, although they formed large aggregates; however, in media lacking glucose, the proliferation of this mutant ceased (not shown).

The PilA1 protein is the major structural component of thick pili in *Synechocystis* (Bhaya *et al.*, 2000) and is presumably the main substrate of the prepilin peptidase. Indeed, the *pilD* strain accumulated a PilA1 form with a lower electrophoretic mobility than the mature PilA1 (Fig. 3A), which corresponded well to the expected size of the prepilin molecule (pPilA1). Detection of this protein supported identity of the *slr1120* gene product as the Type IV prepilin peptidase. However, there was also a second PilA1 form with higher mobility than the mature PilA1 (Fig. 3A). Origin of this band was rather enigmatic and therefore we analysed it in detail by N-terminal sequencing and mass-spectrometry. The analyses showed that the protein contained the entire signal peptide (SP) with exception of the N-terminal methionine but it also contained the C-terminus including tri-methylated Lys residue (Fig. 3B), which excluded a truncation at the C-terminus of the protein. We further tested whether both prepilins contain a disulphide bridge, which is typical feature of the Type IV pilins (Giltner *et al.*, 2012). As shown in Fig. S2, the migration of both prepilins on SDS-PAGE gels was similarly shifted in the presence and absence of dithiothreitol (DTT), suggesting that both prepilins were present in the cells in an oxidized state (Motohashi *et al.*, 2001).

As the lower-mass form of prepilin contained all amino acid residues of the putative prepilin the most probable reason for its faster mobility was its insufficient post-translational modification. Indeed, the *Synechocystis* PilA1 protein has been reported to be *O*-glycosylated between residues 67 and 75 with Thr73 as the most probable residue binding the glycan composed of xylose and fucose (Kim *et al.*, 2009). An increased PilA1 glycosylation has resulted in the reduced electrophoretic mobility (Fig. 3A; Kim *et al.*, 2009), on the other hand insufficient post-translational modification of PilA1, most probably glycosylation, has led to the similar shift, which we observed between the prepilin forms (Kim *et al.*, 2004). Indeed, the mass-spectrometry analysis of the lower-mass prepilin showed no signals that would correspond to *O*-glycosylated peptide 67–75 (Fig. 3B) and therefore, we designated this protein as NpPilA1 (*N*on-glycosylated *p*repilin) and the slower migrating form as pPilA1.

The observed population of NpPilA1 indicated that either the process of prepilin glycosylation was very slow or, alternatively, a pool of prepilin escaped glycosylation. To discriminate between these possibilities we assessed the pPilA1 and NpPilA1 levels after 60 min incubation in the presence of the protein synthesis inhibitor chloramphenicol. As this treatment did not change the ratio

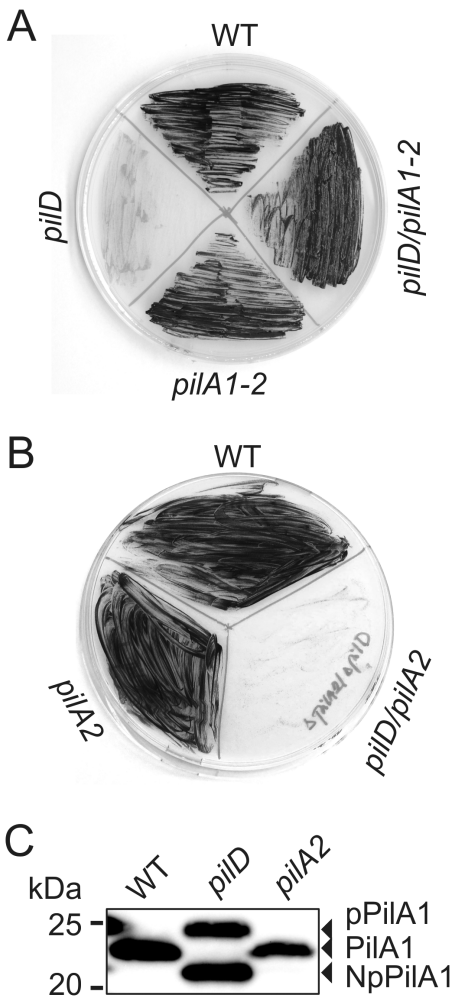

Fig. 2. Growth and complementation of the *pilD* mutant.
A and B. (A) Photoautotrophy of the *pilD* strain is rescued by deletion of the *pilA1-pilA2* chromosomal region (*pilA1-2*) but not by inactivation of the *pilA2* gene alone (B); see Table 1 for strain descriptions. Glucose-free BG11 plates were inoculated with similar amounts of cells and incubated in continuous moderate light (40 μE m^{-2} s^{-1}) for 10 days.
C. Immuno-detection of PilA1 in the *pilA2* strain grown under Glc– conditions; WT and *pilD* were included as controls and immunoblotting was performed as described for Fig. 3A.

between both proteins (Fig. S2), it implied that the *pilD* cells accumulated significant amount of non-glycosylated PilA1 prepilin that was neither additionally processed nor promptly degraded.

The PilD peptidase is essential for the function of the photosynthetic apparatus

The ability of *Synechocystis* cells to grow photoautotrophically apparently did not depend on the functional pilus biogenesis. *Synechocystis* mutants lacking factors essential for pilus assembly (*pilB* and *pilQ*) or the *pilA* genes/operons (*pilA1-2*, *pilA4*, *pilA5-8*, *pilA9-11*; Table 1) had no obvious growth defect (Table 1). Therefore, the presence of mature but unassembled pilin proteins in *pilB* and *pilQ* null mutants did not affect photoautotrophy. Similarly, the absence of either major (PilA1) or minor (pseudo)pilin proteins (PilA2, PilA4, PilA5-8, PilA9-11) had no significant effect on *Synechocystis* viability (Fig. 2, Table 1).

To understand the critical role of PilD in photosynthesis, we analysed the *pilD* strain grown in the presence of glucose (Glc+) and 24 h after its shifting to glucose–free medium (Glc–). The whole-cell spectra showed that the *pilD* cells grown in Glc+ contained virtually normal levels of photosynthetic pigments, except for a lower amount of carotenoids (Fig. 4A). This result was confirmed by the spectroscopic quantification of chlorophyll in the methanol extract (WT = 5.2, *pilD* = 5.5 μg chlorophyll ml^{-1} of cells at OD_{750} = 1). After shifting to Glc–, the total amount of chlorophyll in WT decreased (4.5 μg chlorophyll ml^{-1}; Fig. 4A) because of decreased PSI content, which is a characteristic response of the WT-V sub-strain to Glc– conditions (R. Sobotka and J. Komenda, unpublished data). No decrease in chlorophyll content was observed in the *pilD*, indicating that this regulatory mechanism does not work properly in the mutant (Fig. 4A; see *Discussion*). The PSII/PSI ratio was assessed by low-temperature (77K) chlorophyll emission spectra measured on intact cells. In principle, chlorophyll molecules bound to PSI and PSII complexes emit at characteristic wavelengths, which allows to compare photosystem stoichiometry *in vivo* (Fig. 4B). Most PSII chlorophylls emit at 685 nm except for one emitting at 695 nm which is quite specific for the active intact PSII complexes (Sinha *et al.*, 2012). The origin of the 685 peak is rather complex and includes also inactive PSII and its unassembled subunits (Sinha *et al.*, 2012), other chlorophyll-binding proteins like Hlips (Knoppová *et al.*, 2014) and an emission from phycobilisomes (Hernandez-Prieto *et al.*, 2011). On the other hand, PSI complexes are typical by the emission with maximum around 725 nm. The measurement showed that the mutant contained much less PSII complexes than WT when normalized to PSI level and also the PSI/PSII ratio in the mutant did not changed significantly in Glc– conditions (Fig. 4B), consistently to the whole-cell spectra (Fig. 4A). However, if the PSII level is low, the PSI and 685 peaks can contribute significantly to the 695 emission and, therefore, the evaluation of PSII/PSI ratio from 77K spectra should be made with caution. We therefore also compared levels of PSI (PsaD) and PSII (D1) subunits by immunoblotting using specific antibodies. In Glc+ condition the mutant cells contained higher levels of PsaD and a similar level of D1 relative to the control, but the D1 content decreased markedly after the shift to Glc– conditions whereas the PSI level remained rather constant (Fig. 4D). Finally, PSII activity was addressed directly by measuring oxygen evolution. This analysis revealed that

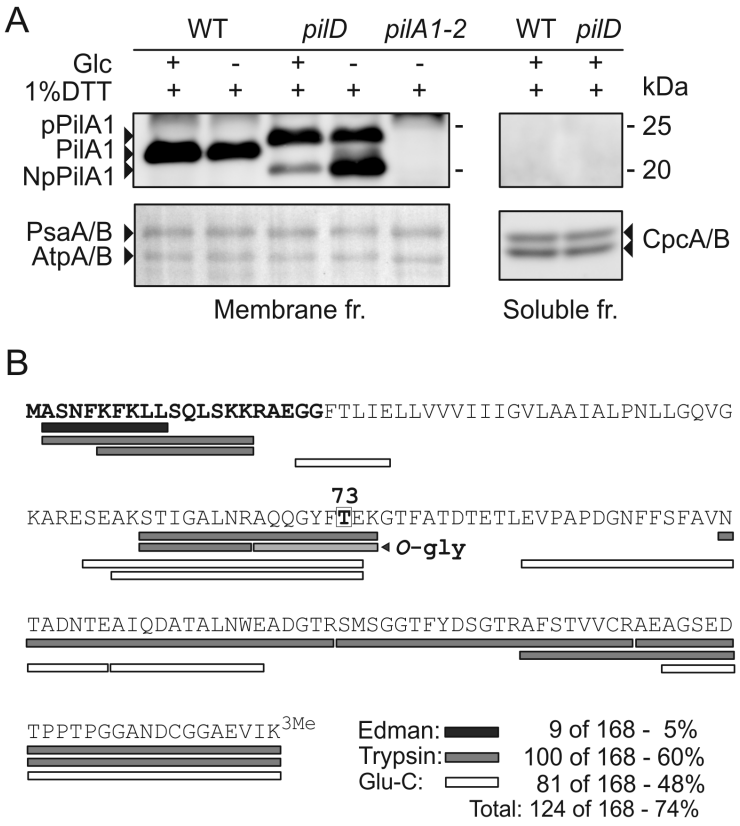

Fig. 3. A. Immuno-detection of the PilA1 prepilin in *Synechocystis pilD* cells. The *pilD* (*slr1120*) mutant lacks the mature form of PilA1 but accumulates the PilA1 prepilin (pPilA1) and a non-glycosylated form of the PilA1 prepilin (NpPilA1), both exclusively in the membrane fraction. Accumulation of the NpPilA1 form is increased after shifting of the *pilD* cells to glucose-free growth medium for 24 h (*pilD* Glc–). The PilA1 protein was detected using a specific antibody, and the membranes isolated from the *pilA1-2* strain were loaded as a control. The blotted proteins stained with Ponceau S are shown below as a loading control; the PsaA/B, AtpA/B and CpcA/B proteins are indicated. The same amount of chlorophyll (0.75 μg) was loaded in each line.
B. Peptide map of the NpPilA1 displaying sequence coverage and peptides generated by trypsin (grey bars, coverage 60%) and Glu-C protease (white bars, coverage 48%). The LC-MS analyses and Edman N-terminal sequencing (black bars, coverage 5%) data cover altogether 74% of the protein sequence. Apart from the absence of initial methionine and the tri-methylation of C-terminal lysine residue (3Me) the data show no other modification of the prepilin sequence. The trypsin peptide 67–75 shown previously to be *O*-glycosylated in the mature PilA1 protein (Kim *et al*., 2009) is highlighted (*O*-gly) including the candidate residue Thr73 (boxed).

the *pilD* cells (Glc+) had approximately half the PSII activity of the WT, and after the shift to Glc–, PSII activity in the mutant further decreased to approximately 20% of the WT (Fig. 4C). Together, these data demonstrated that the mutant maintained enough PSI complexes in both growth conditions tested but the number of functional PSII was low even in presence of glucose and further reduced under photoautotrophic conditions.

While the cell spectra did not suggest extensive changes in the thylakoid membrane system in the *pilD* mutant (Fig. 4A), inspection of the ultrastructure of *pilD* cells by electron microscopy unveiled abundance of abnormal membrane-like structures located in the vicinity of the cytoplasmic membrane (Fig. 5C–F). Vesicle-like and curled forms of membranes can be distinguished. Such structures were not observed in WT cells (Fig. 5A and B). Previously, formation of intracellular membranes has also been observed in *Escherichia coli* mutants lacking the signal recognition particle or SecE components of the translocation machinery (Herskovits *et al*., 2002).

We can conclude that the inactivation of the prepilin peptidase in *Synechocystis* impaired function of the photosynthetic apparatus to such extent that the *pilD* mutant was unable to grow photoautotrophically. Although the *pilD* mutant had capacity to build thylakoid membranes and contained a sufficient level of PSI, it had aberrant membrane ultrastructure and impaired activity of PSII. It appears that in the absence of an external source of reduced carbon, the *pilD* cells failed to maintain a critical number of functional PSII complexes and died.

Elimination of the pilA1 *gene restores the photosynthetic capacity of the* pilD *mutant*

Thick pili are assembled from hundreds of PilA1 subunits (Bhaya *et al*., 2000) hence the PilA1 proteins need to be produced in large quantities. Indeed, based on ^{35}S protein labelling, PilA1 is one of the most intensively synthesized membrane proteins in *Synechocystis* (Fig. 7) and the uncontrolled accumulation of the PilA1 prepilin could somehow impair the photosynthetic apparatus. On the *Synechocystis* chromosome, the *pilA1* gene is followed by *pilA2*, a pilin gene with no essential role in motility (Fig. 1; Yoshihara *et al*., 2001). Strikingly, the parallel deletion of the *pilA1-2* cluster and the *pilD* gene caused no defect in photoautotrophic growth compared to the WT (Fig. 2A), although cell aggregates were formed in liquid culture (not shown). We also generated a strain lacking only the *pilA2* gene (Table 1), and this mutation did not significantly affect the accumulation of the PilA1 protein (Fig. 2C) and did not rescue the *pilD* phenotype (Fig. 2B). These experiments demonstrated

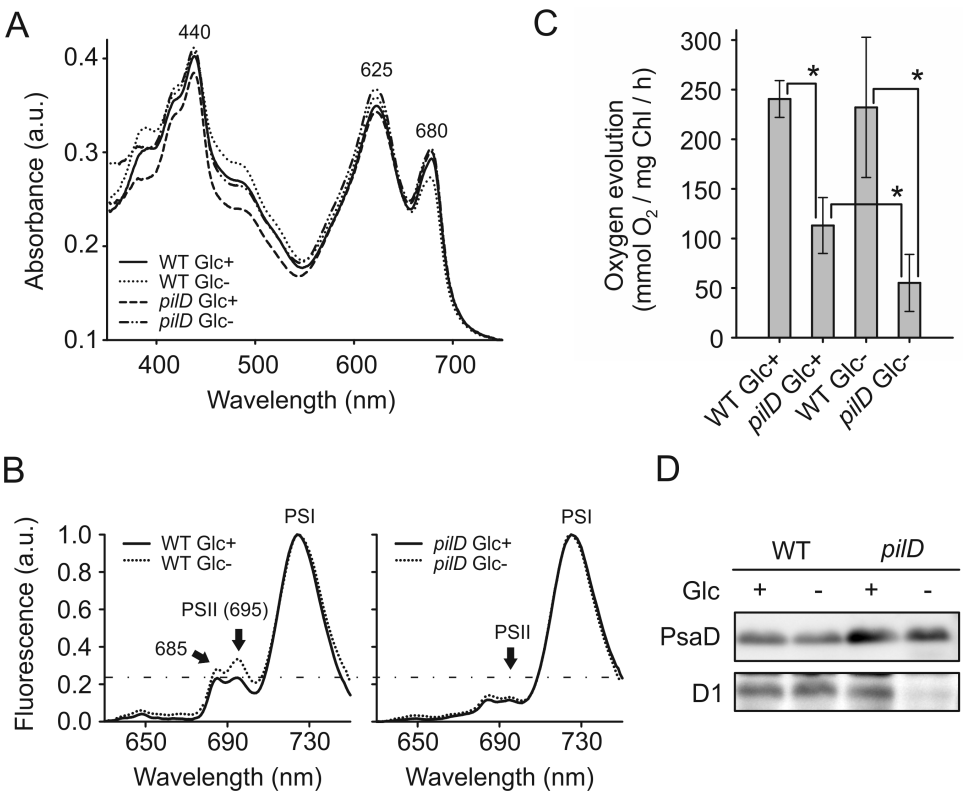

Fig. 4. Level and activity of PSII in the *Synechocystis pilD* strain.
A. Cell absorbance spectra of the WT and *pilD* strains under mixotrophic conditions (Glc+) and after shifting to the glucose-free medium for 24 h (Glc–). Chlorophyll is represented by the 440 and 680 nm peaks, phycobiliproteins by the 625 nm peak and carotenoids by the peaks in the range of 440–520 nm. The spectra were normalized to light scattering at 750 nm.
B. Low-temperature (77 K) fluorescence emission spectra of the WT and *pilD* cells grown under Glc+ and Glc– conditions. Peaks at 695 and 722 nm represent PSII and PSI complexes respectively. a.u., arbitrary units. The spectra were collected using excitation wavelength 435 nm to excite chlorophyll and were normalized to PSI peak.
C. The rate of oxygen evolution in the WT and *pilD* strains under conditions described in (A); the same numbers of cells normalized to light scattering at 750 nm were assayed. The values shown represent the means ± SD from three independent measurements, and asterisks indicate significant differences in oxygen levels as tested using a paired *t*-test ($P = 0.05$).
D. The level of the PSI subunit PsaD and PSII subunit D1 in the WT and *pilD* mutant. The membrane proteins were separated by SDS-PAGE, blotted and probed using specific antibodies; the same amount of chlorophyll (0.75 μg) was loaded in each lane.

that PilA1 prepilin was detrimental to *Synechocystis* cells and caused the *pilD* growth phenotype.

Accumulation of prepilin inhibits the synthesis of essential membrane complexes

To monitor the effect of the *pilD* mutation on protein synthesis/stability, we performed pulse-chase protein radiolabelling of *pilD* and WT strains grown in Glc– conditions. The labelled membrane proteins were separated by SDS-PAGE, and the gel was stained with Sypro Orange, dried and exposed to a phosphorimager plate (Fig. 6A). The autoradiograph demonstrated an inhibition of protein synthesis in the mutant, although the stability of the synthesized proteins was not altered. Significantly, the characteristic bands of the intensively labelled D1 subunit and the partly mature iD1 precursor (Komenda *et al.*, 2007) were practically undetectable in the mutant, suggesting that PSII synthesis and repair were drastically affected by the presence of prepilin. However, the synthesis of core PSI subunits PsaA/B appeared to be similar in the mutant and the WT (Fig. 6). This result suggested that the prepilin inhibited a subset of membrane proteins rather than had a global impact on the protein synthesis. We compared protein labelling pattern in the mutant (Fig. 6A) with a long (8 h) pulse-labelling of WT cells treated with a lethal concentration of chloramphenicol (50 mg l^{-1}; Fig. 6B). Indeed, chloramphenicol drastically reduced the total protein synthesis but the D1 protein synthesis could still be detected while signals of other membrane proteins disappeared completely (Fig. 6B). Given the very intensive labelling of D1 protein in the control (Fig. 6B), the pool of ribosomes translating D1 protein had to comprise a substantial portion of all ribosomes in the cell. If the translation machinery is

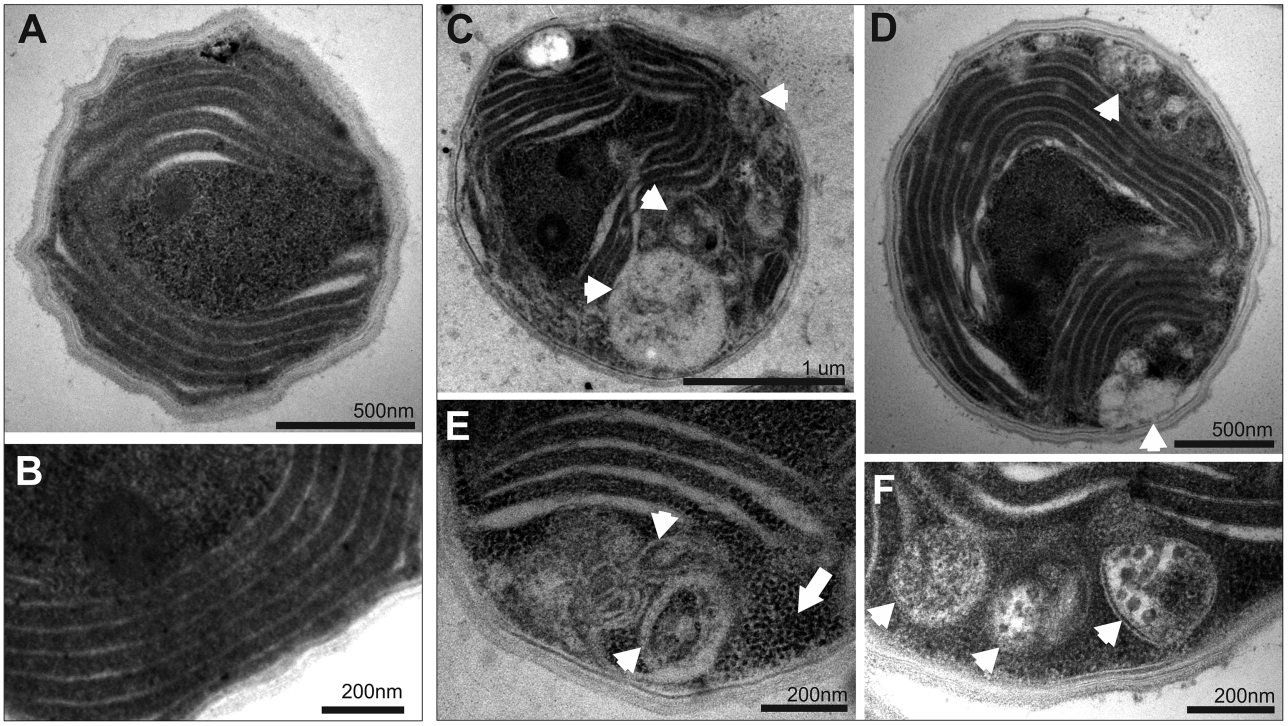

Fig. 5. Transmission electron microscopy of the *Synechocystis* WT and *pilD* cells. Representative stained ultra-thin sections of cells grown for 24 h in glucose-free medium (Glc–). (A) WT cells and (B) a detail of the WT thylakoid membranes. (C and D) *pilD* cells and (E and F) details of unusual membrane structures (marked by white arrowheads) observed in this strain. Note the high concentration of ribosomes in the vicinity of these structures (white arrow).

globally impaired, the D1 protein has certainly better chances to be synthesized, though with limited rate, than e.g. PSI core subunits. We concluded that the observed phenotype of the *pilD* mutant could not be caused by a global defect in protein synthesis but the accumulation of prepilin hit quite specifically otherwise intensive synthesis of PSII subunits.

The toxic effect of prepilin was further explored combining pulse-chase labelling and 2D protein electrophoresis. Similar amounts of WT and *pilD* membranes (based on chlorophyll content) were solubilized using dodecyl-*b*-maltoside (DDM) and subjected to Clear-Native electrophoresis (CN-PAGE, Fig. 7). Consistently with the above data, the native gel revealed significantly lower levels of dimeric and monomeric PSII complexes in the *pilD* sample (note the detection of chlorophyll fluorescence in Fig. 7). Separation of the CN-gel in the second dimension by SDS-PAGE confirmed the low content of individual PSII subunits in the mutant, and it also revealed a strongly reduced level of the NADH dehydrogenase complex (Fig. 7). However, the ATP synthase and the cytochrome b_6f complexes were still fairly abundant in the mutant; refer to (Herranen *et al.*, 2004) for a description of the identification of individual protein spots. The PilA1, pPilA1 and NpPilA1 spots were identified by mass-spectrometry (not shown). Furthermore, no membrane-bound ribosomes were visible in the *pilD* sample, which contrasted with abundance of ribosome subunits running at the top of the CN gel in the WT sample (Fig. 7) and with large numbers of ribosomes in *pilD* cells observed using electron microscopy (Fig. 5).

Notably, the 2D spots of pPilA1 and NpPilA1 were quite weak in the mutant sample, whereas PilA1 was among the most abundant membrane proteins in the WT (Fig. 7). This observation was inconsistent with the comparable levels of pPilA1, NpPilA1 and PilA1 detected by immunoblotting analysis of the completely denatured membrane fractions (Fig. 3A) and suggested that prepilins had limited solubility in DDM. In a separate experiment, we assessed the solubility of membrane proteins and observed that a fraction of pPilA1 and most of NpPilA1 remained insoluble after extraction of the membranes using DDM (Fig. S4). Therefore, it is likely that both forms of prepilins were prevalently localized in a compact structure(s) resistant to mild detergents. As a control, both photosystems were completely solubilized by DDM (Fig. S4); therefore, the analysis of PSII based on the 2D gel system was not biased by its partial solubility.

Exposing the 2D gels to a phosphorimager plate allowed us to assess the synthesis of membrane complexes during

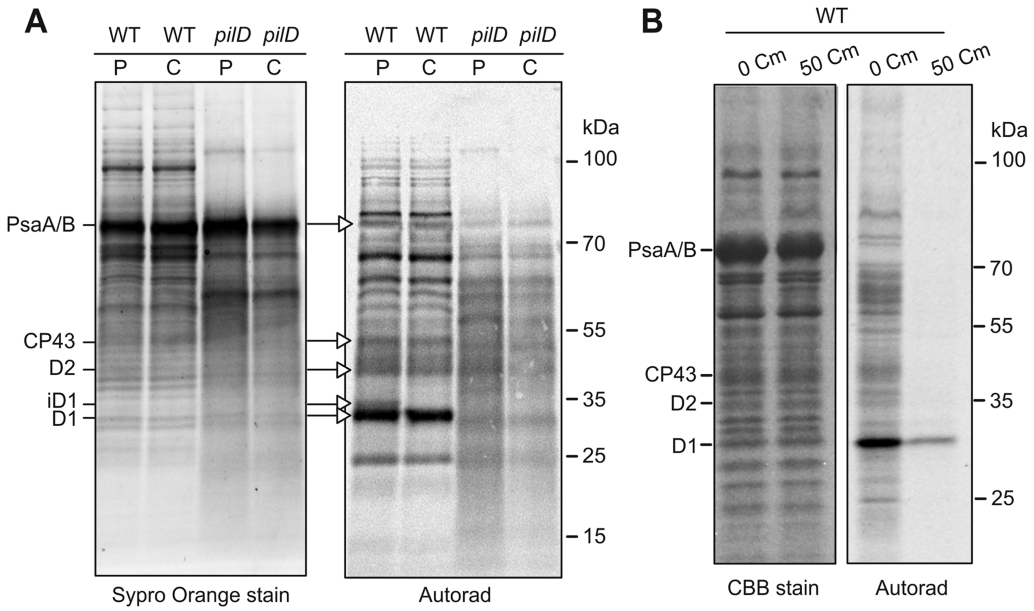

Fig. 6. Pulse-chase [^{35}S] labelling and SDS-PAGE analysis of membrane proteins from WT and *pilD* strains.
A. Cells (Glc–) were radiolabelled with a mixture of [^{35}S] methionine and cysteine for 60 min (line P) and then chased for 60 min in the presence of chloramphenicol (100 mg l^{-1}; line C) at irradiance of 100 μmol photons m^{-2} s^{-1}. Membrane proteins corresponding to 1 μg of chlorophyll were separated using denaturing SDS-PAGE, stained by Sypro Orange, dried and then exposed to a Phosphorimager plate for 7 days (Autorad). The PSI and PSII subunits are marked. The overall incorporation of radioactivity in the *pilD* sample did not exceed 70% of the WT (calculated using the ImageQuant 10 software, GE Healthcare Life Sciences).
B. Eight hours pulse-labelling of WT membrane proteins in presence of 50 mg l^{-1} chloramphenicol. The experiment was performed as described in A except the proteins were stained by Coomassie blue (CBB). A short, 30 min pulse-labelling without chloramphenicol, is shown as a control.

60 min pulse radiolabelling. As expected, PSII core subunits, PilA1 and the PSI subunits PsaA/B were among the most intensely labelled proteins in the WT (Fig. 7). Moreover, the PSII reaction centre assembly intermediate RC* (Knoppová *et al*., 2014) was easily distinguished (see Fig. 8). In the mutant, all PSII subunits were labelled very weakly and detectable only as completely assembled PSII. It is worth to mention that pPilA1 was among the most strongly labelled proteins despite its limited solubility (Fig. 7, Fig. S4). The only mutant proteins labelled to the level comparable with WT were the PSI subunits assembled into trimeric PSI and the subunits of ATP synthase (quantification of selected spots is provided in Table S2). After the 60 min chase, the mutant cells incorporated more radioactivity into monomeric and dimeric PSII complexes (Fig. 8), showing that the process of PSII assembly was drastically limited by the lack of newly synthesized subunits but not completely inhibited. Intriguingly, most of the signal of labelled pPilA1 disappeared during the chase (Fig. 8). Based on the overall stability of pPilA1 and NpPilA1 after treatment with chloramphenicol (Fig. S2), we propose that the pPilA1 became less soluble in DDM during the chase rather than being degraded.

Together, these data provide evidence that the inactivation of the PilD peptidase has an adverse effect on the synthesis of PSII core subunits and on the accumulation of other essential membrane complexes like NADH dehydrogenase. The severe reduction in the levels of these complexes in the mutant cells was in sharp contrast to the continuous production of PSI and the ATP synthase (Fig. 7).

SecY translocons associate with NpPilA1 and undergo proteolytic degradation

The blocked synthesis of certain membrane proteins (Fig. 6), the formation of aberrant membrane structures (Fig. 5) and the low amount of membrane-bound ribosomes in the *pilD* mutant (Figs 7 and 9B) all indicated that prepilins interfered with the translocon machinery. Pilin synthesis requires SecY (Arts *et al*., 2007; Francetic *et al*., 2007), and the Sec translocon machinery is prone to degradation if it is jammed by a substrate (van Stelten *et al*., 2009). *B. subtilis* cells depleted of Type I signal peptidases accumulated pre-proteins, which caused the jamming and inhibition of Sec translocons (Tjalsma *et al*., 1998). Because this is analogous to the situation in the *pilD* strain, we asked whether there was an aberrant physical interaction between pPilA1 or NpPilA1 and components of the translocon apparatus. The SecY translocase was

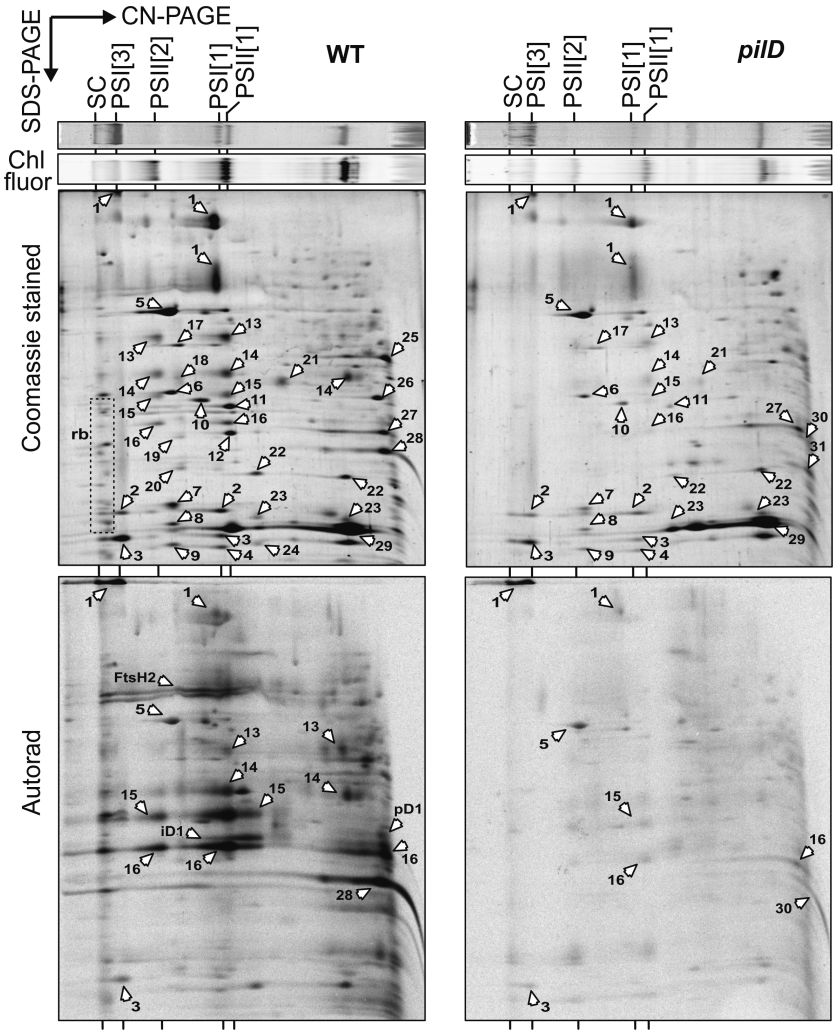

Fig. 7. 2D CN/SDS-PAGE and autoradiograph of membrane proteins from the WT and *pilD* strains. Cells grown under Glc– conditions were radiolabelled as described in the legend of Fig. 6. The isolated membranes were solubilized using DDM, and the obtained protein complexes were separated in the first dimension by clear-native electrophoresis (CN-PAGE). Approximately 4 μg of chlorophyll was loaded per each line. The CN gel was scanned using a LAS 4000 (Fuji) for chlorophyll fluorescence (Chl fluor) to visualize PSII complexes. After the second dimension (SDS-PAGE), the gel was stained with Coomassie blue, dried and then exposed to a Phosphorimager plate for seven days (Autorad). SC indicates high-molecular-mass supercomplexes; PSI[1] and PSI[3] indicate the monomeric and trimeric forms of PSI respectively; PSII[1] and PSII[2] indicate the monomers and dimers of PSII respectively. The individual proteins marked by arrows are 1 – PsaA/B, 2 – PsaD, 3 – PsaF, 4 – PsaL, 5 – AtpA/B, 6 – AtpC, 7 – AtpF, 8 – AtpD, 9 – AtpE, 10 – IlvC, 11 – CpcC1, 12 – CpcG1, 13 – CP47, 14 – CP43, 15 – D2, 16 – D1, 17 – NdhH, 18 – NdhB, 19 – NdhI, 20 – NdhJ, 21 – Amt1, 22 – PetA, 23 – PetB, 24 – PetD, 25 – PstA, 26 – PsbO, 27 – UrtA, 28 – PilA1, 29 – CpcA/B, 30 – pPilA1, 31 – NpPilA1, pD1 – precursor of D1, and iD1 – partially processed precursor of D1; rb indicates ribosome subunits.

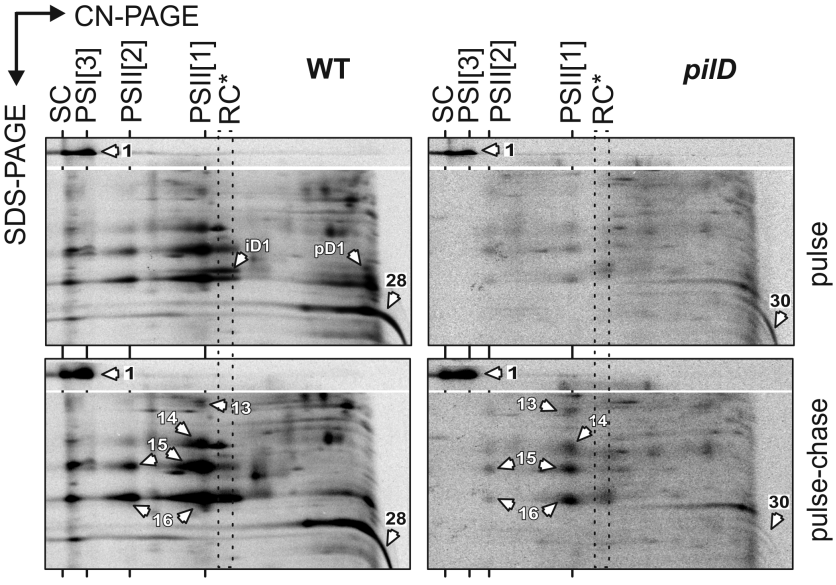

Fig. 8. Pulse-chase [^{35}S] labelling and 2D CN/SDS-PAGE of membrane proteins from the WT and *pilD* strains. Cells (Glc–) were radiolabelled as described for Fig. 6. Dried gels were exposed to a Phosphorimager plate for 7 days, and the *pilD* autoradiographs were further processed using ImageJ software (Knoppová *et al.*, 2014) to enhance the signal. For the same exposure time of the pulse-labelled strains, see Fig. 6. Only the top of the gel showing the PsaA/B proteins and the region between ~ 60 and ~ 20 kDa are shown. The protein complexes and individual proteins are labelled as in Fig. 7; RC* indicates a PSII assembly intermediate (see main text).

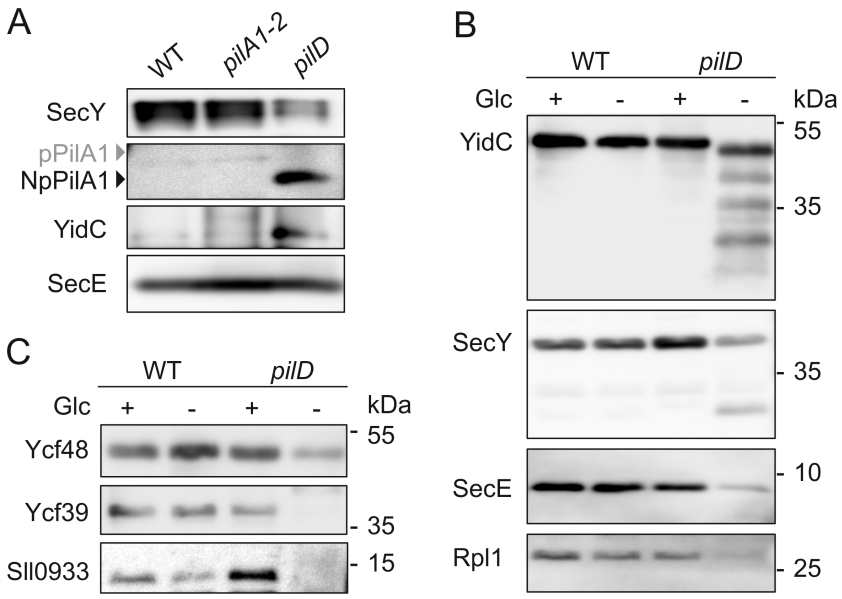

Fig. 9. Immuno-precipitation and immuno-detection of translocon components and PSII assembly factors.
A. Immuno-precipitation of the SecY translocase from solubilized membranes using the anti-SecY antibody and detection of the co-immunoprecipitated proteins. The antibody was incubated overnight with membrane proteins isolated from the WT, *pilA1-2* and *pilD* strains grown at Glc+, and then the antibody was immobilized on Protein A Sepharose 4B (Sigma, Germany). The resin was extensively washed, and the remaining proteins were eluted in a SDS buffer. The eluate was separated by SDS-PAGE, and the gel was blotted and probed with selected antibodies. Only NpPilA1 was detected in the eluate by anti-PilA1 antibody; the expected mobility of pPilA1 is indicated. The anti-SecE antibody was used to re-probe the blot as a control.
B. Immuno-detection of SecY, YidC, SecE and the ribosome subunit Rpl1. Isolated membrane fractions were denatured using 2% SDS and 1% DTT, separated by SDS-PAGE and blotted onto a PVDF membrane. The proteins were detected using specific antibodies as indicated.
C. Immuno-detection of the PSII assembly factors Ycf48, Ycf39 and Sll0933. The immunoblot was prepared essentially as described for (B).

immunoprecipitated from the DDM-solubilized membranes using the anti-SecY antibody, the immunoprecipitate was extensively washed, and the presence of pPilA1 and NpPilA1 was detected using antibodies. As shown in Fig. 9A, NpPilA1co-precipitated with SecY, although the yield of SecY was lower from the *pilD* membranes when compared to the WT (Fig. 9A). In addition to the SecYEG trimer, the YidC insertase/foldase also assists in the synthesis of membrane proteins (Sachelaru *et al.*, 2013) either independently or in a complex with SecY (Dalbey and Kuhn, 2012). Furthermore, YidC is most likely required for pilin synthesis (Saller *et al.*, 2009). Indeed, YidC co-precipitated with SecY specifically from the *pilD* cell membranes; neither PilA1 nor YidC was detected in the precipitate from WT or *pilA1-2* controls (Fig. 9A). As shown in the Fig. S4 the SecY, YidC and PilA1 antibodies are highly specific and it is very unlikely that the NpPilA1 and YidC were co-precipitated with other proteins than SecY.

If the *Synechocystis* major prepilin inhibited SecY, the stability of the translocon should be impaired. Notably, the total SecY level was strongly reduced in *pilD* cells under photoautotrophic conditions, and also a putative product of SecY degradation was detected using the anti-SecY antibody (Fig. 9B). Total SecE level and the pool of membrane-bound ribosomes were similarly reduced in the mutant (Fig. 9B). In addition, all detectable YidC in *pilD* (Glc–) cells appeared truncated and extensive degradation of this protein was evident from the number of YidC fragments (Fig. 9B). Because only residual PSII synthesis occurred in the mutant (Glc–) cells, we measured the levels of the auxiliary factors Ycf48, Ycf39 and Sll0933, which assist during synthesis of PSII core subunits (Rengstl *et al.*, 2013; Knoppová *et al.*, 2014). Consistent with levels of SecY and YidC, the amount of Ycf48 was strongly decreased, and Ycf39 and Sll0933 were completely absent in the mutant after shifting to photoautotrophic conditions (Fig. 9C).

The observed fast depletion of YidC and auxiliary factors involved in PSII synthesis prompted us to investigate putative interactions between these proteins and PilA1 or prepilins. Solubilized membranes from the WT and *pilD* strains were separated on a 2D gel, blotted and probed by selected antibodies. Interestingly, the PilA1 formed three higher-molecular-mass complexes (PilA1-A,B,C) and the A and B complexes co-migrated precisely with the Ycf48 protein. The origin of the Ycf48 spot co-migrating with A complex is unclear but the second Ycf48 signal around ~ 200 kDa indicates an early PSII assembly intermediate named RC*, which consists of D1 and D2 core subunits, several low-mass PSII subunits

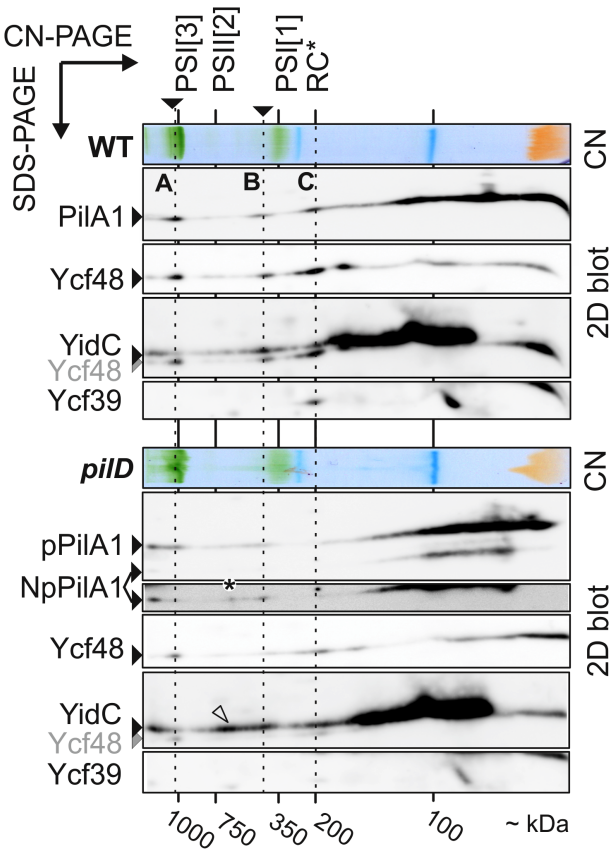

Fig. 10. Immuno-detection of PilA1 and PilA1 prepilins in high-molecular-mass membrane complexes using 2D CN/SDS-PAGE combined with immunoblotting. Membranes isolated from WT and *pilD* cells grown at Glc+ were solubilized by DDM, separated by 2D CN/SDS-PAGE essentially as described for Fig. 7 and blotted. The PVDF membrane was probed by PilA1 antibody and then successively re-probed with Ycf48, Ycf39 and YidC antibodies. In the WT strain, three high-molecular-mass PilA1 signals were detected (A–C, marked by dashed lines). RC* indicates position of the PSII assembly intermediate consisting D1 and D2 core subunits, several low-molecular-mass PSII proteins and Ycf48 and Ycf39 auxiliary factors. A NpPilA1-specific spot is marked by asterisk; the triangle highlights a YidC complex, which accumulates in the mutant strain. Approximate masses of photosynthetic complexes are also indicated.

and the Ycf48 and Ycf39 factors (Fig. 10). The RC* complex has been characterized recently in details and it is quite likely that is assembled in the vicinity of Sec translocon (Knoppová *et al.*, 2014). The PilA1-B complex seemed to co-migrate with a YidC spot (Fig. 10).

The same experiment performed on *pilD* (Glc+) cells showed a different pattern. First, a significant fraction of pPilA1 remained in a very large complex (> 1MDa) on the top of the native gel (Fig. 10). The putative PilA1-A complex was present but no pPilA1 co-migrated with RC* and the level of RC* was quite low (see the signal of Ycf39). The level of NpPilA1 was relatively weak as expected for Glc+ conditions (Fig. 3A); however, a longer exposition also revealed higher-molecular-mass NpPilA1 assemblies. Again, a significant portion of the NpPilA1 was found at the top of the native gel and also a NpPilA1 complex corresponding to PilA1-B was apparent, however practically no NpPilA1 co-migrated with the Ycf48. Interestingly, the immunodetection of YidC protein suggested formation of a relatively abundant YidC complex with size ~ 600 kDa accumulating specifically in the mutant (marked by a triangle in Fig. 10). The migration of this complex was very similar to a distinct NpPilA1 2D spot (marked by asterisk) completely absent in signals of PilA1 and pPilA1 proteins. It is tempting to speculate that the 600 KDa YidC complex is the aberrant structure associated with NpPilA1 co-precipitated from the *pilD* cells (Fig. 9A). It should be noted that prepilins lack competence for assembly into multimeric pilin structures and therefore the observed large complexes were hardly prepilin oligomers (Chen *et al.*, 2006).

Together, these data suggest that the NpPilA1 is physically attached to the Sec translocon and/or YidC. Because of their aberrant interactions, the translocons in the mutant most likely undergo extensive proteolytic degradation and this destructive process seems to include auxiliary factors involved in the synthesis of PSII core subunits. Consistently with the low stability of Ycf48 and Ycf39, the mature PilA1 as well as prepilins were shown to form large membrane complexes and might physically interact with the periplasmic/lumenal Ycf48 protein during formation of RC*.

Discussion

Type IV pilins are inserted into the membrane by the Sec translocase (Arvidson *et al.*, 1999; Arts *et al.*, 2007; Francetic *et al.*, 2007), and the positively charged N-terminus followed by a hydrophobic part (Fig. 1) is the critical feature for virtually any substrates of the Sec pathway (Dalbey and Kuhn, 2012). Although a detailed description of pilin synthesis is not available, knowledge of the synthesis of secreted bacterial proteins with the cleavable type I SP could help us to estimate how pilins are processed by the translocon machinery and why the absence of PilD results in the degradation of SecY and YidC. Unlike the prepilin SP, the cleavable part of the type I SP includes both the charged and hydrophobic parts; however, this makes hardly a fundamental difference in the mode by which the SP promotes translocation.

Once emerged from the ribosome, the hydrophobic residues of the type I SP interact with the signal recognition particle that guides the protein precursor to the Sec translocon. During the early stage of translocation, the nascent chain inside SecY adopts a loop topology and induces a conformational change to open the channel (Simon and Blobel, 1992; Gouridis *et al.*, 2009). As shown recently, the hydrophobic helix of the Type I SP occupies the lateral

gate, whereas the charged and more flexible leading stretch is already exposed to the cytoplasmic surface (Park *et al*., 2014). There, this charged part may interact with lipids, SecY and other components of the translocon machinery. The fate of the SP during the later stages of translation is unclear; however, at least for proteins with more membrane segments, the SP needs to be released from SecY. The SP might move to YidC because YidC attaches to SecY, where nascent membrane segments escape the translocon laterally (Sachelaru *et al*., 2013). Notably, the *E. coli* Type I peptidase has been cross-linked with the SecY-YidC complex but not with SecY alone (Sachelaru *et al*., 2013). This observation indicates that at least for the SecY/YidC-dependent proteins, the SP is cleaved by signal peptidase after it moves from SecY into YidC. This model is consistent with the observed critical length, typically > 80% of the total length the nascent chain has to attain to be processed by the Type I peptidase (Josefsson and Randall, 1981).

According to our current knowledge, the synthesis of pilins follows similar rules except that the charged N-terminus serves as the cleavable SP and that the hydrophobic helix remains a part of the mature pilin. Pilin synthesis requires an interaction with the signal recognition particle (Arvidson *et al*., 1999; Arts *et al*., 2007), and the conformational changes in SecY are most likely induced by the entire N-terminal part of the prepilin including the hydrophobic helix. Maturation of the major XcpT pilin in *P. aeruginosa* depends on functional Sec machinery (Arts *et al*., 2007), which implies that prepilins must be at least partly translocated to expose the SP to the PilD peptidase. However, the cleavage of the XcpT prepilin is very rapid; almost all radiolabelled XcpT is processed after 1 min (Arts *et al*., 2007). Therefore, it is likely that PilD is located near to and operates in parallel with pilin translocation. Arts *et al*. (2007) reported no effect of YidC deletion on the synthesis of XcpT in *E. coli*; however, this result should be considered carefully because it is based on a heterologous system. In *B. subtilis*, the major pilin ComGC was markedly reduced in the YqjG (YidC homologue) deletion strain (Saller *et al*., 2009), which argues for involving of YidC in pilin synthesis. Furthermore, the negatively charged residue in the hydrophobic segment seems to be a signature of YidC-dependence (Zhu *et al*., 2013), and the glutamic acid residue (+ 5) is highly conserved in all pilin proteins (Fig. 1; Giltner *et al*., 2012).

Here, we demonstrated that accumulation of the PilA1 prepilin inhibits the photoautotrophic growth of *Synechocystis* by a process accompanied by degradation of SecY and YidC (Fig. 9B). Based on the observed association of SecY, YidC and the NpPilA1 (Fig. 9A), we propose that pPilA1 is processed by PilD peptidase and most probably also glycosylated near to SecY. The interaction between SecY and YidC is weak (Scotti *et al*., 2000) and probably limited to active translocons (Boy and Koch, 2009). In contrast to the *pilD* mutant sample, in the WT membranes, YidC was not co-precipitated using the SecY antibody (Fig. 9A) and a plausible explanation could be that the inserted NpPilA1 spans both YidC and SecY and links them together. It is tempting to speculate that the charged prepilin SP is exposed and interacts with the cytoplasmic surface of SecY or YidC, and if not removed, it hampers the release of prepilin from the translocon and thereby triggers degradation of the whole translocon machinery.

It is intriguing how much the stability of Sec apparatus in the *pilD* mutant depended on the presence of glucose (Fig. 9B). The detrimental effect of prepilins cannot be completely eliminated by glucose, as documented by the low PSII oxygen evolution (Fig. 4C) and by the reduced content of the RC* complex (Fig. 10); however, the proteolytic degradation of translocons was obvious only under photoautotrophic conditions. Interestingly, the absence of glucose significantly elevated the level of NpPilA1 (Fig. 3A), which might signalize that rather than the total level of prepilin, an increase in the NpPilA1 content has fatal consequences for the cell viability. Glucose as a source of glycosylation substrate could suppress the harmful accumulation of NpPilA1 by increasing the efficiency of glycosylation reaction. Alternatively, glucose could simply provide energy needed for efficient glycosylation in the photosynthesis-deficient mutant cells. The glycosylation of prepilin can make this protein more flexible or less 'sticky' and thus prevent jamming of the translocon. Only a small fraction of NpPilA1 can be solubilized by DDM (Fig. S3), which argues for the formation of a rigid NpPilA1-containing domain in the membranes of mutated cells.

The accumulation of unprocessed Sec substrates is deleterious for bacteria (Dalbey and Wickner, 1985) because it induces the degradation of the jammed Sec translocons (van Stelten *et al*., 2009). Nonetheless, the induction of a similar process by the elimination of the PilD peptidase was rather unexpected because no growth defect has been reported for the well-studied *pilD* strains of *P. aeruginosa* (Pepe and Lory, 1998; Muller *et al*., 2010). This discrepancy could be explained in the following ways: (i) the *Synechocystis* PilA1 has a much longer and strongly charged SP than the major PAK pilin of *P. aeruginosa* (Fig. 1), which might make PilA1 more prone to blocking translocons; (ii) prepilins inhibit the synthesis of PSII, which makes cyanobacteria more sensitive to elimination of *pilD*; and (iii) non-glycosylated and potentially more toxic (lower-mass) prepilins such as NpPilA1 have not been observed in bacterial or archaeal *pilD* mutants (Marsh and Taylor, 1998; Bardy and Jarrell, 2003; Bode *et al*., 2009). Nonetheless, the inactivation of FlaK, a PilD homologue in the archaeon *Methanococcus voltae* that processes preflagellins, has strongly inhibited the cell proliferation (Bardy and Jarrell, 2003). It suggests that the harmful effect of

increased prepilin/pre-flagellin levels might not always be manifested under laboratory conditions.

The *Synechocystis pilD* null mutant has been previously characterized by Devaki Bhaya *et al*. (2000). Intriguingly, the *pilD* mutant in their study (named here *pilD*-DB) has been derived from the glucose-sensitive PCC WT, and although fully segregated, it grew photoautotrophically. The *pilD* strain described here was prepared in a glucose-tolerant background, and we isolated several photoautotrophic *pilD* revertants by growing the mutant on a plate without glucose for more than two weeks (M. Linhartová and R. Sobotka, in preparation). In order to clarify this point we obtained the *pilD*-DB strain directly from the Devaki Bhaya laboratory and found the PilA1 (pre)pilin completely missing (Fig. S5). We expect that the *pilD* segregation under photoautotrophic conditions generated a suppressor mutation(s) that minimized the synthesis of PilA1 prepilin. A point that also calls for an explanation is the constant PSII/PSI ratio observed in the *pilD* mutant shifted to Glc– conditions. The *Synechocystis* controls photosystem stoichiometry mostly by changing PSI level while the PSII cellular content is rather stable (Kopečná *et al*., 2012). But rather than an active PSI degradation, the current model envisages that, if needed, the PSI synthesis is turned down and, as the cell proliferation continues, the existing pool of PSI complexes is 'diluted' due to the growth and cell division (Kopečná *et al*., 2012). The proliferation of the *pilD* strain seems to be quickly inhibited after transfer to photoautotrophic conditions, which rules out this mechanism leaving the PSII/PSI ratio unchanged.

An interesting finding of this work is the completely different sensitivity of PSII and PSI synthesis to prepilin toxicity. The reaction centres of both photosystems are assembled from chlorophyll-binding subunits, and according to the current model, chlorophyll is delivered to apoproteins during their insertion into the membrane (Sobotka, 2014). Our work provides the first clue that photosystems are produced on different, perhaps more specialized or compartmented translocon complexes. The biogenesis of PSI also seems to be less sensitive to degradation of YidC. In cyanobacteria, YidC is strictly required for the biogenesis of the thylakoid membrane, and elimination of this protein is not possible (Spence *et al*., 2004). However, it is not clear whether YidC is essential for the synthesis of all chlorophyll-binding proteins. Furthermore, there might be extrinsic components of the Sec apparatus required for the translocation of PSII subunits and pilins, but not critical for the biogenesis of PSI. Unprocessed prepilins were detected in the *secA* and *secD* mutants of *E. coli* (Francetic *et al*., 2007), and SecA and SecDF could participate in the partitioning of large periplasmic/lumenal domains that are typical for the PSII core subunits.

In modern cyanobacteria the PSII is active in thylakoids; however, an overlap between pilin and PSII biogenesis is not completely surprising. Although the place at which the PSII subunits are synthesized and assembled is not clear yet, various indirect evidences place the PSII synthesis to a putative domain at the interface of thylakoid and cytoplasmic membrane ('PSII biogenesis centres') (Komenda *et al*., 2012; Nickelsen and Rengstl, 2013). Moreover, the cyanobacterium *Gloeobacter violaceus* lacks internal thylakoid membranes and the photosynthetic apparatus has to be synthesized in the cytoplasmic membrane (Rexroth *et al*., 2011). The genome of this living cyanobacterial fossil codes for seven pilin proteins (Table S1) and pilins thus probably coexist with PSII in the cytoplasmic membrane from the oldest cyanobacterial history.

The abovementioned PSII biogenesis centres can be defined by presence of translocons, PSII assembly factors like Ycf48, Ycf39 or Sll0933 (Komenda *et al*., 2012), terminal enzymes of chlorophyll biosynthesis pathway (Chidgey *et al*., 2014; Sobotka, 2014) and early PSII assembly intermediates (Knoppová *et al*., 2014). Indeed, levels of assembly factors are decreased in the *pilD* mutant, and we suggest that these proteins are degraded along with the inhibited Sec-YidC complex. None of these auxiliary factors is essential in *Synechocystis*; however, their inactivation affects the synthesis of PSII core subunits rather than the assembly of PSII (Rengstl *et al*., 2013). It is attractive to speculate that the abundant and large machinery engaged in PSII biogenesis also produces high levels of pilins when motility becomes important. Accumulation of PilA1 prepilin, or perhaps just its non-glycosylated form, induces destruction of this machinery, which results in lack of essential PSII subunits. This model would explain why the first detectable green complexes after the bleaching of *Synechocystis* are 'contaminated' by pilins (He and Vermaas, 1999). However, there is an alternative model, more consistent with the observed co-migration of PilA1 with RC* on the native gel (Fig. 10). Accumulating knowledge about (pseudo)pilins highlights the versatility and adaptability of these proteins in acquiring new functions (Giltner *et al*., 2012). Our results leave open the possibility that a portion of pilins remains in contact with the proposed biosynthetic centre, most probably with the periplasmic/lumenal Ycf48 protein (Fig. 10), and plays a novel role in PSII biogenesis. The delayed re-greening in pilin mutants observed by He and Vermaas (1999) might be due to a missing part in this intricate protein factory.

Experimental procedures

Preparation of Synechocystis *mutants*

All experimental strains were derived from the non-motile glucose-tolerant WT-V sub-strain of the *Synechocystis* PCC 6803 (Trautmann *et al*., 2012). To prepare the *pilD* strain, chromosomal DNA was isolated from the previously reported *pilD* mutant (Bhaya *et al*., 2000), which was a generous gift

from Professor Devaki Bhaya (Carnegie Institution for Science, Stanford, USA). The chromosomal DNA was used to transform the WT-V sub-strain, and full segregation was achieved by re-streaking the transformants several times on plates with increasing concentrations of kanamycin. A similar approach was used to generate the *pilA4* strain using the construct provided by Professor Wim Vermaas (School of Life Sciences, Arizona, USA; He and Vermaas, 1999). To prepare the *pilA1*/*pilA2* (*pilA1-2*), *pilA5-8, pilA9-11, pilB1* and *pilQ* strains, the respective gene or operon was replaced with a zeocin- or chloramphenicol-resistance cassette using the megaprimer PCR method as described in (Kopečná *et al.*, 2013; see Table 1 for a description of all the constructs used). To delete the *pilA2* gene, WT-V cells were transformed with the pGEM-T-*pilA2* vector obtained from Professor Devaki Bhaya, and the fully segregated strain was obtained using increasing concentrations of spectinomycin. Because inactivation of *pilD* or *pilA1* leads to loss of transformation competence (Bhaya *et al.*, 2000; Yoshihara *et al.*, 2001), to construct the *pilA1-2*/*pilD* double mutant, the non-segregated *pilA1-2* was transformed with the *pilD* chromosomal DNA, and then both alleles were fully segregated using increasing concentrations of zeocin and kanamycin simultaneously. Because the *pilA2* mutant is transformation-competent, it was possible to combine this allele with the *pilD* deletion by transformation of the *pilA2* strain with the *pilD* chromosomal DNA.

Growth conditions

Unless stated otherwise, the strains were grown mixotrophically in BG11 medium supplemented with 5 mM glucose on a rotary shaker under moderate light conditions (40 μmol photons m^{-2} s^{-1}) at 28°C. In this work, these conditions are called 'Glc+'. To study the effects of photoautotrophic conditions on the *pilD* strain, cells were harvested, washed, resuspended in fresh BG11 medium without glucose and then incubated in the same conditions for 24 h (Glc– conditions). The photosynthetic competence of pilin mutants was tested by incubating a similar amount of cells from the Glc+ liquid culture on a BG11 plate under moderate light (40 μmol photons m^{-2} s^{-1}) or under high light (300 μmol photons m^{-2} s^{-1}) at 28°C for 10 days.

Whole-cell absorption spectra and measurement of chlorophyll content

The absorption spectra of intact cells were measured using a Shimadzu UV-3000 spectrophotometer. To quantify the chlorophyll content per cell, cell cultures at OD_{750} ~ 0.4 were harvested, the pigments were extracted with methanol, and the chlorophyll concentration determined spectrophotometrically as previously described (Porra *et al.*, 1989). For measurements based on the optical density of the culture, the cell aggregates were disintegrated using an IKA TP 18/10 Ultra-Turrax homogenizer (Janke & Kunkel IKA Werke, Germany).

Measurement of oxygen evolution

The rate of oxygen evolution was measured continuously at 28°C using a customized Clark-type oxygen sensor (OC 223-B atyp, Theta 90, Czech Republic). The measurements were performed in a double-jacketed, multiport electrode chamber with a working volume of 6 ml. Moderate light intensity was set and measured using a submersible spherical micro-quantum sensor US-SQS/L (Walz, Germany) connected to a ULM-500 light meter (Walz, Germany).

Enzymatic digestion and mass spectrometric analysis

Coomassie-stained protein bands were excised from the gel, cut into small pieces and destained using 50 mM 4-ethylmorpholine acetate (pH 8.1) in 50% acetonitrile (MeCN). The proteins were further reduced with 30 mM TCEP in 100 mM Tris-HCl (pH 8.0) at 65°C for 30 min and alkylated by 30 mM iodacetamide in 100 mM Tris-HCl (pH 8.0) for 60 min in the dark. The gel was washed with water, shrunk by dehydration in MeCN and reswelled again in water. The supernatant was removed and the gel was partly dried in a SpeedVac concentrator. The protein samples were then digested overnight by 100 ng of trypsin (Promega) in 25 mM 4-ethylmorpholine acetate/5% MeCN (pH 8.1) at 37°C or by Glu-C protease (Roche) in 25 mM ammonium carbonate (pH 7.8) at 20°C.

In LC-MS and LC-MS/MS analyses the resulting peptides were separated using Ultimate 3000 RSLCnano system (Dionex) on an Acclaim PepMap RSLC column (75 μm × 150 mm, 2 μm, 100 Å; ThermoScientific) connected directly to an ESI source of SolariX XR FT-ICR mass spectrometer (Bruker Daltonics). The spectrometer was calibrated using lock mass calibration resulting in mass accuracy below 1 ppm. LC-MS data were processed using DataAnalysis software (Bruker Daltonics) and LC-MS/MS data were searched by MASCOT (MatrixScience) against a NCBI database.

Edman N-terminal sequencing

N-terminal amino acid analysis was performed using a Procise 491 protein sequencer (Applied Biosystems) according to the manufacturer's manual.

Electron microscopy

WT and *pilD* cells were harvested at OD_{750} ~ 0.4. For negative contrast, the cells were fixed in 1% glutaraldehyde, resuspended in fresh BG11, applied to grids, and then stained with 1% uranylacetate. For making sections, the cells were cryofixed using high-pressure freezing and freeze substitution as previously described (Kopečná *et al.*, 2012). Negative contrast and ultra-thin sections were examined in a JEOL 1010 transmission electron microscope equipped with a Mega View III camera (Olympus – SIS).

Radioactive labelling of proteins and cell fractionation

Radioactive pulse–chase labelling with a mixture of [^{35}S]Met and [^{35}S]Cys was performed as previously described (Dobáková *et al.*, 2009) at irradiance of 100 μmol photons

m^{-2} s^{-1}. The harvested cells were washed and broken by glass beads in buffer A containing 25 mM MES/NaOH, pH 6.5, 10 mM $MgCl_2$, 10 mM $CaCl_2$ and 25% glycerol. The mixture was pelleted at 30 000 *g* for 15 min yielding a soluble fraction containing the supernatant and a membrane fraction pellet, which was re-suspended in an excess volume of thylakoid buffer and then centrifuged to remove the soluble contaminants.

Electrophoresis and immunoblotting

Unless stated otherwise, the membranes or soluble proteins prepared as described above were denatured by incubation in 2% SDS and 1% dithiothreitol (DTT) for 30 min at room temperature and separated on a 12% SDS-gel (SDS-PAGE). The proteins were transferred to a PVDF membrane and incubated with specific primary antibodies and then with a secondary antibody conjugated with horseradish peroxidase (Sigma, Germany). The primary antibodies against the *Synechocystis* PilA1 and SecY proteins were raised in rabbits using the synthetic peptide fragments containing amino acids 147–160 and 4–14 respectively. The antibody raised against the recombinant fragment Arg117-Ser384 of *Synechocystis* YidC was kindly provided by Professor Jörg Nickelsen (Ludwig-Maximilians-University, Munich, Germany). The antibody against *Synechocystis* Ycf48 was kindly provided by Professor Peter Nixon (Imperial College, UK). The Rpl1 antibody was purchased from Agrisera (Sweden). To analyse membrane protein complexes under native conditions, the isolated membranes were resuspended in buffer A, solubilized by 1% n-dodecyl-ß-maltoside and separated on 4–14% Clear-Native electrophoresis gels (CN-PAGE) as described previously (Wittig *et al*., 2007). Approximately 1 ml of cells at OD_{750} = 1 was loaded on a CN gel. The 'in gel' chlorophyll fluorescence of the photosynthetic complexes was quantified using a LAS 4000 imager (Fuji, Japan). Individual components of the protein complexes were resolved by incubation of the gel strip from the first dimension in 2% SDS and 1% DTT for 30 min at room temperature, and then the proteins were separated in the second dimension by SDS-PAGE in a denaturing 12–20% polyacrylamide gel containing 7 M urea (Dobáková *et al*., 2009). The proteins were stained either with Coomassie Blue or by Sypro Orange (Sigma), and in the latter case the proteins were subsequently electro-blotted onto a PVDF membrane and probed with antibodies as described above. When radiolabelled samples were analysed, the gel was dried and exposed to a Phosphorimager plate (GE Healthcare).

Co-immunoprecipitation

The membrane fraction containing 20 µg of chlorophyll was solubilized with 1% n-dodecyl-ß-maltoside and incubated with the specified antibody overnight. Immunoglobulins were bound to Protein A-Sepharose 4B (Sigma) and released using a 25 mM Tris/HCl pH 7.5 buffer containing 1 M sucrose, 1% SDS, 1% DTT, 0.05% BFB at 50°C. The eluate was immediately separated by one-dimensional 12–20% SDS-PAGE, electro-blotted onto a PVDF membrane, which was probed repeatedly with primary antibodies.

Acknowledgements

We are grateful to Professor Devaki Bhaya (Carnegie Institution for Science, Stanford, USA) and Professor Wim Vermaas (School of Life Sciences, Arizona, USA) for various mutants and Professor Jörg Nickelsen (Ludwig-Maximilians-University, Munich, Germany) and Professor Peter Nixon (Imperial College, UK) for antibodies. We thank Eva Prachová for her technical assistance. R.S. and J.K. were supported by projects Algatech and by project 14-13967S of the Grant Agency of the Czech Republic. T.J. and P.T. were supported by Operational Program Prague – Competitiveness (CZ.2.16/3.1.00/24023).

References

Arts, J., van Boxtel, R., Filloux, A., Tommassen, J., and Koster, M. (2007) Export of the pseudopilin XcpT of the *Pseudomonas aeruginosa* type II secretion system via the signal recognition particle-Sec pathway. *J Bacteriol* **189:** 2069–2076.

Arvidson, C.G., Powers, T., Walter, P., and So, M. (1999) *Neisseria gonorrhoeae* PilA Is an FtsY homolog. *J Bacteriol* **181:** 731–739.

Bardy, S.L., and Jarrell, K.F. (2003) Cleavage of preflagellins by an aspartic acid signal peptidase is essential for flagellation in the archaeon *Methanococcus voltae*. *Mol Microbiol* **50:** 1339–1347.

Bhaya, D., Bianco, N.R., Bryant, D., and Grossman, A. (2000) Type IV pilus biogenesis and motility in the cyanobacterium *Synechocystis* sp PCC6803. *Mol Microbiol* **37:** 941–951.

Bhaya, D., Takahashi, A., Shahi, P., and Grossman, A.R. (2001) Novel motility mutants of *Synechocystis* strain PCC 6803 generated by *in vitro* transposon mutagenesis. *J Bacteriol* **183:** 6140–6143.

Bode, S., Quentmeier, C.C., Liao, P.N., Hafi, N., Barros, T., Wilk, L., *et al*. (2009) On the regulation of photosynthesis by excitonic interactions between carotenoids and chlorophylls. *Proc Natl Acad Sci USA* **106:** 12311–12316.

Boy, D., and Koch, H.-G. (2009) Visualization of distinct entities of the SecYEG translocon during translocation and integration of bacterial proteins. *Mol Biol Cell* **20:** 1804–1815.

Burrows, L.L. (2012) *Pseudomonas aeruginosa* twitching motility: type IV pili in action. *Annu Rev Microbiol* **66:** 493–520.

Carbonnelle, E., Helaine, S., Nassif, X., and Pelicic, V. (2006) A systematic genetic analysis in *Neisseria meningitidis* defines the Pil proteins required for assembly, functionality, stabilization and export of type IV pili. *Mol Microbiol* **61:** 1510–1522.

Chen, I., Provvedi, R., and Dubnau, D. (2006) A macromolecular complex formed by a pilin-like protein in competent *Bacillus subtilis*. *J Biol Chem* **281:** 21720–21727.

Chidgey, J.W., Linhartová, M., Komenda, J., Jackson, P.J., Dickman, M.J., Canniffe, D.P., *et al*. (2014) A cyanobacterial chlorophyll synthase-HliD complex associates with the Ycf39 protein and the YidC/Alb3 insertase. *Plant Cell* **26:** 1267–1279.

Dalbey, R.E., and Kuhn, A. (2012) Protein traffic in Gram-

negative bacteria – how exported and secreted proteins find their way. *FEMS Microbiol Rev* **36:** 1023–1045.

Dalbey, R.E., and Wickner, W. (1985) Leader peptidase catalyzes the release of exported proteins from the outer surface of the *Escherichia coli* plasma membrane. *J Biol Chem* **260:** 15925–15931.

Dobáková, M., Sobotka, R., Tichý, M., and Komenda, J. (2009) Psb28 protein is involved in the biogenesis of the photosystem II inner antenna CP47 (PsbB) in the cyanobacterium *Synechocystis* sp PCC 6803. *Plant Physiol* **149:** 1076–1086.

Francetic, O., Buddelmeijer, N., Lewenza, S., Kumamoto, C.A., and Pugsley, A.P. (2007) Signal recognition particle-dependent inner membrane targeting of the PulG pseudopilin component of a type II secretion system. *J Bacteriol* **189:** 1783–1793.

Giltner, C.L., Nguyen, Y., and Burrows, L.L. (2012) Type IV pilin proteins: versatile molecular modules. *Microbiol Mol Biol Rev* **76:** 740–772.

Gouridis, G., Karamanou, S., Gelis, I., Kalodimos, C.G., and Economou, A. (2009) Signal peptides are allosteric activators of the protein translocase. *Nature* **462:** 363–367.

He, Q., and Vermaas, W. (1999) Genetic deletion of proteins resembling Type IV pilins in *Synechocystis* sp. PCC 6803: their role in binding or transfer of newly synthesized chlorophyll. *Plant Mol Biol* **39:** 1175–1188.

Hernandez-Prieto, M.A., Tibiletti, T., Abasova, L., Kirilovsky, D., Vass, I., and Funk, C. (2011) The small CAB-like proteins of the cyanobacterium *Synechocystis* sp PCC 6803: their involvement in chlorophyll biogenesis for Photosystem II. *Biochim Biophys Acta* **1807:** 1143–1151.

Herranen, M., Battchikova, N., Zhang, P.P., Graf, A., Sirpio, S., Paakkarinen, V., *et al*. (2004) Towards functional proteomics of membrane protein complexes in *Synechocystis* sp PCC 6803. *Plant Physiol* **134:** 470–481.

Herskovits, A.A., Shimoni, E., Minsky, A., and Bibi, E. (2002) Accumulation of endoplasmic membranes and novel membrane-bound ribosome-signal recognition particle receptor complexes in *Escherichia coli*. *J Cell Biol* **159:** 403–410.

Holt, N.E., Zigmantas, D., Valkunas, L., Li, X.P., Niyogi, K.K., and Fleming, G.R. (2005) Carotenoid cation formation and the regulation of photosynthetic light harvesting. *Science* **307:** 433–436.

Josefsson, L.-G., and Randall, L.L. (1981) Different exported proteins in *E. coli* show differences in the temporal mode of processing *in vivo*. *Cell* **25:** 151–157.

Kamei, A., Yuasa, T., Orikawa, K., Geng, X.X., and Ikeuchi, M. (2001) A eukaryotic-type protein kinase, SpkA, is required for normal motility of the unicellular cyanobacterium *Synechocystis* sp. strain PCC 6803. *J Bacteriol* **183:** 1505–1510.

Kim, Y.H., Park, Y.M., Kim, S.J., Park, Y.I., Choi, J.S., and Chung, Y.H. (2004) The role of Slr1443 in pilus biogenesis in *Synechocystis* sp. PCC 6803: involvement in post-translational modification of pilins. *Biochem Biophys Res Commun* **315:** 179–186.

Kim, Y.H., Kim, J.Y., Kim, S.Y., Lee, J.H., Lee, J.S., Chung, Y.H., *et al*. (2009) Alteration in the glycan pattern of pilin in a nonmotile mutant of *Synechocystis* sp. PCC 6803. *Proteomics* **9:** 1075–1086.

Knoll, A.H. (2008) Cyanobacteria and earth history. In *The Cyanobacteria – Molecular Biology, Genomics and Evolution*. Herrero, A., and Flores, E. (eds). Norfolk: Caister Academic Press, pp. 1–19.

Knoppová, J., Sobotka, R., Tichý, M., Yu, J., Konik, P., Halada, P., *et al*. (2014) Discovery of a chlorophyll binding protein complex involved in the early steps of photosystem II assembly in *Synechocystis*. *Plant Cell* **26:** 1200–1212.

Komenda, J., Tichý, M., Prášil, O., Knoppová, J., Kuviková, S., de Vries, R., *et al*. (2007) The exposed N-terminal tail of the D1 subunit is required for rapid D1 degradation during photosystem II repair in *Synechocystis* sp PCC 6803. *Plant Cell* **19:** 2839–2854.

Komenda, J., Sobotka, R., and Nixon, P.J. (2012) Assembling and maintaining the Photosystem II complex in chloroplasts and cyanobacteria. *Curr Opin Plant Biol* **15:** 245–251.

Kopečná, J., Komenda, J., Bučinská, L., and Sobotka, R. (2012) Long-term acclimation of the cyanobacterium *Synechocystis* sp PCC 6803 to high light is accompanied by an enhanced production of chlorophyll that is preferentially channeled to trimeric photosystem I. *Plant Physiol* **160:** 2239–2250.

Kopečná, J., Sobotka, R., and Komenda, J. (2013) Inhibition of chlorophyll biosynthesis at the protochlorophyllide reduction step results in the parallel depletion of Photosystem I and Photosystem II in the cyanobacterium *Synechocystis* PCC 6803. *Planta* **237:** 497–508.

Li, X., Dang, S., Yan, C., Gong, X., Wang, J., and Shi, Y. (2013) Structure of a presenilin family intramembrane aspartate protease. *Nature* **493:** 56–61.

Marsh, J.W., and Taylor, R.K. (1998) Identification of the *Vibrio cholerae* type 4 prepilin peptidase required for cholera toxin secretion and pilus formation. *Mol Microbiol* **29:** 1481–1492.

Motohashi, K., Kondoh, A., Stumpp, M.T., and Hisabori, T. (2001) Comprehensive survey of proteins targeted by chloroplast thioredoxin. *Proc Natl Acad Sci USA* **98:** 11224–11229.

Mulkidjanian, A.Y., Koonin, E.V., Makarova, K.S., Mekhedov, S.L., Sorokin, A., Wolf, Y.I., *et al*. (2006) The cyanobacterial genome core and the origin of photosynthesis. *Proc Natl Acad Sci USA* **103:** 13126–13131.

Muller, M.G., Lambrev, P., Reus, M., Wientjes, E., Croce, R., and Holzwarth, A.R. (2010) Singlet energy dissipation in the photosystem II light-harvesting complex does not involve energy transfer to carotenoids. *Chemphyschem* **11:** 1289–1296.

Nickelsen, J., and Rengstl, B. (2013) Photosystem II assembly: from cyanobacteria to plants. *Annu Rev Plant Biol* **64:** 609–635.

Park, E., Menetret, J.F., Gumbart, J.C., Ludtke, S.J., Li, W., Whynot, A., *et al*. (2014) Structure of the SecY channel during initiation of protein translocation. *Nature* **506:** 102–106.

Pepe, J.C., and Lory, S. (1998) Amino acid substitutions in PilD, a bifunctional enzyme of *Pseudomonas aeruginosa*: effect on leader peptidase and n-methyltransferase activities *in vitro* and *in vivo*. *J Biol Chem* **273:** 19120–19129.

Porra, R.J., Thompson, W.A., and Kriedemann, P.E. (1989) Determination of accurate extinction coefficients and simul-

taneous equations for assaying chlorophylls a and b extracted with four different solvents: verification of the concentration of chlorophyll standards by atomic absorption spectroscopy. *Biochim Biophys Acta* **975:** 384–394.
Rengstl, B., Knoppová, J., Komenda, J., and Nickelsen, J. (2013) Characterization of a *Synechocystis* double mutant lacking the photosystem II assembly factors YCF48 and Sll0933. *Planta* **237:** 471–480.
Rexroth, S., Mullineaux, C.W., Ellinger, D., Sendtko, E., Rogner, M., and Koenig, F. (2011) The plasma membrane of the cyanobacterium *Gloeobacter violaceus* contains segregated bioenergetic domains. *Plant Cell* **23:** 2379–2390.
Sachelaru, I., Petriman, N.A., Kudva, R., Kuhn, P., Welte, T., Knapp, B., *et al*. (2013) YidC occupies the lateral gate of the SecYEG translocon and is sequentially displaced by a nascent membrane protein. *J Biol Chem* **288:** 16295–16307.
Saller, M.J., Fusetti, F., and Driessen, A.J. (2009) *Bacillus subtilis* SpoIIIJ and YqjG function in membrane protein biogenesis. *J Bacteriol* **191:** 6749–6757.
Scotti, P.A., Urbanus, M.L., Brunner, J., de Gier, J.W., von Heijne, G., van der Does, C., *et al*. (2000) YidC, the *Escherichia coli* homologue of mitochondrial Oxa1p, is a component of the Sec translocase. *EMBO J* **19:** 542–549.
Simon, S.M., and Blobel, G. (1992) Signal peptides open protein-conducting channels in *E. coli*. *Cell* **69:** 677–684.
Sinha, R.K., Komenda, J., Knoppová, J., Sedlářová, M., and Pospíšil, P. (2012) Small CAB-like proteins prevent formation of singlet oxygen in the damaged photosystem II complex of the cyanobacterium *Synechocystis* sp PCC 6803. *Plant Cell Environ* **35:** 806–818.
Sobotka, R. (2014) Making proteins green; biosynthesis of chlorophyll-binding proteins in cyanobacteria. *Photosynth Res* **119:** 223–232.
Spence, E., Bailey, S., Nenninger, A., Moller, S.G., and Robinson, C. (2004) A homolog of Albino3/OxaI is essential for thylakoid biogenesis in the cyanobacterium *Synechocystis* sp. PCC6803. *J Biol Chem* **279:** 55792–55800.
van Stelten, J., Silva, F., Belin, D., and Silhavy, T.J. (2009) Effects of antibiotics and a proto-oncogene homolog on destruction of protein translocator SecY. *Science* **325:** 753–756.
Takhar, H.K., Kemp, K., Kim, M., Howell, P.L., and Burrows, L.L. (2013) The platform protein is essential for type IV pilus biogenesis. *J Biol Chem* **288:** 9721–9728.
Tammam, S., Sampaleanu, L.M., Koo, J., Manoharan, K., Daubaras, M., Burrows, L.L., *et al*. (2013) PilMNOPQ from the *Pseudomonas aeruginosa* type IV pilus system form a transenvelope protein interaction network that interacts with PilA. *J Bacteriol* **195:** 2126–2135.
Tjalsma, H., Bolhuis, A., van Roosmalen, M.L., Wiegert, T., Schumann, W., Broekhuizen, C.P., *et al*. (1998) Functional analysis of the secretory precursor processing machinery of *Bacillus subtilis*: identification of a eubacterial homolog of archaeal and eukaryotic signal peptidases. *Genes Dev* **12:** 2318–2331.
Trautmann, D., Voss, B., Wilde, A., Al-Babili, S., and Hess, W.R. (2012) Microevolution in *Cyanobacteria*: re-sequencing a motile substrain of *Synechocystis* sp. PCC 6803. *DNA Res* **19:** 435–448.
Wittig, I., Karas, M., and Schagger, H. (2007) High resolution clear native electrophoresis for in-gel functional assays and fluorescence studies of membrane protein complexes. *Mol Cell Proteomics* **6:** 1215–1225.
Yoshihara, S., Geng, X., Okamoto, S., Yura, K., Murata, T., Go, M., *et al*. (2001) Mutational analysis of genes involved in pilus structure, motilityand transformation competency in the unicellular motile cyanobacterium *Synechocystis* sp. PCC6803. *Plant Cell Physiol* **42:** 63–73.
Zhu, L., Wasey, A., White, S.H., and Dalbey, R.E. (2013) Charge composition features of model single-span membrane proteins that determine selection of YidC and SecYEG translocase pathways in *Escherichia coli*. *J Biol Chem* **288:** 7704–7716.

Supporting information

Additional supporting information may be found in the online version of this article at the publisher's web-site.

Publication VI

This article is a *Plant Cell* Advance Online Publication. The date of its first appearance online is the official date of publication. The article has been edited and the authors have corrected proofs, but minor changes could be made before the final version is published. Posting this version online reduces the time to publication by several weeks.

A Cyanobacterial Chlorophyll Synthase-HliD Complex Associates with the Ycf39 Protein and the YidC/Alb3 Insertase[W][OPEN]

Jack W. Chidgey,[a,1] Markéta Linhartová,[b,c,1] Josef Komenda,[b,c] Philip J. Jackson,[a,d] Mark J. Dickman,[d] Daniel P. Canniffe,[a] Peter Koník,[c] Jan Pilný,[b] C. Neil Hunter,[a,2] and Roman Sobotka[b,c]

[a] Department of Molecular Biology and Biotechnology, University of Sheffield, Sheffield S10 2TN, United Kingdom
[b] Institute of Microbiology, Academy of Sciences, 37981 Třeboň, Czech Republic
[c] Faculty of Sciences, University of South Bohemia, 370 05 České Budějovice, Czech Republic
[d] ChELSI Institute, Department of Chemical and Biological Engineering, University of Sheffield, Sheffield S1 3JD, United Kingdom

Macromolecular membrane assemblies of chlorophyll-protein complexes efficiently harvest and trap light energy for photosynthesis. To investigate the delivery of chlorophylls to the newly synthesized photosystem apoproteins, a terminal enzyme of chlorophyll biosynthesis, chlorophyll synthase (ChlG), was tagged in the cyanobacterium *Synechocystis* PCC 6803 (*Synechocystis*) and used as bait in pull-down experiments. We retrieved an enzymatically active complex comprising ChlG and the high-light-inducible protein HliD, which associates with the Ycf39 protein, a putative assembly factor for photosystem II, and with the YidC/Alb3 insertase. 2D electrophoresis and immunoblotting also provided evidence for the presence of SecY and ribosome subunits. The isolated complex contained chlorophyll, chlorophyllide, and carotenoid pigments. Deletion of *hliD* elevated the level of the ChlG substrate, chlorophyllide, more than 6-fold; HliD is apparently required for assembly of FLAG-ChlG into larger complexes with other proteins such as Ycf39. These data reveal a link between chlorophyll biosynthesis and the Sec/YidC-dependent cotranslational insertion of nascent photosystem polypeptides into membranes. We expect that this close physical linkage coordinates the arrival of pigments and nascent apoproteins to produce photosynthetic pigment-protein complexes with minimal risk of accumulating phototoxic unbound chlorophylls.

INTRODUCTION

The photosystem I (PSI) and photosystem II (PSII) chlorophyll-protein complexes of cyanobacteria and plants absorb solar energy and use it for charge separation, which drives downstream processes such as NADPH formation and ATP synthesis. The structures of these complexes (Jordan et al., 2001; Umena et al., 2011) show how chlorophyll molecules are arranged to optimize the absorption of light and efficient energy transfer to the reaction center chlorophylls that act as primary electron donors (Renger and Schlodder, 2011). The biogenesis of PSI and PSII must involve close interplay between enzymes of the chlorophyll biosynthesis pathway and the machinery for synthesis and membrane insertion of the photosystem apoproteins. In vivo and in vitro studies provide circumstantial evidence for such a linkage, suggesting that chlorophyll has to be inserted into proteins cotranslationally, probably as a prerequisite for correct protein folding and for the stable incorporation of chlorophyll protein into membranes (Chua et al., 1976; Eichacker et al., 1996; Müller and Eichacker, 1999). As demonstrated using the Δ*chlL* mutant of the cyanobacterium *Synechocystis* PCC 6803 (hereafter, *Synechocystis*), which is unable to synthesize chlorophyll in the dark, the availability of de novo chlorophyll molecules is essential for the synthesis of all cyanobacterial chlorophyll proteins (Kopečná et al., 2013). By contrast, the absence of the carotenoid cofactor β-carotene has little effect on the synthesis of the PSI in *Synechocystis*, and although synthesis of PSII proteins is impaired, this complex nevertheless accumulates to some extent in the β-carotene-less mutant (Sozer et al., 2010).

A physical linkage between pigment and protein biosynthesis components is likely to be a prerequisite for tight mechanistic coupling between the production of chlorophylls and their attachment to nascent apoproteins, ensuring that there are no deleterious effects arising from unattached, phototoxic chlorophylls, such as the formation of destructive radical oxygen species (Apel and Hirt, 2004). Although there are reports of putative protein factors providing a connection between chlorophyll biosynthesis and PSII biogenesis (Dobáková et al., 2009; Schottkowski et al., 2009), the mechanisms that couple chlorophyll and protein biosynthesis remain unclear. The enzymes involved in the later steps of chlorophyll biosynthesis are considered to be associated with membranes (Masuda and Fujita, 2008), but chlorophyll synthase (ChlG), which attaches the phytol/geranylgeraniol tail to the chlorophyllide (Chlide) macrocycle, is known to be an intrinsic membrane protein (Addlesee et al., 2000). Given that the main chlorophyll binding subunits of

[1] These authors contributed equally to this work.
[2] Address correspondence to c.n.hunter@sheffield.ac.uk.
The authors responsible for distribution of materials integral to the findings presented in this article in accordance with the policy described in the Instructions for Authors (www.plantcell.org) are: C. Neil Hunter (c.n.hunter@sheffield.ac.uk) and Roman Sobotka (sobotka@alga.cz).
[W] Online version contains Web-only data.
[OPEN] Articles can be viewed online without a subscription.
www.plantcell.org/cgi/doi/10.1105/tpc.114.124495

PSI (PsaA and PsaB) and PSII (D1, D2, CP43, and CP47) are relatively large and strongly hydrophobic transmembrane proteins synthesized on membrane-bound ribosomes, the use of ChlG in pull-down assays is a promising strategy to test the idea that this terminal enzyme of chlorophyll biosynthesis is closely associated with the protein synthesis/insertion machinery for the cotranslational attachment of chlorophylls to nascent photosystem apoproteins.

Here, we purified FLAG-tagged ChlG from *Synechocystis* as an enzymatically active pigment-protein complex. Analysis by electrophoresis, mass spectrometry (MS), gel filtration, and enzyme assay demonstrated that ChlG forms a functional complex with the high-light-inducible protein HliD (also named ScpE) and that larger assemblies involving the Alb3/YidC insertase and the Ycf39 protein, a putative assembly factor for PSII, can be isolated. These data provide evidence for the hitherto elusive link between chlorophyll and photosystem apoprotein synthesis.

RESULTS

FLAG-Tagged ChlG Is Purified in a Complex with HliD, Ycf39, and YidC Proteins

In order to identify putative protein partners of ChlG, we constructed a *Synechocystis* strain expressing *chlG* under control of the *psbAII* promoter and with a 3xFLAG-tag encoded at the N terminus of ChlG; subsequently, the original *chlG* gene was deleted. The resulting *psbAII:*Flag-*chlG*/Δ*chlG* (hereafter, Flag-*chlG*) strain exhibited a wild-type pigmentation (Supplemental Figure 1), indicating that the FLAG-tagged ChlG is functional. The cellular level of FLAG-ChlG was somewhat lower than of the native ChlG (Supplemental Figure 2A) but apparently sufficient to provide chlorophyll for maintaining normal levels of photosynthetic complexes.

A membrane fraction was prepared from the photoautotrophically grown Flag-*chlG* strain, solubilized with 1.5% β-dodecyl

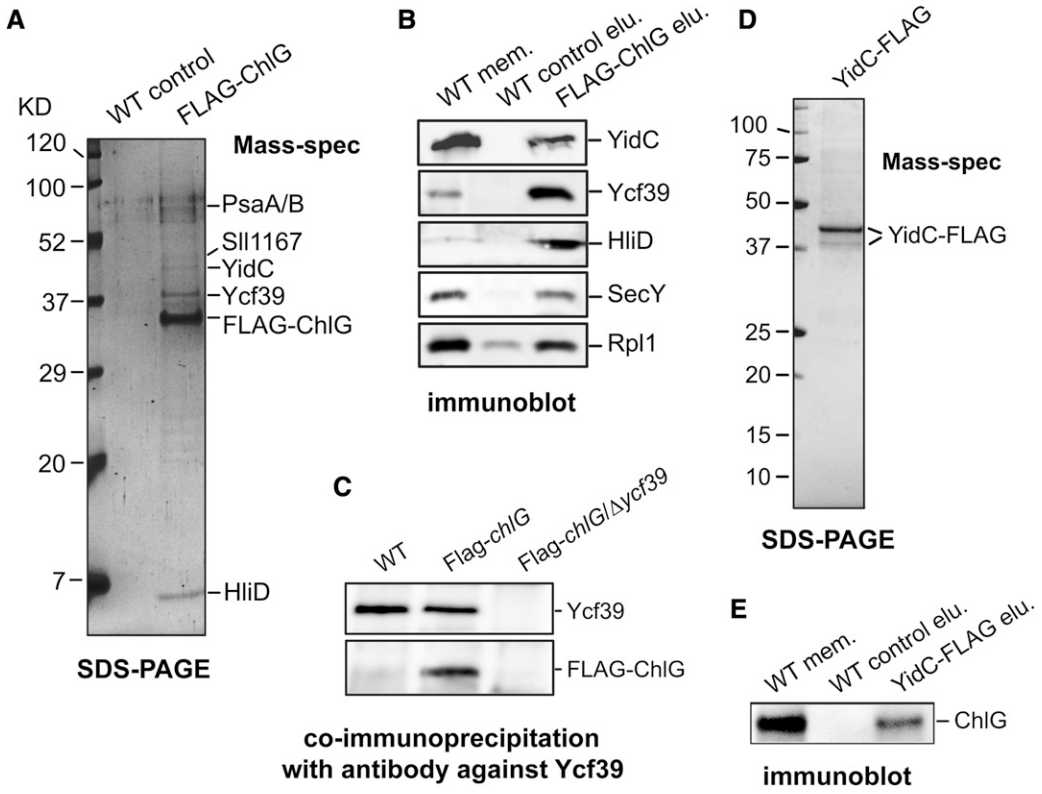

Figure 1. Purification of FLAG-ChlG and YidC-FLAG from *Synechocystis* Cells and Identification of Interacting Protein Partners.

(A) FLAG-ChlG was purified from the Flag-*chlG* strain under native conditions on the anti-FLAG affinity gel. Eluted proteins were separated by SDS-PAGE together with a control pull-down from the *Synechocystis* wild type and stained with Coomassie blue. The amount of protein loaded for each sample corresponded to one-tenth of the total eluate volume. Designated protein bands were identified by MS (see Supplemental Table 1 for detected peptides).

(B) Eluted proteins from the FLAG-ChlG pull-down were resolved by SDS-PAGE, transferred by immunoblot to a PVDF membrane and probed with selected antibodies.

(C) Immunoprecipitation of the Ycf39 protein by the anti-Ycf39 antibody from wild-type and Flag-*ChlG* strains. The FLAG-ChlG protein that coimmunoprecipitated with Ycf39 was detected by an anti-FLAG antibody.

(D) YidC-FLAG was purified from the *yidC*-Flag/Δ*yidC* strain and analyzed as described for FLAG-ChlG.

(E) Eluted proteins from the YidC-FLAG pull-down were resolved by SDS-PAGE, blotted, and probed with the anti-ChlG antibody.

maltoside, and the extract applied to an anti-FLAG affinity column. Following extensive washing, the eluted material was separated by SDS-PAGE (Figure 1A). The Coomassie blue–stained bands were digested with trypsin and identified by MS. In addition to the FLAG-ChlG protein used as bait, we identified the Ycf39 homolog Slr0399, the Slr1471 protein belonging to the Alb3/Oxa1/YidC family (hereafter, YidC), the high-light-inducible protein HliD, the Sll1167 protein from the AmpH family, and the PsaA/B core proteins of PSI (see Supplemental Table 1 for identified peptides). Of these, SDS-PAGE of the control eluate resolved only weakly staining bands of PsaA/B (Figure 1A). Using specific antibodies, we confirmed the presence of Ycf39, YidC, and HliD in the FLAG-ChlG eluate, all of which were absent from the control pull-down (Figure 1B). In addition, we detected a specific signal for SecY for the FLAG-ChlG pull-down, as well as a signal for the Rpl1 ribosome subunit that is clearly stronger than in the control (Figure 1B). We also investigated the ChlG-Ycf39 interaction using an anti-Ycf39 antibody to immunoprecipitate Ycf39 from solubilized membrane proteins prepared from the Flag-ChlG strain; Figure 1C shows that the FLAG-ChlG protein was coimmunoprecipitated with Ycf39 from the Flag-*chlG* strain but not from the control Flag-*chlG* strain lacking Ycf39, providing further evidence for the complex between ChlG and Ycf39.

In order to confirm the association of YidC with ChlG, we constructed a *yidC*- Flag/Δ*yidC* strain that produced near-native amounts of the C-terminally FLAG-tagged YidC (Supplemental Figure 2B) and normal levels of photosynthetic complexes (Supplemental Figure 1). The YidC-FLAG pull-down was analyzed as for FLAG-ChlG; although the MS analysis of stained bands identified only the YidC-FLAG protein (Figure 1D), ChlG was clearly detected in the YidC-FLAG pull-down by the specific antibody (Figure 1E). Ycf39 and HliD were not detectable in this YidC-FLAG pull-down using the cognate antibodies (data not shown), consistent with the low amount of ChlG coeluted with YidC-FLAG, and shown by the lack of a Coomassie blue–stained ChlG band in the gel in Figure 1D. The low ChlG content of the YidC-FLAG pull-down could arise from a weak YidC-ChlG interaction, possibly short-lived, given the transient presence of nascent protein chains within the YidC/Sec translocon. Clear-Native (CN) PAGE was used to examine the YidC-FLAG pull-down in more detail; the complexes were separated in the second dimension by SDS-PAGE (Supplemental Figure 3). Immunodetection of ChlG indicates that this protein comigrates with YidC-FLAG in specific oligomeric states confined to the lower range of YidC aggregates; the rest of the YidC population migrates as a continuum of oligomers ranging from tens to hundreds of kilodaltons in size.

The ChG-HliD Subcomplex Contains Chlorophyll, Chlide, and Carotenoids

The FLAG-ChlG eluate was green-orange in color, in contrast with the very pale-green elution from the wild-type membrane fraction control. Supplemental Figure 4A shows the very low absorption of the wild-type control and the 674-nm absorption maximum of the FLAG-ChlG eluate. The fluorescence emission spectrum recorded at 77K (Supplemental Figure 4B) resolves two emitting components; the major peak at 682 nm is expected to originate from the ChlG-HliD complex, and the 675-nm shoulder likely arises from free (dodecyl-β-maltoside bound) chlorophyll. The presence of some PSI complexes gives rise to the lower 720-nm emission peak. In order to examine the association of these pigments with the ChlG, HliD, Ycf39, and YidC components, which would imply the presence of a hitherto uncharacterized pigment-protein complex, the FLAG-ChlG eluate was concentrated ~5-fold using a 100-kD cutoff ultrafilter and analyzed using CN-PAGE. Two yellow-orange bands, CN1 and CN2, were resolved, each with a mass <100 kD as suggested from migration of the CpcA/B hexamer (107 kD) in the control lane (Figure 2A). In addition, a green band with no correspondence to any abundant chlorophyll-protein complex in *Synechocystis* was present in the FLAG-ChlG pull-down (Figure 2A). As this band exhibited an absorption spectrum typical for the PSI complex (Figure 2C) but it migrated more slowly than monomeric PSI, this complex was designated as PSI[1]*. The green band near the top of the gel corresponded to the trimeric PSI in solubilized membranes (Figure 2A, left lane). Absorption spectra of the CN1 and CN2 bands excised from the gel showed that both bands are associated with Chl(ide) *a* (absorbance at 674 nm) and carotenoids (absorbance at 484 to 514 nm) (Figure 2B). The only difference between CN1 and CN2 complexes seems to be a slightly higher chlorophyll/carotenoid ratio in CN2 (Figure 2B).

Complexes resolved on CN-PAGE were further separated in the second dimension by SDS-PAGE and stained either by Coomassie blue prior to in-gel tryptic digestion and MS analysis or by Sypro Orange for blotting and immunodetection (Figure 3). The CN1 and CN2 bands both contained FLAG-ChlG and HliD, providing clear evidence for the association of this complex with pigments. However, a very faint complex above CN1 can be recognized (white dashed line, left, Figure 3) containing FLAG-ChlG, Ycf39, and Sll1167. Although YidC was not detected on the 2D gels by protein staining, immunoblotting with the anti-YidC antibody shows that it also comigrated with this faint band above CN1. FLAG-ChlG, HliD, and Sll1167 are present in the CN1 band, although not YidC (white dashed line, right, Figure 3). The CN2 band appears to consist only of FLAG-ChlG and HliD, and the fastest migrating FLAG-ChlG spot (white asterisk) was not associated with pigments and probably arose from free ChlG (Figure 3). CN/SDS-PAGE also resolved the ribosome subunits (Figure 3; Supplemental Figure 5), and the immunoblot showed that SecY was bound to the large ribosome subunit. The green PSI[1]* band remained mostly stacked on the top of the resolving gel, which is a characteristic behavior of PSI complexes due to the high stability of PSI core proteins (Komenda et al., 2012b).

Gel filtration was used to further characterize the composition, molecular masses, and spectral properties of FLAG-ChlG assemblies within the FLAG-ChlG eluate. Several complexes were resolved by this method (Figure 4) with the largest one eluting in the void volume (peak GF1). The typical red shift in chlorophyll absorbance seen for the GF1 and GF2 fractions indicated that they consist mainly of PSI complexes (Supplemental Figure 6). Immunoblot analysis of the column fractions corresponding to peaks GF1-4 showed that most of the YidC and Ycf39 eluted

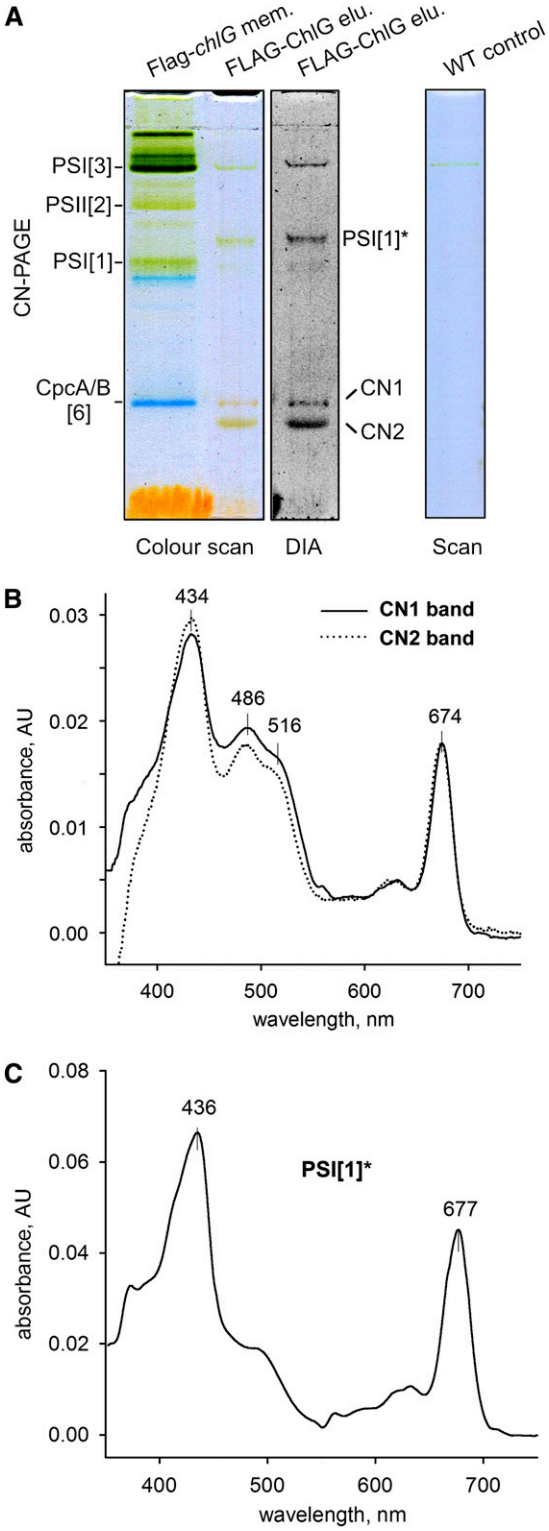

Figure 2. Separation of the Purified FLAG-ChlG Complex by CN-PAGE and Spectroscopy Analysis of Pigmented Bands.

(A) CN-PAGE of the purified FLAG-ChlG complex and a control eluate from wild-type cells, the loading of which corresponded to ~75% of the total eluates. Solubilized membranes (3 μg of chlorophyll) from the Flag-*chlG* strain were used to demonstrate the mobility of photosynthetic complexes: PSI[1] and PSI[3], monomer and trimer of PSI, respectively; PSII[2], dimer of PSII; CpcA/B[6], 107-kD heterohexamer of CpcA and CpcB phycobiliproteins. After separation, the gel was scanned in color by an office scanner and in transmittance mode (DIA) using a LAS 4000 imager (Fuji). CN1, CN2, and PSI[1]* mark protein complexes identified in FLAG-ChlG elution (line 2) but not in the total membrane fraction (line 1).

(B) The orange-yellow CN1 and CN2 bands were excised from the CN-PAGE gel, and absorption spectra were recorded as described in Methods. AU, absorbance units.

(C) Absorption spectra of the PSI[1]* complex; the red shifted absorbance of the chlorophyll Q_y peak is typical for PSI complexes.

slightly later than peak GF1 (~5.7 mL), whereas most of the HliD eluted either in the GF3 peak containing FLAG-ChlG or in the GF4 peak containing neither FLAG-ChlG nor Ycf39 (Figure 4). This analysis showed that YidC and Ycf39 tend to become detached from ChlG but remain in a large complex with molecular mass higher than 400 kD, although small amounts of YidC and Ycf39 retain an association with ChlG. This behavior of YidC might be related to a tendency of this protein to form high-mass oligomers (Supplemental Figure 3). HliD associated preferentially with ChlG forming a complex with an apparent molecular mass of ~70 kD. Given the molecular masses of FLAG-ChlG and HliD, at 38.5 and 6.5 kD, respectively, the complex likely represents ChlG with several bound copies of HliD. A substantial proportion of the HliD in the eluate became detached from FLAG-ChlG and migrated as an ~40-kD aggregate probably consisting of several copies of the protein associated with lipids, detergents, and pigments. In conclusion, gel filtration yielded a pattern of complexes somewhat different from the CN-PAGE analysis, as the FLAG-ChlG-HliD interaction was apparently less stable during this separation method, resulting in an abundant free HliD peak (GF4). On the other hand, this approach validated the conclusion derived from the 2D electrophoresis (Figure 3) showing that the FLAG-ChlG eluate consists of an abundant ChlG-HliD core and less tightly attached Ycf39/YidC components.

In order to obtain a detailed insight into the pigment composition of the FLAG-ChlG-HliD complex, we constructed another strain expressing FLAG-ChlG in a *Synechocystis* mutant lacking PSI due to deletion of the *psaA/B* operon. We purified FLAG-ChlG and then performed a gel filtration separation experiment analogous to the one described above. Elimination of PSI simplified the elution profile without affecting the ChlG-HliD complex, which eluted at 6.8 mL as before (Figure 5A). After elimination of PSI, a significant 5.8 mL elution peak was found with absorption detection at 280 nm (Figure 5A), which corresponded to the elution volume of Ycf39 and YidC in Figure 4. The absorption spectra of peaks GF3 (ChlG-HliD) and GF4 (HliD) in Figure 5B demonstrate the relatively high carotenoid content of HliD-containing fractions, particularly in the ChlG-HliD complex. We noted that the absorption spectrum of the GF3 peak was practically identical to that of the CN1 band (Figure 2B) from the native gel. The pigments in ChlG-HliD complex (GF3 peak), free of any contaminating PSI pigments, were extracted from the collected fractions

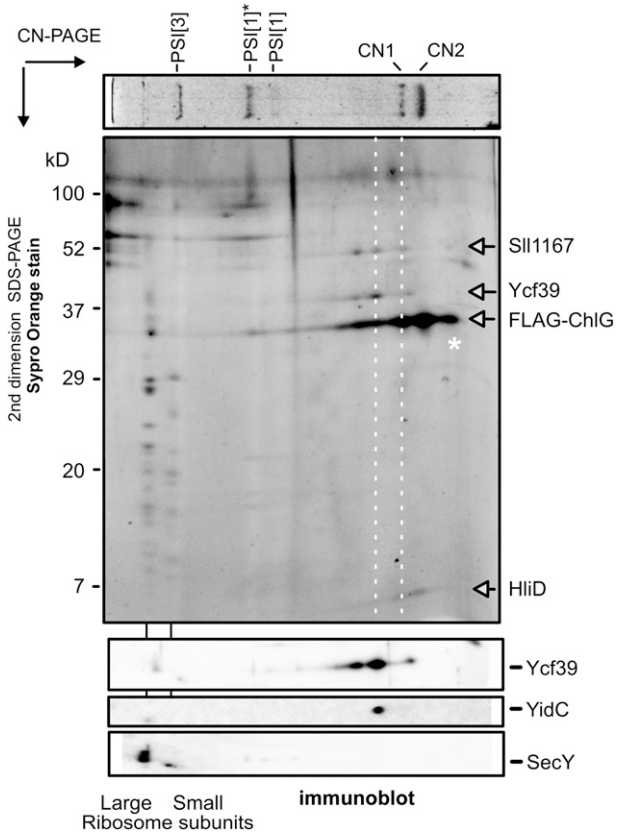

Figure 3. 2D Electrophoresis of the Purified FLAG-ChlG Complex and Identification of Individual Protein Spots.

A gel strip from CN-PAGE with separated FLAG-ChlG complexes (see Figure 2A) was further separated in a second dimension by SDS-PAGE. The gel was stained by Sypro Orange and then blotted onto a PVDF membrane. The identity of designated spots on the stained gel was assigned by MS and further verified by specific antibodies (see Results). PSI[1]* is a form of monomeric PSI migrating slower than a typical PSI[1] (Figures 2A and 2D). YidC, SecY, and Ycf39 were detected using specific antibodies. For identification of individual ribosome subunits migrating close to the top of CN gel, see Supplemental Figure 5.

and analyzed by HPLC. The results (Figure 5C) showed a complex spectrum of pigments associated with the ChlG-HliD complex. In addition to chlorophyll, we also detected Chlide and three carotenoids: zeaxanthin, β-carotene, and myxoxanthophyll. The molar ratio between chlorophyll and carotenoids was estimated to be: Chl(ide) (6): zeaxanthin (3):β-carotene (1): myxoxanthophyll (1) (Figure 5C). The amount of Chlide was rather low, only reaching ~20% of the chlorophyll level.

ChlG Activity of the Purified FLAG-ChlG Complex

Oster et al. (1997) showed that an *Escherichia coli* cell extract containing recombinant ChlG from *Synechocystis* catalyses the attachment of geranylgeraniol or phytol tails to the Chlide macrocycle. In this work, we examined the ChlG activity of purified, native ChlG preparations, initially by assaying the capacity of the FLAG-ChlG eluate to use the endogenous Chlide pool as a source of substrate. Geranylgeranyl-diphosphate was added to the FLAG-ChlG eluate, the stopped assay was terminated at various times during the 32-min time period, and then the geranylgeranyl-chlorophyll product was quantified using HPLC (Figure 6A). The data showed the concomitant increase in geranylgeranyl-chlorophyll and the decrease in Chlide, indicating that the FLAG-ChlG-HliD-Ycf39-YidC complex possesses ChlG activity and the coeluting Chlide is accessible to the ChlG. Furthermore, the subsequent addition of exogenous geranylgeranyl-diphosphate and Chlide stimulated continued ChlG activity (Figures 6B and 6C).

The HliD-Less Strain of *Synechocystis* Lacks ChlG Subcomplexes and Accumulates Chlide

Based on data already presented, we can conclude that a stable, active pigment binding ChlG-HliD core is integrated into larger complexes that also contain Ycf39 and YidC. In order to observe the in vivo effects of genetic removal of HliD on the composition of this complex, the *hliD* gene was deleted from the Flag-*chlG* strain. Detergent-solubilized membrane proteins from the Flag-*chlG* and Flag-*chlG*/Δ*hliD* strains were separated by 2D CN/SDS-PAGE, blotted, and probed with an anti-FLAG antibody (Figure 7A). The pattern of FLAG-ChlG spots in the case of the Flag-*chlG* resembled that of the separated FLAG-ChlG pull-down on CN-PAGE (Figure 3) with putative CN1 and CN2 bands (marked by asterisks in Figure 7A) and with a higher mass complex containing Ycf39 (black arrowhead in Figure 7A). By contrast, the total FLAG-ChlG signal in the Δ*hliD* sample (Figure 7A,

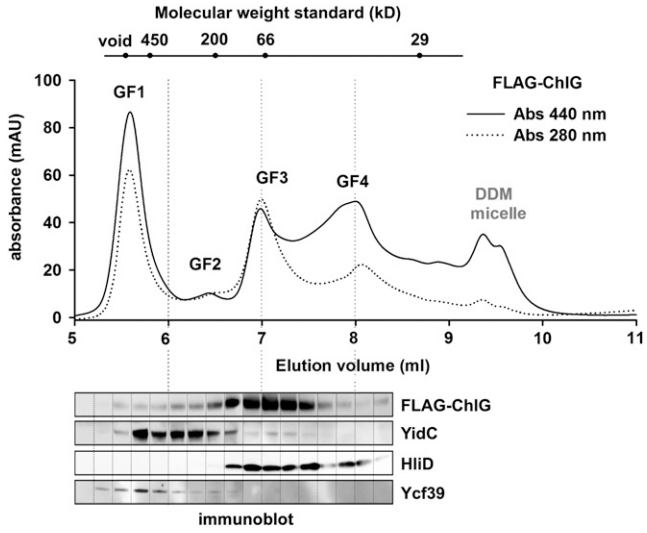

Figure 4. Separation of the Purified FLAG-ChlG Complexes by Gel Filtration Chromatography and Immunodetection of Eluted Proteins.

The FLAG-ChlG pull-down was loaded on a BioSec 3000 column, and eluted protein/complexes were detected by absorbance at 280 and 440 nm. Eluted fractions were collected and subjected to immunoblot analysis; each band corresponds to the 0.2-mL chromatograph fraction with which it is aligned. DDM, dodecyl-β-maltoside.

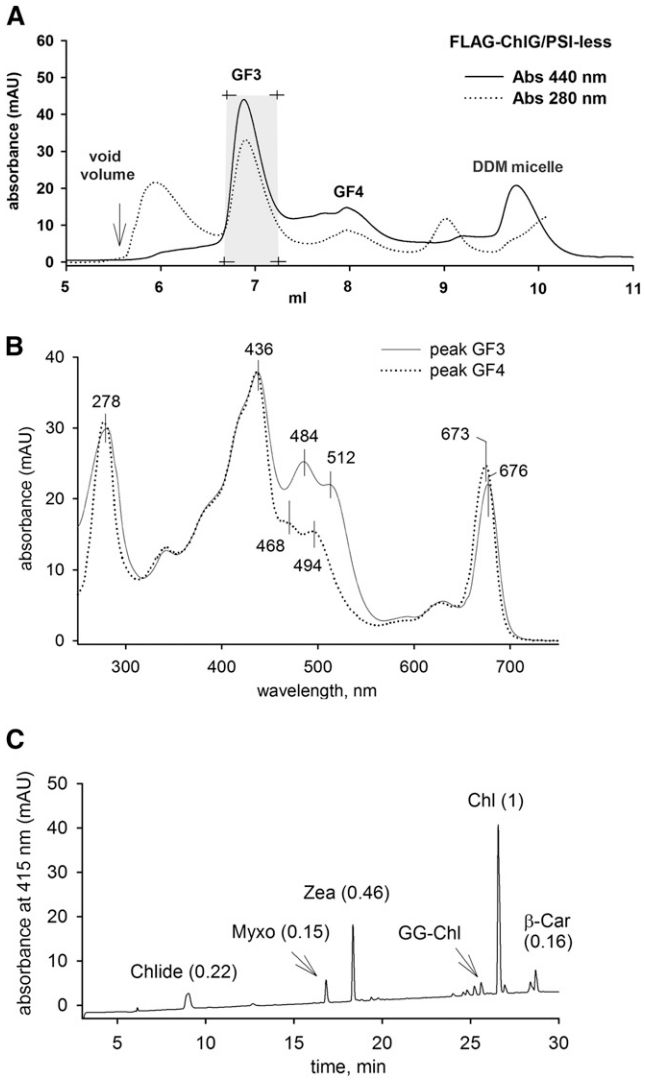

Figure 5. Analysis of Pigments Associated with the FLAG-ChlG-HliD Complex.

(A) FLAG-ChlG pull-down obtained from the PSI-less background was separated on a gel filtration column essentially as described for Figure 4 and the GF3 peak collected (gray box). DDM, dodecyl-β-maltoside.

(B) Absorption spectra of the GF3 and GF4 peaks were recorded by a HPLC diode array detector.

(C) Pigments were extracted from the pooled fractions representing the GF3 peak (gray box in **[A]**), separated by HPLC and detected at 415 nm. The area of each peak was integrated and the molar stoichiometry of individual pigments estimated. Myxo, myxoxanthophyll; Zea, zeaxanthin; GG-Chl, geranylgeranyl chlorophyll; β-Car, β-carotene.

bottom right-hand panel) was much weaker and rather smeared with no apparent spots. Furthermore, reprobing the immunoblot with anti-Ycf39 showed that Ycf39 was undetectable in membranes isolated from the Flag-*chlG*/Δ*hliD* mutant (Figure 7A, bottom right-hand panel). Despite repeated efforts, we were unable to isolate FLAG-tagged ChlG from the HliD-less strain, indicating that the protein is most probably destabilized and degraded during the isolation procedure. Thus, the inherent pigment binding capacity of ChlG could not be determined in the absence of HliD.

As different native electrophoretic systems can provide different pattern of separated complexes (Wittig et al., 2007), we repeated the analysis of Flag-*chlG* membranes using Blue-Native instead of CN/SDS-PAGE (Supplemental Figure 7). In this case, the pattern of FLAG-ChlG complexes detected in Flag-*chlG* membranes was simpler with three clearly separated signals visible in the immunoblot, and only the lowest molecular mass spot retained in the *hliD* mutant (Supplemental Figure 7). In contrast with separation of the same sample on CN-PAGE, Ycf39 seems to be detached from ChlG-HliD and migrates as an oligomer, consistent with a weaker association of Ycf39 with a more stable ChlG-HliD core. Interestingly, Blue-Native electrophoresis resolved a minor fraction of FLAG-ChlG that migrated close to PSII as a large, >400-kD complex that was not affected by the absence of HliD (Supplemental Figure 7, black arrows).

It is intriguing that the *hliD* deletion affected neither cell growth nor the accumulation of photosystems (compared with first dimension CN gel strips in Figure 7A), despite the large decrease in ChlG level, the rearrangement of its complexes and the significant decrease in the amount of Ycf39. Previously, no phenotype has been observed for the *Synechocystis* Δ*hliD* strain (Funk and Vermaas, 1999; He et al., 2001), although multiple deletions of Hli family members including HliD do affect chlorophyll metabolism (Xu et al., 2002). In order to identify a selective effect of *hliD* deletion on chlorophyll biosynthesis, we compared levels of chlorophyll precursors in the Δ*hliD* and wild-type strains (Figure 7B). Interestingly, even under moderate light intensity, the Chlide level was elevated more than 6-fold in the Δ*hliD* mutant, and there was only a very low level (<10% of the wild type) of protoporphyrin IX (Figure 7B); chlorophyll biosynthesis intermediates such as protochlorophyllide were also lowered, but to a smaller extent. For comparison, we also analyzed chlorophyll biosynthesis intermediates in another mutant that lacks the HliC protein, the amino acid sequence of which is very similar to HliD (Supplemental Figure 8). No significant changes in chlorophyll precursor levels were found in this strain (Figure 7C), suggesting that the disturbances in chlorophyll biosynthesis observed in Figure 7B were specifically induced by elimination of HliD.

A reciprocal experiment assessed the effect of deleting the *ycf39* gene on HliD and ChlG. We observed a significant decrease in the HliD level in the Δ*ycf39* strain and elevated levels of ChlG (Figure 8). Levels of chlorophyll precursors were not perturbed by elimination of the Ycf39 protein (data not shown). We conclude that the absence of Ycf39 has a negative impact on synthesis/stability of HliD and that HliD is important for accumulation of both Ycf39 and ChlG in the cell and for maintaining low levels of Chlide.

DISCUSSION

The BchG/ChlG (bacterio)chlorophyll synthases are integral membrane proteins that attach the geranylgeraniol tail to the

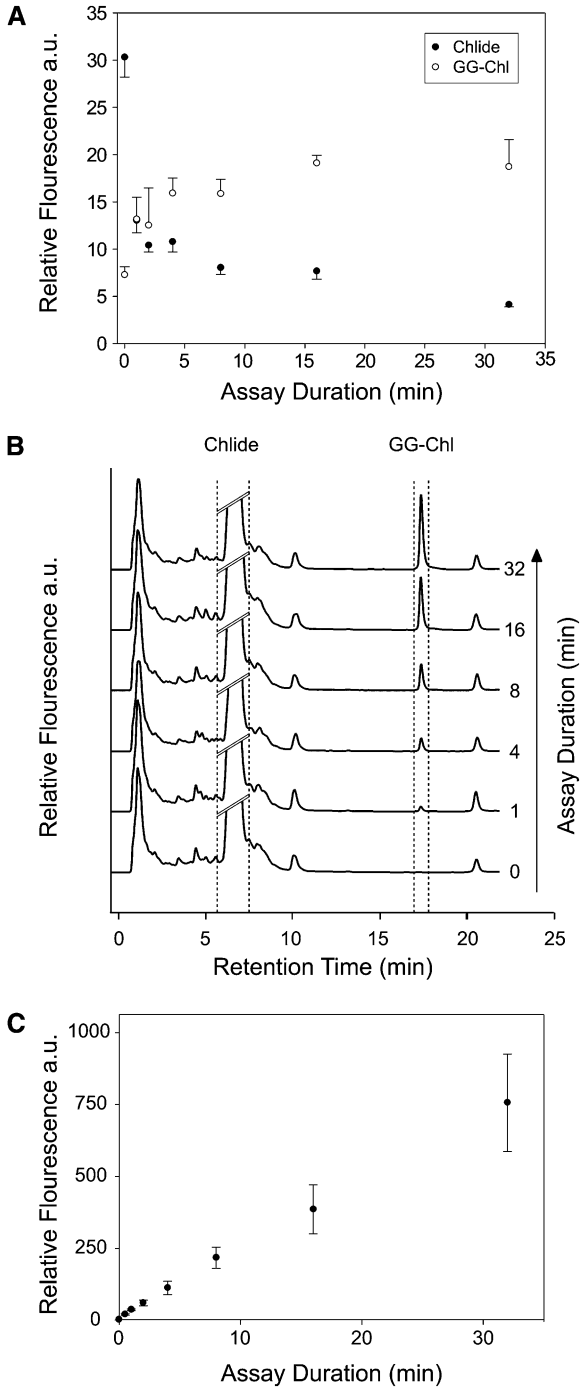

Figure 6. ChlG Activity of the Purified FLAG-ChlG Complex.

(A) Conversion of the endogenous Chlide pool and exogenous Chlide to geranylgeranyl-chlorophyll (GG-Chl). Stopped assays were performed in the presence of 20 μM geranylgeranyl diphosphate. Assays were performed in triplicate and each time point was analyzed by reverse-phase HPLC.

(B) Utilization of exogenously added Chlide by FLAG-ChlG. Assays were performed as in **(A)** but with the addition of 20 μM Chlide. Each chromatography trace is representative of one of three replicates.

(C) Evolution of the geranylgeranyl-chlorophyll product in the exogenous Chlide assays in **(B)**.

(bacterio)chlorophyll macrocycle (Oster et al., 1997), a process that increases the hydrophobicity of (bacterio)chlorophyll pigments and commits them to insertion within the many binding sites within the photosystem apoproteins. Given that photosystem formation requires a supply of chlorophylls, which must be tightly synchronized with synthesis of nascent apoproteins to avoid accumulation of unused pigments, it was reasonable to hypothesize that the (bacterio)chlorophyll synthases are in close proximity to the protein synthesis/insertion/assembly apparatus for the photosystem biogenesis. Such a close connection between biosynthetic components would minimize the time for pigment transfer from the synthase to the translocon channel containing nascent polypeptides and therefore reduce the risk of photooxidative damage to chlorophylls and their surroundings. One way to establish a fully concerted biosynthetic/assembly mechanism would involve a protein supercomplex comprising ChlG and translocon components, as recently suggested (Sobotka, 2014). Here, we used the *Synechocystis* ChlG as bait in pull-down experiments to show that the ChlG forms a relatively stable pigment-protein complex primarily with HliD, a member of CAB-like protein family. More loosely attached are Ycf39, a member of short chain dehydrogenases (Kallberg et al., 2002), and the YidC insertase. Nevertheless, both proteins remain attached to ChlG-HliD during membrane solubilization, affinity chromatography on the anti-FLAG column, and CN-PAGE (Figure 3). Although YidC, as a general insertase, is probably involved in the synthesis of ChlG, it is very unlikely that miniscule amounts of nascent FLAG-ChlG would pull down enough of the YidC involved in ChlG assembly to be detectable by Coomassie blue staining (Figure 1A). We show that FLAG-tagged YidC migrates in CN/SDS-PAGE as a series of oligomers, with a subpopulation of smaller assemblies associating with ChlG (Supplemental Figure 3). There is therefore strong experimental support for indirect association of ChlG, HliD, and YidC with the SecY translocase and ribosome subunits, forming a continuous link from chlorophyll biosynthesis to cotranslational insertion of nascent photosystem polypeptides and their folding and assembly to form functional photosystems.

The HliD Component

HliD is a small, one-helix protein belonging to the high-light-induced protein (Hlip) family that shares a significant sequence similarity to plant chlorophyll *a/b* binding proteins and possesses a highly conserved chlorophyll binding (CAB) motif (Supplemental Figure 8). Genes encoding Hlips are common in cyanobacterial genomes and are strongly expressed under various stress conditions (Bhaya et al., 2002). The *Synechocystis* chromosome encodes four small Hlip members called HliA-D, and another Hlip is fused with ferrochelatase as a C-terminal CAB domain, which is a typical feature of cyanobacterial and chloroplast ferrochelatases (Sobotka et al., 2011). A *Synechocystis* mutant lacking all five Hlips is photosensitive and has markedly reduced levels of chlorophyll and all major carotenoids (Xu et al., 2004). Individual Hlips seem to fulfill distinct although overlapping roles, which is reflected in their different patterns of regulation (He et al., 2001). Deletion of the ferrochelatase CAB domain resulted in an aberrant accumulation

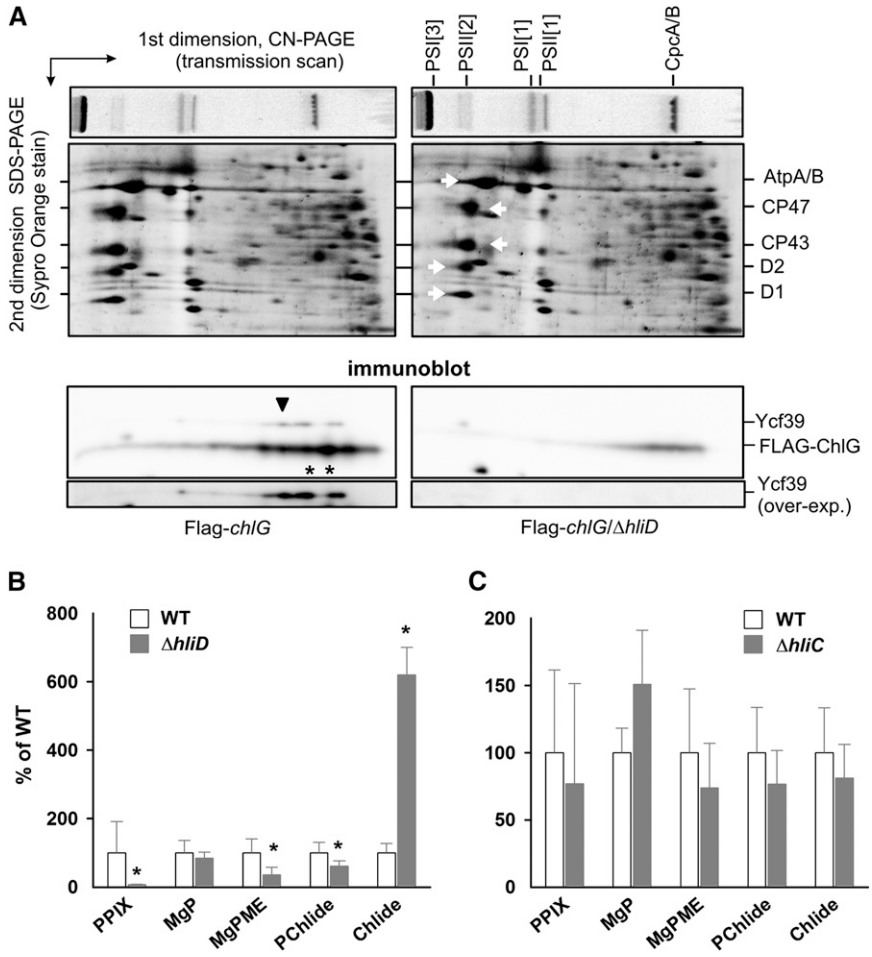

Figure 7. Characterization of *Synechocystis* Δ*hliD* Strains.

(A) Deletion of the *hliD* gene affects abundance of FLAG-ChlG and Ycf39 proteins as well as the formation of higher mass FLAG-ChlG complexes in the membrane. Membrane fractions isolated from the *Synechocystis* Flag-*chlG* (left) and Flag-*chlG*/Δ*hliD* (right) strains were separated by 2D CN/SDS-PAGE, stained by Sypro Orange, and finally blotted onto a PVDF membrane. Only the part of the SDS gel between ~25 and ~70 kD is presented; spots representing PSII core subunits and AtpA/B proteins are marked by white arrows. FLAG-ChlG and Ycf39 were detected by anti-FLAG and anti-Ycf39 antibodies, respectively. Black asterisks indicate the positions of the CN1 and CN2 bands (see Figure 3); the black arrowhead indicates a putative complex between FLAG-ChlG and Ycf39. In the lowest immunoblot panel, the Ycf39 signal was overexposed.

(B) Analysis of chlorophyll precursors in the wild-type and Δ*hliD* strains grown photoautotrophically at 40 μmol of photons m^{-2} s^{-1}. Precursors were extracted with 70% methanol from cells at OD_{750} = 0.4 and analyzed by HPLC equipped with a diode array detector and a pair of fluorescence detectors (Hollingshead et al., 2012). PPIX, protoporphyrin IX; MgP, Mg-protoporphyrin IX; MgPME, Mg-protoporphyrin IX monomethylester; PChlide, protochlorophyllide. Values shown represent means ± SD from three independent measurements. Asterisks indicate statistically significant differences in precursor levels as tested using a paired *t* test (P = 0.05).

(C) An identical measurement of chlorophyll precursors as in **(B)** performed on the Δ*hliC* strain.

of chlorophyll-protein complexes under high light, a phenotype not observed for other Hlip mutants (Sobotka et al., 2011). HliA, HliB, and HliC were found to interact with the PSII subunit CP47, likely to photoprotect the PSII assembly machinery and stabilize chlorophylls released during the process of PSII repair (Promnares et al., 2006; Yao et al., 2007). In contrast, HliD does not colocalize with PSII (Yao et al., 2007) but rather, as shown in this work, HliD copurifies with FLAG-ChlG (Figure 1). A distinct role for HliD is in line with our finding that the *hliD* null mutant, but not a *hliC* mutant, accumulates Chlide under nonstress conditions, and this accumulation is accompanied by significantly lowered levels of precursors earlier in the chlorophyll pathway (Figure 7). The observed disturbance of the whole tetrapyrrole pathway in the *hliD* mutant is consistent with previous analyses of Hlip-less *Synechocystis* strains that exhibit impaired synthesis of chlorophyll proteins due to a chlorophyll deficiency (Hernandez-Prieto et al., 2011; Yao et al., 2012).

The increased pool of Chlide could be the consequence of lowered ChlG activity but could also arise from a defect in chlorophyll recycling. The half-life of chlorophyll in *Synechocystis* is

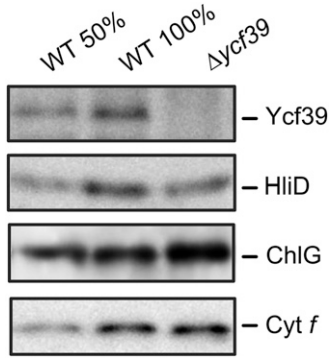

Figure 8. Immunodetection of HliD and ChlG in the *Synechocystis* Δ*ycf39* Strain.

Membrane fractions prepared from wild-type and Δ*ycf39* strains were separated by SDS-PAGE and blotted, and the HliD and ChlG proteins were detected by specific antibodies. The level of cytochrome *f* detected though its peroxidase activity was included as a loading control.

much shorter when all Hlips are deleted (Yao et al., 2012) and Chlide was demonstrated to be an intermediate of chlorophyll reutilization (Vavilin et al., 2005). How exactly Hlips assist the process of chlorophyll recycling is not known; however, our data show that the ChlG-HliD complex binds chlorophyll, carotenoids, and Chlide, possibly released from degraded chlorophyll-proteins in the vicinity of ChlG. This complex is enzymatically active and is able to convert its endogenous Chlide pool, as well as exogenous Chlide, to chlorophyll in the presence of added geranylgeranyl-diphosphate (Figure 6). Thus, we suggest that Chlide could be channeled to HliD from degraded proteins, perhaps via a network of other Hlips, then phytylated by ChlG in its HliD-bound state prior to loading into apoproteins. Associated carotenoids would operate as energy scavengers to prevent formation of oxygen radicals following excitation of Chl(ide). The total carotenoid to Chl (ide) ratio found in the FLAG-ChlG-HliD complex is relatively high (~1:1), and the unexpected presence of three different carotenoids (Figure 5C) suggests that carotenoids play an important protective role during chlorophyll phytolation. It is noteworthy that the absorption spectrum of FLAG-ChlG-HliD suggests a higher carotenoid content in comparison with the putative HliD oligomer detected as peak GF4 (Figure 5B), indicating that some carotenoid(s) might be located at the interface between ChlG and HliD, but this requires further study. Although HliD is not essential for ChlG activity, its absence decreased the cellular ChlG level, and this protein is needed for assembly of FLAG-ChlG into larger complexes with other proteins such as Ycf39 (Figure 7A).

Similar molecular mechanisms are expected to underpin the synthesis of chlorophyll-proteins in cyanobacteria and chloroplasts. Plants are likely to contain a ChlG associated with a light-harvesting complex (LHC)-like protein resembling HliD. The situation in plants is made more complex by the presence of broader spectrum of LHC-like proteins, which includes single-helix (OHP), double-helix (SEP and LIL), and triple-helix (ELIP) proteins. However, strong evidence already exists that implicates plant LHC-like proteins in chlorophyll biosynthesis; overexpression of the *Arabidopsis thaliana ELIP2* gene reduced the levels of chlorophyll precursors and chlorophyll-protein complexes (Tzvetkova-Chevolleau et al., 2007), and LIL3, which physically interacts with geranylgeranyl reductase, is critical for the accumulation of this enzyme in the chloroplast (Tanaka et al., 2010). Geranylgeranyl reductase cooperates with ChlG for chlorophyll phytolation (Rüdiger et al., 2005) and so the association of terminal enzymes of the chlorophyll pathway with HLIPs/LHC-like proteins might be a common theme.

The YidC Component

YidC (Slr1471), which belongs to the evolutionarily conserved YidC/Oxa1/Alb3 protein family involved in biogenesis of membrane proteins in bacteria, mitochondria, and chloroplasts, is thought to be involved in assisting partitioning of transmembrane segments into the lipid bilayer and folding of nascent membrane proteins (Beck et al., 2001; Nagamori et al., 2004). In *E. coli*, YidC binds to the SecY component of the SecYEG protein–conducting channel, where nascent transmembrane segments laterally escape the translocon (Sachelaru et al., 2013). The critical role of YidC/Alb3 for biogenesis of cyanobacterial and plant thylakoid membranes is well documented (Spence et al., 2004; Göhre et al., 2006). Replacement of YidC with YidC-GFP in *Synechocystis* resulted in a photosensitive strain accumulating only limited amounts of both photosystems (Ossenbühl et al., 2006). Like the bacterial YidC, the chloroplast Alb3 associates with the SecY translocase (Klostermann et al., 2002), and in a current model, the core photosystem subunits are synthesized on Sec translocon associated with YidC/Alb3 (Sobotka, 2014). Moreover, various techniques have revealed the interaction between Alb3 and chlorophyll binding proteins (Pasch et al., 2005; Göhre et al., 2006). However, the interaction between SecY and YidC is relatively weak (Scotti et al., 2000) and dynamically responds to the binding of ribosomes (Sachelaru et al., 2013), which might explain why SecY is detectable in the FLAG-ChlG pull-down only using antibodies and not by MS or protein staining as with YidC (Figure 1).

Regarding the foldase activity of YidC (Nagamori et al., 2004), we expect that the YidC/Alb3 assists chlorophyll loading into nascent apoproteins. Interestingly, ribosomal pausing occurs at distinct sites during the elongation of the D1 subunit of PSII, and this pausing seems to be intimately associated with chlorophyll binding (Kim et al., 1994). It is tempting to speculate that the YidC/Alb3 fixes growing polypeptides in a series of programmed configurations amenable for chlorophyll insertion and that ribosome pausing provides the time for attachment of chlorophyll molecules, provided by nearby ChlG. In this context, it is noteworthy that the posttranslational targeting of LHCs into chloroplast membranes is mediated by Alb3 alone with no assistance from the Sec translocon (Moore et al., 2003). Since pigments are loaded into LHCs very probably during integration into the membrane, it is reasonable to expect that the posttranslational insertion of chlorophyll into LHCs is also mediated by an Alb3-ChlG complex.

Our model of a ChlG-HliD complex physically associated with YidC/Sec translocon is in line with accumulating evidence that the translocon machinery can be extended by various factors

involved in postprocessing of the translocated polypeptide. In the endoplasmic reticulum, oligosaccharyl transferase and signal peptidase are components of the translocon (Rapoport, 2007). The bacterial translocon was shown to interact with chaperones such as PpiD (Antonoaea et al., 2008) and with FtsH proteases ensuring quality control of translated proteins or the integrity of translocon itself (van Bloois et al., 2008). It appears that, in addition to its role for protein translocation, the SecYEG/YidC core serves as a platform for accessory proteins devoted to nascent protein modification, cofactor binding, or early steps of complex assembly. We show that whereas ChlG interacts with HliD, Ycf39, and YidC, tagged YidC retrieves only low levels of ChlG, reflecting a possibly transient interaction between these proteins and a wider role for YidC as part of a translocon for many types of membrane complex insertion and assembly. The existence of an extensive machinery for membrane integration, cofactor attachment, and protein folding is consistent with the proposed biogenesis center (Stengel et al., 2012), speculated to be responsible for the early steps of PSII assembly in cyanobacteria (Komenda et al., 2012a). The monomeric PSI[1]* complex, which seems to specifically coelute with FLAG-ChlG (Figures 1 and 2), could be another structural and functional component of the biogenesis center. We can only speculate that the PSI[1]* complex could serve as a scaffold for some other components or/and as an efficient energy scavenger.

The Ycf39 and Sll1167 Components

An interaction between Ycf39 and the ChlG-HliD subcomplex was demonstrated by its purification with FLAG-ChlG and by coimmunoprecipitation (Figure 1). Ycf39 belongs to family of atypical short-chain alcohol dehydrogenase/reductases, which have an NAD(P)H binding motif near the N terminus but lack the canonical Tyr residue critical for activity of typical short-chain alcohol dehydrogenase/reductases (Kallberg et al., 2002). The function of Ycf39 in *Synechocystis* has not been established; deletion of the cognate *slr0399* gene had no effect on cell viability, but it did complement mutations near to the Q_A quinone acceptor of PSII (Ermakova-Gerdes and Vermaas, 1999). This observation led to speculation that Ycf39 is a chaperone-like protein involved in quinone insertion into the PSII complex (Ermakova-Gerdes and Vermaas, 1999). Inactivation of the *Arabidopsis* Ycf39 homolog Hcf244 greatly decreased accumulation of PSII core proteins, and although the mechanism of Hcf244 action was not explained, it appears to be connected to the synthesis of the D1 protein (Link et al., 2012). The association of the cyanobacterial Ycf39 with ChlG and HliD suggests its role in pigment insertion or modification. Indeed, our recent data confirm the involvement of Ycf39 in the delivery of chlorophyll to the newly synthesized D1 protein and stabilization of the PSII reaction center complex (Knoppová et al., 2014).

The Sll1167 protein is related to the AmpH family of bacterial enzymes expected to assist in remodeling of peptidoglycan layer (González-Leiza et al., 2011); its enigmatic occurrence in the vicinity of chlorophyll-protein biosynthesis components raises the possibility that Sll1167 plays a structural or functional role in photosystem biogenesis.

METHODS

Growth Conditions

Synechocystis PCC 6803 (hereafter, *Synechocystis*) strains were grown in a rotary shaker under moderate light conditions (40 μmol of photons m^{-2} s^{-1}) at 30°C in liquid BG11 medium. For purification of protein complexes, 4 liters of cells were grown photomixotrophically in a 10-liter flask under 100 μmol of photons m^{-2} s^{-1} light in BG11 medium supplemented with 5 mM Glc. The cell culture was agitated with magnetic stirrer and bubbled with air.

Construction of *Synechocystis* Strains

To prepare *Synechocystis* strains expressing ChlG with a 3xFLAG (hereafter, FLAG) tag at the N terminus, the *chlG* gene (*slr0056*) was cloned into the pPD-*N*FLAG plasmid and the construct transformed into the wild type. pPD-*N*FLAG contains the *Synechocystis psbAII* promoter, a sequence encoding the 3xFLAG tag, and flanking sequences for homologous recombination that allow insertion of tagged constructs into the *Synechocystis* genome in place of the *psbAII* gene (Hollingshead et al., 2012). The Flag-*yidC* strain was constructed using pPD-*C*FLAG plasmid to place the 3xFLAG tag at the YidC C terminus. The only difference between pPD-*N*FLAG and pPD-*C*FLAG plasmids is in the position of the tag. The *chlG*, *yidC* (*slr1471*), and *ycf39* (*slr0399*) genes were deleted using the megaprimer PCR method essentially as described (Kopečná et al., 2013). The Flag-*chlG* strain lacking the Ycf39 protein was prepared using genomic DNA isolated from the Δ*ycf39* strain, and the PSI-less variant of the Flag-*chlG* strain was constructed using DNA isolated from the *psaAB*$^-$ strain described by Shen et al. (1993). The Δ*hliC* and Δ*hliD* mutants were obtained by the transformation of *Synechocystis* wild-type strain using genomic DNA isolated from previously described Hlip mutants (Xu et al., 2004). In all cases, transformants were selected on a BG11 agar plate containing 5 μg mL^{-1} of appropriate antibiotic and fully segregated by restreaking transformants on plates with increasing concentration of the antibiotic.

Preparation of Solubilized Membrane Fraction and Anti-FLAG Pull-Down

Synechocystis cells expressing genes for FLAG-tagged proteins were grown to an OD_{750} of 0.5 to 0.7. Cells were pelleted, washed, and resuspended with buffer A (25 mM MES/NaOH, pH 6.5, 10 mM $CaCl_2$, 10 mM $MgCl_2$, 25% glycerol, and EDTA-free Protease Inhibitor [Roche]). Cells were mixed in equal proportions with glass beads and broken in a Mini-Beadbeater-16 (BioSpec), and the soluble proteins and membranes were separated by centrifugation (65,000*g*, 45 min). The membrane fraction was washed once with an excess of buffer A, then resuspended in buffer A and solubilized for 30 min at 10°C with 1.5% dodecyl-β-maltoside (Applichem). Finally, insoluble contaminants were removed by centrifugation (65,000*g*, 25 min).

FLAG-ChlG and FLAG-YidC complexes were purified from membrane fraction using an anti-FLAG-M2 agarose column (Sigma-Aldrich). To remove contaminants, the anti-FLAG-resin was washed with 20 resin volumes of buffer A containing 0.25% dodecyl-β-maltoside. The FLAG-tagged proteins were eluted with 2.5 resin volumes of buffer A containing 150 μg/mL 3xFLAG peptide (Sigma-Aldrich) and 0.04% dodecyl-β-maltoside.

Denaturing and 2D Electrophoresis and Protein Immunodetection

The protein composition of the purified complexes was analyzed by electrophoresis in a denaturing 12 to 20% linear gradient polyacrylamide gel containing 7 M urea (Dobáková et al., 2009). Proteins were stained

either by Coomassie Brilliant Blue or subsequently transferred onto a polyvinylidene fluoride (PVDF) membrane for immunodetection (see below). For native electrophoresis, the FLAG-ChlG pull-down was concentrated 5-fold on a 100-kD cutoff microconcentrator (Millipore) and separated on 4 to 12% clear native gel (Wittig et al., 2007). Individual components of protein complexes were resolved by incubating the gel strip from the first dimension in 2% SDS and 1% DTT for 30 min at room temperature, and proteins were separated in the second dimension by SDS-electrophoresis in a denaturing 12 to 20% polyacrylamide gel containing 7 M urea (Dobáková et al., 2009). Proteins were stained either by Coomassie Brilliant Blue or Sypro Orange, and in the latter case, they were subsequently transferred onto a PVDF membrane. Membranes were incubated with specific primary antibodies and then with secondary antibody conjugated with horseradish peroxidase (Sigma-Aldrich). Primary antibodies against SecY, Ycf39, and ChlG were raised in rabbit against synthetic peptides 4-14, 311-322, and 89-104, respectively. The antibody raised against the recombinant fragment Arg-117–Ser-384 of the *Synechocystis* YidC was kindly provided by Jörg Nickelsen (Ludwig-Maximilians-University, Munich, Germany). Antibodies against the HliD and Rpl1 were purchased from Agrisera (Sweden)

Measurement of Absorption and Fluorescence Spectra

Absorption spectra of protein bands cut from CN-PAGE were measured at room temperature with a Shimadzu UV-3000 spectrophotometer. The 77K fluorescence emission spectra were measured in liquid nitrogen with an Aminco spectrofluorimeter (Spectronic Unicam) using an excitation wavelength of 435 nm to excite chlorophyll *a*.

MS

After SDS-PAGE, Coomassie Brilliant Blue–stained protein bands/spots were excised and subjected to in-gel digestion with trypsin (porcine, modified, proteomics grade; Sigma-Aldrich). The tryptic peptides were analyzed by nanoflow liquid chromatography coupled to MS using instrument systems comprising an UltiMate 3000 nano-LC (Dionex) installed with PepMap C_{18} 5 mm × 300-μm (trapping) and 150 mm × 75-μm (analytical) columns (Dionex) operating at flow rates of 30 μL/min and 300 nL/min, respectively, with the same solvents and elution gradient detailed above. Data were acquired online using a Maxis UHR-TOF mass spectrometer (Bruker) with line MS and automated dependent MS/MS scans. For protein identification, mass spectra were converted to Mascot Generic File format using a processing script provided by Bruker and submitted to Mascot Daemon v. 2.1.3 running with Mascot Server v. 2.2.01 against the *Synechocystis* complete proteome database (http://www.uniprot.org/uniprot/?query=organism:1111708).

Gel Filtration and Pigment Analysis

The FLAG-ChlG eluate prepared from 4 liters of cells was immediately injected onto an Agilent-1200 HPLC machine and separated on Bio-sep 3000 column (Phenomenex) using 25 mM HEPES buffer, pH 7.5, containing 0.25% dodecyl-β-maltoside at a flow rate of 0.2 mL min^{-1} at 10°C. Fractions were collected using an Agilent-1200 fraction collector. To analyze the pigments coeluted with the major FLAG-ChlG peak from the gel filtration column, fractions representing the GF3 peak were pooled and concentrated ~10 times on 30-kD cutoff microconcentrators (Millipore). This solution was extracted with an excess of methanol and the extract injected onto an Agilent-1200 HPLC. Separation was performed on a reverse-phase column (Kinetex C8, 2.6-μm particle size, 3.9 × 150 mm; Phenomenex) with 35% methanol and 15% acetonitrile in 0.25 M pyridine (solvent A) and 20% methanol and 20% acetone in acetonitrile as solvents B. Pigments were eluted with a linear gradient of solvent B (30 to 95% in 25 min) followed by 95% of solvent B at a flow rate of 0.8 mL min^{-1} at 40°C. Pigment stoichiometries were estimated using published extinction coefficients for chlorophyll and β-carotene (Eijckelhoff and Dekker, 1997); the extinction coefficient for myxoxanthophyll in methanol (ε412 = 66 mM^{-1} cm^{-1}) was calculated using an authentic standard prepared from *Synechocystis* membranes.

ChlG Activity Assay

FLAG-ChlG eluate from 4 liters of cells was incubated at 30°C with 20 μM geranylgeranyl-pyrophosphate (Sigma-Aldrich) and, where appropriate, 20 μM Chlide (kindly provided by D.J. Heyes, University of Manchester, UK). Assays were stopped at the appropriate time point by the addition of excess methanol and subsequently analyzed on an Agilent-1200 HPLC. Separation was performed on a reverse-phase column (Nova-Pak C18, 4-μm particle size, 3.9 × 150 mm; Waters) with 350 mM ammonium acetate and 30% methanol as solvent A and 100% methanol as solvent B. Pigments were eluted with a linear gradient of solvent B (65 to 100%, 15 min) followed by 100% solvent B at a flow rate of 0.9 mL min^{-1} at 40°C. Pigment content was continuously monitored by the HPLC fluorescence detector (440 nm excitation; 670 nm emission). Relative quantification was performed by integration of relevant chromatograph peaks. All assays were performed in triplicate.

Quantification of Chlorophyll Precursors

For quantitative determination of chlorophyll precursors, 50 mL of culture at OD_{750} = 0.4 was filtered through a 4-μm cellulose filter to remove precipitated pigments in the growth medium and harvested. Pigments were extracted with an excess of 80% methanol/20% water and measured essentially as described previously (Hollingshead et al., 2012).

Accession Numbers

Sequence data from this article can be found in the Arabidopsis Genome Initiative or GenBank/EMBL databases under accession number BAA10281.2 (*chlG*).

Supplemental Data

The following materials are available in the online version of this article.

Supplemental Figure 1. Whole-Cell Absorption Spectra of *Synechocystis* Wild Type and Flag-*chlG*/Δ*chlG* (Hereafter Flag-*chlG*) and *yidC*-Flag/Δ*yidC* Strains Grown Photoautotrophically.

Supplemental Figure 2. Immunodetection of ChlG and YidC Native Proteins and Their Tagged Derivatives Expressed under the *psbAII* Promoter.

Supplemental Figure 3. 2D Electrophoresis of the Purified YidC-FLAG and Immunodetection of ChlG.

Supplemental Figure 4. Absorption and Fluorescence Spectroscopy of FLAG-ChlG and Control Pull-Downs.

Supplemental Figure 5. Identification of Individual Ribosomal Subunits by 2D CN/SDS-PAGE.

Supplemental Figure 6. Absorbance Spectra of GF1 and GF2 Gel Filtration Peaks Measured by a Diode-Array Detector.

Supplemental Figure 7. 2D Electrophoresis of Membrane Complexes from Flag-*chlG* and Flag-*chlG*/Δ*hliD* Strains and Immunodetection of FLAG-ChlG and Ycf39.

Supplemental Figure 8. Amino Acid Sequence Alignment of *Synechocystis* Hli Proteins and the Third Transmembrane Helix of the *Arabidopsis* Lhca2 Protein.

Supplemental Table 1. Identification of Proteins in the FLAG-ChlG Pull-Down Eluate.

ACKNOWLEDGMENTS

We thank Lenka Moravcová for her excellent technical assistance. R.S. and J.K. were supported by project Algatech and by project P501/10/1000 of the Grant Agency of the Czech Republic. J.W.C. gratefully acknowledges a doctoral studentship from the Biotechnology and Biological Sciences Research Council (BBSRC; UK). P.J.J., D.P.C., M.J.D., and C.N.H. were supported by a research grant from the BBSRC.

AUTHOR CONTRIBUTIONS

J.W.C., M.L., P.J.J., J.P., M.J.D., J.K., R.S., and C.N.H. designed experiments. J.W.C., M.L., P.J.J., D.P.C., P.K., J.P., and R.S. performed experiments. R.S., J.K., and C.N.H. wrote the article.

Received February 18, 2014; revised February 18, 2014; accepted February 28, 2014; published March 28, 2014.

REFERENCES

Addlesee, H.A., Fiedor, L., and Hunter, C.N. (2000). Physical mapping of *bchG, orf427*, and *orf177* in the photosynthesis gene cluster of *Rhodobacter sphaeroides*: Functional assignment of the bacteriochlorophyll synthetase gene. J. Bacteriol. **182:** 3175–3182.

Antonoaea, R., Fürst, M., Nishiyama, K., and Müller, M. (2008). The periplasmic chaperone PpiD interacts with secretory proteins exiting from the SecYEG translocon. Biochemistry **47:** 5649–5656.

Apel, K., and Hirt, H. (2004). Reactive oxygen species: Metabolism, oxidative stress, and signal transduction. Annu. Rev. Plant Biol. **55:** 373–399.

Beck, K., Eisner, G., Trescher, D., Dalbey, R.E., Brunner, J., and Müller, M. (2001). YidC, an assembly site for polytopic *Escherichia coli* membrane proteins located in immediate proximity to the SecYE translocon and lipids. EMBO Rep. **2:** 709–714.

Bhaya, D., Dufresne, A., Vaulot, D., and Grossman, A. (2002). Analysis of the hli gene family in marine and freshwater cyanobacteria. FEMS Microbiol. Lett. **215:** 209–219.

Chua, N.H., Blobel, G., Siekevitz, P., and Palade, G.E. (1976). Periodic variations in the ratio of free to thylakoid-bound chloroplast ribosomes during the cell cycle of *Chlamydomonas reinhardtii.* J. Cell Biol. **71:** 497–514.

Dobáková, M., Sobotka, R., Tichý, M., and Komenda, J. (2009). Psb28 protein is involved in the biogenesis of the photosystem II inner antenna CP47 (PsbB) in the cyanobacterium *Synechocystis* sp. PCC 6803. Plant Physiol. **149:** 1076–1086.

Eichacker, L.A., Helfrich, M., Rüdiger, W., and Müller, B. (1996). Stabilization of chlorophyll *a*-binding apoproteins P700, CP47, CP43, D2, and D1 by chlorophyll *a* or Zn-pheophytin *a.* J. Biol. Chem. **271:** 32174–32179.

Eijckelhoff, C., and Dekker, J.P. (1997). A routine method to determine the chlorophyll *a*, pheophytin *a* and β-carotene contents of isolated photosystem II reaction center complexes. Photosynth. Res. **52:** 69–73.

Ermakova-Gerdes, S., and Vermaas, W. (1999). Inactivation of the open reading frame *slr0399* in *Synechocystis* sp. PCC 6803 functionally complements mutations near the $Q_{(A)}$ niche of photosystem II. A possible role of Slr0399 as a chaperone for quinone binding. J. Biol. Chem. **274:** 30540–30549.

Funk, C., and Vermaas, W. (1999). A cyanobacterial gene family coding for single-helix proteins resembling part of the light-harvesting proteins from higher plants. Biochemistry **38:** 9397–9404.

Göhre, V., Ossenbühl, F., Crèvecoeur, M., Eichacker, L.A., and Rochaix, J.D. (2006). One of two alb3 proteins is essential for the assembly of the photosystems and for cell survival in *Chlamydomonas.* Plant Cell **18:** 1454–1466.

González-Leiza, S.M., de Pedro, M.A., and Ayala, J.A. (2011). AmpH, a bifunctional DD-endopeptidase and DD-carboxypeptidase of *Escherichia coli.* J. Bacteriol. **193:** 6887–6894.

He, Q., Dolganov, N., Bjorkman, O., and Grossman, A.R. (2001). The high light-inducible polypeptides in *Synechocystis* PCC6803. Expression and function in high light. J. Biol. Chem. **276:** 306–314.

Hernandez-Prieto, M.A., Tibiletti, T., Abasova, L., Kirilovsky, D., Vass, I., and Funk, C. (2011). The small CAB-like proteins of the cyanobacterium *Synechocystis* sp. PCC 6803: Their involvement in chlorophyll biogenesis for photosystem II. Biochim. Biophys. Acta **1807:** 1143–1151.

Hollingshead, S., Kopecná, J., Jackson, P.J., Canniffe, D.P., Davison, P.A., Dickman, M.J., Sobotka, R., and Hunter, C.N. (2012). Conserved chloroplast open-reading frame *ycf54* is required for activity of the magnesium protoporphyrin monomethylester oxidative cyclase in *Synechocystis* PCC 6803. J. Biol. Chem. **287:** 27823–27833.

Jordan, P., Fromme, P., Witt, H.T., Klukas, O., Saenger, W., and Krauss, N. (2001). Three-dimensional structure of cyanobacterial photosystem I at 2.5 A resolution. Nature **411:** 909–917.

Kallberg, Y., Oppermann, U., Jörnvall, H., and Persson, B. (2002). Short-chain dehydrogenases/reductases (SDRs). Eur. J. Biochem. **269:** 4409–4417.

Kim, J., Klein, P.G., and Mullet, J.E. (1994). Synthesis and turnover of photosystem II reaction center protein D1. Ribosome pausing increases during chloroplast development. J. Biol. Chem. **269:** 17918–17923.

Klostermann, E., Droste Gen Helling, I., Carde, J.P., and Schünemann, D. (2002). The thylakoid membrane protein ALB3 associates with the cpSecY-translocase in *Arabidopsis thaliana.* Biochem. J. **368:** 777–781.

Knoppová, J., Sobotka, R., Tichý, M., Yu, J., Koník, P., Halada, P., Nixon, P.J., and Komenda, J. (2014). Identification of a novel chlorophyll binding protein complex involved in the early steps of photosystem II assembly. Plant Cell, in press.

Komenda, J., Knoppová, J., Kopečná, J., Sobotka, R., Halada, P., Yu, J.F., Nickelsen, J., Boehm, M., and Nixon, P.J. (2012b). The Psb27 assembly factor binds to the CP43 complex of photosystem II in the cyanobacterium *Synechocystis* sp. PCC 6803. Plant Physiol. **158:** 476–486.

Komenda, J., Sobotka, R., and Nixon, P.J. (2012a). Assembling and maintaining the Photosystem II complex in chloroplasts and cyanobacteria. Curr. Opin. Plant Biol. **15:** 245–251.

Kopečná, J., Sobotka, R., and Komenda, J. (2013). Inhibition of chlorophyll biosynthesis at the protochlorophyllide reduction step results in the parallel depletion of photosystem I and photosystem II in the cyanobacterium *Synechocystis* PCC 6803. Planta **237:** 497–508.

Link, S., Engelmann, K., Meierhoff, K., and Westhoff, P. (2012). The atypical short-chain dehydrogenases HCF173 and HCF244 are jointly involved in translational initiation of the *psbA* mRNA of Arabidopsis. Plant Physiol. **160:** 2202–2218.

Masuda, T., and Fujita, Y. (2008). Regulation and evolution of chlorophyll metabolism. Photochem. Photobiol. Sci. **7:** 1131–1149.

Moore, M., Goforth, R.L., Mori, H., and Henry, R. (2003). Functional interaction of chloroplast SRP/FtsY with the ALB3 translocase in thylakoids: Substrate not required. J. Cell Biol. **162:** 1245–1254.

Müller, B., and Eichacker, L.A. (1999). Assembly of the D1 precursor in monomeric photosystem II reaction center precomplexes precedes chlorophyll a-triggered accumulation of reaction center II in barley etioplasts. Plant Cell **11:** 2365–2377.

Nagamori, S., Smirnova, I.N., and Kaback, H.R. (2004). Role of YidC in folding of polytopic membrane proteins. J. Cell Biol. **165:** 53–62.

Ossenbühl, F., Inaba-Sulpice, M., Meurer, J., Soll, J., and Eichacker, L.A. (2006). The *synechocystis* sp PCC 6803 oxa1 homolog is essential for membrane integration of reaction center precursor protein pD1. Plant Cell **18:** 2236–2246.

Oster, U., Bauer, C.E., and Rüdiger, W. (1997). Characterization of chlorophyll *a* and bacteriochlorophyll *a* synthases by heterologous expression in *Escherichia coli.* J. Biol. Chem. **272:** 9671–9676.

Pasch, J.C., Nickelsen, J., and Schünemann, D. (2005). The yeast split-ubiquitin system to study chloroplast membrane protein interactions. Appl. Microbiol. Biotechnol. **69:** 440–447.

Promnares, K., Komenda, J., Bumba, L., Nebesarova, J., Vacha, F., and Tichy, M. (2006). Cyanobacterial small chlorophyll-binding protein ScpD (HliB) is located on the periphery of photosystem II in the vicinity of PsbH and CP47 subunits. J. Biol. Chem. **281:** 32705–32713.

Rapoport, T.A. (2007). Protein translocation across the eukaryotic endoplasmic reticulum and bacterial plasma membranes. Nature **450:** 663–669.

Renger, T., and Schlodder, E. (2011). Optical properties, excitation energy and primary charge transfer in photosystem II: Theory meets experiment. J. Photochem. Photobiol. B Biol. **104:** 126–141.

Rüdiger, W., Böhm, S., Helfrich, M., Schulz, S., and Schoch, S. (2005). Enzymes of the last steps of chlorophyll biosynthesis: Modification of the substrate structure helps to understand the topology of the active centers. Biochemistry **44:** 10864–10872.

Sachelaru, I., Petriman, N.A., Kudva, R., Kuhn, P., Welte, T., Knapp, B., Drepper, F., Warscheid, B., and Koch, H.G. (2013). YidC occupies the lateral gate of the SecYEG translocon and is sequentially displaced by a nascent membrane protein. J. Biol. Chem. **288:** 16295–16307.

Schottkowski, M., Ratke, J., Oster, U., Nowaczyk, M., and Nickelsen, J. (2009). Pitt, a novel tetratricopeptide repeat protein involved in light-dependent chlorophyll biosynthesis and thylakoid membrane biogenesis in *Synechocystis* sp. PCC 6803. Mol. Plant **2:** 1289–1297.

Scotti, P.A., Urbanus, M.L., Brunner, J., de Gier, J.W., von Heijne, G., van der Does, C., Driessen, A.J., Oudega, B., and Luirink, J. (2000). YidC, the *Escherichia coli* homologue of mitochondrial Oxa1p, is a component of the Sec translocase. EMBO J. **19:** 542–549.

Shen, G.Z., Boussiba, S., and Vermaas, W.F.J. (1993). Synechocystis sp PCC 6803 strains lacking photosystem I and phycobilisome function. Plant Cell **5:** 1853–1863.

Sobotka, R. (2014). Making proteins green; biosynthesis of chlorophyll-binding proteins in cyanobacteria. Photosynth. Res. **119:** 223–232.

Sobotka, R., Tichy, M., Wilde, A., and Hunter, C.N. (2011). Functional assignments for the carboxyl-terminal domains of the ferrochelatase from *Synechocystis* PCC 6803: The CAB domain plays a regulatory role, and region II is essential for catalysis. Plant Physiol. **155:** 1735–1747.

Sozer, O., Komenda, J., Ughy, B., Domonkos, I., Laczkó-Dobos, H., Malec, P., Gombos, Z., and Kis, M. (2010). Involvement of carotenoids in the synthesis and assembly of protein subunits of photosynthetic reaction centers of *Synechocystis* sp. PCC 6803. Plant Cell Physiol. **51:** 823–835.

Spence, E., Bailey, S., Nenninger, A., Møller, S.G., and Robinson, C. (2004). A homolog of Albino3/OxaI is essential for thylakoid biogenesis in the cyanobacterium *Synechocystis* sp. PCC6803. J. Biol. Chem. **279:** 55792–55800.

Stengel, A., Gügel, I.L., Hilger, D., Rengstl, B., Jung, H., and Nickelsen, J. (2012). Initial steps of photosystem II de novo assembly and preloading with manganese take place in biogenesis centers in *Synechocystis.* Plant Cell **24:** 660–675.

Tanaka, R., Rothbart, M., Oka, S., Takabayashi, A., Takahashi, K., Shibata, M., Myouga, F., Motohashi, R., Shinozaki, K., Grimm, B., and Tanaka, A. (2010). LIL3, a light-harvesting-like protein, plays an essential role in chlorophyll and tocopherol biosynthesis. Proc. Natl. Acad. Sci. USA **107:** 16721–16725.

Tzvetkova-Chevolleau, T., Franck, F., Alawady, A.E., Dall'Osto, L., Carrière, F., Bassi, R., Grimm, B., Nussaume, L., and Havaux, M. (2007). The light stress-induced protein ELIP2 is a regulator of chlorophyll synthesis in *Arabidopsis thaliana.* Plant J. **50:** 795–809.

Umena, Y., Kawakami, K., Shen, J.R., and Kamiya, N. (2011). Crystal structure of oxygen-evolving photosystem II at a resolution of 1.9 Å. Nature **473:** 55–60.

van Bloois, E., Dekker, H.L., Fröderberg, L., Houben, E.N., Urbanus, M.L., de Koster, C.G., de Gier, J.W., and Luirink, J. (2008). Detection of cross-links between FtsH, YidC, HflK/C suggests a linked role for these proteins in quality control upon insertion of bacterial inner membrane proteins. FEBS Lett. **582:** 1419–1424.

Vavilin, D., Brune, D.C., and Vermaas, W. (2005). ^{15}N-labeling to determine chlorophyll synthesis and degradation in *Synechocystis* sp. PCC 6803 strains lacking one or both photosystems. Biochim. Biophys. Acta **1708:** 91–101.

Wittig, I., Karas, M., and Schägger, H. (2007). High resolution clear native electrophoresis for in-gel functional assays and fluorescence studies of membrane protein complexes. Mol. Cell. Proteomics **6:** 1215–1225.

Xu, H., Vavilin, D., Funk, C., and Vermaas, W. (2002). Small Cab-like proteins regulating tetrapyrrole biosynthesis in the cyanobacterium Synechocystis sp. PCC 6803. Plant Mol. Biol. **49:** 149–160.

Xu, H., Vavilin, D., Funk, C., and Vermaas, W. (2004). Multiple deletions of small Cab-like proteins in the cyanobacterium *Synechocystis* sp. PCC 6803: Consequences for pigment biosynthesis and accumulation. J. Biol. Chem. **279:** 27971–27979.

Yao, D., Kieselbach, T., Komenda, J., Promnares, K., Prieto, M.A. H., Tichy, M., Vermaas, W., and Funk, C. (2007). Localization of the small CAB-like proteins in photosystem II. J. Biol. Chem. **282:** 267–276.

Yao, D.C.I., Brune, D.C., Vavilin, D., and Vermaas, W.F.J. (2012). Photosystem II component lifetimes in the cyanobacterium *Synechocystis* sp. strain PCC 6803: small Cab-like proteins stabilize biosynthesis intermediates and affect early steps in chlorophyll synthesis. J. Biol. Chem. **287:** 682–692.

Publication VII

This article is a *Plant Cell* Advance Online Publication. The date of its first appearance online is the official date of publication. The article has been edited and the authors have corrected proofs, but minor changes could be made before the final version is published. Posting this version online reduces the time to publication by several weeks.

Discovery of a Chlorophyll Binding Protein Complex Involved in the Early Steps of Photosystem II Assembly in *Synechocystis*[W]

Jana Knoppová,[a,b] Roman Sobotka,[a,b] Martin Tichý,[a,b] Jianfeng Yu,[c] Peter Konik,[b] Petr Halada,[d] Peter J. Nixon,[c] and Josef Komenda[a,b,1]

[a] Institute of Microbiology, Academy of Sciences, 37981 Třeboň, Czech Republic
[b] Faculty of Science, University of South Bohemia, 370 05 České Budějovice, Czech Republic
[c] Department of Life Sciences, Sir Ernst Chain Building-Wolfson Laboratories, Imperial College London, London SW7 2AZ, United Kingdom
[d] Laboratory of Molecular Structure Characterization, Institute of Microbiology, Academy of Sciences, 14220 Praha 4-Krč, Czech Republic

Efficient assembly and repair of the oxygen-evolving photosystem II (PSII) complex is vital for maintaining photosynthetic activity in plants, algae, and cyanobacteria. How chlorophyll is delivered to PSII during assembly and how vulnerable assembly complexes are protected from photodamage are unknown. Here, we identify a chlorophyll and β-carotene binding protein complex in the cyanobacterium *Synechocystis* PCC 6803 important for formation of the D1/D2 reaction center assembly complex. It is composed of putative short-chain dehydrogenase/reductase Ycf39, encoded by the *slr0399* gene, and two members of the high-light-inducible protein (Hlip) family, HliC and HliD, which are small membrane proteins related to the light-harvesting chlorophyll binding complexes found in plants. Perturbed chlorophyll recycling in a Ycf39-null mutant and copurification of chlorophyll synthase and unassembled D1 with the Ycf39-Hlip complex indicate a role in the delivery of chlorophyll to newly synthesized D1. Sequence similarities suggest the presence of a related complex in chloroplasts.

INTRODUCTION

Photosystem II (PSII) embedded in the thylakoid membranes of plants, algae, and cyanobacteria is the multisubunit enzyme complex that uses light energy to catalyze the highly energetically demanding reaction of water splitting. Recent three-dimensional structures of active dimeric PSII complexes from cyanobacteria have revealed the spatial organization of the protein subunits and cofactors involved in excitation energy transfer and electron transport (Ferreira et al., 2004; Guskov et al., 2009; Umena et al., 2011). Within the core of the complex there are two reaction center (RC) subunits called D1 and D2, which bind the cofactors involved in primary charge separation (Rappaport and Diner, 2008). On either side are CP43 and CP47, which both bind chlorophyll *a* and β-carotene and serve as inner light-harvesting complexes or antennae. On the periphery of these large subunits are 13 small, mostly single helix transmembrane subunits, while the lumenal part of the complex is shielded by the PsbO, PsbU, and PsbV extrinsic subunits (reviewed in Roose et al., 2007).

PSII biogenesis in the cyanobacterium *Synechocystis* sp PCC 6803 (hereafter, *Synechocystis*) occurs in a stepwise fashion from four preassembled smaller subcomplexes or modules (Komenda et al., 2012a). Each module consists of one large chlorophyll binding subunit (D1, D2, CP47, and CP43) and several neighboring low molecular mass membrane polypeptides plus bound pigment and other cofactors. PSII assembly is initiated through interaction of the D1 and D2 modules to form a RC intermediate, termed the RCII complex. The CP47 module (Boehm et al., 2011) is then attached to RCII forming a CP43-less complex, called RC47 (Boehm et al., 2012a). Oxygen-evolving monomeric and dimeric PSII are formed after addition of the CP43 module (Boehm et al., 2011), attachment of the luminal extrinsic proteins, and light-driven assembly of the oxygen-evolving Mn_4CaO_5 complex (Komenda et al., 2008; Nixon et al., 2010). Accessory factors, such as Ycf48, Psb27, and Psb28, associate transiently with PSII at specific stages of assembly but their functions remain unclear (Komenda et al., 2012b). PSII assembly in chloroplasts is likely to occur by a similar pathway, although additional accessory proteins appear to have been recruited (Chi et al., 2012; Nickelsen and Rengstl, 2013).

PSII is vulnerable to light-induced inactivation and is repaired via the selective replacement of the D1 protein, which is accompanied by a partial disassembly and reassembly of the complex (reviewed in Nixon et al., 2010). This process is especially important under high irradiance, which in cyanobacteria induces the synthesis of a group of single transmembrane helix proteins called Hlips (high-light-inducible proteins; Dolganov et al., 1995) or Scps (small CAB-like proteins; Funk and Vermaas, 1999) with sequence similarities to plant light-harvesting

[1] Address correspondence to komenda@alga.cz.
The author responsible for distribution of materials integral to the findings presented in this article in accordance with the policy described in the Instructions for Authors (www.plantcell.org) is: Josef Komenda (komenda@alga.cz).
[W] Online version contains Web-only data.
www.plantcell.org/cgi/doi/10.1105/tpc.114.123919

complexes. Hlips have been detected in monomeric PSII and RC47 complexes (Promnares et al., 2006; Yao et al., 2007) and have been shown to prevent generation of singlet oxygen in PSII (Sinha et al., 2012) and to participate in regulation of chlorophyll biosynthesis (Xu et al., 2002; Hernandez-Prieto et al., 2011). Hlips contain a domain implicated in chlorophyll and carotenoid binding, and several studies have suggested binding of pigments to Hlips/Scps (Xu et al., 2004; Storm et al., 2008), but clear and convincing experimental evidence is still lacking.

In this study, we discovered that *Synechocystis* Ycf39, encoded by the *slr0399* gene, and two members of the Hlip family, HliC (ScpB) and HliD (ScpE), associate with the RCII complex. Our data demonstrate that Ycf39 and the two Hlips form a separate pigment-protein complex (designated the Ycf39-Hlip complex) containing chlorophyll and β-carotene, which is important for accumulation of the RC in vivo. Our data also suggest that the Ycf39-Hlip complex is involved in the delivery of recycled chlorophyll to newly synthesized D1 protein during the formation of the RCII subcomplex and protects newly synthesized D1 and RCII from light damage.

RESULTS

Identification of Ycf39 as a Component of a PSII RC Subcomplex

Our previous studies of PSII assembly in *Synechocystis* have revealed that strains unable to synthesize the inner antenna CP47 accumulate two RC assembly intermediate complexes designated RCII* and RCIIa (Sobotka et al., 2005; Dobáková et al., 2007; Komenda et al., 2008). These complexes differ in size on native gels, most probably due to the presence of additional component(s) in the larger RCII* complex. To explore this further, we separated solubilized membrane complexes isolated from the CP47-less strain (ΔCP47) by clear-native (CN) electrophoresis (Figure 1A). After separation by SDS-PAGE in the second dimension and staining of protein subunits, we used mass spectrometry (MS) to identify two well-stained proteins that comigrated with the RCII* complex. The larger one was the Ycf48 assembly factor found previously in RCII* (Komenda et al., 2008), while the smaller protein, of ~40 kD, was identified as Ycf39, the product of the *slr0399* gene (Figure 1A, 2D Sypro).

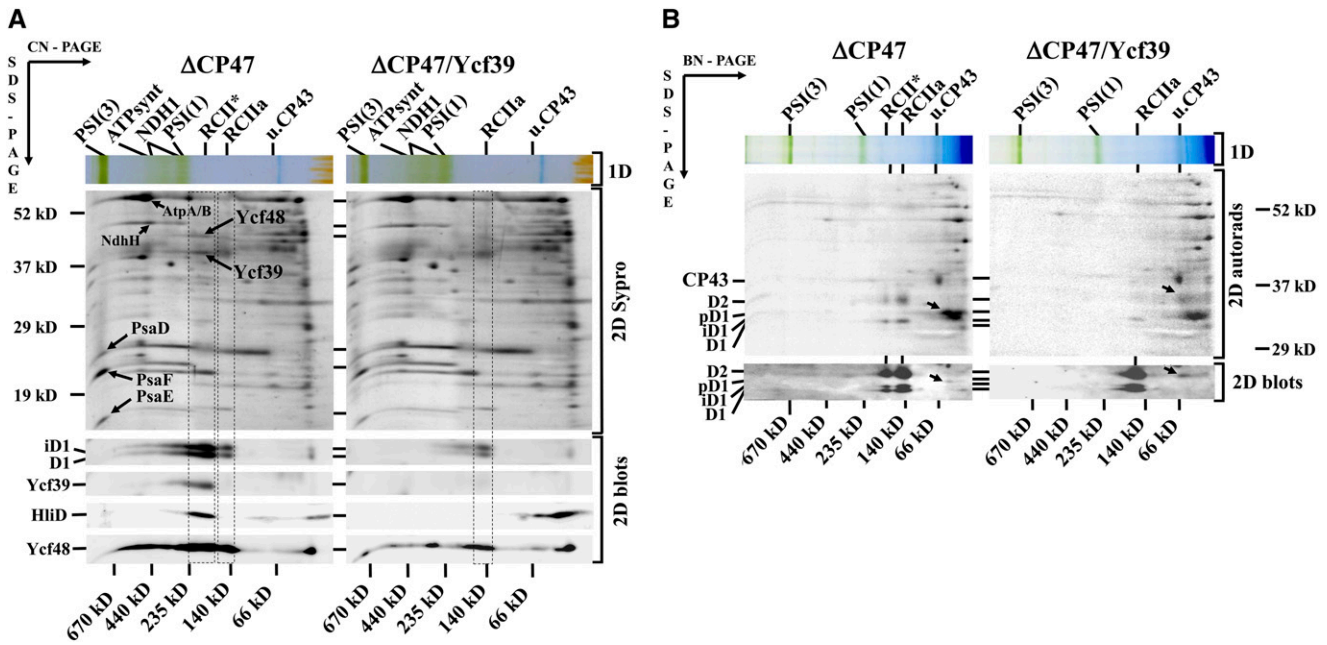

Figure 1. Identification of Ycf39 as a Component of the PSII RC Complex RCII* and Effect of Ycf39 on Protein Biosynthesis in a Strain Lacking the PSII Antenna CP47.

(A) Membranes isolated from cells of ΔCP47 and ΔCP47/Ycf39 deletion strains grown in the presence of Glc were analyzed by 2D-CN/SDS-PAGE. The first-dimension native gel was photographed (1D) and after SDS-PAGE in the 2nd dimension the gel was stained by Sypro (2D Sypro), and bands designated by arrows were identified by MS. Alternatively, the gel was blotted and probed with antibodies specific for D1, Ycf39, HliD, and Ycf48 (2D blots). The designation of complexes: PSI(3) and PSI(1), trimeric and monomeric PSI; ATPsynt, ATP synthase; NDH1, NADH dehydrogenase; RCII* and RCIIa, two PSII RC complexes lacking CP47 and CP43; u.CP43, unassembled CP43; iD1 and D1 indicate the partially and fully processed forms of the D1 protein, respectively. Each loaded sample contained 5 μg chlorophyll.

(B) Membranes isolated from cells of ΔCP47 and the ΔCP47/Ycf39 labeled by radioactive Met and Cys were analyzed by 2D-blue native (BN)/SDS-PAGE, the gel was blotted, the blot dried and exposed to a phosphor imager plate (2D autorads), and later used for detection of the D1 and D2 proteins by specific antibodies (2D blots). pD1 indicates the unprocessed form of D1, other designations are as in **(A)**. Unassembled pD1 (left panel) and D2 (right panel) are designated by oblique arrows.

The presence of Ycf39 in RCII* but not in the smaller RCIIa complex was also supported by immunoblotting experiments (Figure 1A, 2D blots). Surprisingly, a member of the Hlip family, HliD, was also present in RCII* but absent in RCIIa (Figure 1A, 2D blots), suggesting a link between Ycf39 and Hlips. To test the importance of Ycf39 for accumulation of RCII complexes, we deleted the *slr0399* gene in the ΔCP47 strain and membrane complexes of the resulting double mutant were subjected to analysis by 2D-CN/SDS-PAGE. The absence of RCII* in the ΔCP47/Ycf39 double mutant provided further confirmation that Ycf39 was an additional component of RCII*. Moreover, the overall level of RCII complexes markedly decreased (Figure 1A, 2D blots).

We also assessed the effect of deleting *ycf39* on the biosynthesis of membrane proteins in the ΔCP47 strain by radioactive protein labeling and subsequent 2D protein analysis (Figure 1B). The autoradiograms showed a significantly reduced incorporation of radiolabel into D1 in the double mutant, suggesting a limitation in the biosynthesis of D1 in the absence of Ycf39. This was further supported by immunoblot analysis of the 2D blot using antibodies specific for D1 and D2 (Figure 1B, 2D blots). While in the single ΔCP47 strain a small fraction of precursor D1 (pD1) is always observed in the region of unassembled proteins (see also Komenda et al., 2004), this fraction was missing in the double mutant and, instead, there was an increased level of unassembled D2 protein, shown previously to accumulate in the absence of D1 (Komenda et al., 2004).

Ycf39 Is Associated with the Cytoplasmic Surface of the Membrane

Ycf39 is predicted to contain an NAD(P)H binding domain and to be a soluble member of the short-chain alcohol dehydrogenase/reductase superfamily (Ermakova-Gerdes and Vermaas, 1999). Analysis of membrane and soluble fractions by immunoblotting revealed that Ycf39 was actually strongly associated with the membrane despite the lack of a predicted transmembrane region (Supplemental Figure 1B). Furthermore the sensitivity of Ycf39 to degradation by trypsin in right-side-out membrane vesicles (Komenda, 2000; Dobáková et al., 2009) and the lack of a predicted lumenal-targeting sequence suggested a location on the cytoplasmic side of the membrane.

Identification of a Chlorophyll Binding Complex Containing Ycf39, HliC, and HliD

To isolate complexes associated with Ycf39, we constructed a CP47-less strain expressing a 3xFlag-tagged version of the protein (Flag-Ycf39), which we purified under native conditions using a Flag-affinity column. The obtained eluate contained both chlorophyll and carotenoids as indicated by its absorption spectrum (Supplemental Figure 2A) and confirmed by HPLC analysis which demonstrated the presence of chlorophyll, β-carotene, and pheophytin (Supplemental Figure 3). Trace amounts of the carotenoids myxoxanthophyll and zeaxantin were detected but are likely to be impurities rather than regular components of the complexes. Moreover, the maximum of the 77K chlorophyll fluorescence spectrum at 682 nm suggested the isolated preparation was related to PSII as photosystem I (PSI) emits at ~720 to 730 nm under these conditions (Shen et al., 1993) (Supplemental Figure 2A).

Pigment proteins pulled down with Flag-Ycf39 were identified following 2D-CN/SDS-PAGE (Figure 2A). The analysis by native PAGE revealed the presence of four pigmented bands. The most intense yellow-green band corresponded to RCII* as revealed by its relative size (~200 kD) and polypeptide composition. Immunoblot and/or MS analysis (Supplemental Table 1) revealed the presence of D2, D1 (in its mature form as well as its incompletely processed form iD1), PsbE and PsbF of Cyt *b*-559, and PsbI. Furthermore, in the region around 45 kD, we detected Flag-Ycf39 and Ycf48. Finally, in the region around 5 to 7 kD, we also identified members of the Hlip family: HliD (ScpE) and HliC (ScpB).

A second smaller pigment-protein complex (of ~60 kD) contained Flag-Ycf39 together with HliD and HliC and represents a previously undiscovered pigment-protein complex of *Synechocystis*, which we designate the Ycf39-Hlip complex. A third pigmented band at the edge of the native gel most probably represented free pigments in detergent/lipid micelles, but there was also a distinct band of HliD, which might also bind pigment. We always detected a variable amount of another pigment-protein complex, migrating slightly faster than the RCII* complex. This complex contained most of the proteins detected in RCII* but did not contain Ycf39 and the Hlips, and its size corresponded to the size of RCIIa complex detected in thylakoids of the CP47-less strain. The lack of Ycf39 suggests that this complex results from fragmentation of the RCII* complex during purification or electrophoresis. Interestingly, this complex was highly fluorescent (Figure 2A, 1D LAS fluor), a feature that is usual for pigment-protein complexes related to PSII (Kopečná et al., 2013). However, both RCII* and the Flag-Ycf39-Hlip complex showed much lower fluorescence at room temperature, indicating efficient quenching of the absorbed light energy. Finally, the largest green nonfluorescent band was assigned as the trimeric PSI complex according to its size of ~750 kD, detection of the PsaD subunit (Figure 2A), and a 77K fluorescence emission band at 722 nm. However, the absence of a 722-nm chlorophyll fluorescence band at 77K in the pull-down preparation (Supplemental Figure 2) indicated that the trimeric PSI complex was only a minor component.

The use of the CN gel system allowed us to measure the absorption and low-temperature fluorescence spectra of the pigmented bands directly in the gel. Both Flag-Ycf39-Hlip and RCII* contained chlorophyll and carotenoids, with absorption maxima at around 675 and 450 to 530 nm, respectively. A small shoulder at ~543 nm in the absorption spectrum of the RCII* complex also indicated the presence of pheophytin (Figure 2B, arrow), which was also detected in the crude Flag-Ycf39 preparation by HPLC (Supplemental Figure 3). The spectrum of the Flag-Ycf39-Hlip complex was typified by a distinct absorption band at around 520 nm. Such a red shift in the β-carotene absorption band would suggest a special environment of this pigment within the complex (Figure 2B, left panel). The 77K chlorophyll fluorescence maximum at 681 nm was similar for both complexes (Figure 2B, right panel). Finally, the absorption maximum at 678 nm and 77K chlorophyll fluorescence band at ~722 nm confirmed the identity of the largest green band as PSI.

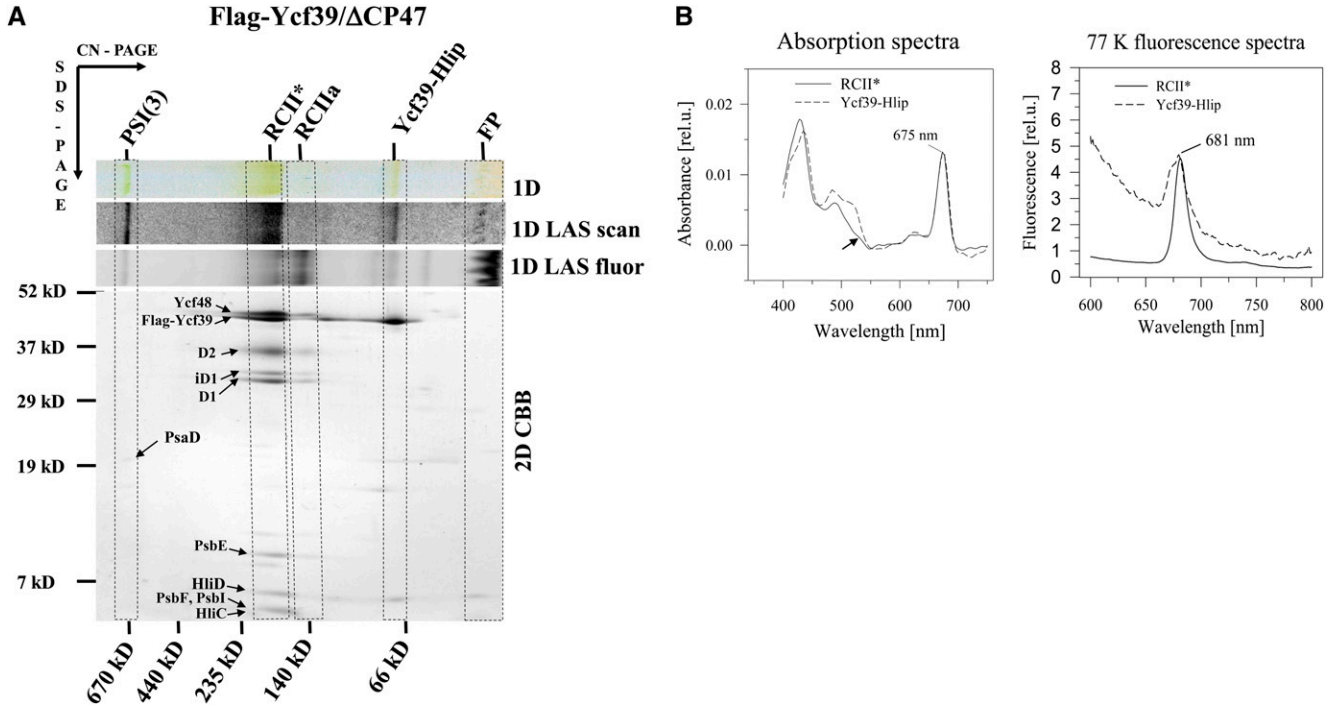

Figure 2. Analysis of the Flag-Ycf39 Preparation Using 2D-CN/SDS-PAGE and Room Temperature Absorption and 77K Chlorophyll Fluorescence Spectra of RCII* and Ycf39-Hlip Complexes in Gel.

(A) The preparation was isolated using anti-Flag affinity resin from membranes of the *Synechocystis* mutant expressing Flag-Ycf39 instead of Ycf39 and lacking CP47. It was subsequently analyzed by 2D-CN/SDS-PAGE. The first-dimension native gel was photographed (1D) or scanned by LAS 4000 for absorption (1D LAS scan) or fluorescence (1D LAS fluor) and after SDS-PAGE in the 2nd dimension, the gel was stained by Coomassie blue (2D CBB) and the designated spots were identified by MS (Supplemental Table 1). FP are free pigments, and other designations are as in Figure 1. Due to the high resistance of the PSI(3) band to SDS, most of its subunits are not released from it on 2D gels and are therefore hardly visible.
(B) The left panel shows room temperature absorption spectra, and the right panel the 77K chlorophyll fluorescence spectra of RCII* (solid lines) and Ycf39-Hlip complexes (dashed lines) in gel. The arrow in the RCII* absorption spectrum designates the shoulder at 543 nm belonging to pheophytin.

In order to prove that the attachment of Flag-Ycf39 with the RCII* complex was not an artifact related to the use of a mutant lacking CP47, we performed the pull-down experiment with a wild-type strain expressing Flag-tagged Ycf39. Although the yield of the preparation was much lower on a cell basis, the composition of the isolated preparation was similar to that obtained from the ΔCP47 strain (Figure 3A). We analyzed this preparation by 2D-CN/SDS-PAGE in combination with immunoblotting and detected Ycf48, D1, D2, HliC, HliD, and the PsbI proteins. As in the ΔCP47 strain, Ycf39, HliC, and HliD were present both in the RCII* complex and in a separate pigmented Ycf39-Hlip complex. In both preparations, we also detected a fluorescent band between the Ycf39-Hlip complex and free pigments. Based on the result of the immunoblot, it was ascribed to the D1-PsbI complex (Figure 3A, 1D LAS fluor) with its strong fluorescence suggesting the presence of bound chlorophyll.

HliC and HliD Are Needed for Pigment Binding and Stable Association of Ycf39 with PSII

To assess the importance of the Hlips for binding of Ycf39 to RCII, we constructed and analyzed CP47-less mutants lacking either HliC or HliD. The 2D electrophoresis confirmed that the absence of HliC, and especially HliD, led to a significant decrease in the abundance of RCII* (Supplemental Figure 4). We also constructed a CP47-less mutant expressing Flag-tagged Ycf39 but lacking HliD. The preparation isolated from this strain contained almost 10-fold less chlorophyll but lacked RCII and instead contained PSI as judged by absorption spectroscopy and 77K fluorescence emission spectroscopy (Supplemental Figure 2B). The preparation also lacked HliC, consistent with the previously identified close relationship between expression of HliC and HliD (Kufryk et al., 2008). Importantly, the Flag-tagged Ycf39 protein isolated from this strain did not bind detectable pigment following native gel electrophoresis (Figure 3B). This experiment showed that Hlips are required for binding of chlorophyll and β-carotene in the Ycf39-Hlip complex, while Ycf39 alone does not bind pigments.

The Ycf39-Hlip Complex Binds to D1 at an Early Stage in Assembly

To test whether the Ycf39-Hlip complex was able to bind to unassembled D1, we also expressed and isolated Flag-tagged Ycf39 from a strain lacking D2, which accumulates low levels of D1 but is unable to assemble RCII or larger PSII core complexes

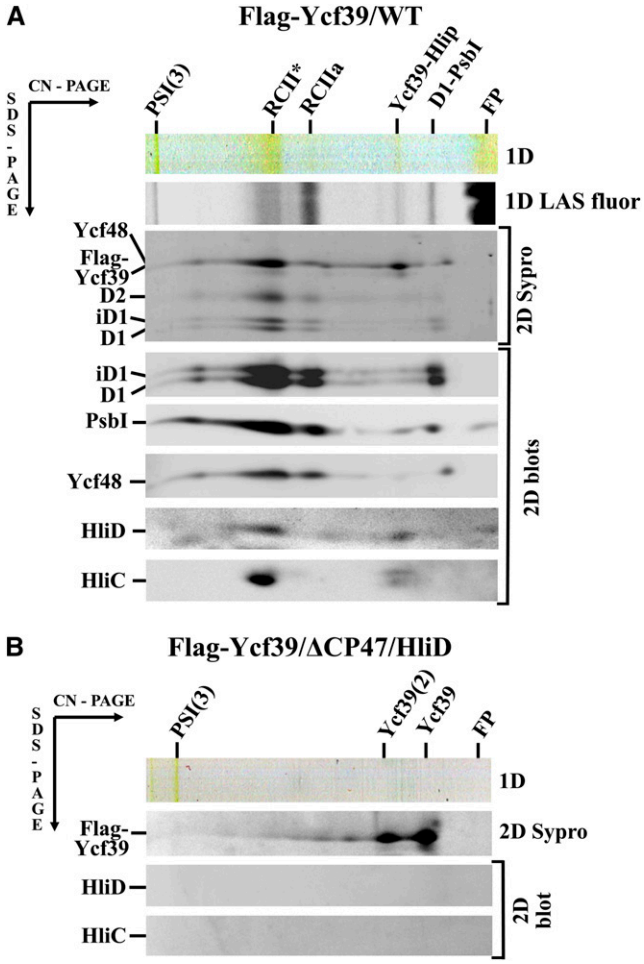

Figure 3. Pigment Proteins in Flag-Ycf39 Preparations from the Wild Type and a Strain Lacking CP47 and HliD.

The preparations from the wild type **(A)** and from the strain lacking CP47 and HliD **(B)**, both expressing Flag-Ycf39 instead of Ycf39, were isolated using anti-Flag affinity resin. Pigment proteins were subsequently separated by 2D-CN/SDS-PAGE. The first-dimension native gel was photographed (1D) and scanned by LAS 4000 for fluorescence (1D LAS fluor), after SDS-PAGE in the second dimension the gel was stained by Sypro orange (2D Sypro), electroblotted to polyvinylidene fluoride membrane, and probed with specific antibodies [2D blot(s)]. Designation of complexes is as in Figures 1 and 2, the Ycf39(2) is most probably the dimeric form of Ycf39, and D1-PsbI is a small fluorescent complex of (i) D1 and the small PSII subunit PsbI.

(Komenda et al., 2004). In the preparation we detected, in addition to Flag-Ycf39, D1 in the mature as well as incompletely processed form (iD1) together with Ycf48, HliC, and HliD (Figure 4A). Interestingly, the FtsH2/FtsH3 heterocomplex involved in D1 degradation during PSII repair was also present. By contrast, the Flag-Ycf39 preparation isolated from a D1-less strain, which is still able to accumulate low levels of the D2/Cyt b-559 subcomplex (Komenda et al., 2008), contained HliD, HliC but neither D2 nor Ycf48 (Figure 4B; Supplemental Table 1).

The DE Loop of D1 Is Important for Binding of Ycf39-Hlip Complex

The results thus far suggested that the D1 protein provides the binding site for the Ycf39-Hlip complex within RCII*. To locate this site more precisely, we tested two strains having either a 20–amino acid deletion at the N terminus (A20; Komenda et al., 2007) or a 25–amino acid deletion in the DE loop between the fourth and fifth transmembrane helices of D1 (R225-V249, PCD mutant; Mulo et al., 1997) for the presence of RCII* during radioactive labeling at low temperature, which leads to an increased accumulation of RCII subcomplexes (Komenda et al., 2008). The result showed the lack of RCII* accumulation in the PCD but not in the A20 mutant (Supplemental Figure 5), indicating a possible Ycf39 binding site in the R225-V249 segment of D1. During biosynthesis of the D1 protein, this segment is released from the ribosome and becomes available for Ycf39 binding when the fifth transmembrane helix is still buried within the ribosome. This moment corresponds well to a putative pause in biosynthesis of chloroplast D1, which is assumed to allow chlorophyll binding (Kim et al., 1991).

The preparations from both RCII-less strains and especially from the D1-less strain showed a significant content of 50S and 30S ribosomal subunits and, even more importantly, chlorophyll synthase (ChlG), which is the ultimate enzyme responsible for attachment of geranylgeranyl/phytyl group to Chlide during chlorophyll biosynthesis (Bollivar, 2006) (Figure 4B). Thus, the Ycf39-Hlip complex appears to associate with ribosomes and ChlG, implicating Ycf39 as playing a role at an early stage in D1 biosynthesis when chlorophyll is required for insertion into the growing polypeptide chain.

A Mutant Lacking Ycf39 Is More Sensitive to Photoinhibition

To gain more information on the physiological importance of Ycf39, we characterized a *ycf39* deletion strain and compared it with the wild type. In agreement with a previous report (Ermakova-Gerdes and Vermaas, 1999), there was no detectable difference in the phenotype between ΔYcf39 and the wild type in terms of growth rate, pigment composition, 77K chlorophyll fluorescence spectra, and rate of oxygen evolution at different irradiances. However, PSII in the ΔYcf39 strain was clearly more sensitive than in wild type to high irradiance as judged by the more rapid decline in the rate of oxygen evolution during the first 45 min of illumination at 700 μmol photons m^{-2} s^{-1} (Figure 5A). After this period, oxygen evolution stabilized in the mutant, which suggested that the photoprotective processes counteracting fast PSII photodamage are less efficient in the mutant during the initial period of high-light treatment but not at later points. Moreover, assessment of D1 protein turnover did not show any significant difference between the strains (Supplemental Figure 6). However, more detailed analysis by 2D gels revealed that the amount of labeled D1 protein was slightly lower in the PSII core complexes of the mutant (Figure 5B), and the mutant also showed a dramatic reduction in the level of labeled iD1 in the RCII complexes. Compared with the wild type, the mutant also showed increased accumulation of newly synthesized D1, D2, CP47, and CP43 in the unassembled protein region of the gel, consistent with a block in

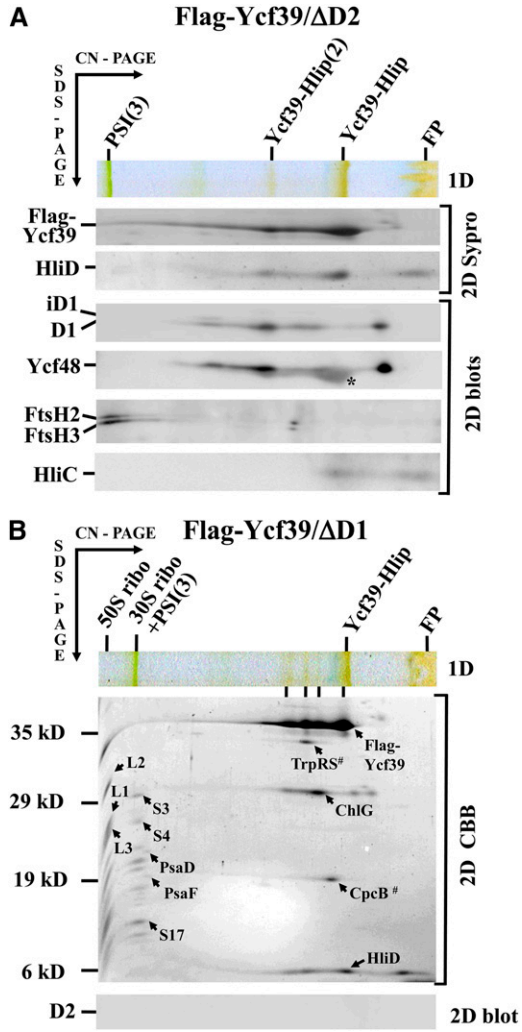

Figure 4. 2D-CN/SDS-PAGE Analysis of the Flag-Ycf39 Preparations from D2-Less and D1-Less Strains Expressing Flag-Ycf39.

The preparations from D2-less **(A)** and D1-less **(B)** strains expressing Flag-Ycf39 instead of Ycf39 were isolated using anti-Flag affinity resin. Pigment-proteins were subsequently separated by 2D-CN/SDS-PAGE. The first-dimension native gel was photographed (1D), and after SDS-PAGE in the second dimension, the gel in **(A)** was stained by Sypro Orange (2D Sypro), blotted onto polyvinylidene fluoride membrane, and D1, Ycf48, FtsH2, FtsH3, and HliC were detected by specific antibodies (2D blots). Asterisk indicates unspecific reaction of the flagged Ycf39 partly overlapping the signal of Ycf48. In **(B)**, the gel was stained with Coomassie blue (2D CBB) and selected proteins identified by MS. Complexes are designated as in Figure 3. 50S and 30S ribo designate large and small subunit of ribosomes, and other designations are as in Figure 2. The following proteins were identified in the preparation from the D1-less strain by MS: L1 (Rpl1, Sll1744), L2 (Rpl2, Sll1260), and L3 (Rpl3, Sll1799) of the large 50S ribosomal subunit subunit; S3 (Rps3, Sll1804), S4 (Rps4, Slr0469), and S17 (Rps17, Ssl3437) of the small ribosomal subunit; Flagged Ycf39 (Slr0399); ChlG (chlorophyll synthase, Slr0056); HliD (ScpE, Ssr1789). The bands with hashtag, CpcB (Sll157) and TrpRS (tryptophanyl-tRNA-synthetase, Slr1884), are standard unspecific interactors of the Flag resin. The 2D blot indicates the lack of the D2 protein in the preparation.

the formation of RCII and larger complexes. Overall, these data suggest that the Ycf39-Hlip complex is important for maintaining PSII activity upon sudden exposure to high irradiances at the level of D1 incorporation into RCII complexes.

Ycf39 Is Needed for Efficient Chlorophyll Recycling

Association of Ycf39 with D1, Hlips, ChlG, and ribosomes implies the possible involvement of Ycf39 in the insertion of chlorophyll into newly synthesized D1, either during de novo assembly or PSII repair. To investigate this further, we analyzed differences in the level of pigments and chlorophyll precursors and their changes induced by exposure of the wild-type and Ycf39-less cells to high light. No significant differences were observed between the strains under the experimental conditions used and a similar result was also obtained for the strains lacking CP47. However, since the role of Ycf39 seems to be restricted to the biosynthesis of the D1 protein, which contains only a small fraction of total cellular chlorophyll present in wild-type cells, specific changes related just to the D1 protein could be masked by the insertion of chlorophyll into other chlorophyll binding proteins. Therefore, we constructed a mutant that contains the D1 and D2 proteins but lacks PSI, CP47, and CP43, together with its variant lacking Ycf39. We exposed these mutants to a short high-light treatment in the presence of the chlorophyll biosynthesis inhibitor gabaculine (Guikema et al., 1986) and simultaneously monitored the levels of the D1 protein and early chlorophyll precursors Mg-protoporphyrin and its monomethyl ester. The ΔPSI/CP47/CP43/Ycf39 strain showed a strong depletion of Mg protoporphyrin during 30-min exposure to high light indicating consumption of chlorophyll biosynthesis intermediates for biosynthesis of new chlorophyll while the precursors in the control strain remained stable (Figure 6A). Immunoblots showed a stable content of both iD1 and D1 proteins during light treatment in the control strain, while the level of both proteins decreased by ~30% after light treatment of the Ycf39-less strain (Figure 6B). These data suggest a block in the reuse of chlorophyll and a higher requirement of newly synthesized chlorophyll for de novo biosynthesis of the D1 protein in the absence of Ycf39.

DISCUSSION

Despite its obvious physiological importance, little is known about how chlorophyll is delivered to the apo-polypeptides during assembly and repair of the photosynthetic apparatus in cyanobacteria and chloroplasts. Here, we provide evidence that the Ycf39-Hlip pigment-protein complex is important for chlorophyll delivery to the D1 subunit during the initial stages of PSII assembly in *Synechocystis*.

Ycf39 was identified following analysis of the polypeptide composition of the RCII* complex, an early assembly intermediate of PSII lacking the inner antennae CP47 and CP43 (Figure 1). Isolation of Flag-tagged Ycf39 revealed that this protein forms a chlorophyll and β-carotene binding protein complex with two members of the Hlip family, HliC and HliD. In the wild type, the complex was mostly present in its free form due to the low content of RCII subcomplexes (Supplemental

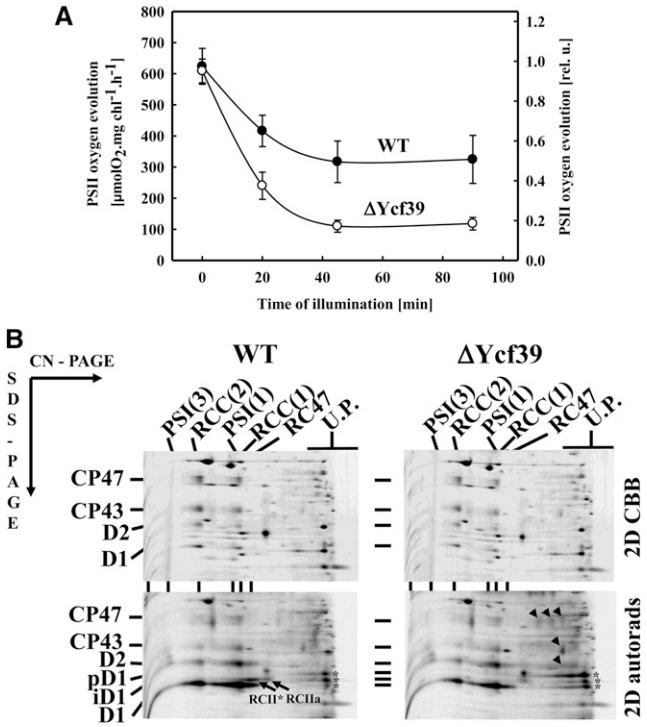

Figure 5. PSII Repair and Biosynthesis of PSII Proteins in Wild-Type and ΔYcf39 Strains under High Irradiance.

(A) Wild-type cells (closed symbols) and ΔYcf39 (empty symbols) were illuminated with 700 μmol photons m^{-2} s^{-1} of white light for 90 min, and during illumination, PSII oxygen-evolving activity was assayed in whole cells to examine PSII repair. The initial values of oxygen evolution were 624 ± 58 and 609 ± 38 μmol O_2 mg chlorophyll^{-1} h^{-1} for the wild type and ΔYcf39, respectively (values are means of six measurements ± SD from three independent experiments).

(B) Membranes isolated from radioactively labeled cells were analyzed by 2D-CN/SDS-PAGE. The gels were stained by Coomassie blue (2D CBB) and exposed to a phosphor imager plate (2D autorads). Designation of complexes: RCC(2) and RCC(1), dimeric and monomeric PSII core complexes; RC47, PSII core complex lacking CP43; U.P., unassembled proteins; other designations are as in Figure 1. Asterisks indicate unassembled forms of unprocessed, partially processed, and processed D1 protein (their identity was confirmed by immunodetection), arrows indicate RCII complexes, which are almost missing in the mutant; arrowheads designate unassembled CP47, CP43, and D2 waiting for the D1 protein. Each loaded sample contained 5 μg chlorophyll.

Figure 4), but in the strain lacking CP47 and therefore unable to form larger PSII core complexes, a significant portion of Ycf39-Hlip was found attached to the RCIIa subcomplex forming the larger subcomplex RCII* (Figures 1 and 2). The RCII* subcomplex contains the previously identified PSII subunits: Mature D1 and its incompletely processed form iD1, D2, both subunits of Cyt *b*-559 (PsbE and PsbF), and PsbI (Komenda et al., 2004, 2008; Dobáková et al., 2007). Occasionally, the PsbY subunit could also be detected in the complex (Supplemental Table 1). The subunit composition of the RCII* complex corresponds well to the latest PSII structural models (Ferreira et al., 2004; Guskov et al., 2009; Umena et al., 2011) since the presence of most other small subunits and lumenal PSII proteins is dependent on the antenna chlorophyll-proteins CP47 and CP43. These two chlorophyll-proteins attach to the RCII complex as separate modules, together with neighboring small subunits and pigments, later in the process of PSII assembly (Boehm et al., 2011; Komenda et al., 2012a). In agreement with a previous report (Komenda et al., 2008), RCII* also contained the Ycf48 assembly factor (Figure 1A). Several minor protein bands that we did not succeed in identifying due to their low abundance, were also present so the existence of other substoichiometric accessory factors in RCII* remains possible.

The low abundance of the RCII complexes in vivo has until now prevented their isolation and characterization. The absorption spectrum of the RCII* separated by native gel electrophoresis indicated the presence of a higher number of chlorophyll and β-carotene molecules in comparison with the RCII complex previously isolated from *Synechocystis* by stripping off the inner PSII antennae from the PSII core (Tomo et al., 2008), which is consistent with additional binding of pigments to the Ycf39-Hlip complex. Moreover, a small shoulder at ~545 nm is consistent with the presence of pheophytin. There are two pheophytin molecules in the D1/D2 complex isolated by fragmentation of larger core complexes, one of which is used as the primary electron acceptor (Nanba and Satoh, 1987). So, it is possible that during PSII assembly, the pigments needed for primary charge separation are already present in the RCII assembly intermediates.

Separation of the Ycf39-Hlip complex from other complexes and proteins by native gel electrophoresis and measurement of its absorption spectra also provided the strongest support yet for chlorophyll and β-carotene binding to Hlips. When we isolated Flag-Ycf39 from the strain lacking both CP47 and HliD, no pigmented band appeared in the low molecular weight region of the gel despite the large amount of the Flag-Ycf39 present (Figure 3B). This is consistent with bioinformatic analyses of Ycf39 indicating it to be a member of the short-chain alcohol dehydrogenase/reductase family unrelated to pigment binding.

The Ycf39 protein overaccumulated in several mutants unable to form either PSII core or RCII complexes due to the lack of D1, D2, or CP47. Immunoblot analysis showed increased amounts of Ycf39 in all three of the tested PSII mutants with its amount agreeing well with the increased content of HliD (and carotenoids) (Supplemental Figure 7A). Amounts of Ycf39 and HliD also increased in parallel in wild-type cells exposed to high light (Supplemental Figure 7B). Interestingly, using 2D gel analysis, we detected much higher levels of two other members of the Hli family, HliA/B, bound to the PSII core complex of the Ycf39-less strain in comparison with the wild-type strain (Supplemental Figure 8). Accumulation of HliA/B could represent a possible compensatory mechanism induced in the absence of Ycf39.

Flag-Ycf39-Hlip was the main complex isolated from strains lacking either the D1 or D2 proteins (Figure 4), but in these strains, it was copurified with other protein components. Purification of the complex from the strain expressing Flag-tagged Ycf39 and lacking D2 revealed association of the complex with the D1 protein together with PsbI and Ycf48, confirming the involvement of these two latter proteins in the very early stage of D1 biosynthesis (Dobáková et al., 2007; Komenda et al., 2008).

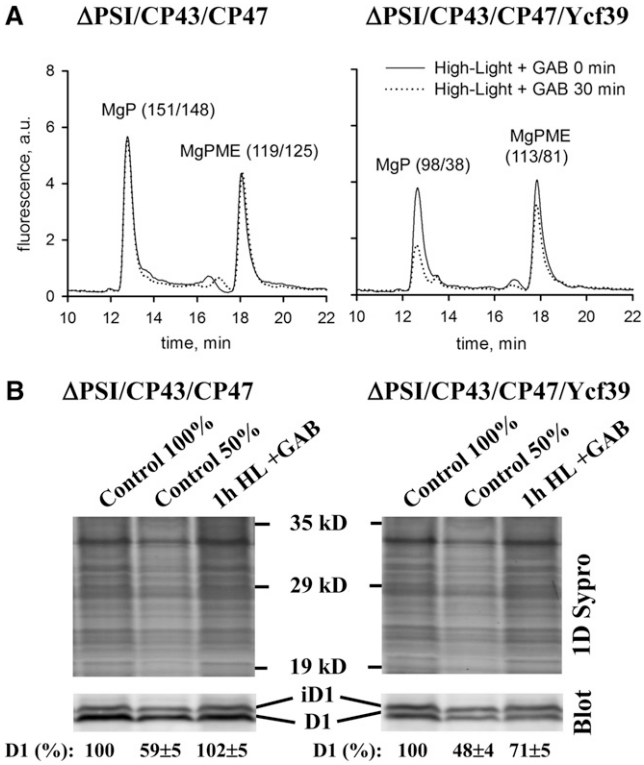

Figure 6. Analysis of Early Chlorophyll Precursors and the D1 Protein Level in Cells of ΔPSI/CP47/CP43 and ΔPSI/CP47/CP43/Ycf39 Strains after Exposure to 300 μmol Photons m^{-2} s^{-1}.

(A) Chromatograms of chlorophyll precursors separated by HPLC from cells of both strains after 30-min dark incubation with 20 μM gabaculine (GAB 0 min) and after an additional 30-min high-light treatment (GAB 30 min).
(B) Membrane proteins from control and cells treated with high light for 60 min in the presence of gabaculine (1 h HL + GAB) were analyzed by SDS-PAGE, the gels were electroblotted to polyvinylidene fluoride membrane and probed with antibodies specific for D1 (blot). Loading of the gel was checked by staining with Sypro Orange (1D Sypro). Chlorophyll (0.2 and 0.1 μg) was loaded for control 100 and 50%, respectively, 0.2 μg for the Ycf39-less mutant. The values represent mean ± SD from three measurements.

The binding of Ycf39 to D1 may occur during a pause in translation of D1, possibly related to insertion of chlorophyll into D1 (Kim et al., 1991). By contrast, the main binding partners of the complex in the strain lacking D1 were ribosomes (namely the large ribosomal 50S subunit) and the enzyme chlorophyll synthase. Indeed, purified chlorophyll synthase has been recently shown to contain small amounts of Ycf39 (Chidgey et al., 2014). Based on these data, we hypothesize that the Ycf39-Hlip complex is present in a complex that participates in the coordinated delivery of chlorophyll to newly synthesized D1 protein. Free chlorophyll is known to be highly toxic in the membrane due to its ability to produce reactive oxygen species in the light (Apel and Hirt, 2004), and its biosynthesis and delivery must be carefully controlled. However, the almost identical phenotype of the wild type and ΔYcf39 under standard growth conditions is not consistent with the essential role of Ycf39 in this process. Given its crucial physiological importance, chlorophyll delivery to the D1 protein may occur via multiple pathways with some not involving Ycf39 as an essential component. Vermaas and colleagues have shown that most chlorophylls are actually recycled via Chlide during PSII repair (Vavilin and Vermaas, 2007). Based on our data (Figure 6), we hypothesize that the Ycf39-Hlip complex plays an important role in the reuse of chlorophyll released from degraded proteins for biosynthesis of D1.

According to our current working model, damaged D1 is degraded in *Synechocystis* by the FtsH2/FtsH3 heterohexameric protease complex (Boehm et al., 2012b); indeed, this complex was identified in the Ycf39 pull-down from the strain lacking D2 (Figure 4B). The released chlorophylls might then be immediately reused with the help of Hlips (Vavilin et al., 2007) via reactions involving detachment of the phytol tail (catalyzed by unknown enzyme) and its reattachment (Vavilin and Vermaas, 2007) catalyzed most probably by chlorophyll synthase. After association of Ycf39, Hlips, and chlorophyll synthase, the D1 protein emerging from membrane-bound ribosomes will be loaded with the reused chlorophylls and finally bound to the D2 protein to form RCII* (Figure 7). After attachment of the CP47 module (Komenda et al., 2012a), the Ycf39-Hlip complex is detached from the resulting RC47 complex (Boehm et al., 2012a) and used for biosynthesis and assembly of other D1 modules. The sensitivity of PSII activity in the *ycf39* null mutant to high light (Figure 5A) suggests that the use of recycled chlorophyll for D1 biosynthesis might be especially important at the initial stages of high light stress when de novo biosynthesis of chlorophyll is not yet fully induced. Upon onset of high light, PSII damage can be so fast that the biosynthesis of D1 is not fast enough to quickly replace D1 at the level of the RC47 complex and RCII complexes synthesized with the help of recycled chlorophyll might represent an alternative mode of repair in which either D1 or both D1 and D2 can be replaced.

A minor component of all isolated Flag-Ycf39 preparations was trimeric PSI, which is the most abundant complex of *Synechocystis* thylakoids. This complex was also present in the negative control eluate obtained after passing solubilized

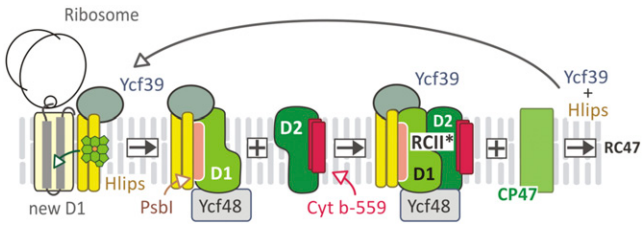

Figure 7. The Hypothetical Scheme for the Role of Ycf39-Hlip Complex in the Biosynthesis of D1 and Assembly of the RCII Complex.

Recycled chlorophylls are inserted via Ycf39-Hlip into D1 as it is synthesized and inserted into the membrane at a translocon-associated ribosome. D1 is then released and associates with PsbI and Ycf48 to form a D1 module, which binds to the D2 module, containing D2 and both subunits of cytochrome b-559, to form the RCII* assembly complex. Subsequent attachment of CP47, forming the RC47 complex, releases the Ycf39-Hlip complex for reuse.

thylakoids of the wild type through the anti-Flag affinity resin and therefore is possibly a contaminant. However, the level of trimer in isolated Ycf39-containing eluates was higher than in the control, so we do not yet exclude the possibility that Ycf39 binds to PSI and is involved in the release of chlorophyll from PSI for insertion into other pigment binding proteins, such as the D1 protein, as suggested recently (Kopečná et al., 2012).

The function of a NAD(P)H binding motif near the N terminus of Ycf39 remains elusive. Link et al. (2012) have pointed out that this motif could in fact bind RNA instead of being involved in redox reactions typical for the family of atypical short-chain dehydrogenases/reductases to which Ycf39 can be assigned (Kavanagh et al., 2008). As RNAs are components of ribosomes, the motif might represent a binding site for ribosomes or possibly for mRNA.

The strong quenching of chlorophyll fluorescence in RCII* but not in RCIIa also provides evidence for a role of the Ycf39-Hlip complex in safely dissipating excess excitation energy in the RCII* complex through nonphotochemical quenching, thereby protecting the RCII complex from light damage. We hypothesize that β-carotene bound to the Ycf39-Hlip complex may directly or indirectly via its own chlorophylls quench excitation energy from chlorophylls bound to the D1 protein. Although the orange carotenoid protein is known to play a photoprotective role in cyanobacteria (Kirilovsky and Kerfeld, 2012), it acts by binding to the phycobilisome light-harvesting complex, which is not able to bind to PSII assembly complexes (Wilson et al., 2006). The Ycf39-Hlip complex may also temporarily bind chlorophylls released from degraded RCII when the biosynthesis of new D1 is not yet completed. In both cases, formation of triplet chlorophylls and reactive singlet oxygen will be prevented (Sinha et al., 2012), thereby preventing damage to D1 (Figure 6B).

Ycf39 has previously been suggested to act as a chaperone helping to insert quinone into mutated Q_A binding pockets of PSII (Ermakova-Gerdes and Vermaas, 1999). However, Ycf39 is not actually needed for Q_A insertion into wild-type PSII (Ermakova-Gerdes and Vermaas, 1999), so it seems more likely that binding of Ycf39 protein on the cytoplasmic surface of RCII might have indirect effects on the access/binding of quinone to the Q_A binding pocket.

Hlips and Ycf39 have homologs in *Arabidopsis thaliana*, which suggests that these proteins might play a similar role in chloroplasts. Genes for one-helix-proteins (Ohps) homologous to Hlips have been identified in the *Arabidopsis* genome (Engelken et al., 2010) and like Hlips are also induced by high irradiance (Jansson et al., 2000; Andersson et al., 2003). The Ycf39 homolog from *Arabidopsis* called High Chlorophyll Fluorescence 244 (HCF244) (Link et al., 2012) is essential for normal accumulation of PSII and the protein has been shown to be needed for biosynthesis of the D1 protein, although the mechanism of its action has not been explained. Our data are in accordance with the close relationship between Ycf39 and biosynthesis of the D1 protein. It is possible that in *Arabidopsis* the absence of HCF244 does not allow de novo biosynthesis of the D1 protein, which would agree with the observed phenotype of the *hcf244* null mutant. However, in *Synechocystis* D1, biosynthesis is not completely blocked in the *ycf39* mutant and the block seems to mainly concern just a small fraction of the D1 protein destined for the assembly of new RCII complexes. On the other hand, most of the protein used for replacement of the damaged D1 protein appears to be synthesized normally as in the wild type (in agreement with this, no apparent difference in the *psbA* transcript level was found between the wild type and ΔYcf39); consequently, the phenotypes of the wild type and the ΔYcf39 mutant are very similar. This contrasts with the situation observed in *Arabidopsis* in which the absence of HCF244 leads to the almost complete loss of PSII accumulation in the mutant. This comparison again emphasizes the more drastic effect of a similar mutation in chloroplasts in comparison with cyanobacteria. It is possible that during de novo assembly of PSII in the chloroplast the newly synthesized D1 protein lacking bound HCF244 is efficiently recognized and degraded by proteases such as FtsH, while D1 in *Synechocystis* is able to escape the quality control system to some degree to allow formation of new PSII complexes.

METHODS

Construction and Cultivation of Cyanobacterial Strains

The previously constructed strains used in this study were derived from the Glc-tolerant strain of *Synechocystis* sp PCC 6803 (Williams, 1988) referred to as the wild type. The following previously described strains of the Glc-tolerant *Synechocystis* sp PCC 6803 strain were used: (1) the CP47 deletion strain (ΔCP47), in which the *psbB* gene is replaced by a spectinomycin resistance cassette (Eaton-Rye and Vermaas, 1991); (2) the *psbA* triple deletion strain (ΔD1) with cassette-less deletions in *psbA1* and *psbA3* genes and the *psbA2* gene replaced by a chloramphenicol resistance cassette (Nagarajan et al., 2011); (3) the *psbDIC*/*psbDII* deletion strain (ΔD2) with the *psbDIC* and *psbDII* genes encoding the D2 protein replaced by a chloramphenicol and a spectinomycin resistance cassette, respectively (Vermaas et al., 1990), and the *psaAB* deletion strain (ΔPSI) in which *psaAB* operon was replaced with a chloramphenicol resistance cassette (Shen et al., 1993). The ΔPSI strain was used to prepare the *psaAB*/*psbB*/*psbC* triple deletion strain (ΔPSI/CP47/CP43) in which *psbB* was additionally replaced by a spectinomycin resistance cassette and *psbC* interrupted by a kanamycin resistance cassette. The Hlip-lacking strains were transformed using genomic DNAs isolated from strains lacking HliC and HliD (Xu et al., 2002).

The transformation vector used to disrupt the *slr0399* gene encoding Ycf39 was constructed in two steps. First, *slr0399* along with 445 bp of upstream and 555 bp of downstream sequences were amplified from wild-type genomic DNA with primer set Slr0399-F (5′-GCCCCAGGACACG GATTTTACCGTCAA-3′) and Slr0399-R (5′-GTTCAGGGAGAGCGCTTCC CATAAAAGGTT-3′). The resulting fragments were then cloned into the multiple cloning region of pGEM-T Easy vector (Promega) to yield the initial vector pSlr0399 (Supplemental Figure 9A). Further modifications on pSlr0399 was then performed by replacing the open reading frame for Ycf39 between the *Eco*NI and *Hpa*I sites with an erythromycin resistance cassette via restriction digestion and ligation to create the final transformation vector termed pSlr0399ErmA (Supplemental Figure 9A). Sequencing confirmed that the orientation of the resistance cassette was the same as the orientation of *slr0399*. The pSlr0399ErmA plasmid was then used to transform the wild-type cells. Transformants were selected for erythromycin resistance and PCR was used to show integration of the selectable marker and elimination of the wild-type *slr0399* gene copy (Supplemental Figure 9B). The pSlr0399ErmA plasmid was also used for the transformation of other mutants like ΔD1, ΔD2, and ΔCP47 to create their Ycf39-less variants and their complete segregation was again checked by PCR (Supplemental Figure 9B).

Plasmid pPsbAIpetJ-Flag was used for construction of the strains expressing Flag-tagged Ycf39 under the control of the copper-regulated *petJ* promoter at the *psbAI* locus. The plasmid was constructed as follows: a 600-bp XbaI-Cfr9I fragment upstream and a 600-bp BglII-XmaJI fragment downstream of the *psbAI* gene were amplified by PCR and cloned into pETBlue-2 plasmid (Novagen). The *petJ* promoter from *Synechocystis* sp PCC 6803 (positions 846,614 to 846,331 according to CyanoBase) and 3xFlag coding sequence (Sigma-Aldrich) were amplified by PCR, ligated, and again amplified by PCR for cloning between the *psbAI* fragments. Finally, the kanamycin resistance gene (aphX) from pUC4K, amplified as a BamHI-*Bgl*II fragment, was cloned into the *Bgl*II site upstream of the second *psbAI* fragment leaving a single *Bgl*II site for cloning of *slr0399*. To clone the *slr0399* into the Flag plasmid, the *slr0399* gene was amplified by PCR using the following primers: NotI+*slr0399*-Fw, 5′-ATTAAAGCGGCCGCACGAGTTTTGGTGGTAGGCGG-3′, and *slr0399*+BglII-Rev, 5′- CAAACTAGTAGATCTAGAAAAAGAA-3′. After *Not*I and *Bgl*II digestion and ligation into the plasmid, the construct was used for the transformation of ΔSlr0399 deletion mutants. Mutants were selected for kanamycin resistance and were examined for segregation in the *psbAI* locus by PCR using gene-specific primers. To induce expression of the Flag-tagged Ycf39 protein, the strains were cultivated in BG-11 medium lacking $CuSO_4$.

The strains were grown in BG-11 as described previously (Kopečná et al., 2012). Growth media of nonautotrophically growing mutants were supplemented with 5 mM Glc. For gabaculine experiments, the cells of the strain ΔPSI/CP47/CP43 and its Ycf39-less variant were incubated with 20 μM gabaculine in the dark for 30 min, then the control samples for precursor assessment and immunoblot analysis were taken and the cells were subsequently exposed to irradiance of 300 μmol photons m^{-2} s^{-1} for additional 30 and 60 min, after which other samples were taken and analyzed. All experiments and measurements with cells were performed at least in triplicate and typical results are shown in figures.

Radioactive Labeling

Radioactive pulse (for 2D analysis) and pulse-chase (for 1D analysis) labeling of the cells was performed using a mixture of [^{35}S]Met and [^{35}S]Cys (Trans-label; MP Biochemicals) as described previously (Dobáková et al., 2009).

Preparation of Cellular Fractions and Isolation of Flag-Ycf39

Membranes were prepared by breaking the cells with zirkonia/silica beads according to the procedure described by Komenda and Barber (1995) and Dobáková et al. (2009). Flag-tagged Ycf39 was isolated using the anti-Flag M2 affinity gel (Sigma-Aldrich) after solubilization of membranes in 1.5% (w/v) *n*-dodecyl-β-D-maltoside.

Analysis of Proteins and Their Complexes

The membrane protein complexes were analyzed by blue-native or CN electrophoresis in combination with SDS-PAGE and immunoblotting as described (Komenda et al., 2012b). The previously described primary antibodies against the following proteins were used in this study: D1, D2, CP47, CP43, PsbI (Dobáková et al., 2007), and FtsH2 and FtsH3 (Boehm et al., 2012b). Moreover, we also used commercial anti-HliA/B and HliD (Agrisera), anti-Flag (Sigma-Aldrich) and our own antibodies against Ycf48, Ycf39, and HliC. The antiserum to *Synechocystis* Ycf48 (Slr2034) was raised against residues 37 to 342 expressed in *Escherichia coli* as an N-terminal His-tagged fusion protein and isolated by immobilized nickel affinity chromatography as described by Michoux et al. (2010). It was used as a crude antiserum at a dilution of 5000. Antibodies against Ycf39 (Slr0399) and HliC (Ssl1633) were raised in rabbit against a conjugate of keyhole limpet hemocyanin with a peptide 311-322 of Ycf39 and 2-17 of HliC, respectively. Antisera were purified using the corresponding immobilized peptides and used at a dilution of 2000 for anti Ycf39 and 500 for anti-HliC.

Tryptic in-Gel Digestion and Protein Identification by MS

The initial identification of Ycf39 in the Coomassie Brilliant Blue–stained protein spot separated by 2D-CN/SDS-PAGE from the CP47-less strain was performed by the Ultraflex III MALDI-TOF/TOF instrument (Bruker Daltonics) as described (Komenda et al., 2012b); all other MS analyses were done on a NanoAcquity UPLC (Waters) online coupled to an ESI Q-ToF Premier mass spectrometer (Waters) as described (Janouškovec et al., 2013).

Pigment Analyses, Spectroscopy, and Polarography Methods

Chlorophyll concentration was measured in 100% methanol according to Wellburn (1994), and quantitative determination of pigments in isolated preparations was performed by HPLC as described (Kopečná et al., 2012). For quantitative determination of chlorophyll precursors, a 3-mL culture at OD_{750} = 0.5 to 0.6 was spun down and resuspended in 20 μL water. Pigments were extracted with an excess of 70% methanol/30% water, filtered, and immediately injected onto an HPLC (Agilent-1200). Separation was performed on a reverse phase column (ReproSil pur 100, C8, 3-μm particle size, 4 × 150 mm; Watrex) with 35% methanol and 15% acetonitrile in 0.25 M pyridine (solvent A) and 50% methanol in acetonitrile as solvents B. Pigments were eluted with a gradient of solvent B (40 to 52% in 5 min) followed by 52 to 55% of solvent B in 30 min at a flow rate of 0.8 mL min^{-1} at 40°C. Eluted pigments were detected by a fluorescence detector set at 416/595 nm to detect Mg-protoporphyrin and Mg-protoporphyrin methylester. Chlorophyll fluorescence emission spectra at 77K were measured using an Aminco Bowman Series 2 luminescence spectrometer (Spectronic Unicam) as described (Sinha et al., 2012). Absorption spectra were measured using a Shimadzu UV3000 spectrophotometer, and the light-saturated steady state rate of oxygen evolution was assessed polarographically in the presence of artificial electron acceptors as described (Komenda et al., 2007).

Accession Numbers

Sequence data from this article can be found in the GenBank/EMBL databases under the following accession numbers: Ycf39 (Slr0399), NP_441851; HliC (Ssl1633), NP_440923; and HliD (Ssr1789), NP_440269.

Supplemental Data

The following materials are available in the online version of this article.

Supplemental Figure 1. Localization of Ycf39 in the Cells of *Synechocystis*.

Supplemental Figure 2. Room Temperature Absorption and 77K Chlorophyll Fluorescence Spectra of Flag-Tagged Ycf39 Preparations Isolated from the *Synechocystis* CP47-Less Mutant Expressing Flag-Ycf39 and Containing or Lacking HliD.

Supplemental Figure 3. HPLC Analysis of Pigments Present in the Flag-Tagged Ycf39 Preparation Isolated from the *Synechocystis* CP47-Less Mutant Expressing Flag-Ycf39 Instead of Ycf39.

Supplemental Figure 4. 2D Analysis of Membrane Protein Complexes of the Wild Type, ΔCP47, and ΔCP47 Lacking HliC or HliD Proteins.

Supplemental Figure 5. Biosynthesis of the PSII Proteins in Strains with N-Terminal Deletion (A20) and Deletion in the DE Loop of D1 [Δ(R225-V249)] under High Irradiance.

Supplemental Figure 6. The Rate of the D1 Degradation under High Irradiance Is Not Changed upon the Deletion of Ycf39.

Supplemental Figure 7. Levels of Ycf39 and HliD in Various PSII Mutants Unable to Assemble PSII Core Complexes and in Wild Type Exposed to High Irradiance.

Supplemental Figure 8. 2D Analysis of Membranes from Cells of the Wild Type and ΔYcf39 Deletion Strain before and after Their Treatment under High Irradiance of 500 μmol Photons m^{-2} s^{-1}.

Supplemental Figure 9. Construction and Verification of the *slr0399* Deletion.

Supplemental Table 1. PSII-Related Proteins Identified by MS and Immunoblotting in the RCII* Complex Separated by 2D-CN/SDS PAGE from the Flag-Ycf39 Preparation Isolated from the ΔCP47 Strain.

Supplemental Table 2. List of PSII- and Chlorophyll Biosynthesis-Related Proteins Identified in Preparations of Flag-Ycf39 Isolated from Wild-Type, HliD-, CP47-, D1-, and D2-Less Strains Expressing Flag-Ycf39.

ACKNOWLEDGMENTS

We thank Jan Pilný, Lenka Moravcová, and Vendula Krynická for excellent technical assistance during protein, pigment, and transcript analyses. J. Knoppová, J. Komenda, R.S., and M.T. were supported by projects Algatech (CZ.1.05/2.1.00/03.0110), RVO61388971, and P501/11/0377 of the Grant Agency of the Czech Republic; P.H. by project "Prague Infrastructure for Structure Biology and Metabolomics" (CZ.2.16/3.1.00/24023); and J.Y. and P.J.N. were supported by the UK Biotechnology and Biological Sciences Research Council (Grants BB/F020554/1 and BB/L003260/1).

AUTHOR CONTRIBUTIONS

J. Knoppová, R.S., P.J.N., and J. Komenda designed research. J. Knoppová, R.S., M.T., J.Y., P.K., P.H., and J. Komenda performed research. J. Knoppová, R.S., P.K., P.H., P.J.N., and J. Komenda analyzed the data. J. Knoppová, R.S., P.J.N., and J. Komenda wrote the article.

Received February 5, 2014; revised February 25, 2014; accepted March 7, 2014; published March 28, 2014.

REFERENCES

Andersson, U., Heddad, M., and Adamska, I. (2003). Light stress-induced one-helix protein of the chlorophyll a/b-binding family associated with photosystem I. Plant Physiol. **132:** 811–820.

Apel, K., and Hirt, H. (2004). Reactive oxygen species: Metabolism, oxidative stress, and signal transduction. Annu. Rev. Plant Biol. **55:** 373–399.

Boehm, M., Romero, E., Reisinger, V., Yu, J.F., Komenda, J., Eichacker, L.A., Dekker, J.P., and Nixon, P.J. (2011). Investigating the early stages of photosystem II assembly in Synechocystis sp. PCC 6803: Isolation of CP47 and CP43 complexes. J. Biol. Chem. **286:** 14812–14819.

Boehm, M., Yu, J., Reisinger, V., Bečková, M., Eichacker, L.A., Schlodder, E., Komenda, J., and Nixon, P.J. (2012a). Subunit composition of CP43-less photosystem II complexes of Synechocystis sp PCC 6803: Implications for the assembly and repair of photosystem II. Philos. Trans. R. Soc. B Biol. Sci. **367:** 3444–3454.

Boehm, M., Yu, J.F., Krynická, V., Barker, M., Tichý, M., Komenda, J., Nixon, P.J., and Nield, J. (2012b). Subunit organization of a *Synechocystis* hetero-oligomeric thylakoid FtsH complex involved in photosystem II repair. Plant Cell **24:** 3669–3683.

Bollivar, D.W. (2006). Recent advances in chlorophyll biosynthesis. Photosynth. Res. **90:** 173–194.

Chi, W., Ma, J.F., and Zhang, L.X. (2012). Regulatory factors for the assembly of thylakoid membrane protein complexes. Philos. Trans. R. Soc. B Biol. Sci. **367:** 3420–3429.

Chidgey, J.W., Linhartová, M., Komenda, J., Jackson, P.J., Dickman, M.J., Canniffe, D.P., Koník, P., Pilný, J., Hunter, C.N., and Sobotka, R. (2014). A cyanobacterial chlorophyll synthase-HliD complex associates with the Ycf39 protein and the YidC/Alb3 insertase. Plant Cell **26:** 10.1105/tpc.114.124495.

Dobáková, M., Tichý, M., and Komenda, J. (2007). Role of the PsbI protein in photosystem II assembly and repair in the cyanobacterium Synechocystis sp. PCC 6803. Plant Physiol. **145:** 1681–1691.

Dobáková, M., Sobotka, R., Tichý, M., and Komenda, J. (2009). Psb28 protein is involved in the biogenesis of the photosystem II inner antenna CP47 (PsbB) in the cyanobacterium *Synechocystis* sp. PCC 6803. Plant Physiol. **149:** 1076–1086.

Dolganov, N.A.M., Bhaya, D., and Grossman, A.R. (1995). Cyanobacterial protein with similarity to the chlorophyll a/b binding proteins of higher plants: Evolution and regulation. Proc. Natl. Acad. Sci. USA **92:** 636–640.

Eaton-Rye, J.J., and Vermaas, W.F.J. (1991). Oligonucleotide-directed mutagenesis of psbB, the gene encoding CP47, employing a deletion mutant strain of the cyanobacterium Synechocystis sp. PCC 6803. Plant Mol. Biol. **17:** 1165–1177.

Engelken, J., Brinkmann, H., and Adamska, I. (2010). Taxonomic distribution and origins of the extended LHC (light-harvesting complex) antenna protein superfamily. BMC Evol. Biol. **10:** 233.

Ermakova-Gerdes, S., and Vermaas, W. (1999). Inactivation of the open reading frame slr0399 in Synechocystis sp. PCC 6803 functionally complements mutations near the Q(A) niche of photosystem II. A possible role of Slr0399 as a chaperone for quinone binding. J. Biol. Chem. **274:** 30540–30549.

Ferreira, K.N., Iverson, T.M., Maghlaoui, K., Barber, J., and Iwata, S. (2004). Architecture of the photosynthetic oxygen-evolving center. Science **303:** 1831–1838.

Funk, C., and Vermaas, W. (1999). A cyanobacterial gene family coding for single-helix proteins resembling part of the light-harvesting proteins from higher plants. Biochemistry **38:** 9397–9404.

Guikema, J.A., Freeman, L., and Fleming, E.H. (1986). Effects of gabaculine on pigment biosynthesis in normal and nutrient deficient cells of *Anacystis nidulans*. Plant Physiol. **82:** 280–284.

Guskov, A., Kern, J., Gabdulkhakov, A., Broser, M., Zouni, A., and Saenger, W. (2009). Cyanobacterial photosystem II at 2.9-A resolution and the role of quinones, lipids, channels and chloride. Nat. Struct. Mol. Biol. **16:** 334–342.

Hernandez-Prieto, M.A., Tibiletti, T., Abasova, L., Kirilovsky, D., Vass, I., and Funk, C. (2011). The small CAB-like proteins of the cyanobacterium *Synechocystis* sp. PCC 6803: their involvement in chlorophyll biogenesis for photosystem II. Biochim. Biophys. Acta **1807:** 1143–1151.

Janouškovec, J., Sobotka, R., Lai, D.H., Flegontov, P., Koník, P., Komenda, J., Ali, S., Prášil, O., Pain, A., Oborník, M., Lukeš, J., and Keeling, P.J. (2013). Split photosystem protein, linear-mapping topology, and growth of structural complexity in the plastid genome of *Chromera velia*. Mol. Biol. Evol. **30:** 2447–2462.

Jansson, S., Andersson, J., Kim, S.J., and Jackowski, G. (2000). An *Arabidopsis thaliana* protein homologous to cyanobacterial high-light-inducible proteins. Plant Mol. Biol. **42:** 345–351.

Kavanagh, K.L., Jörnvall, H., Persson, B., and Oppermann, U. (2008). Medium- and short-chain dehydrogenase/reductase gene and protein families: The SDR superfamily: functional and structural diversity within a family of metabolic and regulatory enzymes. Cell. Mol. Life Sci. **65:** 3895–3906.

Kim, J.M., Klein, P.G., and Mullet, J.E. (1991). Ribosomes pause at specific sites during synthesis of membrane-bound chloroplast reaction center protein D1. J. Biol. Chem. **266:** 14931–14938.

Kirilovsky, D., and Kerfeld, C.A. (2012). The orange carotenoid protein in photoprotection of photosystem II in cyanobacteria. Biochim. Biophys. Acta **1817:** 158–166.

Komenda, J. (2000). Role of two forms of the D1 protein in the recovery from photoinhibition of photosystem II in the cyanobacterium Synechococcus PCC 7942. Biochim. Biophys. Acta **1457:** 243–252.

Komenda, J., and Barber, J. (1995). Comparison of psbO and psbH deletion mutants of Synechocystis PCC 6803 indicates that degradation of D1 protein is regulated by the QB site and dependent on protein synthesis. Biochemistry **34:** 9625–9631.

Komenda, J., Knoppová, J., Kopečná, J., Sobotka, R., Halada, P., Yu, J.F., Nickelsen, J., Boehm, M., and Nixon, P.J. (2012b). The Psb27 assembly factor binds to the CP43 complex of photosystem II in the cyanobacterium *Synechocystis* sp. PCC 6803. Plant Physiol. **158:** 476–486.

Komenda, J., Nickelsen, J., Tichý, M., Prášil, O., Eichacker, L.A., and Nixon, P.J. (2008). The cyanobacterial homologue of HCF136/YCF48 is a component of an early photosystem II assembly complex and is important for both the efficient assembly and repair of photosystem II in Synechocystis sp. PCC 6803. J. Biol. Chem. **283:** 22390–22399.

Komenda, J., Reisinger, V., Müller, B.C., Dobáková, M., Granvogl, B., and Eichacker, L.A. (2004). Accumulation of the D2 protein is a key regulatory step for assembly of the photosystem II reaction center complex in Synechocystis PCC 6803. J. Biol. Chem. **279:** 48620–48629.

Komenda, J., Sobotka, R., and Nixon, P.J. (2012a). Assembling and maintaining the photosystem II complex in chloroplasts and cyanobacteria. Curr. Opin. Plant Biol. **15:** 245–251.

Komenda, J., Tichý, M., Prásil, O., Knoppová, J., Kuviková, S., de Vries, R., and Nixon, P.J. (2007). The exposed N-terminal tail of the D1 subunit is required for rapid D1 degradation during photosystem II repair in Synechocystis sp PCC 6803. Plant Cell **19:** 2839–2854.

Kopečná, J., Sobotka, R., and Komenda, J. (2013). Inhibition of chlorophyll biosynthesis at the protochlorophyllide reduction step results in the parallel depletion of Photosystem I and photosystem II in the cyanobacterium Synechocystis PCC 6803. Planta **237:** 497–508.

Kopečná, J., Komenda, J., Bučinská, L., and Sobotka, R. (2012). Long-term acclimation of the cyanobacterium *Synechocystis* sp. PCC 6803 to high light is accompanied by an enhanced production of chlorophyll that is preferentially channeled to trimeric photosystem I. Plant Physiol. **160:** 2239–2250.

Kufryk, G., Hernandez-Prieto, M.A., Kieselbach, T., Miranda, H., Vermaas, W., and Funk, C. (2008). Association of small CAB-like proteins (SCPs) of *Synechocystis* sp. PCC 6803 with photosystem II. Photosynth. Res. **95:** 135–145.

Link, S., Engelmann, K., Meierhoff, K., and Westhoff, P. (2012). The atypical short-chain dehydrogenases HCF173 and HCF244 are jointly involved in translational initiation of the psbA mRNA of Arabidopsis. Plant Physiol. **160:** 2202–2218.

Michoux, F., Takasaka, K., Boehm, M., Nixon, P.J., and Murray, J.W. (2010). Structure of CyanoP at 2.8Å: Implications for the evolution and function of the PsbP subunit of photosystem II. Biochemistry **49:** 7411–7413.

Mulo, P., Tyystjarvi, T., Tyystjarvi, E., Govindjee, Maenpaa, P., and Aro, E.M. (1997). Mutagenesis of the D-E loop of photosystem II reaction centre protein D1. Function and assembly of photosystem II. Plant Mol. Biol. **33:** 1059–1071.

Nagarajan, A., Winter, R., Eaton-Rye, J., and Burnap, R. (2011). A synthetic DNA and fusion PCR approach to the ectopic expression of high levels of the D1 protein of photosystem II in Synechocystis sp PCC 6803. J. Photochem. Photobiol. B Biol. **104:** 212–219.

Nanba, O., and Satoh, K. (1987). Isolation of a photosystem II reaction center consisting of D-1 and D-2 polypeptides and cytochrome b-559. Proc. Natl. Acad. Sci. USA **84:** 109–112.

Nickelsen, J., and Rengstl, B. (2013). Photosystem II assembly: From cyanobacteria to plants. Annu. Rev. Plant Biol. **64:** 609–635.

Nixon, P.J., Michoux, F., Yu, J.F., Boehm, M., and Komenda, J. (2010). Recent advances in understanding the assembly and repair of photosystem II. Ann. Bot. (Lond.) **106:** 1–16.

Promnares, K., Komenda, J., Bumba, L., Nebesářová, J., Vácha, F., and Tichý, M. (2006). Cyanobacterial small chlorophyll-binding protein ScpD (HliB) is located on the periphery of photosystem II in the vicinity of PsbH and CP47 subunits. J. Biol. Chem. **281:** 32705–32713.

Rappaport, F., and Diner, B.A. (2008). Primary photochemistry and energetics leading to the oxidation of the (Mn)4Ca cluster and to the evolution of molecular oxygen in photosystem II. Coord. Chem. Rev. **252:** 259–272.

Roose, J.L., Wegener, K.M., and Pakrasi, H.B. (2007). The extrinsic proteins of photosystem II. Photosynth. Res. **92:** 369–387.

Shen, G.Z., Boussiba, S., and Vermaas, W.F.J. (1993). Synechocystis sp PCC 6803 strains lacking photosystem I and phycobilisome function. Plant Cell **5:** 1853–1863.

Sinha, R.K., Komenda, J., Knoppová, J., Sedlářová, M., and Pospíšil, P. (2012). Small CAB-like proteins prevent formation of singlet oxygen in the damaged photosystem II complex of the cyanobacterium *Synechocystis* sp. PCC 6803. Plant Cell Environ. **35:** 806–818.

Sobotka, R., Komenda, J., Bumba, L., and Tichý, M. (2005). Photosystem II assembly in CP47 mutant of *Synechocystis* sp. PCC 6803 is dependent on the level of chlorophyll precursors regulated by ferrochelatase. J. Biol. Chem. **280:** 31595–31602.

Storm, P., Hernandez-Prieto, M.A., Eggink, L.L., Hoober, J.K., and Funk, C. (2008). The small CAB-like proteins of Synechocystis sp. PCC 6803 bind chlorophyll. In vitro pigment reconstitution studies on one-helix light-harvesting-like proteins. Photosynth. Res. **98:** 479–488.

Tomo, T., Akimoto, S., Tsuchiya, T., Fukuya, M., Tanaka, K., and Mimuro, M. (2008). Isolation and spectral characterization of photosystem II reaction center from Synechocystis sp. PCC 6803. Photosynth. Res. **98:** 293–302.

Umena, Y., Kawakami, K., Shen, J.R., and Kamiya, N. (2011). Crystal structure of oxygen-evolving photosystem II at a resolution of 1.9 Å. Nature **473:** 55–60.

Vavilin, D., and Vermaas, W. (2007). Continuous chlorophyll degradation accompanied by chlorophyllide and phytol reutilization for chlorophyll synthesis in *Synechocystis* sp. PCC 6803. Biochim. Biophys. Acta **1767:** 920–929.

Vavilin, D., Yao, D., and Vermaas, W. (2007). Small Cab-like proteins retard degradation of photosystem II-associated chlorophyll in Synechocystis sp. PCC 6803: Kinetic analysis of pigment labeling with 15N and 13C. J. Biol. Chem. **282:** 37660–37668.

Vermaas, W., Charite, J., and Eggers, B. (1990). System for site-directed mutagenesis in the *psb*DI/C operon of *Synechocystis* sp. PCC 6803. In Current Research in Photosynthesis. I. M. Baltscheffsky, ed (Dordrecht, The Netherlands: Kluwer Academic Publishers), pp. 231–238.

Wellburn, A.R. (1994). The spectral determination of chlorophyll a and chlorophyll b as well as carotenoids using various solvents with spectrophotometers of different resolution. J. Plant Physiol. **144:** 307–313.

Williams, J.G.K. (1988). Construction of specific mutations in PSII photosynthetic reaction center by genetic engineering methods in *Synechocystis* 6803. Methods Enzymol. **167:** 766–778.

Wilson, A., Ajlani, G., Verbavatz, J.M., Vass, I., Kerfeld, C.A., and Kirilovsky, D. (2006). A soluble carotenoid protein involved in phycobilisome-related energy dissipation in cyanobacteria. Plant Cell **18:** 992–1007.

Xu, H., Vavilin, D., Funk, C., and Vermaas, W. (2002). Small Cab-like proteins regulating tetrapyrrole biosynthesis in the cyanobacterium Synechocystis sp. PCC 6803. Plant Mol. Biol. **49:** 149–160.

Xu, H., Vavilin, D., Funk, C., and Vermaas, W. (2004). Multiple deletions of small Cab-like proteins in the cyanobacterium *Synechocystis* sp. PCC 6803: Consequences for pigment biosynthesis and accumulation. J. Biol. Chem. **279:** 27971–27979.

Yao, D., Kieselbach, T., Komenda, J., Promnares, K., Prieto, M.A. H., Tichý, M., Vermaas, W., and Funk, C. (2007). Localization of the small CAB-like proteins in photosystem II. J. Biol. Chem. **282:** 267–276.

Publication VIII

nature chemical biology

ARTICLE

PUBLISHED ONLINE: 23 FEBRUARY 2015 | DOI: 10.1038/NCHEMBIO.1755

Mechanism of photoprotection in the cyanobacterial ancestor of plant antenna proteins

Hristina Staleva[1], Josef Komenda[1,2], Mahendra K Shukla[1,2], Václav Šlouf[1], Radek Kaňa[1,2], Tomáš Polívka[1,3] & Roman Sobotka[1,2]*

Plants collect light for photosynthesis using light-harvesting complexes (LHCs)—an array of chlorophyll proteins that are able to reversibly switch from harvesting to energy-dissipation mode to prevent damage of the photosynthetic apparatus. LHC antennae as well as other members of the LHC superfamily evolved from cyanobacterial ancestors called high light–inducible proteins (Hlips). Here, we characterized a purified Hlip family member HliD isolated from the cyanobacterium *Synechocystis* sp. PCC 6803. We found that the HliD binds chlorophyll-*a* (Chl-*a*) and β-carotene and exhibits an energy-dissipative conformation. Using femtosecond spectroscopy, we demonstrated that the energy dissipation is achieved via direct energy transfer from a Chl-*a* Q_y state to the β-carotene S_1 state. We did not detect any cation of β-carotene that would accompany Chl-*a* quenching. These results provide proof of principle that this quenching mechanism operates in the LHC superfamily and also shed light on the photoprotective role of Hlips and the evolution of LHC antennae.

All photosynthetic organisms have to cope with unpredictable changes in light intensity as overexcitation of photosystems results in generation of reactive oxygen species. To prevent this, the LHCs of plants and algae have an inbuilt ability to switch from light harvesting to a quenching state in which energy is dissipated. Although researchers have proposed multiple molecular mechanisms that directly involve a carotenoid molecule to explain the principle of energy dissipation in LHCs, the mechanics behind this process remain unconfirmed. Scientists have suggested reductive quenching of the Chl-*a* excited state via electron transfer to carotenoid[1], energy transfer quenching through energy transfer from Chl-*a* to carotenoid[2] and quenching due to excitonic interaction between Chl-*a* and carotenoid[3] in plants. Researchers observed the reductive quenching *in vivo*, but for the individual LHCs, they observed a low yield of carotenoid radical formation only in minor LHCs and have not yet reported reductive quenching in major LHCII antenna[4,5]. Researchers have proposed that the quenching attributed to excitonic interaction operates both *in vivo* and in isolated LHCs[3], whereas they proposed that energy transfer quenching works mainly in isolated complexes[2,6] even though others have challenged the experimental evidence for this mechanism[7]. Thus, the quenching mechanism operating at the level of individual LHCs remains an open question.

Cyanobacteria harvest light predominantly using phycobilisomes, but they also have a family of Hlips that are considered ancestors of the whole LHC superfamily[8–10]. Hlips are small (~7 kDa), single-helix proteins that exhibit similarity to the first and third helix of plant LHC antenna and have a characteristic Chl-*a*–binding motif conserved in the whole LHC superfamily[8,10]. Genes encoding Hlips are common in cyanobacterial genomes and are strongly expressed under various stress conditions[11], but their exact role in the cell is mostly unknown. Hlips most likely have a photoprotective function[12] during various processes that deal with Chl-*a* molecules, including synthesizing Chl-binding proteins[13], recycling Chl-*a*[14] and assembling photosystem II[15]. We have shown recently in the cyanobacterium *Synechocystis* sp. PCC 6083 that two Hli proteins named HliD and HliC assist in synthesizing photosystem II's functional core. Particularly, we identified these Hlips as components of a larger protein complex designated RC*, which consists of the photosystem II assembly intermediate RCa and the Ycf39 protein belonging to short-chain dehydrogenase/reductase superfamily[16]. Notably, a subcomplex consisting of Ycf39 and Hlips as well as Hlips alone partially dissociated from RC* during native electrophoresis and migrated as pigmented bands[16]. Here, we purified the Ycf39–HliD subcomplex and demonstrated that HliD binds Chl-*a* with β-carotene and dissipates absorbed energy via direct energy transfer from the Chl-*a* Q_y state to the β-carotene S_1 state. These results provide proof of principle that the carotenoid-induced Chl-*a* quenching achieved via energy transfer can operate in LHC superfamily. Because we proved this quenching in a Hlip, the ancestor of the whole LHC superfamily, we hypothesize that the mechanism of LHC-based nonphotochemical quenching may be an ancient cyanobacterial invention redesigned later by algae and plants for the control of light harvesting.

RESULTS

HliD protein binds Chl-*a* and β-carotene pigments

To determine the composition of pigments attached to Hlips, we employed 3×Flag-tagged Ycf39 (f.Ycf39) and isolated an almost pure yellowish f.Ycf39–Hlip complex (**Fig. 1a** and **Supplementary Results**, **Supplementary Fig. 1a**). Although analysis of the eluate by MS revealed the presence of HliC (**Supplementary Table 1**), HliD was the only Hli protein detectable in the preparation by the two-dimensional gel (**Supplementary Fig. 1b**), and deletion of the *hliC* gene caused no apparent difference in size or pigmentation of the purified complex (**Supplementary Fig. 1c**). Because we have previously found no pigmentation of the isolated Hlip-free f.Ycf39 protein[16], we concluded that the HliD alone bound all pigments in the purified complex, which we termed the f.Ycf39–HliD complex.

Native electrophoresis demonstrated that f.Ycf39–HliD quenched chlorophyll fluorescence in a way that is comparable to the quenching in the trimeric photosystem I (**Supplementary Fig. 2**), and the

[1]Faculty of Science, University of South Bohemia, České Budějovice, Czech Republic. [2]Institute of Microbiology, Academy of Sciences of the Czech Republic, Třeboň, Czech Republic. [3]Biology Centre, Institute of Plant Molecular Biology, Academy of Sciences of the Czech Republic, České Budějovice, Czech Republic. *e-mail: sobotka@alga.cz

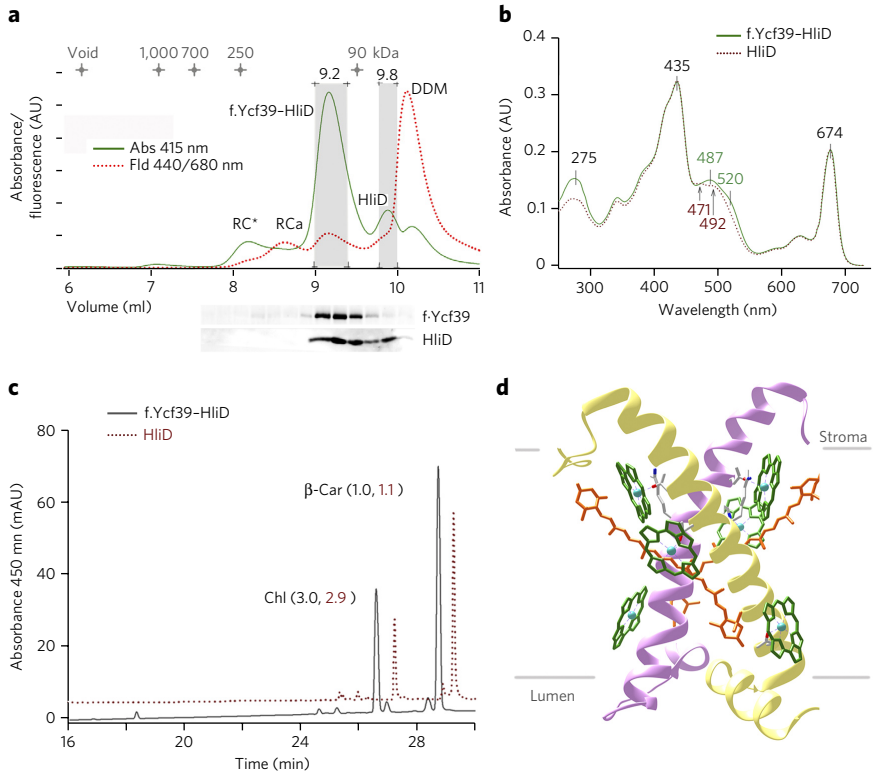

Figure 1 | Biochemical characterization of the f.Ycf39–HliD complex. (**a**) Gel filtration of the f.Ycf39–HliD pull-down assay. Pigments eluted from the column were detected by absorbance and by Chl-*a* fluorescence (Online Methods); collected fractions were subjected to immunoblot analysis. AU, arbitrary units; RC*, photosystem II reaction center associated with Ycf39–HliD. RCa, photosystem II reaction center; DDM, dodecyl-β-maltoside. (**b**) Absorption spectra of f.Ycf39–HliD and HliD as recorded by a diode-array detector. (**c**) HPLC analysis of pigments co-eluted with f.Ycf39–HliD and HliD and extracted from pooled fractions (indicated by gray columns in **a**). The calculated molar stoichiometry of Chl-*a* (Chl) and β-carotene (β-Car) is shown in parentheses. (**d**) A structural model of the putative HliD dimer with bound Chl-*a* and carotenoid pigments shown as a side view along the membrane plane. Model was prepared using the crystal structure of pea LHCII[18] and thus contains xanthophyll lutein instead of the β-carotene that should be present in the HliD structure. For clarity, only porphyrin rings of Chl-*a* molecules are shown.

strong chlorophyll quenching was evident also during purification of the complex by gel filtration (**Fig. 1a**). The quantum yield of f.Ycf39–HliD fluorescence was ~0.01 (**Supplementary Fig. 3**). We eluted the f.Ycf39–HliD complex from the column with a relative molecular weight of ~100 kDa (f.Ycf39 = 39 kDa), and it exhibited chlorophyll (435 nm and 674 nm) and carotenoid absorbance (487 nm and 520 nm; **Fig. 1b**). Moreover, we observed the less abundant pigmented complex that eluted later, which also quenched chlorophyll fluorescence but had a slightly blue-shifted carotenoid absorbance (**Fig. 1a**,**b**). We believe that this peak represented an HliD oligomer dissociated from f.Ycf39–HliD (**Fig. 1b**); we also saw this 'free' HliD on the two-dimensional gel (**Supplementary Fig. 1**). The analysis of pigments co-eluted with f.Ycf39–HliD and HliD peaks showed that both complexes contained Chl-*a* and β-carotene with the ratio 3:1 (**Fig. 1c**). On the basis of the sequence similarity between LHCII antennae and HliD protein, we expect that at least two copies of HliD are essential for pigment binding in a 3:1 stoichiometry. In LHCII, two of four Chl-*a* bound to the conserved ExxH/NxR motif are coordinated by glutamate-arginine ion pairs[17,18], and to achieve such a configuration, the HliD protein has to form an oligomer. Therefore, we proposed a hypothetical model for HliD: a dimer containing six Chl-*a* and two β-carotene molecules (**Fig. 1d**).

Chlorophyll-to-carotenoid energy transfer in HliD

To measure the Chl-*a* lifetime, we investigated the f.Ycf39–HliD complex by femtosecond transient absorption spectroscopy. We excited the complex at 620 nm to allow recording of absorption kinetics in the Q_y region (**Fig. 2**). The Chl-*a* signal exhibited multiexponential decay, and the magnitude of the initial bleaching decreased to less than 50% during the first 100 ps (**Fig. 2a**), confirming the efficient quenching of excited Chl-*a* observed in the native gel (**Supplementary Fig. 2**). To obtain information about excited-state dynamics, we fitted the whole spectro-temporal data set recorded in the 450–720-nm spectral window globally. To visualize the dynamics, we used a sequential model for the fitting, in which the initially excited state decays into other states with increasing lifetimes. The resulting spectra of individual states are depicted in **Figure 2b**. The first spectrum was clearly caused by Chl-*a* as it consisted of a sharp bleaching signal peaking at 675 nm because of the Q_y absorption band of Chl-*a* and the weak, featureless excited-state absorption extending from 450 nm to 650 nm. This Chl-*a* spectrum decayed in 2.1 ps to another state whose most interesting feature was the presence of a new band peaking at 580 nm, accompanied by a negative signal in the 450–520-nm region. Clearly, this signal was not associated with Chl-*a*; instead, such signals are typically observed when a carotenoid molecule is in its first excited state, S_1. The population of the carotenoid S_1 state is identified by its characteristic S_1-S_n excited-state absorption, which peaks in the 520–600-nm region[19]. Thus, the straightforward interpretation of the red spectrum in **Figure 2b** is that the 580-nm band is the S_1-S_n transition of β-carotene in the f.Ycf39–HliD complex. This assignment was further supported by the bleaching signal below 520 nm that matched the absorption profile of β-carotene in the complex. Appearance of the β-carotene signal monitored at the S_1-S_n maximum at 580 nm is shown in **Figure 2c**. The same kinetics were likewise obtained after direct excitation into the Q_y band at 670 nm (**Supplementary Fig. 4**). **Figure 2a** depicts decay of the Chl-*a* bleaching signal at 675 nm.

Associating the red spectrum in **Figure 2b** with the β-carotene S_1 state implies that we should obtain essentially the same S_1 spectrum if the carotenoid is excited directly. We thus measured transient absorption spectra after direct excitation of β-carotene at 490 and 530 nm (**Fig. 3a**). Whereas the S_1 spectrum of β-carotene excited at 490 nm differed from the spectrum obtained after Chl-*a* excitation, exciting β-carotene at 530 nm provided a reasonable match. Also, the bleaching regions of the spectra taken after 530- and 620-nm excitations were similar. Although the S_1 spectrum of β-carotene excited at 530 nm correlated with that obtained after Chl-*a* excitation (**Fig. 3a**), the lifetimes of the S_1 states were clearly different (**Fig. 3b**). The S_1 state of β-carotene populated via the Q_y-S_1 channel decayed predominantly with a 12-ps time constant, but direct excitation of β-carotene led to <10-ps S_1 lifetimes (**Fig. 3b**). To provide deeper insight into the excited-state dynamics of β-carotene, we carried out full analysis of the data recorded after direct excitation

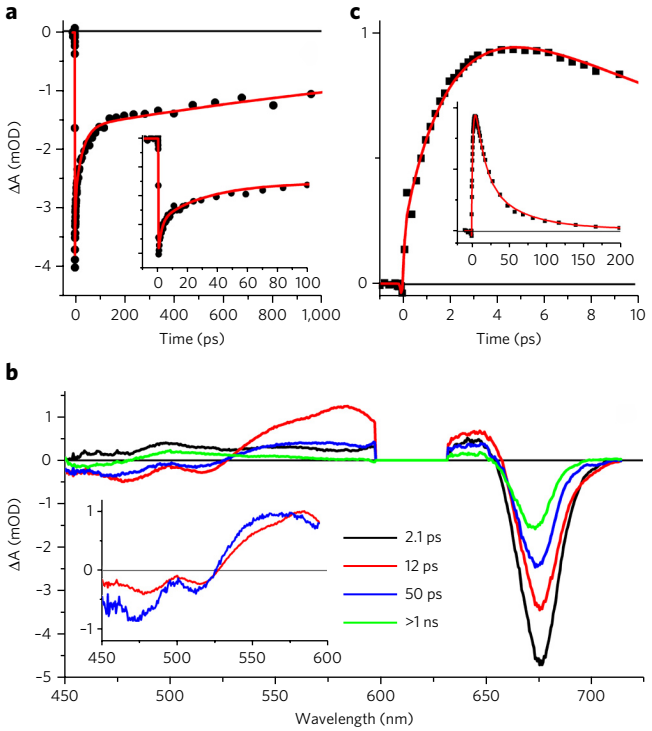

Figure 2 | Transient absorption spectroscopy of the f.Ycf39–HliD complex. (**a**–**c**) The sample was excited into the Chl-*a* vibrational band at 620 nm. (**a**) Decay of the Chl-*a* signal monitored at the maximum of ground state bleaching at 675 nm. Inset: the dynamics within the first 100 ps. (**b**) EAD spectra obtained from global fitting of the data. The initially excited state (black EADS) decays in 2.1 ps to form the red EADS that has features of the β-carotene spectrum. Inset: normalized EAD spectra corresponding to two decay component of the S_1 state. (**c**) Kinetics showing the rise of the carotenoid signal at 580 nm after excitation of Chl-*a*. Inset: the dynamics at a longer timescale, demonstrating the decay of the β-carotene excited state.

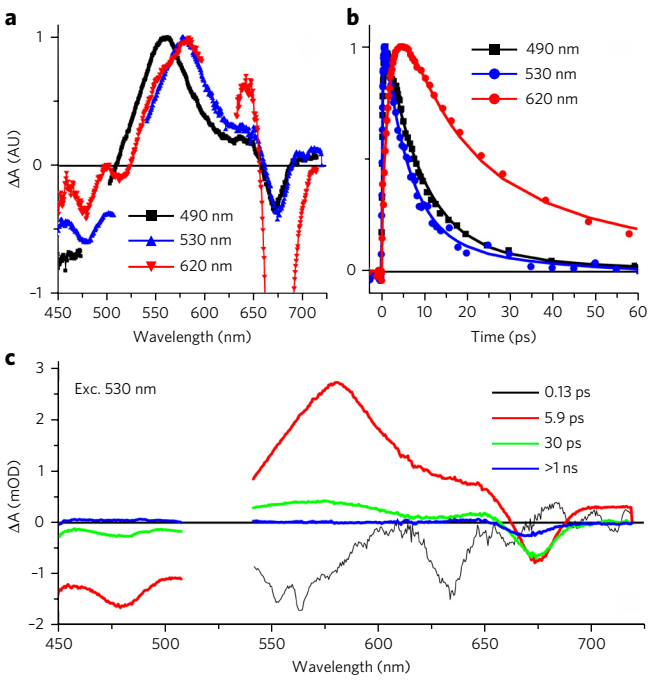

Figure 3 | Transient absorption data recorded after direct excitation of β-carotene. (**a**) Transient absorption spectra recorded at 3 ps either after direct excitation of β-carotene (490 and 530 nm) or after excitation of Chl-*a* (620 nm). The spectrum of β-carotene excited at 530 nm matches the spectrum of the β-carotene S_1 state populated from Chl-*a* excited at 620 nm. Spectra are normalized to the maximum of β-carotene excited-state absorption. (**b**) Kinetics monitoring the decay of β-carotene S_1 state after different excitation wavelengths. Decay of the β-carotene S_1 state populated via Chl-*a* (excitation at 620 nm) is substantially slower than that of the S_1 state populated by direct excitation of β-carotene at either 490 or 530 nm. (**c**) EAD spectra extracted from globally fitting the data recorded after direct excitation of β-carotene in the f.Ycf39–HliD complex at 530 nm (exc. 530 nm). The black EADS corresponds to the initially excited state (carotenoid S_2 state), and the red EADS has typical features of the S_1 state with the minor contribution of Chl-*a* bleaching caused by carotenoid-Chl energy transfer.

of β-carotene in the f.Ycf39–HliD complex at 530 nm (**Fig. 3c**) or at 490 nm (**Supplementary Fig. 5**). For both excitations, the first evolution-associated difference spectrum (EADS) corresponding to the excited S_2 state of β-carotene decayed within 130 fs. The S_1 lifetimes of β-carotene in the f.Ycf39–HliD complex are readily determined from the time constants associated with the red EADS, which have the typical shape associated with the S_1 spectrum. The S_1 lifetimes obtained after direct excitation of β-carotene, 8.7 ps (excitation at 490 nm) and 5.9 ps (excitation at 530 nm), were markedly shorter than the S_1 lifetimes of β-carotene populated via Chl-*a* (12 ps; **Fig. 3b**). The fitting results shown in **Figure 2b** revealed the presence of slower channels characterized by the time constants of 12 ps and 50 ps, which both occurred with substantial amplitude in the Chl-*a* bleaching region.

The presence of the 12-ps time constant in the Chl-*a* bleaching region may be due to the fact that fitting the multiexponential decay of Chl-*a* can easily pick a time constant associated with the carotenoid decay (12 ps). To clarify this, we fitted the carotenoid and Chl-*a* regions separately (**Supplementary Fig. 6**). Indeed, although the carotenoid region must be fitted with both 12- and 50-ps time constants, which monitor decays of two spectrally distinct S_1 states, in the Chl-*a* bleaching region these two components merged into one 30-ps time constant that precisely reproduced the slower phase of Chl-*a* decay. Thus, the slower channel is most likely associated with 30-ps energy transfer from Chl-*a*, populating the spectrally distinct carotenoid S_1 state, whose lifetime is 50 ps.

To test whether electron transfer between excited Chl-*a* and carotenoid, a process that has also been associated with quenching in photosynthetic systems[1], occurs in the HliD protein we recorded transient absorption spectra in the near-infrared region. The signal of a carotenoid cation would be expected to be in the 900–1,000-nm spectral range if such a mechanism were active in the HliD protein[20]. Because the spectra in the near-infrared region did not exhibit any hint of a carotenoid cation (**Supplementary Fig. 7**), we concluded that no electron transfer between carotenoid and Chl-*a* occurred in the f.Ycf39–HliD complex.

DISCUSSION

Population of the S_1 state of β-carotene after Chl-*a* excitation at 620 nm provided clear evidence for quenching of the Chl-*a* Q_y state via energy transfer to the S_1 state of β-carotene. A quenching mechanism based on direct energy transfer from a Chl-*a* Q_y state to a carotenoid S_1 state has previously been proposed to operate in LHCII from higher plants[2] and in the IsiA protein from cyanobacteria[21]. However, because of the suggested slow (>100 ps) Chl-*a*–to-carotenoid energy transfer, the carotenoid S_1 state could not be sufficiently populated. Consequently, signatures of the carotenoid S_1 state have not been apparent, and the validity of the model has been challenged[7]. Here, the appearance of the β-carotene

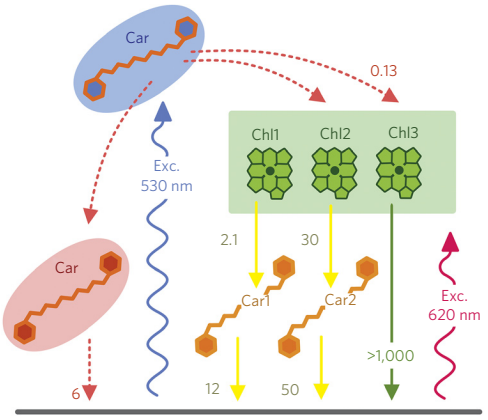

Figure 4 | Scheme of energy transfer pathways in HliD. Solid lines denote processes induced by the excitation of Chl-*a* at 620 nm (exc. 620 nm); dashed lines represent processes observed after excitation of the carotenoid S_2 state at 530 nm (exc. 530 nm; blue oval). Global fitting reveals two quenching channels (yellow arrows). Energy acceptors in these two quenching processes are two spectrally distinct carotenoid S_1 states (Car1 and Car2). A different S_1 state (red oval) is populated via internal conversion from the S_2 state (blue oval). Color coding of carotenoid states does not necessarily imply these states belong to different carotenoid pools. Time constants (in picoseconds) are associated with each pathway in diagram. Car, carotenoid.

signal after Chl-*a* excitation was evident. The kinetic trace recorded at 580 nm in the maximum of the S_1-S_n band of β-carotene (**Fig. 2c**) showed that the 2.1-ps rise, which monitors the arrival of excitations to the S_1 state of β-carotene after excitation of Chl-*a* in the f.Ycf39–HliD complex, accounted for about 80% of the signal. We excluded the possibility of reductive quenching by electron transfer from carotenoid to Chl-*a*[1] (**Supplementary Fig. 7**), and the slow, 2.1-ps rise of the S_1 signal after Chl-*a* excitation also ruled out any mechanism involving excitonic coupling between carotenoid and Chl-*a*[3].

Matching the S_1 spectrum of β-carotene excited at 530 nm to the carotenoid spectrum observed after Q_y excitation of Chl-*a* (**Fig. 3a**) led us to the conclusion that a red-shifted β-carotene in the f.Ycf39–HliD complex was responsible for the quenching associated with the 2.1-ps component. Different populations of β-carotene are consistent with the observed shift in β-carotene absorbance between the f.Ycf39–HliD complex and the dissociated HliD (**Fig. 1b**). In our structural model of HliD, two β-carotene molecules bind symmetrically to a dimer (**Fig. 1d**); however, the interaction with Ycf39 protein might influence the binding pocket of one β-carotene and consequently facilitate energy transfer via this carotenoid. It should be noted that the association with Ycf39 is not required for such quenching because the overall ability to quench Chl-*a* fluorescence was comparable for the Ycf39–HliD complex and 'free' HliD (**Fig. 2a** and **Supplementary Fig. 1a**).

Although there was a spectral similarity between the S_1 states populated directly from the carotenoid S_2 state and those populated via the Q_y pathway, the difference in lifetimes suggested that the situation is more complex. As direct excitation of β-carotene did not generate an S_1 state whose lifetime would be comparable to that of a quencher (12 ps), we suggest that excitations arriving from the Q_y state likely end in a minimum at the S_1 potential surface that is not accessible from the S_2 state. The key difference between the direct excitation of β-carotene and the Q_y quenching pathway lies in the fact that the former process generates the S_1 state via S_2-S_1 relaxation. The latter process occurs via energy transfer from Q_y to S_1; thus, β-carotene is initially in its ground state, implying that it is formally an S_0-S_1 transition. Because the S_1 potential surface of carotenoids is believed to be rather complicated, with multiple minima, it is not unrealistic that approaching the S_1 state 'from above' (S_2) or 'from below' (S_0) may result in different minima at the S_1 potential surface. Indeed, researchers have observed longer S_1 lifetimes of β-carotene in solution after populating the S_1 state directly from the ground state via two-photon excitation[22].

The global fitting of data recorded after direct excitation of carotenoid also revealed two interesting features. First, the fast 130-fs decay characterizing depopulation of the S_2 state was associated with appearance of Chl-*a* bleaching at 674 nm, indicating that some fraction of the S_2 population was transferred to Chl-*a*. Comparing the magnitudes of Chl-*a* bleaching and S_1-S_n excited state absorption (**Fig. 3c**) suggested that this energy transfer channel is only minor. The f.Ycf39–HliD complex is tuned to be an efficient quencher, and weak carotenoid-to-Chl-*a* energy transfer is likely an inevitable consequence of pigment arrangement within the f.Ycf39–HliD complex. Second, global fitting revealed the presence of a long decay component of 50 ps (excitation at 490 nm) and 30 ps (excitation at 530 nm). These components characterize the dominant Chl-*a* decay channel after carotenoid excitation, proving that Chl-*a*, populated via the minor energy transfer channel from β-carotene, is also efficiently quenched. Notably, the shape of the EADS associated with these components is reminiscent of the carotenoid S* state in the 450–600-nm region[23]. This indicates that the Chl-*a* molecules in the f.Ycf39–HliD complex that are populated via energy transfer from β-carotene are quenched through a slower channel correlating to either a population of the S* state or an S_1 state of some β-carotene, which was spectrally distinct from the main quencher. A scheme of energy transfer pathways is shown in **Figure 4**.

The inability to correlate the lifetimes of β-carotene S_1 state populated via S_2-S_1 internal conversion and via the Q_y-S_1 pathway indicated that the carotenoid S_1 potential surface is likely more complex than previously thought. Yet the data presented here unequivocally identified the energy transfer from the Q_y state of Chl-*a* to the S_1 state of a carotenoid as the mechanism of nonphotochemical quenching in the f.Ycf39–HliD complex. Pigments in the complex were clearly bound to HliD (**Fig. 1a**,**b**), which belongs to proteins assumed to be ancestors of the whole LHC superfamily[10]. Although LHC antenna proteins are the best-characterized members of the LHC superfamily, this large and diverse group also includes single-helix, double-helix and triple-helix proteins that certainly do not contribute to light harvesting but rather play a similar photoprotective role in eukaryotes like the Hlips in cyanobacteria[24].

As we clarified here, the function of Hlips relies on efficient dissipation of the Chl-*a* excited state energy via the carotenoid S_1 state. Given the highly conserved Chl-*a*–binding motif, it is feasible that the arrangement of Chl-*a* molecules and surrounding carotenoids shares a similar pattern in the whole LHC superfamily, though the carotenoid species (quencher) may vary in different proteins[18,25,26]. Researchers have already revealed such variation on a common theme by solving crystal structures of plant major and minor LHC antennae[26]. We therefore propose a hypothesis that the quenching mechanism described for HliD may be principally unchanged in LHC-like proteins as well as in LHC antennae[2]. The situation for intact thylakoid membranes is likely more complicated, and this type of quenching may work along with other quenching mechanisms[1,3]. However, if our hypothesis is correct, the evolution of LHC antennae had to include structural changes that allowed high flexibility between energy dissipation and harvesting[27]. The subfamily of LHC proteins specialized for light harvesting is thought to emerge at the basis of the green and red algal lineage, and apart from the plant-like antennae, it also involves fucoxanthin Chl-*a*/*c*-binding proteins[9,28]. Notably, the quenching in both LHC and fucoxanthin Chl-*a*/*c*–binding protein antennae is strongly enhanced by low pH[29,30], but we observed a rather negative effect for low pH on f.Ycf39–HliD quenching (**Supplementary Fig. 8**).

It is therefore possible that the eukaryotic invention of pH-activated quenching in an ancient, photoprotective LHC-like protein was a critical step for the evolution of LHC antennae. A gradual transition from fixed to flexible quenching is supported by the recent discovery of LHC stress-related (LHCSR) proteins in green algae and mosses[31]. LHCSRs exhibit constitutive, yet pH-sensitive, quenching and might represent a transition state between photoprotective LHC-like proteins and the LHC-based light-harvesting systems.

Received 17 September 2014; accepted 13 January 2015; published online 23 February 2015

METHODS

Methods and any associated references are available in the online version of the paper.

References

1. Holt, N.E. *et al.* Carotenoid cation formation and the regulation of photosynthetic light harvesting. *Science* **307**, 433–436 (2005).
2. Ruban, A.V. *et al.* Identification of a mechanism of photoprotective energy dissipation in higher plants. *Nature* **450**, 575–578 (2007).
3. Bode, S. *et al.* On the regulation of photosynthesis by excitonic interactions between carotenoids and chlorophylls. *Proc. Natl. Acad. Sci. USA* **106**, 12311–12316 (2009).
4. Avenson, T.J. *et al.* Zeaxanthin radical cation formation in minor light-harvesting complexes of higher plant antenna. *J. Biol. Chem.* **283**, 3550–3558 (2008).
5. Fuciman, M. *et al.* Role of xanthophylls in light harvesting in green plants: a spectroscopic investigation of mutant LHCII and Lhcb pigment-protein complexes. *J. Phys. Chem. B* **116**, 3834–3849 (2012).
6. Berera, R., van Stokkum, I.H.M., Kennis, J.T.M., van Grondelle, R. & Dekker, J.P. The light-harvesting function of carotenoids in the cyanobacterial stress-inducible IsiA complex. *Chem. Phys.* **373**, 65–70 (2010).
7. Müller, M.G. *et al.* Singlet energy dissipation in the photosystem II light-harvesting complex does not involve energy transfer to carotenoids. *ChemPhysChem* **11**, 1289–1296 (2010).
8. Dolganov, N.A.M., Bhaya, D. & Grossman, A.R. Cyanobacterial protein with similarity to the chlorophyll a/b binding proteins of higher plants: evolution and regulation. *Proc. Natl. Acad. Sci. USA* **92**, 636–640 (1995).
9. Neilson, J.A.D. & Durnford, D.G. Structural and functional diversification of the light-harvesting complexes in photosynthetic eukaryotes. *Photosynth. Res.* **106**, 57–71 (2010).
10. Engelken, J., Brinkmann, H. & Adamska, I. Taxonomic distribution and origins of the extended LHC (light-harvesting complex) antenna protein superfamily. *BMC Evol. Biol.* **10**, 233 (2010).
11. Bhaya, D., Dufresne, A., Vaulot, D. & Grossman, A. Analysis of the *hli* gene family in marine and freshwater cyanobacteria. *FEMS Microbiol. Lett.* **215**, 209–219 (2002).
12. He, Q., Dolganov, N., Bjorkman, O. & Grossman, A.R. The high light-inducible polypeptides in *Synechocystis* PCC6803. Expression and function in high light. *J. Biol. Chem.* **276**, 306–314 (2001).
13. Chidgey, J.W. *et al.* A cyanobacterial chlorophyll synthase-HliD complex associates with the Ycf39 protein and the YidC/Alb3 insertase. *Plant Cell* **26**, 1267–1279 (2014).
14. Vavilin, D., Yao, D. & Vermaas, W.F.J. Small cab-like proteins retard degradation of photosystem II-associated chlorophyll in *Synechocystis* sp PCC 6803—Kinetic analysis of pigment labeling with N-15 and C-13. *J. Biol. Chem.* **282**, 37660–37668 (2007).
15. Yao, D. *et al.* Localization of the small CAB-like proteins in photosystem II. *J. Biol. Chem.* **282**, 267–276 (2007).
16. Knoppová, J. *et al.* Discovery of a chlorophyll binding protein complex involved in the early steps of photosystem II assembly in *Synechocystis*. *Plant Cell* **26**, 1200–1212 (2014).
17. Liu, Z. *et al.* Crystal structure of spinach major light-harvesting complex at 2.72 Å resolution. *Nature* **428**, 287–292 (2004).
18. Standfuss, J., Terwisscha van Scheltinga, A.C., Lamborghini, M. & Kühlbrandt, W. Mechanisms of photoprotection and nonphotochemical quenching in pea light-harvesting complex at 2.5 Å resolution. *EMBO J.* **24**, 919–928 (2005).
19. Polívka, T. & Sundström, V. Ultrafast dynamics of carotenoid excited states—from solution to natural and artificial systems. *Chem. Rev.* **104**, 2021–2071 (2004).
20. Jeevarajan, J.A., Wei, C.C., Jeevarajan, A.S. & Kispert, L.D. Optical absorption spectra of dications of carotenoids. *J. Phys. Chem.* **100**, 5637–5641 (1996).
21. Berera, R. *et al.* A mechanism of energy dissipation in cyanobacteria. *Biophys. J.* **96**, 2261–2267 (2009).
22. Kosumi, D. *et al.* Ultrafast relaxation kinetics of the dark S-1 state in all-*trans*-β-carotene explored by one- and two-photon pump-probe spectroscopy. *Chem. Phys.* **373**, 33–37 (2010).
23. Gradinaru, C.C. *et al.* An unusual pathway of excitation energy deactivation in carotenoids: singlet-to-triplet conversion on an ultrafast timescale in a photosynthetic antenna. *Proc. Natl. Acad. Sci. USA* **98**, 2364–2369 (2001).
24. Tanaka, R. *et al.* LIL3, a light-harvesting-like protein, plays an essential role in chlorophyll and tocopherol biosynthesis. *Proc. Natl. Acad. Sci. USA* **107**, 16721–16725 (2010).
25. Adamska, I., Roobol-Boza, M., Lindahl, M. & Andersson, B. Isolation of pigment-binding early light-inducible proteins from pea. *Eur. J. Biochem.* **260**, 453–460 (1999).
26. Pan, X. *et al.* Structural insights into energy regulation of light-harvesting complex CP29 from spinach. *Nat. Struct. Mol. Biol.* **18**, 309–315 (2011).
27. Krüger, T.P., Wientjes, E., Croce, R. & van Grondelle, R. Conformational switching explains the intrinsic multifunctionality of plant light-harvesting complexes. *Proc. Natl. Acad. Sci. USA* **108**, 13516–13521 (2011).
28. Koziol, A.G. *et al.* Tracing the evolution of the light-harvesting antennae in chlorophyll a/b-containing organisms. *Plant Physiol.* **143**, 1802–1816 (2007).
29. Ruban, A.V., Young, A. & Horton, P. Modulation of chlorophyll fluorescence quenching in isolated light-harvesting complex of photosystem II. *Biochim. Biophys. Acta* **1186**, 123–127 (1994).
30. Kaňa, R., Kotabová, E., Sobotka, R. & Prášil, O. Non-photochemical quenching in cryptophyte alga *Rhodomonas salina* is located in chlorophyll a/c antennae. *PLoS ONE* **7**, e29700 (2012).
31. Bonente, G. *et al.* Analysis of LhcSR3, a protein essential for feedback de-excitation in the green alga *Chlamydomonas reinhardtii*. *PLoS Biol.* **9**, e1000577 (2011).

Acknowledgments

The authors thank M. Durchan and J. Tichý for their help with fluorescence measurements. J.K., T.P., V.Š. and R.S. were supported by the project P501/12/G055 from the Czech Science Foundation and by project Algatech. M.K.S. was supported by the project 14-13967S from the Czech Science Foundation and H.S. by the project CZ.1.07/2.3.00/30.0049.

Author contributions

M.K.S. purified the f.Ycf39–HliD complex under the supervision of R.S.; J.K., R.K. and R.S. performed biochemical analyses. H.S. and V.Š. performed ultrafast spectroscopic experiments and analyzed data under the supervision of T.P.; R.S., T.P. and J.K. designed the study and wrote the paper. The whole study was supervised by R.S. All authors discussed the results and commented on the manuscript.

Competing financial interests

The authors declare no competing financial interests.

Additional information

Supplementary information is available in the online version of the paper. Reprints and permissions information is available online at http://www.nature.com/reprints/index.html. Correspondence and requests for materials should be addressed to R.S.

ONLINE METHODS

Construction of *Synechocystis* strains. Construction of the *Synechocystis* f.*ycf39*/Δ*ycf39*/Δ*psbB* strain was described in a previous study[16]. An identical strain lacking HliC protein was obtained by the transformation of f.*ycf39*/Δ*ycf39*/Δ*psbB* strain by genomic DNA isolated from the *Synechocystis* Δ*hliC* mutant[32].

Purification of the f.Ycf39–HliD complex. For purification of the f.Ycf39–HliD complex, 20 L of the *Synechocystis* f.*ycf39*/Δ*ycf39*/Δ*psbB* cells or the f.*ycf39*/Δ*ycf39*/Δ*psbB*/Δ*hliC* cells were grown in 10-L flasks under 40 µmol of photons m^{-2} s^{-1} light at 28 °C in BG11 medium supplemented with 5 mM glucose. The cell culture was agitated with a magnetic stirrer and bubbled with air. Purification of the f.Ycf39–HliD complex was performed essentially as described[16] except the MES buffer containing divalent cations was replaced by a phosphate buffer (25 mM potassium phosphate, pH 7.5, 50 mM $NaCl_2$, 10% glycerol).

Two-dimensional clear-native/SDS-electrophoresis and immunoblot. For native electrophoresis, the f.Ycf39 eluate was concentrated fivefold on a 100-kDa cutoff micro-concentrator (Millipore) and separated on 4–12% clear-native gel[33]. Individual components of protein complexes were resolved by incubating the gel strip from the first dimension in 2% SDS and 1% dithiothreitol for 30 min at room temperature, and proteins were separated in the second dimension by SDS electrophoresis in a denaturing 12–20% polyacrylamide gel containing 7 M urea[34]. For immunoblotting, proteins were separated by SDS electrophoresis, transferred onto a PVDF membrane (Sigma-Aldrich, Germany) and incubated with specific primary antibodies as well as with secondary antibody conjugated with horseradish peroxidase (Sigma-Aldrich, Germany, catalog number A6154). Primary antibody against Ycf39 was raised in rabbits against synthetic peptides 4–14, and the antibody against the HliD was purchased from Agrisera (Sweden, catalog number AS10 1610).

Gel filtration and pigment analysis. The f.Ycf39–HliD eluate was immediately injected onto an Agilent-1200 HPLC machine and separated on Bio-sep 3000 column (Phenomenex) using 25 mM MES buffer, 10 mM $MgCl_2$, 10 mM $CaCl_2$, pH 6.5, containing 0.1% dodecyl-β-maltoside at a flow rate of 0.2 ml min^{-1} at 10 °C. Eluted proteins and complexes were detected by a diode-array detector and a fluorescence detector set to 440/680 nm (excitation/emission wavelengths). The column was calibrated using photosynthetic complexes with known size: trimeric photosystem I (~1 MDa), dimeric photosystem II (~700 kDa), monomeric photosystem II lacking oxygen-evolving complex (~250 kDa) and the purified His-tagged CP43 subcomplex (~90 kDa)[35]. To identify the pigments associated with f.Ycf39–HliD and HliD, fractions representing the 9.2-ml and 9.8-ml peaks were pooled and concentrated ~20 times on 30-kDa cutoff micro-concentrators (Millipore). This solution was extracted with 90% methanol and the extract analyzed by Agilent-1200 HPLC. Separation was carried out on a reverse phase column (Kinetex C8, 2.6 µm particle size, 3.9 × 150 mm; Phenomenex) with 35% methanol and 15% acetonitrile in 0.25M pyridine (solvent A) and 20% methanol, 20% acetone in acetonitrile as solvent B. Pigments were eluted with a linear gradient of solvent B (30–95% in 25 min) followed by 95% of solvent B at a flow rate of 0.8 ml min^{-1} at 40 °C. Pigment stoichiometries were estimated using extinction coefficients for Chl-*a* and β-carotene[36].

Fluorescence quantum yield. The fluorescence quantum yield was calculated according to the equation[37]

$$Q = Q_R \times \frac{I}{I_R} \times \frac{OD_R}{OD} \times \frac{n^2}{n_R^2}$$

where Q is the fluorescence quantum yield, I is the integrated fluorescence intensity, OD is the optical density and n the refractive index of the sample. The subscript R indicates a reference fluorophore with known quantum yield.

Femtosecond spectroscopy. The femtosecond spectrometer used for collecting transient absorption spectra is based on a laser system Integra-i (Quantronix). It consists of Er-fiber oscillator and Ti:Sapphire amplifier producing ~130-fs pulses at a repetition rate of 1 kHz. The central wavelength of the output pulses is 795 nm with 1.7 mJ per pulse. The amplified pulses were divided into two paths. The first one was directed to the optical parametric amplifier TOPAS (Light Conversion, Lithuania) to generate tunable excitation pulses. The second one was used to produce white light–continuum probe pulses by focusing a fraction of the amplifier output to a 3-mm sapphire plate. The white-light pulses, which were directed and focused only by reflective optics to prevent dispersion, were further divided into the probe beam that overlapped with the excitation beam at the sample and a reference beam that passed through the sample outside the excitation spot. The probe and the reference beams were brought to the slit of a spectrograph, where it was dispersed onto a dual CCD detector with 2,048 elements allowing measurements of transient spectra in a spectral window of ~240 nm. During all measurements, we kept the number of photons per pulse per cm^2 under 2×10^{14} to achieve reasonable signal-to-noise ratio while avoiding sample degradation and/or annihilation processes. In all measurements, the mutual polarization of the pump and probe beams was set to the magic angle (54.7°) by placing a polarization rotator in the pump beam. All measurements were carried out in a 2-mm quartz cuvette with a micro-stirrer to continuously mix the sample during measurements.

Global fitting. The spectro-temporal data sets obtained from the measurements were analyzed globally by fitting package DAFit (Pascher Instruments). The data were fitted to a sum of exponentials, including numerical deconvolution of the response function, and a fourth degree polynomial describing the chirp. The fitting procedure used general linear regression for the amplitudes of the exponentials and the Nelder-Mead simplex method for the rate constants, the FWHM and the chirp polynomial. To visualize the excited state dynamics, we assumed that the excited states evolved according to a sequential, irreversible scheme A → B, B → C, C → D. The arrows represent increasingly slower monoexponential processes, and the time constants of these processes correspond to lifetimes of the species A, B, C, D, etc. The spectral profiles of the species are called EAD spectra, and although in complex systems they do not directly correspond to the individual excited state species, they provide information about the time evolution of the whole system[38].

32. Xu, H., Vavilin, D., Funk, C. & Vermaas, W.F.J. Multiple deletions of small cab-like proteins in the cyanobacterium *Synechocystis* sp PCC 6803—Consequences for pigment biosynthesis and accumulation. *J. Biol. Chem.* **279**, 27971–27979 (2004).
33. Wittig, I., Karas, M. & Schägger, H. High resolution clear native electrophoresis for in-gel functional assays and fluorescence studies of membrane protein complexes. *Mol. Cell. Proteomics* **6**, 1215–1225 (2007).
34. Dobáková, M., Sobotka, R., Tichý, M. & Komenda, J. Psb28 protein is involved in the biogenesis of the photosystem II inner antenna CP47 (PsbB) in the cyanobacterium *Synechocystis* sp PCC 6803. *Plant Physiol.* **149**, 1076–1086 (2009).
35. Boehm, M. *et al.* Investigating the early stages of Photosystem II assembly in *Synechocystis* sp PCC 6803. Isolation of CP47 and CP43 complexes. *J. Biol. Chem.* **286**, 14812–14819 (2011).
36. Eijckelhoff, C. & Dekker, J.P. A routine method to determine the chlorophyll alpha, pheophytin-α and β-carotene contents of isolated Photosystem II reaction center complexes. *Photosynth. Res.* **52**, 69–73 (1997).
37. Lakowicz, J.R. *Principles of Fluorescence Spectroscopy* 1st edn. (Kluwer Academic, 1999).
38. van Stokkum, I.H., Larsen, D.S. & van Grondelle, R. Global and target analysis of time-resolved spectra. *Biochim. Biophys. Acta* **1657**, 82–104 (2004).

doi:10.1038/nchembio.1755

Publication IX

frontiers in Plant Science

ORIGINAL RESEARCH
published: 17 March 2016
doi: 10.3389/fpls.2016.00292

Synthesis of Chlorophyll-Binding Proteins in a Fully Segregated Δ*ycf54* Strain of the Cyanobacterium *Synechocystis* PCC 6803

*Sarah Hollingshead[1,2], Jana Kopečná[3], David R. Armstrong[1], Lenka Bučinská[3,4], Philip J. Jackson[1,5], Guangyu E. Chen[1], Mark J. Dickman[5], Michael P. Williamson[1], Roman Sobotka[3,4] and C. Neil Hunter[1]**

[1] Department of Molecular Biology and Biotechnology, University of Sheffield, Sheffield, UK, [2] Sir William Dunn School of Pathology, University of Oxford, Oxford, UK, [3] Institute of Microbiology, Centre Algatech, Academy of Sciences of the Czech Republic, Třeboň, Czech Republic, [4] Faculty of Science, University of South Bohemia, České Budějovice, Czech Republic, [5] ChELSI Institute, Department of Chemical and Biological Engineering, University of Sheffield, Sheffield, UK

OPEN ACCESS

Edited by:
John Love,
University of Exeter, UK

Reviewed by:
Peter Jahns,
University of Düsseldorf, Germany
Caiji Gao,
The Chinese University of Hong Kong, China

***Correspondence:**
C. Neil Hunter
c.n.hunter@sheffield.ac.uk

Specialty section:
This article was submitted to Plant Cell Biology, a section of the journal Frontiers in Plant Science

Received: *09 November 2015*
Accepted: *23 February 2016*
Published: *17 March 2016*

Citation:
Hollingshead S, Kopečná J, Armstrong DR, Bučinská L, Jackson PJ, Chen GE, Dickman MJ, Williamson MP, Sobotka R and Hunter CN (2016) Synthesis of Chlorophyll-Binding Proteins in a Fully Segregated Δycf54 Strain of the Cyanobacterium Synechocystis PCC 6803. Front. Plant Sci. 7:292. doi: 10.3389/fpls.2016.00292

In the chlorophyll (Chl) biosynthesis pathway the formation of protochlorophyllide is catalyzed by Mg-protoporphyrin IX methyl ester (MgPME) cyclase. The Ycf54 protein was recently shown to form a complex with another component of the oxidative cyclase, Sll1214 (CycI), and partial inactivation of the *ycf54* gene leads to Chl deficiency in cyanobacteria and plants. The exact function of the Ycf54 is not known, however, and further progress depends on construction and characterization of a mutant cyanobacterial strain with a fully inactivated *ycf54* gene. Here, we report the complete deletion of the *ycf54* gene in the cyanobacterium *Synechocystis* 6803; the resulting Δ*ycf54* strain accumulates huge concentrations of the cyclase substrate MgPME together with another pigment, which we identified using nuclear magnetic resonance as 3-formyl MgPME. The detection of a small amount (∼13%) of Chl in the Δ*ycf54* mutant provides clear evidence that the Ycf54 protein is important, but not essential, for activity of the oxidative cyclase. The greatly reduced formation of protochlorophyllide in the Δ*ycf54* strain provided an opportunity to use ^{35}S protein labeling combined with 2D electrophoresis to examine the synthesis of all known Chl-binding protein complexes under drastically restricted *de novo* Chl biosynthesis. We show that although the Δ*ycf54* strain synthesizes very limited amounts of photosystem I and the CP47 and CP43 subunits of photosystem II (PSII), the synthesis of PSII D1 and D2 subunits and their assembly into the reaction centre (RCII) assembly intermediate were not affected. Furthermore, the levels of other Chl complexes such as cytochrome b_6f and the HliD–Chl synthase remained comparable to wild-type. These data demonstrate that the requirement for *de novo* Chl molecules differs completely for each Chl-binding protein. Chl traffic and recycling in the cyanobacterial cell as well as the function of Ycf54 are discussed.

Keywords: Ycf54, *Synechocystis* 6803, chlorophyll, photosystem II, protochlorophyllide, Mg-protoporphyrin IX methylester cyclase

INTRODUCTION

Chlorophylls (Chl) and Chl binding proteins are essential components of the photosynthetic apparatus. Together they act as principal light harvesting and energy transforming cofactors in photosynthetic organisms, as demonstrated by the structures of both photosystem I (PSI) and photosystem II (PSII; Jordan et al., 2001; Zouni et al., 2001; Umena et al., 2011). It is likely that at least for large Chl-binding subunits of PSI (PsaA, PsaB) and PSII (CP43, CP47) Chl molecules must be inserted into these proteins co-translationally as a prerequisite for correct protein folding (Chua et al., 1976; Eichacker et al., 1996; Müller and Eichacker, 1999; Chidgey et al., 2014). As demonstrated recently using a cyanobacterial Δ*chlL* mutant, which is unable to synthesize Chl in the dark, the availability of *de novo* Chl molecules is ultimately essential for synthesis of all central subunits of both photosystems (Kopečná et al., 2013). Nonetheless, there are unexplained aspects of the assembly of PSII subunits, such as the particular sensitivity of the CP47 subunit to the lack of *de novo* Chl (Dobáková et al., 2009; Kopečná et al., 2015).

The Chls are a group of modified tetrapyrrole molecules distinguished by their fifth isocyclic or E ring, the geranylgeranyl/phytol moiety esterified at C17 and a centrally chelated magnesium ion. The isocyclic ring arises from the cyclisation of the methyl-propionate side-chain at C-13 to the C-15 bridge carbon between rings C and D. In oxygenic phototrophs this biosynthetic reaction is catalyzed by the oxidative Mg-protoporphyrin IX monomethyl ester cyclase (MgPME-cyclase), which incorporates atmospheric oxygen into the $C13^1$ carbonyl group (Porra et al., 1996). Although studied in some detail, the enzyme responsible for the aerobic cyclisation reaction remains the least understood in the Chl biosynthesis pathway. The first gene identified as encoding an oxidative cyclase component was the *Rubrivivax gelatinosus acsF* (aerobic cyclisation system iron containing protein) locus (Pinta et al., 2002). Subsequently, AcsF homologs have been identified in all studied oxygenic photosynthetic organisms (Boldareva-Nuianzina et al., 2013).

The Ycf54 protein (12.1 kDa) has been shown recently to interact with the AcsF homolog Sll1214 (hereafter CycI; Peter et al., 2009) in the cyanobacterium *Synechocystis* PCC 6803 (hereafter *Synechocystis*; Hollingshead et al., 2012). Demonstrations that partial elimination of Ycf54 strongly impairs the formation of PChlide and causes Chl deficiency in both cyanobacteria and plants (Albus et al., 2012; Hollingshead et al., 2012) led to speculations that this protein is a catalytic subunit of the MgPME cyclase (Bollivar et al., 2014). Here, we clarify this issue by achieving the complete deletion of the *ycf54* gene in *Synechocystis*. Although the Chl content in this strain was very low, the MgPME-cyclase was apparently active, which demonstrated that the Ycf54 protein is not an essential subunit of the MgPME cyclase. On the other hand, the mutant contained a very low level of CycI and lacked a high-mass complex associated with the light-dependent PChlide oxidoreductase enzyme (POR). The greatly limited formation of PChlide in the *ycf54* mutant provided an opportunity to assess the sensitivity of assembly pathways for all known Chl-proteins in cyanobacteria to the availability of *de novo* Chl. Interestingly, the deletion of the *ycf54* gene almost abolished the synthesis of PsaA/B subunits and PSII antennas CP47 and CP43, whereas the accumulation of other Chl-proteins showed little or no defects.

EXPERIMENTAL PROCEDURES

Growth Conditions

Synechocystis strains were grown photomixotrophically in a rotary shaker under low light conditions (5 μmol photons m^{-2} s^{-1}) at 30°C in liquid BG11 medium (Rippka et al., 1979) supplemented with 10 mM TES-KOH (pH 8.2) and 5 mM glucose.

Construction of the Δ*ycf54 Synechocystis* Strain

In order to disrupt open reading frame *slr1780* (*ycf54*), we prepared a construct for replacing the most this gene (bp 64–276) by a Zeocin resistance cassette. The sequences up- and down-stream (∼300 bp) of the *ycf54* gene were amplified with the relevant primers and fusion PCR in conjunction with megaprimers (Ke and Madison, 1997) were used to anneal these either side of the Zeocin resistance cassette. The resulting PCR product was transformed into the GT-W *Synechocystis* substrain (Bečková et al., submitted) and transformants were selected on a BG11 agar plate containing 2 μg ml^{-1} Zeocin. Complete segregation was achieved by sequentially doubling the concentration of antibiotic to a final concentration of 32 μg ml^{-1} Zeocin.

Cell Absorption Spectra and Determination of Chl Content

Absorption spectra of whole cells were measured at room temperature using a Shimadzu UV-3000 spectrophotometer (Kyoto, Japan). To determine Chl levels, pigments were extracted from cell pellets (2 ml, OD_{750} = ∼0.5) with 100% methanol and the Chl concentration was determined spectroscopically (Porra et al., 1989).

Analysis of Pigments by HPLC

Pigments were extracted from equal quantities of cells by the method described in Canniffe et al. (2013) and separated on a Phenomenex Aqua C_{18} reverse phase column (5 μM particle size, 125 Å pore size, 250 mm × 4.6 mm) at a flow rate of 1 ml min^{-1}. 3-formyl-MgPME was purified on a Fortis Universil C_{18} reverse phase column (5 μM particle size, 125 Å pore size, 150 mm × 10 mm) at a flow rate of 3.5 ml min^{-1}. Reverse phase columns were run using a method modified from Sobotka et al. (2011). Solvents A and B were 350 mM ammonium acetate pH 6.9/30% methanol (v/v) and 100% methanol, respectively. Pigments were

eluted over a linear gradient of 65 to 75% buffer A over 35 min.

Purification of 3-Formyl-MgPME for NMR Analysis

Pigments were extracted by phase partitioning from 6 L of Δ*ycf54* culture grown to an $OD_{750\,nm}$ 1.2. One volume of diethyl ether was added to two volumes of cell culture in a separation funnel and the diethyl ether phase containing 3-formyl-MgPME was separated from the cell culture. Pigments were extracted from the cell culture three times. The diethyl ether was removed by rotary evaporation and the extracted pigments were re-suspended in a small volume of HPLC grade methanol. After centrifugation at 15,000 × *g* for 10 min, 3-formyl-MgPME was purified by preparative HPLC. Ammonium acetate was removed from the HPLC purified 3-formyl-MgPME by solid-phase extraction on DSC-18 reverse-phase columns (Supelco). Solvents C, D, and E were QH_2O, 50% methanol (v/v) and 100% methanol, respectively. After equilibration of the column with 1.0 ml solvent D, the purified 3-formyl-MgPME, diluted 1/3 with QH_2O, was loaded and allowed to enter the column by gravity flow. The column was washed with 1 ml solvent C, then 1 ml solvent D to remove the ammonium acetate. The pigment was eluted into a glass vial with 300 μl methanol. The purified pigment was completely dried in a vacuum centrifuge and stored at –20°C.

NMR Assignment of 3-Formyl-MgPME

The dried pigment from HPLC was re-suspended in 500 μl methanol-d4 (Sigma), centrifuged to remove any insoluble pigment, transferred to a 5 mm NMR tube and sealed. All NMR experiments were carried out on a Bruker Avance DRX 600 instrument equipped with a cryoprobe at an acquisition temperature of 298 K.

The one-dimensional selective Nuclear Overhauser Enhancement (NOE) experiments were recorded using a double pulsed field gradient spin echo selective NOE experiment (Stott et al., 1995) using an 80 ms 180° Gaussian pulse for the selective excitation and a 1 s mixing time, acquiring 1024 transients at each saturation frequency. The Total Correlation Spectroscopy (TOCSY) experiment was recorded using a 45 ms spin lock at a power of 8.3 kHz. Two carbon Heteronuclear Single Quantum Correlation (HSQC) experiments were recorded with carbon offsets of 60 and 140 ppm.

2D Electrophoresis, Immunodetection, and Protein Radiolabeling

Membrane and soluble protein fractions were isolated from 50 ml of cells at $OD_{750\,nm}$ ~0.4 according to Dobáková et al. (2009) using buffer A (25 mM MES/NaOH, pH 6.5, 5 mM $CaCl_2$, 10 mM $MgCl_2$, 20% glycerol). Isolated membrane complexes (0.25 mg/ml Chl) were solubilized in buffer A containing 1% *n*-dodecyl-β-D-maltoside.

To assess protein levels by immunodetection, the protein content of *Synechocystis* lysates was quantified spectroscopically (Kalb and Bernlohr, 1977), separated by SDS-PAGE (Novagen) and transferred to a nitrocellulose membrane. The membranes were probed with specific primary antibodies and then with secondary antibodies conjugated to horseradish peroxidise (Sigma). The primary antibodies used in this study were raised in rabbits as described in Hollingshead et al. (2012), with the exception of CHL27 (anti-CycI), which was purchased from Agrisera (Sweden).

Two-dimensional clear-native electrophoresis was performed essentially as described in Kopečná et al. (2013). Proteins separated in the gel were stained either by Coomassie Blue, or Sypro Orange, followed by transfer onto a PVDF membrane. Membranes were incubated with specific primary antibodies, and then with a secondary antibody conjugated with horseradish peroxidase (Sigma).

Radioactive pulse labeling of the proteins in cells was performed using a mixture of [^{35}S]Met and [^{35}S]Cys (Translabel; MP Biochemicals). After 30 min incubation of cells with labeled amino-acids, the solubilized membranes isolated from radiolabelled cells were separated by 2D-electrophoresis. The stained 2D gel was finally exposed to a phosphor-imager plate, which was scanned by Storm (GE Healthcare) to visualize labeled protein spots.

Relative Quantification of FLAG-CycI and Captured Proteins in Pulldown Assays

Pulldown assays using N-terminal FLAG-tagged CycI as bait, with both wild-type (WT) and Δ*ycf54* backgrounds, were carried out according to Hollingshead et al. (2012). FLAG eluates were concentrated to 100 μl using Amicon Ultra 0.5 ml 3 kDa MWCO ultrafiltration devices (Millipore). The proteins were then precipitated, reduced and *S*-alkylated according to Zhang et al. (2015). Proteolytic digestion was carried out with 1:25 w/w (enzyme:substrate) pre-mixed trypsin/Lys-C (1 μg/μL, Promega, mass spectrometry grade) at 37°C for 2 h. The samples were then diluted with 75 μl 100 mM Tris-HCl, pH 8.5, 10 mM $CaCl_2$ and the digestion allowed to proceed for a further 18 h at 37°C. After the addition of 5μl 10% TFA, the samples were desalted using C_{18} spin columns (Thermo Fisher) and analyzed by nano-flow liquid chromatography (Ultimate 3000 RSLCnano system, Dionex) coupled to a mass spectrometer (Maxis UHR-TOF, Bruker or Q Exactive HF Orbitrap, Thermo Scientific). For Maxis data, mass spectra were internally calibrated with the lock-mass ion at m/z 1221.9906 then converted to MGF format using a script provided by Bruker. Q Exactive data-files were converted to MGFs using MSConvert[1]. Protein identification was carried out by searching against the *Synechocystis* PCC 6803 proteome database (release date 02-08-2015, 3507 entries[2] using Mascot Daemon v. 2.5.1 running with Mascot Server v. 2.5 (Matrix Science), specifying trypsin as the enzyme in the search parameters and allowing for one missed cleavage. *S*-carbamidomethyl-cysteine and methionine oxidation were selected as fixed and variable modifications, respectively. MS and MS/MS tolerances were set to 0.01 Da and false discovery rates determined by searching of a decoy database composed of reversed protein sequences. The data-files and search results have

[1] www.proteowizard.sourceforge.net

[2] www.uniprot.org/proteomes/UP000001425

been uploaded to the ProteomeXchange Consortium[3] via the PRIDE partner repository (identifier DOI 10.6019/PXD003149).

Electron Microscopy

Wild-type and Δ*ycf54* cells were harvested in the log phase by centrifugation. Cell pellets were loaded into 200 μm deep specimen carriers (Leica Microsystems), pre-treated with 1% lecithin in chloroform and cryo-immobilized by high-pressure freezing using EM PACT2 (Leica Microsystems). Freeze-substitution was carried out as described by van de Meene et al. (2006) using an automatic freeze substitution unit (EM ASF, Leica). Samples were then infiltrated with graded series (1:2, 1:1, 2:1) of Spurr-acetone mixture (6–8 h for each), twice with 100% Spurr's resin (SPI Supplies) and finally embedded in fresh resin. The polymerization was performed at 60°C for 48 h. Ultra-thin 70 nm sections were cut on ultramicrotome (UCT, Leica), collected on formvar-coated copper grids and stained with uranyl acetate (5 min) and lead citrate (3 min). Grids were viewed with a JEOL 1010 transmission electron microscope operating at 80 kV equipped with a Mega View III camera (SIS GmbH).

RESULTS

Ycf54 Is Not Essential for Activity of MgPME Cyclase

In our previous report (Hollingshead et al., 2012) we described a *ycf54*$^{-}$ *Synechocystis* strain harboring an insertion of the Erythromycin resistance cassette in the *ycf54* gene. Although prolonged attempts to fully segregate the mutant allele into all copies of the chromosome were unsuccessful, the phenotype of the partially segregated strain was informative nevertheless, and it exhibited an obvious defect in PChlide formation. However, the capability of *Synechocystis* cells to tolerate deletions of important genes also depends on the 'WT' substrain used. For instance, a previous attempt to inactivate *gun4*, another gene crucial for Chl biosynthesis, was achieved in the non-motile *Synechocystis* GT-P substrain but it failed in the motile PCC-M (compare Wilde et al., 2004; Sobotka et al., 2008). Thus, in order to obtain a fully segregated *ycf54* mutant, we prepared a new construct for replacement of the *ycf54* gene and transformed GT-P, GT-S, GT-W and PCC-M substrains; the GT-P substrain has been used in our previous work (Hollingshead et al., 2012). Interestingly, the *ycf54* deletion readily segregated in the GT-W substrain (**Figure 1A**) under low light (5 μmol photons.m^{-2}.s^{-1}) and photomixotrophic conditions; all attempts to segregate the *ycf54* deletion in other substrains failed (not shown). For the purposes of the work reported here the GT-W substrain is designated as the WT; a detailed analysis of GT-P and GT-W including genome sequencing is presented elsewhere in this issue (Bečková et al., submitted).

The fully segregated Δ*ycf54* strain did not grow photoautotrophically, although supplementation of the growth medium with glucose made photomixotrophic growth possible at light intensities up to 100 μmol photons.m^{-2}.s^{-1}. Examination of the absorption spectra from cells normalized for optical density at 750 nm (OD_{750}), shows that the Chl absorbance maxima at 439 and 679 nm and the carotenoid absorbance maximum at 494 nm are severely depleted in Δ*ycf54*, whilst the absorbance maximum of the phycobiliproteins at 624 nm remains unchanged when compared to the WT (**Figure 1B**). Mutant cells contained only about 13% of WT Chl (**Figure 1B**) and the whole cell spectrum showed a large absorbance peak at 422 nm, indicating a substantial accumulation of MgPME (**Figure 1B**) (Hollingshead et al., 2012).

Identification of the Chl Precursors that Accumulate in the Δ*ycf54* Mutant

Previously we reported that Chl biosynthesis in a partially segregated *ycf54*$^{-}$ mutant was blocked at the MgPME cyclase step, which causes accumulation of high levels of MgPME, the substrate of the cyclase, and lesser levels of an unknown pigment with a Soret peak at 433 nm (Hollingshead et al., 2012). To examine the photosynthetic precursor pigments present in Δ*ycf54*, methanol extracts from low light grown cells were separated by HPLC (**Figure 2A**). As with *ycf54*$^{-}$, Δ*ycf54* synthesized high levels of MgPME and lesser levels of the unknown pigment. Given that the Soret band of this pigment is situated between the Soret peaks of MgPME at 416 nm and PChlide at 440 nm (**Figure 2B**) we proposed that it could be an intermediate of the cyclase reaction.

Nuclear magnetic resonance spectroscopy was used to determine the identity and structure of this unknown pigment, which was extracted by diethyl ether/water phase partitioning from the medium of Δ*ycf54* cells grown under very low light conditions. This pigment was purified to homogeneity by preparative HPLC. The one-dimensional ^{1}H spectrum (**Figure 3A**) shows the reasonable degree of purity of the pigment, with impurities indicated by an asterisk; the signals downfield of 5 ppm represent minor contaminants and methanol, whilst the impurity signals upfield of 5 ppm represent solvents, including water. Signals from the unknown pigment were assigned using a combination of ^{1}H TOCSY, gradient-selected 1D NOE, and natural abundance ^{13}C HSQC spectra.

NOE experiments were carried out with selective saturation of all proton peaks downfield from 3 ppm in order to identify protons with through-space correlation (**Figure 3A**). To cover the full range of ^{13}C shifts, two ^{13}C HSQC spectra were run with ^{13}C offsets of 60 ppm and 140 ppm. Many of the signals have ^{1}H and ^{13}C chemical shifts similar in frequency to those from MgPME (**Figure 3B**), with the expected TOCSY and NOE connectivities, and can therefore be assigned straightforwardly. The ^{13}C HSQC spectra (**Figure 3C**) confirmed the assignments of the four meso protons and the five methyl groups (with the four imidazole methyls having ^{13}C shifts of around 10 ppm and the propionate methyl having a shift of 50 ppm). The signals from the 3-vinyl protons were absent, but there is a new signal with ^{1}H and ^{13}C shifts of 11.6 and 190 ppm, respectively, which can only come from an aldehyde. This

[3]http://proteomecentral.proteomexchange.org

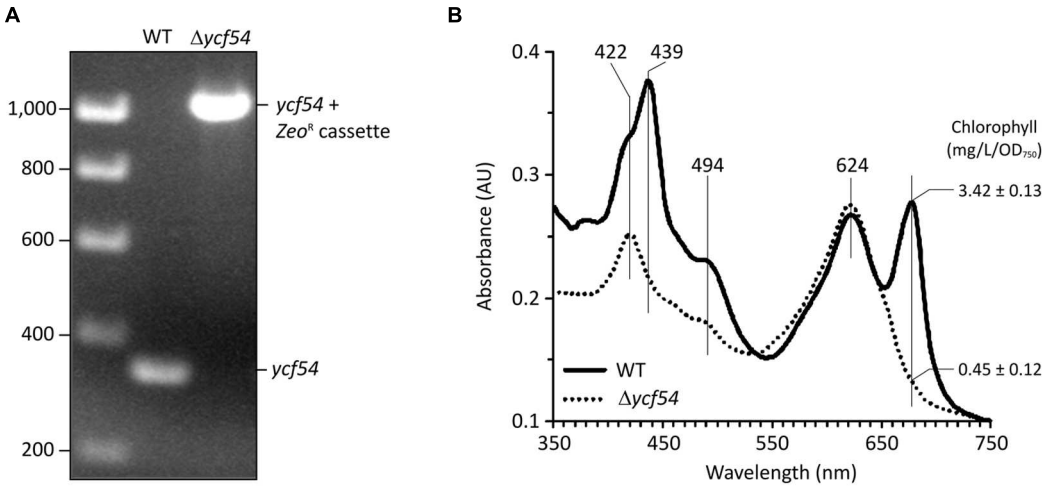

FIGURE 1 | Deletion of the *ycf54* gene in *Synechocystis* and the whole-cell spectra the resulting Δ*ycf54* strain. (A) PCR amplification of the *slr1780* (*ycf54*) region to confirm full segregation of the Zeocin resistance cassette. WT, wild-type. **(B)** Whole cell absorbance spectra of *Synechocystis* whole cells grown photomixotrophically under low light conditions. Chl *a* is represented by the 682-nm peak, and phycobiliproteins are represented by the 625-nm peak. Spectra were measured with cells at a similar optical density ($OD_{750\ nm}$ = ∼0.3) and normalized to light scattering at 750 nm.

signal has NOEs to both the 5-meso and 2-methyl protons, both of which were shifted downfield, and no through-bond connectivity in the TOCSY, verifying that this was a 3-formyl group which had replaced the 3-vinyl group of the MgPME. The NMR data are compiled, together with details of the acquisition parameters, in Supplementary Table 1, including Supplementary Figures S1–S3. Further confirmation that this signal represents a 3-formyl group comes from the ^{1}H-NMR spectra of Chl *d* (Fukusumi et al., 2012), which has a clear signal at ∼11.5 assigned as the 3-formyl group. Thus, the unknown pigment is magnesium 3-formyl-protoporphyrin IX monomethyl ester (**Figure 2D**).

Effects of Removal of Ycf54 on Other Chl Biosynthesis Enzymes

In order to investigate levels of Chl biosynthetic enzymes, and to verify the loss of Ycf54 in the Δ*ycf54* mutant, lysates from WT and Δ*ycf54* cells were fractionated into membrane and soluble components. The appearance of the cell lysate fractions (**Figure 4A**) reflects their pigment composition; the WT whole cell lysate and membrane fractions are green, and in Δ*ycf54* whole cell lysate and membrane fractions are blue and orange, respectively, because of the near-absence of Chl. A western blot of each of these extracts was probed with antibodies raised against a wide range of Chl biosynthesis enzymes (**Figure 4B**). The immunoblot probed with the antibody to Ycf54 shows this protein is distributed evenly between the soluble and insoluble fractions and is not detected in Δ*ycf54*, confirming the full segregation of this mutant. The absence of Ycf54 is also accompanied by a decrease in CycI and geranylgeranyl reductase (ChlP) and increased relative levels of the Mg-chelatase subunits ChlI and ChlD, although no change was detected in the levels of ChlH (**Figure 4B**).

Mass spectrometry was used to quantify the effects of *ycf54* deletion, in terms of the ability of CycI to associate with partner proteins *in vivo*. Pulldown assays with FLAG-tagged CycI are already known to retrieve Ycf54 from cell extracts (Hollingshead et al., 2012), so this experiment was repeated using FLAG- CycI in a Δ*ycf54* background. The amounts of PChlide oxidoreductase (POR), 3,8-divinyl (proto)chorophyllide reductase (DVR) and ChlP captured in pulldown assays by FLAG- CycI/WT and FLAG-CycI in Δ*ycf54* were compared by mass spectrometry. Proteins extracted from FLAG eluates were digested with a combination of endoproteinase LysC and trypsin and the peptide fragments analyzed by nanoLC-MS/MS. The captured proteins were quantified relative to the CycI bait as shown in **Figure 5**. Captured POR levels had decreased significantly in the Δ*ycf54* strain while DVR was reduced to an undetectable level. ChlP was only just detectable in one Δ*ycf54* replicate and relative to CycI by three orders of magnitude in the other two.

Lack of PChlide Impairs Synthesis of PsaA/B and Inner PSII Antennae but the Accumulation of Other Chl-Binding Proteins Is Not Affected

To evaluate the effects of greatly reduced Chl on the photosystems in Δ*ycf54* compared to the WT, photosynthetic membranes isolated from an equal biomass were gently solubilized with β-DDM and the membrane complexes were resolved by clear native electrophoresis (CN-PAGE), followed by SDS-PAGE in the second dimension. The resulting 2D CN/SDS-PAGE (**Figure 6A**) showed that Δ*ycf54* has drastically reduced levels of both photosystems, whilst the levels of other abundant membrane complexes such as ATP synthase, NADH:ubiquinone oxidoreductase and the cytochrome b_6f complex (shown by the western blot) are comparable between the two strains.

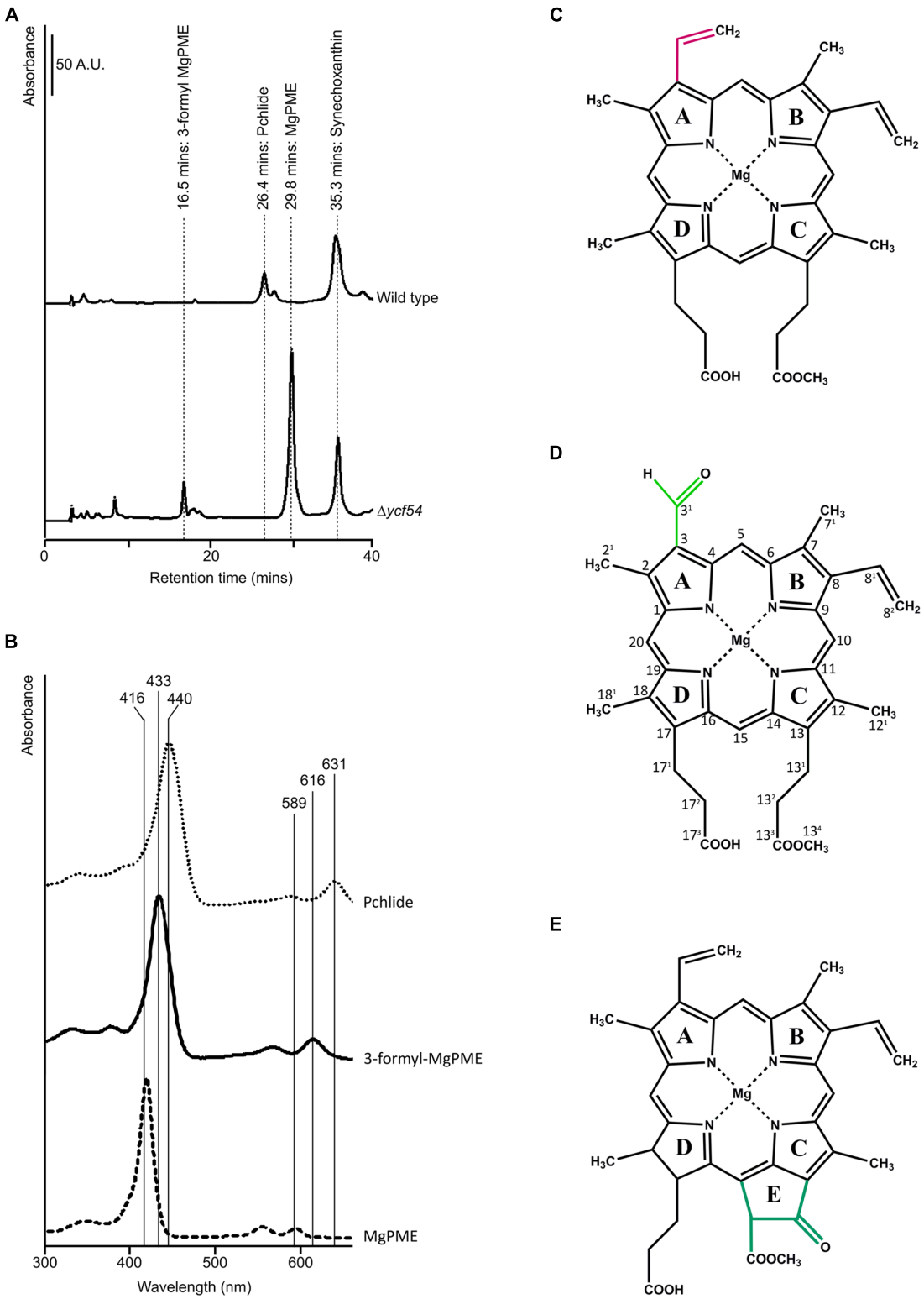

FIGURE 2 | HPLC analyses of pigments from WT and Δ*ycf54* cells. (A) Polar pigments were extracted with 80% methanol containing 0.2% (v/v) ammonium from an equal volume of cells at an $OD_{750\ nm}$ = ~0.7 and analyzed on a Phenomenex C_{18} column. Separation of precursors was detected by a diode array detector set to 432 nm, the Soret peak of 3-formyl MgPME, which is observed in Δ*ycf54* cells. The elution times of the pigments of interest are indicated. **(B)** Absorbance spectra of MgPME, PChlide and 3-formyl-MgPME, **(C)** Mg-protoporphyrin IX monomethyl ester (MgPME), **(D)** Mg-3-formyl-protoporphyrin IX monomethyl ester (3-formyl-MgPME), **(E)** protochlorophyllide (PChlide).

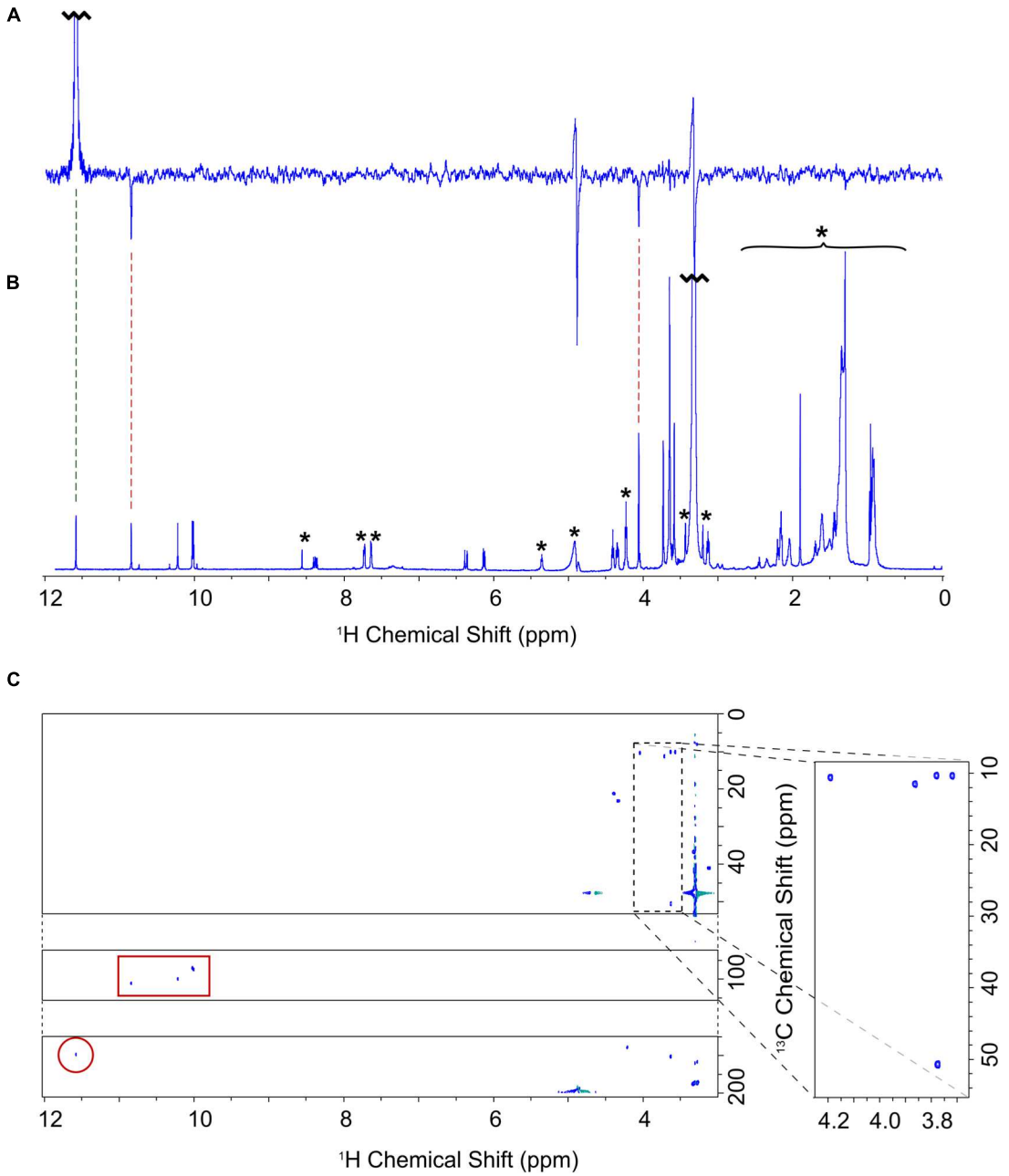

FIGURE 3 | NMR assignment of the A432 pigment accumulating in the Δ*ycf54* strain. (A) One dimensional selective NOE spectrum of 3-formyl-MgPME, selectively pulsed at 11.60 ppm (selectively exciting proton 3^1). Negative signals indicate NOE cross signal with protons 5 and 2^1 at 10.86 and 4.07 ppm, respectively. **(B)** ^{1}H-NMR spectrum of 3-formyl-MgPME. Signals marked with an asterisk are either solvent signals (methanol, water) or impurities (e.g., column matrix). **(C)** ^{13}C-HSQC spectrum for 3-formyl-MgPME. The carbon axis is split for clarity. The dashed box indicates methyl signals, expanded on the right. The red box indicates signals from meso protons. The red circle indicates a 3^1 aldehyde signal.

Interestingly, although the fully assembled PSII complexes in the mutant were barely detectable, this strain still accumulated relatively high levels of unassembled CP43 (**Figure 6A**). This observation suggests a block in formation of the early PSII assembly intermediates, which precedes attachment of the CP43 module and finalization of PSII reaction center core assembly (Komenda et al., 2004).

PSII assembly occurs in a stepwise fashion from four preassembled modules. These consist of one large Chl binding subunit (D1, D2, CP47, or CP43) in addition to several low molecular mass membrane polypeptides, bound pigments and other co-factors (Komenda et al., 2012). Assembly is initiated via the association of D1 and D2 to form the intermediate complex RCII* Knoppová et al. (2014), next the CP47 assembly

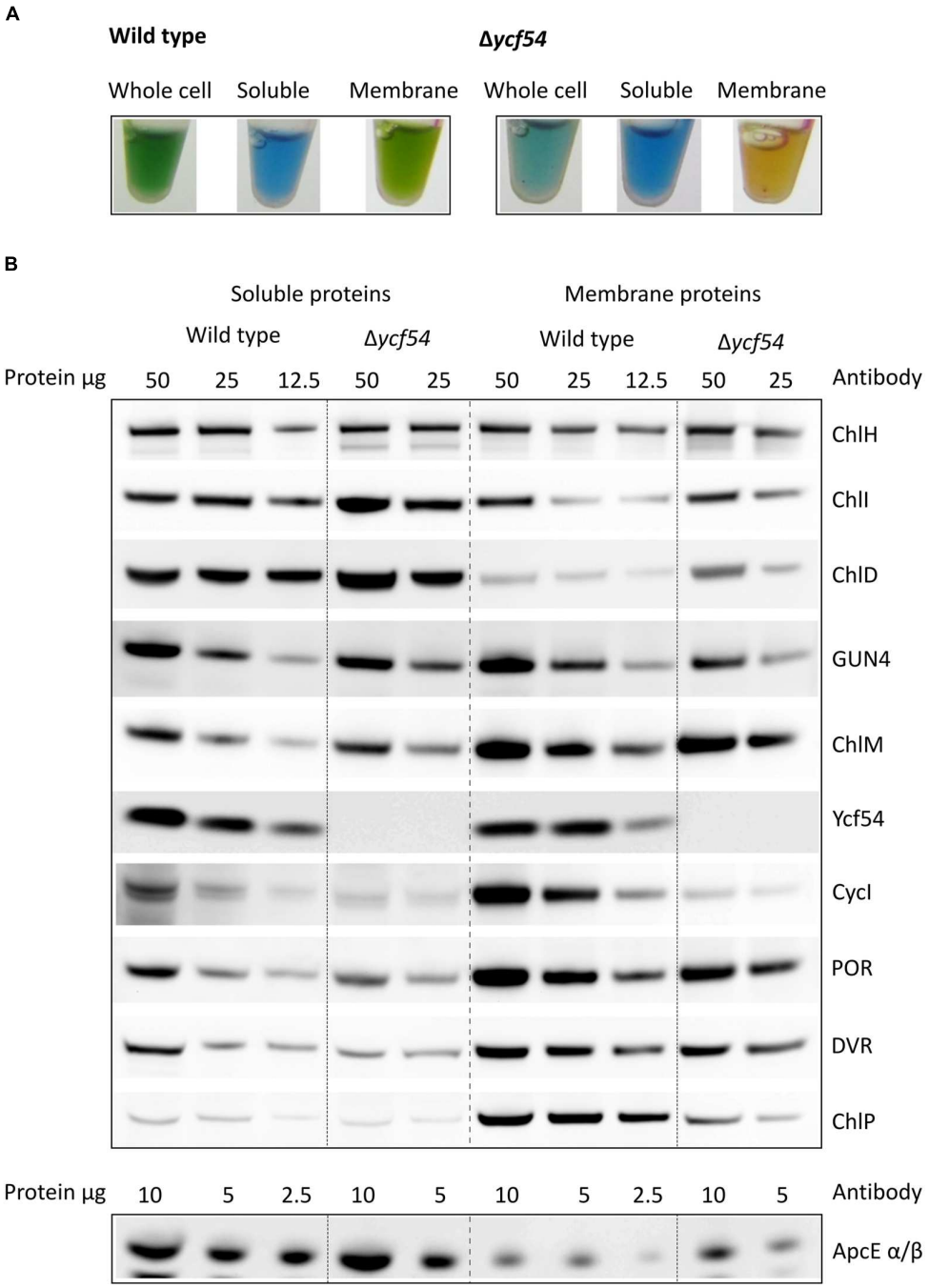

FIGURE 4 | Levels of Chl biosynthesis enzymes in WT and Δ*ycf54* cells. (A) Photographs of the whole cell, soluble and solubilized membrane lysate fractions, illustrating the changes in pigmentation between WT and Δ*ycf54*. **(B)** Western blot analysis of the soluble and membrane fractions from WT and Δ*ycf54 Synechocystis* strains. Samples of known protein concentration were separated by SDS-electrophoresis and transferred to a nitrocellulose membrane, which was probed with antibodies to the magnesium chelatase subunits (ChlH, ChlI, ChlD, and GUN4), CycI (CHL27), Mg-protoporphyrin IX methyltransferase (ChlM), Ycf54, PChlide oxidoreductase (POR), 3,8-divinyl (proto)chorophyllide reductase (DVR), geranylgeranyl reductase (ChlP). Detection of phycobiliprotein ApcE α/β served as a loading control.

module is attached, forming RC47, and finally mature PSII is formed by addition of the CP43 module (Boehm et al., 2011, 2012), attachment of the lumenal extrinsic proteins, and light-driven assembly of the oxygen-evolving Mn_4CaO_5 complex (Komenda et al., 2008; Nixon et al., 2010). To further investigate the perturbations in PSII assembly, the levels of individual PSII assembly sub-complexes were ascertained by 2D gel electrophoresis and immunodetection (**Figure 6B**). To assess

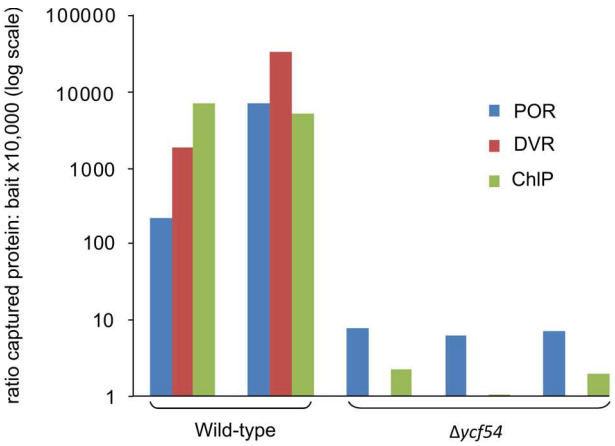

FIGURE 5 | Relative quantification of CycI, POR, DVR, and ChlP in FLAG-CycI pulldowns against WT and Δ*ycf54* backgrounds, using mass spectrometry. The bait and captured proteins in FLAG-CycI elutes were identified by mass spectrometry and database searching as described in Materials and Methods. For each analysis, a representative tryptic peptide ion was extracted from the full scan spectra as follows: CycI, AILEEFR, m/z 439.24, 2+; POR, VADELGFPK, m/z 488.26, 2+; DVR (Slr1923), VNKPTLSPNLSVLEEVEK, 666.03 3+; ChlP, AGIETYLFER, 599.81, 2+.

accumulation of the RCII* complex, the immunoblot was probed with antibodies raised against the RCII* components D1, Ycf39, and HliD (Knoppová et al. (2014). **Figure 6B** shows that the level of RCII* is unaffected by the large reduction in cellular Chl levels in the Δ*ycf54* mutant. Next, we investigated if PSII maturation was blocked at CP47 attachment and formation of RC47, by probing the blots with antibodies raised against HliA, a specific component of the CP47 assembly module (Promnares et al., 2006). We found that HliA, and hence the CP47 assembly module, was readily detectable in WT, but could not be detected in Δ*ycf54* (**Figure 6B**), indicating that low Chl abundance in Δ*ycf54* is impairing accumulation of the CP47 assembly module.

Our FLAG-pulldown experiments show that the interactions between CycI, POR, and DVR are significantly reduced in the Δ*ycf54* strain (**Figure 5**), therefore we compared the co-migration of these enzymes on a 2D gel (**Figure 6C**). Evident in the WT is a putative high-mass complex of ∼400 kDa (highlighted by the green box), which contains both CycI and POR; this complex was not detectable in the mutant (**Figure 6C**). Interestingly, our 2D gel shows that levels of Chl synthase, ChlG, HliD, and Ycf39, components of a chlorophyll biosynthetic/membrane insertase assembly complex (Chidgey et al., 2014), are unaffected in the Δ*ycf54* mutant (**Figure 6C**).

To understand the flux of photosystem biogenesis, we used ^{35}S pulse radio-labeling coupled with 2D CN/SDS-PAGE (**Figure 7**; a Coomassie stained gel is provided as Supplementary Figure S4), to compare the levels of protein synthesis between the WT and Δ*ycf54* mutant. As demonstrated in **Figure 7**, the ability of Δ*ycf54* to synthesize the Chl-binding PSI subunits PsaA/B is limited and synthesis of CP47 and CP43 subunits is hardly detectable even though 3-times more Δ*ycf54* protein was loaded onto the gel (See Supplementary Figure S4 for overexposed signal of the CP47). In contrast, there were comparable levels of synthesis of the PSII reaction center core subunits D1 and D2 in the WT and Δ*ycf54* strains. This observation, coupled with the data from our 2D-immunoblot (**Figure 6B**), shows that the D1 and D2 subunits are rapidly assembled into RCII* in Δ*ycf54*, but given the lack of assembled PSII complexes, these RCII* are presumably rapidly degraded in the mutant. Interestingly, in the mutant the unassembled CP43 was still detectable on the stained gel, which contrasted to virtually zero level of unassembled CP47 (**Figures 6A,B** and **7**; Supplementary Figure S4). This observation indicates that both synthesis and stability of the CP47 are impaired in the mutant, whereas the structurally similar CP43 antenna can still accumulate though the synthesis is also very weak (Supplementary Figure S4). Taken together, our data suggest that the depleted levels of *de novo* Chl in Δ*ycf54* specifically hinder the synthesis of PSI and the inner antennae of the PSII. However, given different stability of CP47 and CP43, it is the lack of CP47 protein that blocks assembly of RC47 and thus PSII maturation, sensitizing the PSII assembly pathway to the availability of *de novo* Chl.

Lack of *De Novo* Chl Affects Ultrastructure of Δ*ycf54* Cells

In order to investigate the effects of removal of 87% of the cellular Chl on the ultrastructure of Δ*ycf54* cells, electron microscopy of negatively stained thin cell sections was performed. Electron micrographs are shown in **Figure 8**. In the WT the thylakoids are observed as parallel stacks of two to five membranes that closely follow the contour of the cell membrane (**Figures 8A–C**), but no such organized thylakoid membranes are visible in micrographs of the Δ*ycf54* mutant (**Figures 8B–D**). Instead, membrane-like structures are dispersed throughout the cytoplasm of the cell. These results suggest key role of photosystems in the formation of the highly ordered thylakoid structures.

DISCUSSION

The MgPME-cyclase is the least understood component in the Chl biosynthetic pathway, and current knowledge of the individual components of the MgPME-cyclase had been limited to homologs of the *Rubrivivax gelatinosus* AcsF protein. Previous work identified two genes in *Synechocystis*, *sll1214*, and *sll1874*, as *acsF* homologs, which encode a membrane associated component of the MgPME-cyclase (Minamizaki et al., 2008; Peter et al., 2009). AcsF and its homologs contain a putative di-iron site and are thus viewed as the true catalytic subunit of the MgPME-cyclase (Tottey et al., 2003). The discovery of another gene, *ycf54*, that plays an important role in cyclase activity (Albus et al., 2012; Hollingshead et al., 2012) showed that other components are required, but so far it is not possible to assign a catalytic or assembly-related function to the Ycf54 protein. Further work on the role of Ycf54 required a fully segregated Δ*ycf54* mutant, which is reported herein.

In our efforts to construct a fully segregated Δ*ycf54* mutant, we discovered it was only possible to completely delete the *ycf54* gene in one specific substrain of *Synechocystis* (GT-W).

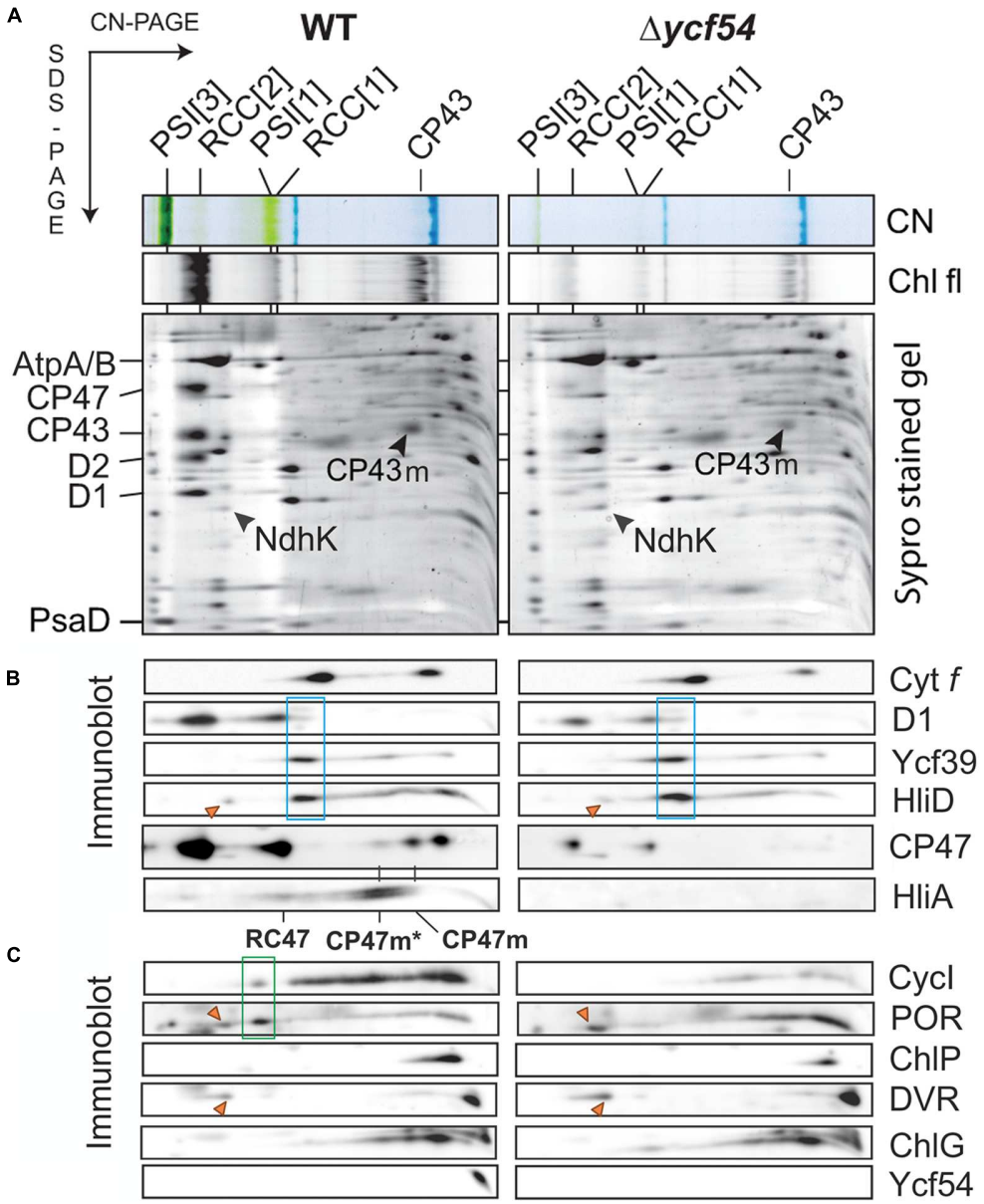

FIGURE 6 | 2D gel-electrophoresis of membrane complexes isolated from WT and Δ*ycf54* cells, followed by immunodetection of PSII assembly complexes and enzymes involved in Chl biosynthesis. (A) Membrane proteins were separated by 4–14% CN-PAGE, and then in the second dimension by 12–20% SDS-PAGE. The loading corresponds to the same number of cells. The SDS gel was stained by Sypro Orange, blotted and the cytochrome *f* visualized by heme *f* peroxidase activity. Chl fluorescence emitted by PSII and by unassembled CP43 (Chl fl) was detected by Fuji LAS 4000 after excitation by blue light. Designation of complexes is: PSI[3] and PSI[1], trimeric and monomeric PSI, respectively; RCC[2] and RCC[1], dimeric and monomeric PSII core complexes, respectively. **(B)** Immunodetection of PSII assembly complexes. RCII* complex (boxed in blue) was detected using D1, Ycf39, and HliD antibodies. The positions of the CP47 assembly module CP47m, and CP47m associated with High-Light-Inducible proteins HliA/B (CP47m*), are indicated. The HliA signal also marks the position of the PSII core complex lacking CP43 (RC47). **(C)** Immunodetection of Ycf54 proteins and enzymes involved in Chl biosynthesis in the membrane fraction separated by 2D electrophoresis. Highlighted by the green box is a putative high-mass complex (~400 kDa) containing CycI and POR; this complex is not detectable in the mutant. Orange triangles indicate unspecific cross-reactions with a subunit of the NDH complex. ChlG is Chl-synthase; other enzymes are designated as in **Figure 2**.

One possible explanation for this finding was elucidated by analysis of the GT-W genome, which contains a long (~100 kbp) chromosomal duplication that covers one hundred genes, including *cycI (sll1214*; Bečková et al., submitted). This chromosomal duplication is not present in any of the other *Synechocystis* substrains for which a genome sequence is available (Kanesaki et al., 2012; Trautmann et al., 2012). Given the duplication of *cycI* in GT-W, it is likely that *cycI* expression is

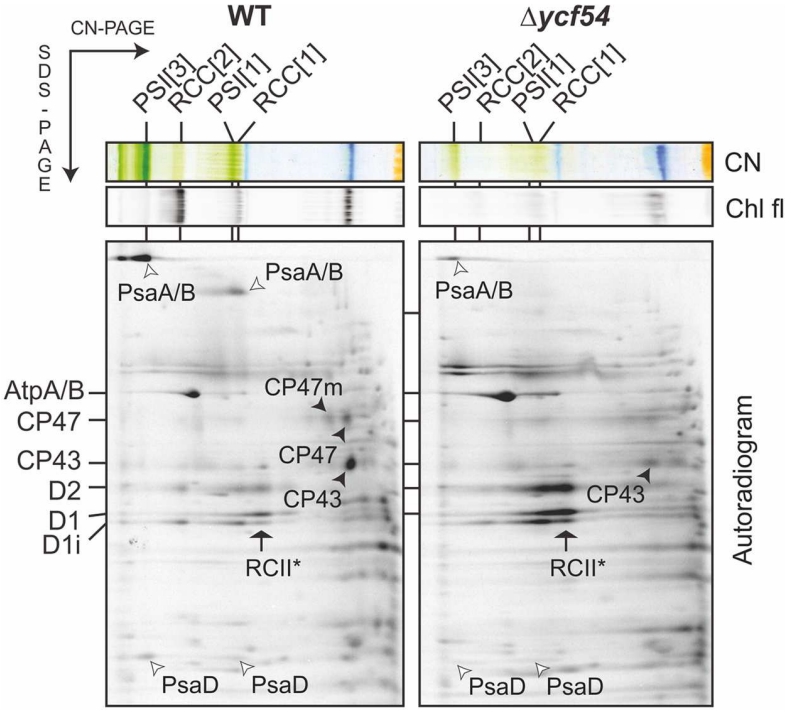

FIGURE 7 | Synthesis of the Chl-binding proteins in the Δ*ycf54* strain. WT and mutant cells were radiolabeled with [^{35}S]Met/Cys mixture using a 30-min pulse. Isolated membrane proteins were separated by CN-PAGE on a 4–14% linear gradient gel, and another 12–20% SDS-electrophoresis was used for the second dimension. For Δ*ycf54* membrane proteins three-times more cells were loaded than for the control to obtain a detectable signal for weakly labeled proteins (PsaA/B). The 2D gels were stained with Coomassie Blue (the stained gel is shown as Supplementary Figure S4) then dried, and the labeled proteins were then detected by a phosphorimager (Autorad). Protein complexes are designated as in **Figure 6**.

increased in this strain. A very low level of CycI is a hallmark of the strains in which we partially or completely inactivated the *ycf54* gene. Thus, we hypothesize that the doubled expression of the *sll1214* gene coding for CycI may suppress the lethality of inactivating the *ycf54* gene. This hypothesis is in agreement with our observation that in the absence of Ycf54 the CycI cyclase component is destabilized (**Figures 4** and **5**) and the remaining CycI content is probably very close to a threshold essential for viability.

Analysis of the pigments that accumulate in the Δ*ycf54* mutant could provide clues regarding the role of the Ycf54 protein, and a previous analysis showed that the partially segregated *ycf54* mutant accumulates MgPME, the substrate of the cyclase. In addition, there was an unknown pigment (**Figure 2**) that was suggested to be an intermediate in the cyclase reaction (Hollingshead et al., 2012), on the basis that the 433 nm Soret absorbance peak falls between the Soret peaks of the cyclase substrate MgPME (416 nm) and the PChlide product (440 nm). Similarly, early work with greening cucumber cotyledons had found pigments with emission maxima between 434 and 436 nm, proposed to be biosynthetic intermediates between MgPME and PChlide (Rebeiz et al., 1975). Identification of the unknown pigment as Mg-3-formyl-PME suggests that this pigment is not an intermediate in the cyclase reaction, as it is highly unlikely that this would produce a Chl pigment modified at the C3 position. Rather, Mg-3-formyl-PME bears a striking resemblance to Chl *d*, the major light harvesting pigment found in the cyanobacterium *Acaryochloris marina* (Miyashita et al., 1996). The pathway and reaction mechanism of Chl *d* biosynthesis in *Acaryochloris marina* have not yet been elucidated but, based on the genome sequence, Chl *d* is thought to be derived from Chl *a* (Swingley et al., 2008). Previously, Chl *d* has been synthesized in low yields in aqueous acetone from Chl *a* by treatment with papain (Koizumi et al., 2005) and peroxide (Aoki et al., 2011) and in much higher yields from Chl *a* incubated with thiophenol and acetic acid in tetrahydrofuran (Fukusumi et al., 2012). Given the high accumulation of MgPME in Δ*ycf54*, it is likely that reactive oxygen species, including peroxide, convert the MgPME 3-vinyl group, leading to the formation of Mg-3-formyl-PME.

The identification of Mg-3-formyl-PME as an oxidation product of the substrate rather than a catalytic intermediate is not consistent with a catalytic role for Ycf54 in the MgPME-cyclase complex. However, the hypothesis by Hollingshead et al. (2012) that Ycf54 plays a role in the assembly or stabilization of the catalytic MgPME-cyclase enzyme complex remains valid. By using FLAG-CycI as bait in pulldown assays, combined with quantitative MS analysis, we demonstrated that the absence of Ycf54 affects formation of a complex between CycI and enzymes further down the pathway (POR, DVR, and ChlP). In particular, the almost complete absence of DVR in the pulldown from the Δ*ycf54* strain provides a strong evidence that Ycf54 facilitates formation of such a complex; in contrast to POR and ChlP the

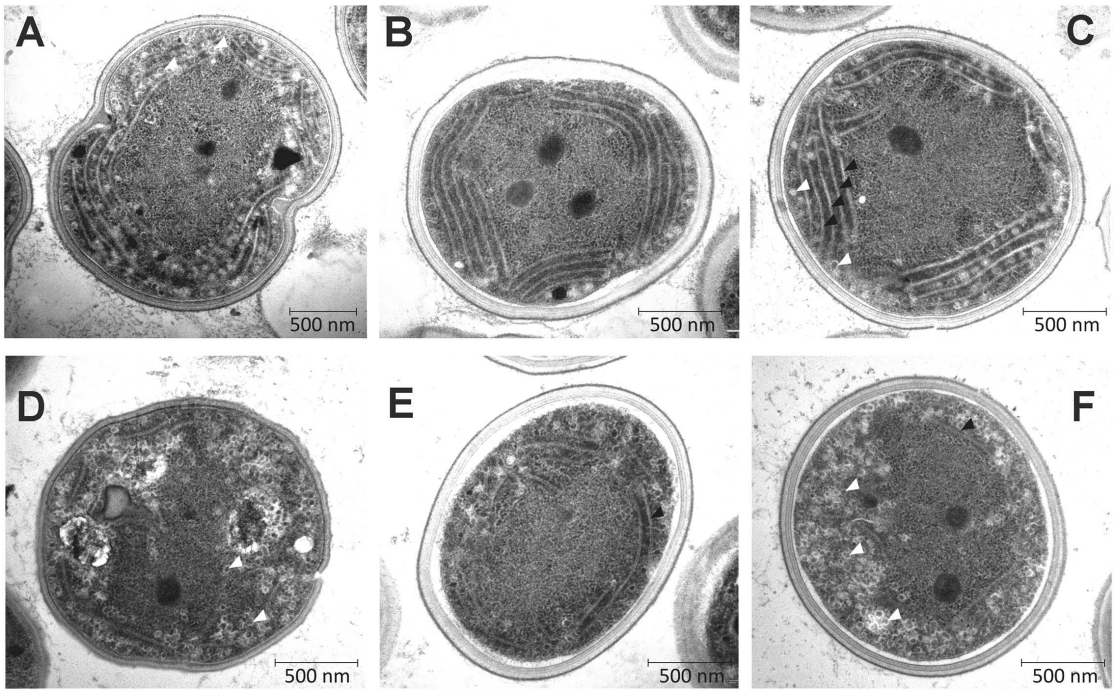

FIGURE 8 | Transmission electron micrographs of WT and Δ*ycf54* cells. Ultrathin sections from *Synechocystis* WT **(A–C)** and Δ*ycf54* cells **(D–F)** grown photomixotrophically under low light conditions. White arrows indicate thylakoid membranes and white triangles indicate glycogen granules.

stability of DVR in the mutant does not seem to be compromised and thus this result cannot be explained by a hypothetical fast degradation of this enzyme during pulldown assay. Indeed, the present data also provide evidence for an interaction between Cycl1 and POR, DVR, and ChlP, which aligns well with data obtained by Kauss et al. (2012) who performed pulldown experiments with the *Arabidopsis* FLU protein. These analyses found that FLU forms a complex with CHL27, the *Arabidopsis* AcsF homolog, PORB, PORC, and ChlP. In *Synechocystis* at least, it appears that Ycf54 plays no direct catalytic role, and that it is important for the formation and maintenance of a Chl biosynthetic complex, with disruption of this complex possibly triggering degradation of CycI and consequently Chl deficiency. However, a wider role for Ycf54 in governing the whole pathway appears to be excluded by the lack of effect of the Δ*ycf54* on components of the ChlG-HliD-Ycf39 complex that operates at the end of the pathway. This complex likely coordinates Chl delivery to the membrane-intrinsic apparatus for insertion and translocation of apoproteins of the photosynthetic apparatus (Chidgey et al., 2014). It is notable that although the CycI is almost exclusively associated with the membrane fraction under moderate light conditions Ycf54 is distributed equally between membrane and soluble fractions (**Figure 4B**). It is not known whether membrane-bound or soluble Ycf54 is critical for the CycI stability but there is a possibility that dissociation of Ycf54 from a membrane-bound assembly of CycI, POR, and DVR enzymes triggers degradation of CycI. Such a mechanism might regulate CycI activity at post-translational level and allow the cell to respond quickly to fluctuations in the environment.

Deletion of the *ycf54* gene generated a *Synechocystis* strain with very low levels of Chl, facilitating our studies on the cellular effects of a greatly lowered flux down the Chl biosynthetic pathway. It has long been known that photosystem biosynthesis requires Chl (Mullet et al., 1990; Eichacker et al., 1992; Müller and Eichacker, 1999), so we took advantage of the low Chl levels in the Δ*ycf54* mutant to investigate the effects of Chl depletion on the synthesis and assembly of the photosystems. Although the levels of some Chl biosynthesis enzymes are altered in the Δ*ycf54* mutant the ChlG-HliD-Ycf39 complex is unaffected, allowing the effects of reduced flux down the Chl pathway on Chl binding proteins to be investigated without disrupting ChlG-HliD-Ycf39 interactions with the YidC/Alb3 insertase and the consequent synthesis of nascent photosystem polypeptides. In addition, we were able to investigate the accumulation of "minor" Chl binding proteins, including cytochrome b_6f (Kurisu et al., 2003), the Hli proteins (Staleva et al., 2015) and the Chl-synthase complex (Chidgey et al., 2014). Our findings show that whilst the Chl binding proteins PsaA/B and CP47 are highly sensitive to cellular Chl levels, the accumulation of CP43 and "minor" Chl binding proteins, including cytochrome b_6f, is robust under Chl limiting conditions.

PSI is the main sink for *de novo* Chl (Kopečná et al., 2013); our results (**Figure 7**) show that synthesis of the core PSI subunits PsaA/B is impaired in the absence of Ycf54, i.e., under *de novo* Chl limiting conditions, suggesting that *Synechocystis* is unable to recycle Chl molecules released from degraded complexes for the synthesis of new PSI complexes. In comparison, the dependence of PSII biogenesis on the availability of *de novo* Chl

modules appears to be more complex, as previous studies show Chl molecules are re-cycled during PSII synthesis and repair (Kopečná et al., 2013, 2015) via re-phytylation of chlorophyllide (Vavilin and Vermaas, 2007). The PSII complex assembles in a modular fashion, starting with the association of D1 and D2 assembly modules, to form the RCII* complex. This is followed by attachment of a CP47 module, then a CP43 module, then the lumenal extrinsic proteins and the oxygen-evolving Mn_4CaO_5 complex (reviewed in Komenda et al., 2012). Despite the large decrease in cellular Chl levels in Δ*ycf54*, all components of the RCII* complex are synthesized in adequate amounts and assembled. We hypothesize that synthesis of the RCII* complex is enabled by the continuous recycling of a relatively stable pool of Chl molecules made available during the RCII* assembly/degradation cycle. Evidence that RCII* contains Chl as well pheophytin, carotenoids and heme cofactors has been shown previously (Knoppová et al., 2014). We cannot exclude the possibility that in the Δ*ycf54* mutant there is a pool of the RCII* complex that lacks Chl. However, we did not observe any shift of electrophoretic mobility even for the ^{35}S labeled RCII* that would indicate presence of a hypothetical Chl-less RCII*. Furthermore, Δ*ycf54* contains some functional PSII complexes, which requires that at least some RCII* with cofactors has to be synthesized en route to the fully assembled PSII.

Our findings also show that CP43 can accumulate as an unassembled module in Δ*ycf54* even though the synthesis is very limited (**Figures 6A** and **7**). In contrast, CP47 seems to be unstable in Δ*ycf54*, which suggests that CP47 is the *de novo* Chl sensitive component of PSII biogenesis. This observation is consistent with previous work on the accumulation of PSII subunits in Δ*por* (Kopečná et al., 2013) and Δ*gun4* (Sobotka et al., 2008) mutants, disrupted in the PChlide reduction and Mg-chelatase steps, respectively. As also seen for Δ*ycf54*, the Δ*por* and Δ*gun4* strains accumulate the PSII core complex RCII* and the PSII antenna CP43, but CP47 synthesis is not observed (Sobotka et al., 2008; Kopečná et al., 2013). It is not currently known why CP47 is more sensitive to the availability of *de novo* Chl than the similar CP43 subunit, although it has been recently observed that the newly synthesized CP43, but not CP47, subunit is attached to a PSI complex (Kopečná et al., 2015). We tentatively speculate that the situation in the mutant leads frequently to the synthesis of aberrant CP47 lacking one or more Chl molecules. The synthesis of CP43 might be less error-prone because Chl molecules bound to the periphery of PSI could be used for the assembly of this complex.

In summary, the role of Ycf54 in the MgPME-cyclase complex has been elucidated further. This work shows that whilst Ycf54 is required for stabilization of Cyc1, the known catalytic component of the MgPME-cyclase, the protein itself is unlikely to play a key catalytic role in the formation of the fifth isocyclic ring. Furthermore, Ycf54 does not appear to be directly implicated in Chl phytolation or Chl insertion into proteins. The construction of a Δ*ycf54* mutant has provided a useful tool to investigate the effects of reduced *de novo* Chl on the biosynthesis of cyanobacterial Chl binding proteins, highlighting the differing requirements for Chl exhibited by proteins within the PSI and PSII light harvesting complexes that bind this pigment. Insights into the catalytic cycle of the MgPME-cyclase remain elusive and further work is required to determine the exact molecular mechanisms of this enzyme.

AUTHOR CONTRIBUTIONS

SH, JK, DA, LB, PJ, and GC performed the research; MD, MW, RS, and CNH designed the experiments, and SH, DA, PJ, MD, MW, RS, and CNH wrote the paper.

ACKNOWLEDGMENTS

SH, PJ, CNH, and MD gratefully acknowledge financial support from the Biotechnology and Biological Sciences Research Council (BBSRC UK), award numbers BB/G021546/1 and BB/M000265/1. MD acknowledges support from the Biotechnology and Biological Sciences Research Council (UK; BB/M012166/1). CNH was also supported by Advanced Award 338895 from the European Research Council. SH was supported by a doctoral studentship from the University of Sheffield. GC and DA were supported by a BBSRC doctoral studentship. JK, LB, and RS were supported by project 14-13967S of the Czech Science Foundation, and by the National Programme of Sustainability I (LO1416).

SUPPLEMENTARY MATERIAL

The Supplementary Material for this article can be found online at: http://journal.frontiersin.org/article/10.3389/fpls.2016.00292

REFERENCES

Albus, C. A., Salinas, A., Czarnecki, O., Kahlau, S., Rothbart, M., Thiele, W., et al. (2012). LCAA, a novel factor required for magnesium protoporphyrin monomethylester cyclase accumulation and feedback control of aminolevulinic acid biosynthesis in Tobacco. *Plant Physiol.* 160, 1923–1939. doi: 10.1104/pp.112.206045

Aoki, K., Itoh, S., Furukawa, H., Nakazato, M., Iwamoto, K., Shiraiwa, Y., et al. (2011). "Enzymatic and non-enzymatic conversion of Chl a to Chl d," in *Proceedings of the 5th Asia and Oceania Conference on Photobiology*, Nara.

Boehm, M., Romero, E., Reisinger, V., Yu, J., Komenda, J., Eichacker, L. A., et al. (2011). Investigating the early stages of Photosystem II assembly in *Synechocystis* sp PCC 6803: isolation of CP47 and CP43 complexes. *J. Biol. Chem.* 286, 14812–14819. doi: 10.1074/jbc.M110.207944

Boehm, M., Yu, J., Reisinger, V., Bečková, M., Eichacker, L. A., Schlodder, E., et al. (2012). Subunit composition of CP43-less photosystem II complexes of *Synechocystis* sp PCC 6803: implications for the assembly and repair of photosystem II. *Philos. Trans. R. Soc. B Biol. Sci.* 367, 3444–3454. doi: 10.1098/rstb.2012.0066

Boldareva-Nuianzina, E. N., Bláhová, Z., Sobotka, R., and Koblížek, M. (2013). Distribution and origin of oxygen-dependent and oxygen-independent forms of Mg-protoporphyrin monomethylester cyclase among phototrophic *proteobacteria*. *Appl. Environ. Microbiol.* 79, 2596–2604. doi: 10.1128/AEM.00104-13

Bollivar, D., Braumann, I., Berendt, K., Gough, S. P., and Hansson, M. (2014). The Ycf54 protein is part of the membrane component of Mg-protoporphyrin IX monomethyl ester cyclase from barley (*Hordeum vulgare* L.). *FEBS J.* 281, 2377–2386. doi: 10.1111/febs.12790

Canniffe, D. P., Jackson, P. J., Hollingshead, S., Dickman, M. J., and Hunter, C. N. (2013). Identification of an 8-vinyl reductase involved in bacteriochlorophyll biosynthesis in *Rhodobacter sphaeroides* and evidence for the existence of a third distinct class of the enzyme. *Biochem. J.* 450, 397–405. doi: 10.1042/BJ20121723

Chidgey, J. W., Linhartová, M., Komenda, J., Jackson, P. J., Dickman, M. J., Canniffe, D. P., et al. (2014). A cyanobacterial chlorophyll synthase-HliD complex associates with the Ycf39 protein and the YidC/Alb3 insertase. *Plant Cell* 26, 1267–1279. doi: 10.1105/tpc.114.124495

Chua, N. H., Blobel, G., Siekevitz, P., and Palade, G. E. (1976). Periodic variations in the ratio of free to thylakoid-bound chloroplast ribosomes during the cell cycle of *Chlamydomonas reinhardtii*. *J. Cell Biol.* 71, 497–514. doi: 10.1083/jcb.71.2.497

Dobáková, M., Sobotka, R., Tichý, M., and Komenda, J. (2009). Psb28 protein is involved in the biogenesis of the photosystem II inner antenna CP47 (PsbB) in the cyanobacterium *Synechocystis* sp. PCC 6803. *Plant Physiol.* 149, 1076–1086. doi: 10.1104/pp.108.130039

Eichacker, L., Paulsen, H., and Rüdiger, W. (1992). Synthesis of chlorophyll a regulates translation of chlorophyll a apoproteins P700, CP47, CP43 and D2 in barley etioplasts. *Eur. J. Biochem.* 205, 17–24. doi: 10.1111/j.1432-1033.1992.tb16747.x

Eichacker, L. A., Helfrich, M., Rüdiger, W., and Muller, B. (1996). Stabilization of chlorophyll a-binding apoproteins P700, CP47, CP43, D2, and D1 by chlorophyll a or Zn-pheophytin a. *J. Biol. Chem.* 271, 32174–32179. doi: 10.1074/jbc.271.50.32174

Fukusumi, T., Matsuda, K., Mizoguchi, T., Miyatake, T., Ito, S., Ikeda, T., et al. (2012). Non-enzymatic conversion of chlorophyll-a into chlorophyll-d in vitro: a model oxidation pathway for chlorophyll-d biosynthesis. *FEBS Lett.* 586, 2338–2341. doi: 10.1016/j.febslet.2012.05.036

Hollingshead, S., Kopečná, J., Jackson, P. J., Canniffe, D. P., Davison, P. A., Dickman, M. J., et al. (2012). Conserved chloroplast open-reading frame ycf54 is required for activity of the magnesium protoporphyrin monomethylester oxidative cyclase in *Synechocystis* PCC 6803. *J. Biol. Chem.* 287, 27823–27833. doi: 10.1074/jbc.M112.352526

Jordan, P., Fromme, P., Witt, H. T., Klukas, O., Saenger, W., and Krauss, N. (2001). Three-dimensional structure of cyanobacterial photosystem I at 2.5 Å resolution. *Nature* 411, 909–917. doi: 10.1038/35082000

Kalb, V. F., and Bernlohr, R. W. (1977). A new spectrophotometric assay for protein in cell extracts. *Anal. Biochem.* 82, 362–371. doi: 10.1016/0003-2697(77)90173-7

Kanesaki, Y., Shiwa, Y., Tajima, N., Suzuki, M., Watanabe, S., Sato, N., et al. (2012). Identification of substrain-specific mutations by massively parallel whole-genome resequencing of *Synechocystis* sp. PCC 6803. *DNA Res.* 19, 67–79. doi: 10.1093/dnares/dsr042

Kauss, D., Bischof, S., Steiner, S., Apel, K., and Meskauskiene, R. (2012). FLU, a negative feedback regulator of tetrapyrrole biosynthesis, is physically linked to the final steps of the Mg++-branch of this pathway. *FEBS Lett.* 586, 211–216. doi: 10.1016/j.febslet.2011.12.029

Ke, S. H., and Madison, E. L. (1997). Rapid and efficient site-directed mutagenesis by single-tube 'megaprimer' PCR method. *Nucleic Acids Res.* 25, 3371–3372. doi: 10.1093/nar/25.16.3371

Knoppová, J., Sobotka, R., Tichý, M., Yu, J., Koník, P., Halada, P., et al. (2014). Discovery of a chlorophyll binding protein complex involved in the early steps of photosystem II assembly in *Synechocystis*. *Plant Cell* 26, 1200–1212. doi: 10.1105/tpc.114.123919

Koizumi, H., Itoh, Y., Hosoda, S., Akiyama, M., Hoshino, T., Shiraiwa, Y., et al. (2005). Serendipitous discovery of Chl d formation from Chl a withpapain. *Sci. Technol. Adv. Mater.* 6, 551–557. doi: 10.1016/j.stam.2005.06.022

Komenda, J., Nickelsen, J., Tichý, M., Prášil, O., Eichacker, L. A., and Nixon, P. J. (2008). The cyanobacterial homologue of HCF136/YCF48 is a component of an early photosystem II assembly complex and is important for both the efficient assembly and repair of photosystem II in *Synechocystis* sp PCC 6803. *J. Biol. Chem.* 283, 22390–22399. doi: 10.1074/jbc.M801917200

Komenda, J., Reisinger, V., Müller, B. C., Dobáková, M., Granvogl, B., and Eichacker, L. A. (2004). Accumulation of the D2 protein is a key regulatory step for assembly of the photosystem II reaction center complex in *Synechocystis* PCC 6803. *J. Biol. Chem.* 279, 48620–48629. doi: 10.1074/jbc.M405725200

Komenda, J., Sobotka, R., and Nixon, P. J. (2012). Assembling and maintaining the Photosystem II complex in chloroplasts and cyanobacteria. *Curr. Opin. Plant Biol.* 15, 245–251. doi: 10.1016/j.pbi.2012.01.017

Kopečná, J., Pilný, J., Krynická, V., Tomèala, A., Kis, M., Gombos, Z., et al. (2015). Lack of phosphatidylglycerol inhibits chlorophyll biosynthesis at multiple sites and limits chlorophyllide reutilization in *Synechocystis* sp. Strain PCC 6803. *Plant Physiol.* 169, 1307–1317. doi: 10.1104/pp.15.01150

Kopečná, J., Sobotka, R., and Komenda, J. (2013). Inhibition of chlorophyll biosynthesis at the protochlorophyllide reduction step results in the parallel depletion of Photosystem I and Photosystem II in the cyanobacterium *Synechocystis* PCC 6803. *Planta* 237, 497–508. doi: 10.1007/s00425-012-1761-4

Kurisu, G., Zhang, H. M., Smith, J. L., and Cramer, W. A. (2003). Structure of the cytochrome b6f complex of oxygenic photosynthesis: tuning the cavity. *Science* 302, 1009–1014. doi: 10.1126/science.1090165

Minamizaki, K., Mizoguchi, T., Goto, T., Tamiaki, H., and Fujita, Y. (2008). Identification of two homologous genes, chlAI and chlAII, that are differentially involved in isocyclic ring formation of chlorophyll a in the cyanobacterium *Synechocystis* sp PCC 6803. *J. Biol. Chem.* 283, 2684–2692. doi: 10.1074/jbc.M708954200

Miyashita, H., Ikemoto, H., Kurano, N., Adachi, K., Chihara, M., and Miyachi, S. (1996). Chlorophyll d as a major pigment. *Nature* 383, 402. doi: 10.1038/383402a0

Müller, B., and Eichacker, L. A. (1999). Assembly of the D1 precursor in monomeric photosystem II reaction center precomplexes precedes chlorophyll a-triggered accumulation of reaction center II in barley etioplasts. *Plant Cell* 11, 2365–2377. doi: 10.2307/3870961

Mullet, J. E., Klein, P. G., and Klein, R. R. (1990). Chlorophyll regulates accumulation of the plastid encoded chlorophyll apoprotein CP43 and apoprotein D1 by increasing apoprotein stability. *Proc. Natl. Acad. Sci. U.S.A.* 87, 4038–4042. doi: 10.1073/pnas.87.11.4038

Nixon, P. J., Michoux, F., Yu, J., Boehm, M., and Komenda, J. (2010). Recent advances in understanding the assembly and repair of photosystem II. *Ann. Bot.* 106, 1–16. doi: 10.1093/aob/mcq059

Peter, E., Salinas, A., Wallner, T., Jeske, D., Dienst, D., Wilde, A., et al. (2009). Differential requirement of two homologous proteins encoded by sll1214 and sll1874 for the reaction of Mg protoporphyrin monomethylester oxidative cyclase under aerobic and micro-oxic growth conditions. *Biochim. Biophys. Acta* 1787, 1458–1467. doi: 10.1016/j.bbabio.2009.06.006

Pinta, V., Picaud, M., Reiss-Husson, F., and Astier, C. (2002). *Rubrivivax gelatinosus* acsF (previously orf358) codes for a conserved, putative binuclear-iron-cluster-containing protein involved in aerobic oxidative cyclization of Mg-protoporphyrin IX monomethylester. *J. Bacteriol.* 184, 746–753. doi: 10.1128/JB.184.3.746-753.2002

Porra, R., Thompson, W., and Kriedemann, P. (1989). Determination of accurate extinction coefficients and simulataneous equations for assaying chlorophylls a and b extracted with four different solvents: verification of the concentration of chlorophyll standards by atomic absorption spectroscopy. *Biochim. Biophys. Acta* 975, 384–389. doi: 10.1016/S0005-2728(89)80347-0

Porra, R. J., Schafer, W., Gadon, N., Katheder, I., Drews, G., and Scheer, H. (1996). Origin of the two carbonyl oxygens of bacteriochlorophyll alpha – Demonstration of two different pathways for the formation of ring E in *Rhodobacter sphaeroides* and *Roseobacter denitrificans*, and a common hydratase mechanism for 3-acetyl group formation. *Eur. J. Biochem.* 239, 85–92. doi: 10.1111/j.1432-1033.1996.0085u.x

Promnares, K., Komenda, J., Bumba, L., Nebesarova, J., Vacha, F., and Tichy, M. (2006). Cyanobacterial small chlorophyll-binding protein ScpD (HliB) is located on the periphery of photosystem II in the vicinity of PsbH and CP47 subunits. *J. Biol. Chem.* 281, 32705–32713. doi: 10.1074/jbc.M606360200

Rebeiz, C. A., Mattheis, J. R., Smith, B. B., Rebeiz, C., and Dayton, D. F. (1975). Chloroplast biogenesis. Biosynthesis and accumulation of Mg-protoprophyrin IX monoester and longer wavelength metalloporphyrins by greening cotyledons. *Arch. Biochem. Biophys.* 166, 446–465. doi: 10.1016/0003-9861(75)90408-7

Rippka, R., Deruelles, J., Waterbury, J., Herdman, M., and Stanier, R. (1979). Generic assignments, strain histories and properties of pure cultures of cyanobacteria. *Microbiology* 111, 1–61. doi: 10.1099/00221287-111-1-1

Sobotka, R., Duerhring, U., Komenda, J., Peter, E., Gardian, Z., Tichy, M., et al. (2008). Importance of the cyanobacterial GUN4 protein for chlorophyll metabolism and assembly of photosynthetic complexes. *J. Biol. Chem.* 283, 25794–25802. doi: 10.1074/jbc.M803787200

Sobotka, R., Tichy, M., Wilde, A., and Hunter, C. N. (2011). Functional assignments for the carboxyl-terminal domains of the ferrochelatase from *Synechocystis* PCC 6803: the CAB domain plays a regulatory role, and region II is essential for catalysis. *Plant Physiol.* 155, 1735–1747. doi: 10.1104/pp.110.167528

Staleva, H., Komenda, J., Shukla, M. K., Šlouf, V., Kaòa, R., Polívka, T., et al. (2015). Mechanism of photoprotection in the cyanobacterial ancestor of plant antenna proteins. *Nat. Chem. Biol.* 11, 287–291. doi: 10.1038/nchembio.1755

Stott, K., Stonehouse, J., Keeler, J., Hwang, T., and Shaka, A. (1995). Excitation sculpting in high-resolution nuclear magnetic resonance spectroscopy: application to selective NOE experiments. *J. Am. Chem. Soc.* 117, 4199–4200. doi: 10.1021/ja00119a048

Swingley, W. D., Chen, M., Cheung, P. C., Conrad, A. L., Dejesa, L. C., Hao, J., et al. (2008). Niche adaptation and genome expansion in the chlorophyll d-producing cyanobacterium *Acaryochloris marina*. *Proc. Natl. Acad. Sci. U.S.A.* 105, 2005–2010. doi: 10.1073/pnas.0709772105

Tottey, S., Block, M. A., Allen, M., Westergren, T., Albrieux, C., Scheller, H. V., et al. (2003). *Arabidopsis* CHL27, located in both envelope and thylakoid membranes, is required for the synthesis of protochlorophyllide. *Proc. Natl. Acad. Sci. U.S.A.* 100, 16119–16124. doi: 10.1073/pnas.2136793100

Trautmann, D., Voss, B., Wilde, A., Al-Babili, S., and Hess, W. R. (2012). Microevolution in cyanobacteria: re-sequencing a motile substrain of *Synechocystis* sp. PCC 6803. *DNA Res.* 19, 435–448. doi: 10.1093/dnares/dss024

Umena, Y., Kawakami, K., Shen, J. R., and Kamiya, N. (2011). Crystal structure of oxygen-evolving photosystem II at a resolution of 1.9 Å. *Nature* 473, 55–60. doi: 10.1038/nature09913

van de Meene, A. M., Hohmann-Marriott, M. F., Vermaas, W. F., and Roberson, R. W. (2006). The three-dimensional structure of the cyanobacterium *Synechocystis* sp. PCC 6803. *Arch. Microbiol.* 184, 259–270.

Vavilin, D., and Vermaas, W. (2007). Continuous chlorophyll degradation accompanied by chlorophyllide and phytol reutilization for chlorophyll synthesis in *Synechocystis* sp PCC 6803. *Biochim. Biophys. Acta* 1767, 920–929. doi: 10.1016/j.bbabio.2007.03.010

Wilde, A., Mikolajczyk, S., Alawady, A., Lokstein, H., and Grimm, B. (2004). The gun4 gene is essential for cyanobacterial porphyrin metabolism. *FEBS Lett.* 571, 119–123. doi: 10.1016/j.febslet.2004.06.063

Zhang, H., Liu, H., Blankenship, R. E., and Gross, M. L. (2015). Isotope-encoded carboxyl group footprinting for mass spectrometry-based protein conformational studies. *J. Am. Soc. Mass Spectrom.* 27, 178–181. doi: 10.1007/s13361-015-1260-5

Zouni, A., Witt, H. T., Kern, J., Fromme, P., Krauss, N., Saenger, W., et al. (2001). Crystal structure of photosystem II from *Synechococcus elongatus* at 3.8 Å resolution. *Nature* 409, 739–743. doi: 10.1038/35055589

Conflict of Interest Statement: The authors declare that the research was conducted in the absence of any commercial or financial relationships that could be construed as a potential conflict of interest.